Liouville theory and random maps

Séverin Charbonnier

université PARIS-SACLAY

IPhT SACLAY

UNIVERSITÉ PARIS SUD
Comprendre le monde, construire l'avenir

NNT : 2018SACLS265

Thèse de doctorat

Liouville theory and random maps

Thèse de doctorat de l'Université Paris-Saclay
préparée à Université Paris-Sud

Ecole doctorale n°564 École doctorale Physique en Île-de-France (EDPIF)
Spécialité de doctorat: Physique

Thèse présentée et soutenue à Gif-sur-Yvette, le 10 septembre 2018, par

Séverin Charbonnier

Composition du Jury :

Timothy Budd Professeur assistant, Radboud University (Pays-Bas)	Rapporteur
François David Professeur, CEA Saclay, CNRS	Directeur de thèse
Enrica Duchi Maître de conférence, Université Paris Diderot, CNRS	Examinatrice
Bertrand Eynard Directeur de recherche, CEA Saclay, CNRS	Co-directeur de thèse
Robert Penner Professeur, University of California - Los Angeles (États-Unis)	Examinateur
Vincent Rivasseau Professeur, Université Paris-Sud, CNRS	Président
Adrian Tanasa Professeur, Université de Bordeaux, CNRS	Rapporteur

Acknowledgements

Je veux tout d'abord remercier mes deux formidables directeurs de thèse, François David et Bertrand Eynard. Vous m'avez constamment aiguillé vers des projets prometteurs, m'avez intégré à vos recherches, et avez écouté avec attention et patience mes pistes – souvent infructueuses. Vous avez été toujours de prompts et infaillibles soutiens, que ce soit pour participer à des écoles, pour rendre visite à des chercheurs, pour trouver un postdoc, ou pour me pousser à parler et écrire. François, qui as d'abord été un enseignant hors pair en théorie statistique des champs, ta connaissance sans pareil du domaine de la gravité quantique fut précieuse. Ta rigueur et ta ténacité dans les recherches ont été des modèles, ainsi que ton humilité : il n'est pas rare de te voir exécuter une de tes marches aléatoires devant ton tableau, et affirmer que tel résultat tout juste prouvé n'est qu'un simple exercice bien connu des écoliers. Bertrand, dont la capacité à rendre un sujet ardu accessible en ciblant l'essentiel, est inestimable pour un doctorant. Ta propension à voir loin (il est arrivé que je ne comprenne que des mois plus tard là où sans doute tu voulais me mener dès le début) et à tisser des liens entre des domaines très différents des mathématiques, est enthousiasmante et a aiguisé mon intérêt pour divers sujets. Je vous suis reconnaissant à tous les deux d'avoir su vous rendre disponibles durant ces trois ans, même dans les périodes chargées.

I am very grateful to Timothy Budd and Adrian Tanasa, for reading meticulously this manuscript and allowing me to defend my thesis. Also, you have been very reactive to my various administrative demands: this has been very important for preparing the defense peacefully. I am aware and sorry to have shorten your summer. Also, I particularly wish to thank Enrica Duchi, Robert Penner and Vincent Rivasseau, who accepted to be part of my jury.

Mes remerciements s'adressent à tous mes collaborateurs : Gaëtan, dont la rapidité dans les calculs et les idées sont insondables ; Raphaël, au moins autant poète que mathématicien ; Linxiao and Joonas, and the legendary « moules cocotte au muscat Corse » ; et Emmanuel, qui as toujours pris le temps de m'expliquer ses autres projets en cours. Cette thèse a été réalisée à l'IPhT, aussi je souhaite remercier toutes les personnes avec qui j'ai pu avoir des échanges enrichissants : Sylvain, Riccardo, Vincent, Jean-Yves, Bertrand, Jérémie. Parmi eux se trouvent les organisateurs des cours et des séminaires, qui font de ce laboratoire un centre bien vivant. Merci à Jean-Marc et Philippe, respectivement parrain et tuteur de thèse, pour vos judicieux conseils en deuxième année. Par ailleurs, les Journées Cartes ont toujours été des moments stimulants d'échange, et c'est pourquoi j'en remercie les organisateur-ices et les participant-e-s.

Je suis aussi redevable envers le personnel du laboratoire et d'abord Sylvie Zaffanella, Laure Sauboy et le service informatique, si prompt-e-s à répondre à mes questions. Merci à toi Stéphane qui as sauvé notre bureau de moult naufrages, dus à ma propension à créer de l'entropie. Merci au personnel du restaurant des Algorithmes, qui souvent s'inquiétait de ma santé quand je ne prenais qu'une assiette de légumes. Note pour plus tard : ne pas grignoter entre les repas. Merci aussi à toutes les mains invisibles qui m'ont permis d'aller à des conférences, des écoles, tou-te-s les secrétaires que je ne saurais nommer. Santi, tu m'as souvent guidé dans le dédale de la bureaucratie universitaire et surtout tu m'as initié à l'art du réveil adiabatique réversible lorsqu'on partageait une chambre à l'institut de physique de Cargèse ; merci d'avoir supporté mon chaos de bureau et moi durant trois ans. Promis je goûterai au maté. Christian et Pierre, plus amis que collègues aussi, dont je n'oublierai pas les talents au frisbee. Enfin, merci à tou-te-s les autres (post)doctorant-e-s qui ont égayé les déjeuners : Soumya, Laïs, Hannah, Riccardo, Luca, Federico, Niall, Étienne, Romain, Lilian, Jonathan, Kemal, Benoit, Tiago, Orazio, Stefano, Dinh-Long. Je m'excuse pour

mes éventuelles prises de positions radicales concernant vos préférences alimentaires ou politiques, mais il faut bien dire que vous avez le chic pour avoir systématiquement tort.

Je souhaite remercier les professeurs du master 2 de physique théorique de l'ENS pour leurs enseignements de grande qualité, ainsi que Christoph, dont les cours, les conseils, le soutien et la bonne humeur proverbiale ont été nécessaires le long de mon cursus.

Bien sûr, mes ami-e-s ont été d'importants soutiens, d'abord Frédéric, Antoine et Adrien, toujours déters, festifs et offensifs. Quant à Farrah, Matthieu et Thomas : il est si doux d'avoir des ami-e-s capables de s'astreindre à m'insulter car on ne se voit pas assez. Je pense aussi chaleureusement à Marie-Laure, Mireille, Ambroise et Florian.

En tant qu'étudiant et moniteur de l'Université Paris-Sud, je souhaite remercier les personnels et étudiant-e-s des différentes universités qui ont occupé les campus – entre autre pour loger des exilé-e-s –, qui ont lutté contre les lois Travail et ORE, enfin qui ont renforcé d'autres luttes. Vous avez nourri mes réflexions sur la place de l'enseignement et de la recherche au sein de la société. Plus largement, je remercie les différentes composantes du cortège de tête pour avoir ouvert des brèches salutaires. Mes pensées vont aux victimes de la massive répression policière et judiciaire qui a émaillé ces trois dernières années. Et un fol esprit sait : le silence n'est pas un oubli.

Je suis reconnaissant envers ma famille, d'abord mes parents, qui m'avez élevé dans un milieu aimant et réparateur, et m'avez transmis la curiosité : la visite de tous les musées accessibles en moins de deux heures de tout lieu de vacances y est sans doute pour quelque chose. Ensuite mes sœurs et frères, qui avez participé indirectement à ce manuscrit : Aldée, par ton écoute et tes bons conseils dans les périodes de doute ; Liselotte, par ton soutien logistique qui me permet de venir au laboratoire, et l'évasion musicale du музыка дня, et Régis, qui me trouves les voies pour m'élever ; Théophane et Violaine, qui me poussez à me dépasser techniquement ; et Ghislain, dont la sérénité à toute épreuve m'est un modèle.

Enfin, je rends hommage à Lucie, rayonnante et géniale ; tu as été indispensable à ce manuscrit, et tu fais de ma vie une fête permanente.

Il tempo correva, il suo battito silenzioso scandisce sempre più precipitoso la vita, non ci si può fermare neanche un attimo, neppure per un'occhiata indietro.
Dino Buzzati, Il deserto dei Tartari

Entrez en vous-même, cherchez le besoin qui vous fait écrire : examinez s'il pousse ses racines au plus profond de votre cœur. Confessez-vous à vous-même : mourriez-vous s'il vous était défendu d'écrire ?
Rainer Maria Rilke, Lettres à un jeune poète

Liouville theory and random maps

Contents

Part I
Introduction

1 2d quantum gravity and Liouville theory: context

1.1 2d quantum gravity and Liouville theory

In a quest of simplification of our understanding of the world into one consistent theory with respect to the experiments, the aim of quantum gravity is to get a quantum description of general relativity. In classical general relativity, the gravitational force is governed by the geometry of space-time. Space-time is a (pseudo) Riemannian space, and its geometry is supposed to be determined from the matter (and equivalently the energy) content of the universe, and conversely, the geometry of space-time acts on the matter content of the universe and constrains its movement. The interaction between geometry and matter content is governed by the celebrated Einstein equation:

$$G_{\mu\nu} = \kappa T_{\mu\nu}. \tag{1.1}$$

Einstein tensor $G_{\mu\nu} = R_{\mu\nu} - \frac{1}{2}g_{\mu\nu}R$, expressed in terms of the *metric* $g_{\mu\nu}$ and the Ricci tensor $R_{\mu\nu}$, contains the information on the geometry of space-time, whereas the stress-energy tensor $T_{\mu\nu}$ describes the matter content part. The curvature of the space and the matter content are related through a proportionality constant κ. In classical general relativity – in opposition to quantum general relativity –, Einstein tensor must be a solution of equation 1.1, and corresponds to the saddle-point of the Einstein-Hilbert action:

$$S_{EH}[g_{\mu\nu}, \Phi] = \int_{\mathbb{R}^D} \left(\frac{R[g_{\mu\nu}]}{2\kappa} + \mathcal{L}_M[\Phi] \right) \sqrt{-\det g_{\mu\nu}} d^D x, \tag{1.2}$$

where we consider here D dimensional space-time (one dimension for time and $D-1$ dimensions for space) so the measure is $d^D x$. The Greek indices run from 1 to D. The term $\mathcal{L}_M$ stands for the Lagrangian associated to the matter fields, generically denoted by Φ, present in the universe, and the signature of the metric is $(-,+,+,\dots)$. In a pure gravity description, we forget about matter field in order to focus exclusively on the geometry of space-time, so in that case, Einstein-Hilbert action reduces to the curvature term. It is also customary to add a cosmological term – here to reproduce the expansion of the universe – to this action, namely:

$$S_\Lambda[g_{\mu\nu}] = \int_{\mathbb{R}^D} \Lambda \sqrt{-\det g_{\mu\nu}} d^D x. \tag{1.3}$$

The constant Λ is the cosmological constant. In the end, the pure gravity action is the sum of the Einstein-Hilbert action and the cosmological term:

$$S_{\text{grav}}[g_{\mu\nu}] = S_{EH}[g_{\mu\nu}] + S_{\Lambda}[g_{\mu\nu}].$$

In a quantum description of general relativity, one allows the topology of the space and the geometry itself to have fluctuations away from the classical solution, that is to say, the actual Einstein tensor may differ from the solution of Einstein equation. Potentially any Einstein tensor can appear, and to each of those instances is assigned a probability of occurrence. The most probable event must be the tensor which is solution of the Euler-Lagrange equations associated to the pure gravity action, that is to say the classical solution of Einstein equation. For other generic instance $G_{\mu\nu}$ that may not correspond to the saddle-point of the action, the assigned probability is related to the gravity action evaluated on this instance $S_{\text{grav}}[g_{\mu\nu}]$. The closer to the saddle point the tensor is, the more probable the Einstein tensor is. The action of the matter fields Φ is denoted $S_{\text{matter}}[\Phi, g]$, it depends on the geometry of the space. In the path-integral formalism, the partition function of quantum gravity coupled with matter fields is:

$$\mathcal{Z}_{\text{grav}} = \sum_{\text{topology}} \int \mathcal{D}g\mathcal{D}\Phi e^{-(S_{\text{grav}}[g]+S_{\text{matter}}[\Phi,g])}. \tag{1.4}$$

The measures $\mathcal{D}g$, $\mathcal{D}\Phi$ on the metric and the scalar fields are ill-defined, and they suppose a choice of gauge for the metric, as the action is invariant under reparametrization. This path-integral is supposed to quantize gravity. The procedure to quantize a theory by path-integral formalism in quantum field theory usually uses a perturbative expansion in the coupling constants of the theory. Here, the coupling constants associated to the metric are κ and Λ. However, in $D = 4$ (the dimension of the physical macroscopic world), this perturbative procedure is doomed to fail, since gravity is not *renormalizable* in this case. In this thesis, in order to dodge this problem, we study quantum gravity in 2 dimensions (called thereon *2d quantum gravity*) for Euclidean spaces instead of Minkowskian spaces, in a non perturbative way. It is quite unphysical, but mathematically interesting though. Also there is an indirect link between 2d quantum gravity and D dimensional quantum gravity. Indeed, a way to overpass the renormalization problem and to define a perturbative quantification of gravity, is to turn the point-like particles into (closed or open) one-dimensional objects, called the *strings*. When a string propagates in a target flat space X of dimension D, it sweeps out a 2 dimensional *world sheet* M. This world sheet is endowed with a metric tensor g^{ij} (where $i, j = 1, 2$), the space X is endowed with Minkowski metric $\eta_{\mu\nu} = (-, +, +, \dots)$.

The action associated to a field Φ propagating in a D is the area of the world sheet:

$$S_{\text{world sheet}} = -\frac{1}{4\pi\alpha'}\int_M d^2\xi\sqrt{\det g^{ij}}g^{ij}\partial_i\Phi_\mu\partial_j\Phi_\nu\eta^{\mu\nu}, \tag{1.5}$$

with $\alpha' = \begin{cases}\frac{1}{2} \text{ open string}\\ \frac{1}{4} \text{ closed string}\end{cases}$ Polyakov, in one of the founding papers of 2d quantum gravity [Polyakov, 1981], showed that this action, initially designed to explain the 4d macroscopic world, can be turned so as to study 2d Euclidean quantum gravity, provided that one adds a cosmological constant term to the world sheet action : $\int_M \Lambda\sqrt{\det g^{ij}}d^2\xi$. Let us precise that the usual trick to turn from an Euclidean quantum theory to a Minkowskian one is to use Wick rotation, but in the case of quantum gravity, this trick may not work. Now that we have motivated a little bit the study of 2d qantum gravity, we may expose how it is related to Liouville action.

In 2d quantum gravity on closed Riemann surfaces, the topology surface M as well as its metric can fluctuate. The partition function writes

$$\mathcal{Z}_{2dQG} = \sum_{\substack{\text{topology}\\ \text{of } M}}\int \mathcal{D}g\mathcal{D}\Phi e^{-\frac{\kappa}{4\pi}\int_M\sqrt{\det g_{ij}}Rd^2\xi-\mu\int_M\sqrt{\det g_{ij}}d^2\xi-S_{\text{matter}}[\Phi,g]}. \tag{1.6}$$

where the metric tensors g on M are Riemannian, and the cosmological constant is now denoted μ. The scalar curvature is still denoted R. In two dimensions, the integral of the curvature is a topological invariant, as it is proportional to the Euler characteristic of the surface, and the cosmological constant multiplies the area of the surface M measure with the metric g:

$$\begin{cases}\int_M\sqrt{\det g_{ij}}Rd^2\xi = 4\pi\chi(M)\\ \int_M\sqrt{\det g_{ij}}d^2\xi = A(M,g).\end{cases} \tag{1.7}$$

This decomposition of the action into the Euler characteristic and the area will be visible at the level of discretized approach, but we shall forget about it for the moment, and first transform the partition function according to Polyakov's ideas [Polyakov, 1981]. The latter involves a formal integration over the possible metric tensors, with the "measure" $\mathcal{D}g$ over all the possible compact Riemann surfaces. The topology of a compact Riemann surface M is entirely described by its genus h, which is the number of handles of the surface, so the sum over the possible topology of M is actually a sum over the genera. For a given genus h, two Riemann surfaces M and M' with metric tensors g and g' are *conformally equivalent* (they have the same *conformal structure*), if there exist coordinate systems ξ_1, ξ_2 in which $g_{ij} = \lambda(\xi_1,\xi_2)g'_{ij}$. By Riemann uniformization theorem, a class of conformal structure of a Riemann surface of a given genus is described by the moduli m of the surface. It means that if m is fixed, and M, g^m is a

Riemann surface along with a metric tensor corresponding to this moduli, any other metric g' on M which corresponds to the same moduli is conformally equivalent to g. For each moduli m, let us choose a *background* metric g^m, this gives a family of metrics indexed by the moduli. The choice of the family $(g^m)_m$ is a gauge fixing choice, that gives birth to Faddeev-Popov ghost fields. All the possible metrics one can construct from a Riemann surface of moduli m take the form $g(z) = e^{\gamma\phi(z)}g^m(z)$. For a given genus, the space of moduli is finite dimensional, so the measure $\mathcal{D}g$ can be decomposed into a finite dimensional measure dm over the moduli, a measure over the ghosts, and an infinite dimensional measure $\mathcal{D}\phi$ over the conformal factors. In the end, Polyakov showed that for a metric tensor $g = e^{\gamma\phi}$ the action of 2d gravity coupled with matter can be decomposed in three actions:

$$S_{2dQG}[g, \Phi] = S_L^{\gamma,\mu}[\phi] + S_{\text{ghosts}}[g^m] + S_{\text{CFT}}[g^m, \Phi], \tag{1.8}$$

where the action $S_{\text{ghosts}}[g^m]$ accounts for the coupling between the background metric and the ghosts field, the action $S_{\text{CFT}}[g^m, \Phi]$ describes the conformal field theory of the matter content on a surface with fixed background metric g^m. Last, the gravitational action is given by Liouville action:

$$S_L^{\gamma,\mu}[\phi, g^m] = \frac{1}{4\pi}\int_M \left(|\nabla_{g^m}\phi(z)|^2 + R[g^m]Q\phi(z) + 4\pi\mu e^{\gamma\phi(z)}\right)\sqrt{\det g_{ij}^m(z)}d^2z, \tag{1.9}$$

where ∇_{g^m} is the gradient associated to the background metric g^m, $R[g^m]$ is the curvature measured with the background metric, $\gamma \in]0, 2[$ is a parameter of the theory, the *charge* Q satisfies $Q = \frac{\gamma}{2} + \frac{2}{\gamma}$. The cosmological constant μ is a strictly positive parameter of the the theory. The pure gravity part of the action associated is thus Liouville action, and the partition function of 2d pure quantum gravity on a compact Riemann surface M with given genus and moduli m depends on the parameters γ, μ of the Liouville action, and can be written in this form:

$$\mathcal{Z}^{\gamma,\mu}_{\text{puregravity}} = \int \mathcal{D}\phi e^{-S_L^{\gamma,\mu}[\phi,g^m]}. \tag{1.10}$$

The *observables* of pure quantum gravity on M are the so-called *vertex operators* $V_\alpha(z) = e^{\alpha\phi(z)}$, where $z \in M$. The parameter α is the charge of the operator. Then, the correlation functions one wants to compute are the expectation values of the vertex operators:

$$\left\langle \prod_{i=1}^k V_{\alpha_i}(z_i) \right\rangle^{\gamma,\mu} = \int \mathcal{D}\phi e^{-S_L^{\gamma,\mu}[\phi,g^m] + \sum_{i=1}^k \alpha_i\phi(z_i)}. \tag{1.11}$$

Remark 1.1. *Let us address a vocabulary point here. In this thesis, the term "observable" is used for a quantity or an event $\mathcal{O}$ one can observe in the framework of a theory,*

it is the equivalent of "random variable" in mathematics. The "expectation value" $\langle \mathcal{O} \rangle$ of an observable is the average value when one observes this very event or quantity. If the observable $\mathcal{O}$ can be decomposed into k similar sub-observables $\mathcal{O}_1, \ldots, \mathcal{O}_k$, that is to say the event $\mathcal{O}$ is the simultaneous realization of events $\mathcal{O}_1, \ldots, \mathcal{O}_k$, then its expectation value is called a "correlation function" or equivalently a "k-point function".

Hence, this is the framework of 2d quantum gravity. However, there are many unknowns in this theory, coming from the fact that the objects are ill-defined mathematically, that is to say the probability theory of 2d quantum gravity is not defined. First, in the partition function, the set of fields ϕ over which one has to integrate is not precised – put another way, the space of probability is not defined. In order to get the most general set of possible metrics, the possible fields ϕ can be generalizations of functions, that is to say, distributions. Then, the measure $\mathcal{D}\phi$ is supposed to be a kind of Lebesgue measure over the set of metrics on which we integrate, and it is not obvious how to define it in the path-integral formalism – thus the probability measure is not defined either. What is more, in Liouville action, the term that multiplies the cosmological constant involves the exponential of a potential distribution, which is not defined. Therefore, the path-integral is ill-defined, and one has to make sense of it. We sum up in few words the general ideas of the different approaches developed to address these problems up to now, in order to situate the approach used in this thesis.

1.2 A brief review of the approaches of 2d quantum gravity

1.2.1 The path integral formalism

During the eighties, 2d quantum gravity was extensively studied with path integral methods in complement with discretized approaches (see [David, 1988a], [Distler and Kawai, 1989]). The path integral formulation, which is a continuous approach, is very efficient for physical predictions, and computing various critical exponents. The matter content is supposed to be described by a conformal field theory (CFT). CFTs are indexed by their central charges c, and a matter field in 2 dimensions is described by a CFT with a given central charge. If the matter field does not interact with the metric (*i.e.* with gravity), the study reduces to the study of the CFT. If the matter field is coupled with gravity, then the CFT is "dressed" by gravity. The celebrated KPZ formula (for Knizhnik, Polyakov and Zamolodchikov) relates critical exponents for a CFT without coupling to gravity and critical exponents for CFT dressed with gravity, see [Knizhnik - Polyakov - Zamolodchikov, 1988]. Later, Dorn, Otto, Zamolodchikov and Zamolodchikov conjectured a formula for the three point functions, the DOZZ formula [Dorn and Otto, 1994], [Zamolodchikov and Zamolodchikov, 1995],

[Zamolodchikov and Zamolodchikov, 1996]. However, the drawback of path integral is that it is mathematically ill-defined. There are two essential hurdles, already discussed in previous section:

- the set of fields on which to integrate needs to be defined properly, as well as the measure $\mathcal{D}\phi$.
- if one integrates over distributions, the term of the cosmological constant $4\pi\mu e^{\gamma\phi}$ needs also to be defined, as the exponential of distribution is ill defined.

In order to overpass those difficulties, other approaches were developed at the same time.

1.2.2 Discretized approaches

As the set of all possible fields ϕ on a surface M is infinite dimensional, a first idea is to discretize the surface by a polygonal decomposition of the surface (called a map) with n faces. For 2d surfaces, the faces are polygons, and a discretized field on a polygon f_k gets a single value ϕ_k on the whole polygon. If the map has finitely many faces, the space of possible fields is finite dimensional. Therefore, the discretization allows to make sense of the measure $\mathcal{D}\phi$ and of the Liouville action. The partition function is transformed:

$$\sum_{\text{topologies}} \int \mathcal{D}\phi \longrightarrow \sum_{h} \sum_{\substack{m\text{map of} \\ \text{genus h} \\ \text{size } n}} \prod_{k=1}^{n} d\phi_k. \tag{1.12}$$

The hope is that when the mesh of the discretized surface tends to 0 (the number n of faces grows to infinity), one recovers a limiting theory, also called the continuous limit, which is Liouville quantum gravity. This thesis stands in this framework, so we dwell on the ideas and results of this approach in more details in chapter II. At the discretized level, decorations of the polygons can mimic some matter content, so in this case, if a continuous limit exists, it shall be described by a CFT coupled with gravity.

Those discretized approaches were first used to prove convergence of observables that do not take into account metric information (distances between two points in the surface for instance), see for instance [David, 1985]. Then, Ambjørn and Watabiki [Ambjørn and Watabiki, 1995] studied distances properties in this framework, by developing a sort of peeling process of the random maps. The critical exponents are the same as the ones found by path integral methods. Later, mathematicians proved that for some discretized models, the limit of random maps in terms of metric spaces exists,

and the continuous limit is the Brownian map (see [Le Gall, 2013], [Miermont, 2013]). The techniques employed are mainly combinatorial methods in order to enumerate maps of a certain size, and probabilistic tools to prove convergence of correlations in the continuous limit. Most of the results of this thesis concern enumeration of maps and are purely combinatorial.

1.2.3 Continuous approaches

Another way of making sense of Liouville theories is to tackle the problem directly in the continuum. Let us mention 3 approaches here, in which we can distinguish algebraic methods and probabilistic ones. Those methods were developed at the same time as discretized approaches, and they often are complementary. The presentation adopted here is not chronological. Also, the diverse methods benefit from each other through fruitful interchanges.

First, an algebraic approach for continuous is the conformal bootstrap. The bootstrap idea comes from Polyakov [Polyakov, 1974], it consists in assuming symmetries satisfied by a theory and in deducing constraints satisfied by the correlation functions. If those constraints are strong enough, the correlation functions can be computed. In 2 dimensions, conformal bootstrap was initiated by Belavin, Polyakov and Zamolodchikov [Belavin et al., 1984], and involves the study of representations of the Virasoro algebra. In the bootstrap approach, the theory is defined by a set of axioms, which are so constraining in 2 dimensions that they allow to determine all the *amplitudes* $\left\langle \prod_{i=1}^{k} V_{\sigma_i}(x_i) \right\rangle$ (this is the probability amplitude for k particles of of respective types $\sigma_1, \dots, \sigma_k$ located at $x_1, \dots, x_k$ to interact). They are even *over* determined in the sense that there are several different ways to compute a given amplitude. The difficult goal of the conformal bootstrap approach is to prove that the axioms are consistent, that is to say that the constraints do not contradict each other, or that the different ways of computing the amplitudes yield the same result. Conformal bootstrap is used for the study of CFT, and for 2d quantum gravity, the interesting CFT is Liouville CFT. It has known many developments since it has been defined [Teschner, 1995], [Ribault, 2014].

A second continuous approach was initiated by David, Kupiainen, Rhodes and Vargas (see [David et al., 2015] and the course of Vargas on the subject [Vargas, 2017]), who have been defining properly Liouville quantum gravity as a probabilistic theory. Their study relies on the Gaussian free field (GFF) on a domain of the complex plane. They define rigorously the "Gaussian multiplicative chaos" in order to make sense of the term $e^{\gamma\phi}$, and are able to make the k-point functions of vertex operators

$$\left\langle \prod_{i=1}^{k} V_{\alpha_i}(z_i) \right\rangle^{\gamma,\mu} \tag{1.13}$$

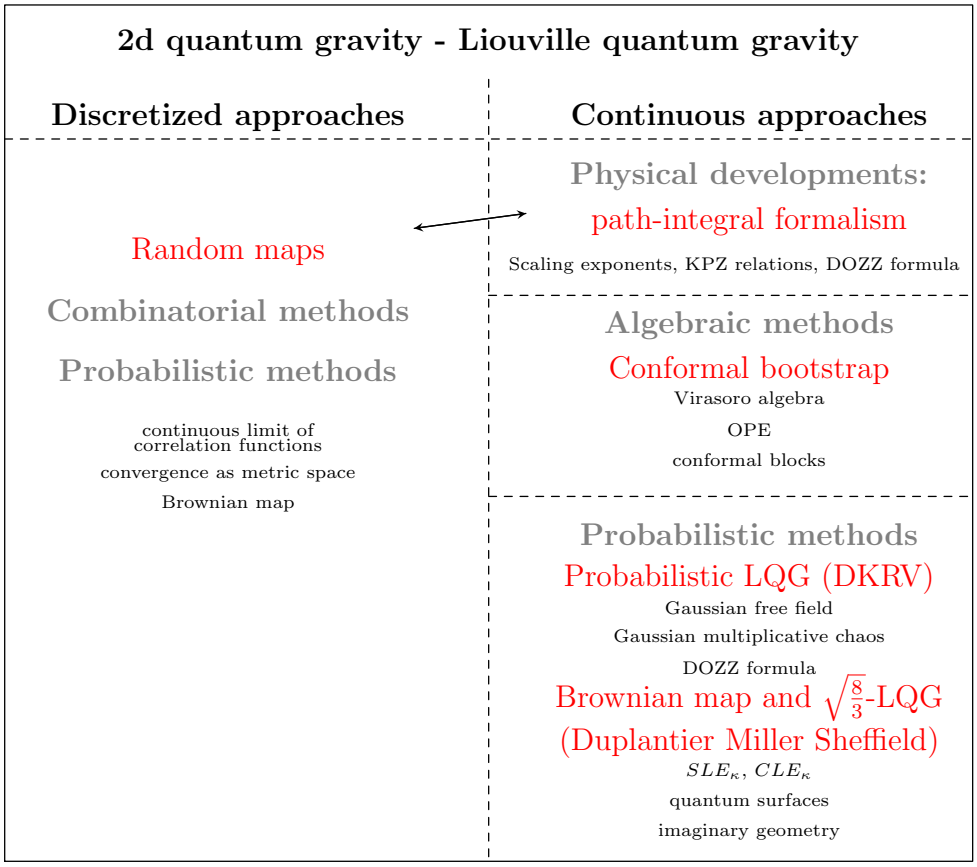

Figure 1: Summary of approaches to 2d quantum gravity. In red, the type of approach, and in small font, some keywords of the approach.

meaningful. By this powerful approach, Kupiainen, Rhodes and Vargas have recently managed to prove DOZZ formula [Kupiainen et al., 2017].

Third, another probabilistic approach was initiated by Duplantier, Miller and Sheffield [Duplantier et al., 2014]. They have been relating the Brownian map – which is a continuous object – with $\gamma = \sqrt{\frac{8}{3}}$-Liouville quantum gravity, which is suspected to describe pure 2d quantum gravity. The theory needs the machinery of imaginary geometry and the study of fractal objects such as SLE_κ curves and conformal loop ensembles CLE_κ.

Figure 1 summarizes the different approaches for 2d quantum gravity.

2 Content of the thesis

This thesis adresses three aspects of discretized approaches to 2d quantum gravity. It is organized as follow.

In the second chapter, the main ideas behind discretized methods are introduced. To do so, we define random maps and what we mean by their continuous limit. A powerful tool to study random maps combinatorics is the formulation in terms of matrix models: since we will encounter them throughout the thesis, they are also introduced as well as some subsequent techniques.
The contributions of the thesis sit in the four following chapters. They form three groups: chapter III, chapters IV and V together, and chapter VI. Each group is dedicated to the study of a specific random maps model, which is introduced in the beginning of the chapters. Also, each group is dedicated to the study of an aspect of random maps. In chapter III, we use Delaunay triangulations and circle patterns in order to study various properties of the measure defined on this set. Those properties are of two types: first we show that the measure is related to the widely studied Weil-Petersson measure on moduli space of Riemann surfaces, second we prove some local inequalities on the measure as preliminary steps for the study of the continuous limit of Delaunay triangulations.
Chapters IV and V tackle the computation of expectation values of observables on random maps and their convergence in the continuous limit in the context of Strebel graphs, that, as we discuss in chapter IV, look like duals of Delaunay triangulations. The expectation values are first explicitely computed in chapter IV thanks to Kontsevich's bijection on Strebel graphs. Then, in chapter V, the computation is made more systematic by resorting to topological recursion. This procedure allows to study the convergence of the expectation value in the continuous limit. We then identify the continuous limit of Strebel graphs with (3,2) minimal model.
A third aspect of random maps addressed in this thesis concerns the symmetry of correlation functions defined from random maps combinatorics. Those symmetries have consequences in terms of constrains imposed, and for further study of the correlation functions as amplitudes of an integrable system. Certain symmetries of the correlation functions computed from the Ising model on random maps are proven. The proof allows to reformulate the recursion which determines planar correlation functions, and we show that the correlation functions are expressed in terms of link patterns.
Each chapter comes with a related flipbook in the bottom right corner. They are complete when the chapter, and the observation of the progress of the animation during the reading may plummet the reader into despair, or fill him/her with hope.
Along the thesis, some additional concepts are required, such as moduli space of Riemann surfaces, intersection numbers, minimal models or topological recursion. They are introduced when they appear the first time in the manuscript.
Last, the appendices are dedicated to technical details of computations and proofs, and

to the special functions appearing in the thesis.

Part II
Random maps and matrix models

"*Tout ce qui est simple, tout ce qui est fort en nous, tout ce qui est durable même, est le don d'un instant.*

Pour lutter tout de suite sur le terrain le plus difficile, soulignons par exemple que le souvenir de la durée est parmi les souvenirs les moins durables. On se souvient d'avoir été, on ne se souvient pas d'avoir duré."

Gaston Bachelard, *L'intuition de l'instant*

We define precisely the discretization method to approach Liouville quantum gravity. A hope of the discretization in 2d quantum gravity is that a continuous surface can be approached by a lattice with sufficiently "small" mesh. Hence, we overpass Zeno of Elea's paradox of the arrow, and take as paradigm that the continuous space-time can be approached by little pieces of discrete space-time. A central notion is random maps, that we introduce here.

3 Random maps

In order to define maps, we need various preliminary definitions. Maps are subclass of graphs, that are combinatorial objects.

Definition 3.1. *A finite connected* graph Γ *is the data of a finite set of vertices* $\mathcal{V}(\Gamma)$ *and a set* $\mathcal{E}(\Gamma)$ *of adjacency relations (the* edges*) between them.*

If $v_1, v_2 \in \mathcal{V}(\Gamma)$ are adjacent, there exists $e \in \mathcal{E}(\Gamma)$, and we write $e = (v_1, v_2)$. A graph is a purely combinatorial object that does not come with a canonical way to represent it. An embedding gives a way to draw a graph (see figure 2):

Definition 3.2. *Let M be a compact orientable smooth surface. A* embedding $\Gamma^{f,M}$ *of Γ into M is a map $f : \Gamma \hookrightarrow M$, which sends vertices $v_i \in \mathcal{V}(\Gamma)$ to distinct points of M, and sends any edges $e = (v_i, v_j) \in \mathcal{E}(\Gamma)$ to a curve of M whose ends are v_i and v_j. The embedding is* proper *if (i) distinct edges do not intersect, except at their extremities, and (ii) the set $M \backslash \Gamma^{f,M}$ is a union of domains homeomorphic to disks.*

To illustrate the second condition for proper embeddings, figure 3 shows an improper embedding. The *genus* of a properly embedded graph $\Gamma^{f,M}$ is the genus g of the surface M. For a graph Γ, the notion of face is not rigid, as it depends on the embedding. Figure 2 shows two embeddings of a same graph that define different sets of faces.

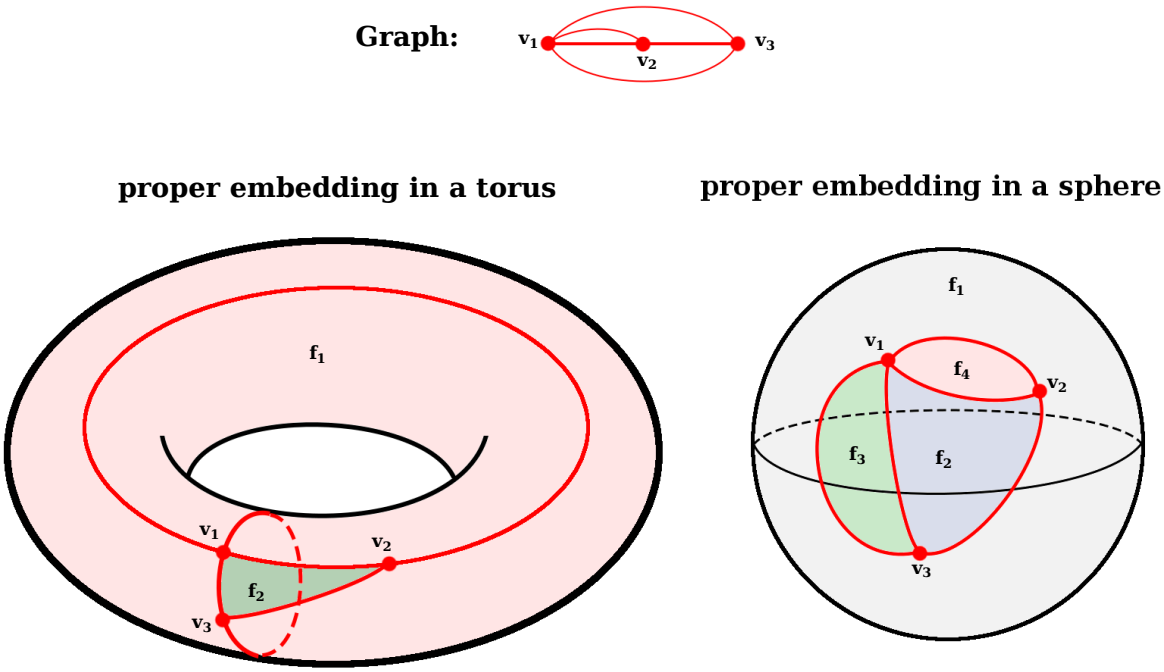

Figure 2: A graph and two possible proper embeddings. The embedding on the torus has 2 faces, whereas the embedding on the sphere has 4 faces. All the faces have the topology of a disk.

Maps are combinatorial objects that allow to define faces. In order to define maps, let us introduce an equivalence relation between embeddings:

Definition 3.3. *Two embeddings* $\Gamma^{f,M}$, $\Gamma^{h,N}$ *of* Γ *are* equivalent $\Gamma^{f,M} \sim \Gamma^{h,N}$ *if there exists a homeomorphism* $\varphi : M \to N$ *that preserves orientation, such that* $h = \varphi \circ f$.

Then, we can give a definition of maps:

Definition 3.4. *A map* m *of genus* g *is an equivalence class of a finite connected graph properly embedded in a surface of genus* g. $\mathcal{V}(m)$, $\mathcal{E}(m)$ *and* $\mathcal{F}(m)$ *refer respectively to the sets of vertices, edges and faces of* m.

A map is an equivalence class of embedded graph. Figure 4 shows an example of two embedded graphs in the same equivalence class. If the genus of a map is 0, we call it a *planar* map, and it can be drawn on a sphere. To show that a map is a purely combinatorial object, we give another equivalent definition, equivalent to definition 3.4, which does not refer to embeddings. To construct a map with n edges, one can "cut" those edges in two to obtain $2n$ half-edges, that we label by $1, 2, \ldots, 2n$. The following definition defines a map by connecting those half edges thanks to permutations:

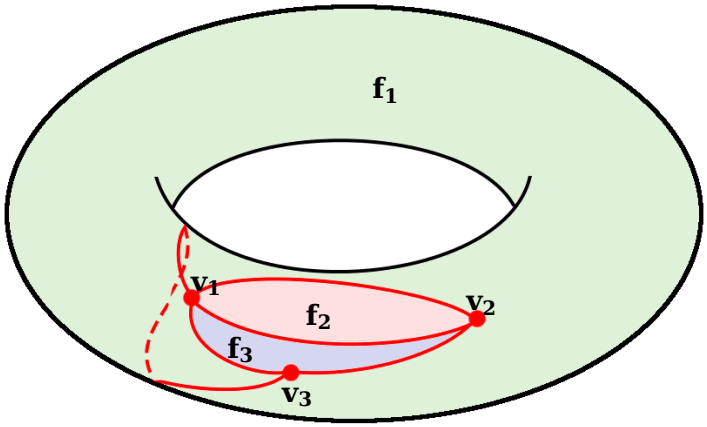

Figure 3: Example of an improper embedding. Although none of the edges intersect each other, the face f_1 has the topology of a cylinder.

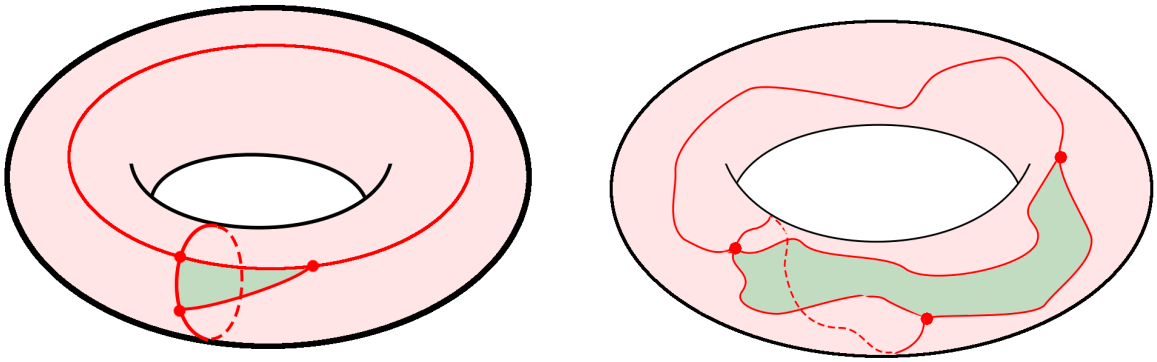

Figure 4: Two equivalent embeddings of a graph, depicting the same map.

Definition 3.5. *A connected map with n edges is the data of 2 permutations $\alpha, \psi \in \mathfrak{S}_{2n}$ such that α is a fixed point free involution and the group generated by α and ψ acts transitively on $\{1, 2 \dots, 2n\}$.*

The fact that α is a fixed point free involution means that it can be written as a product of n transposition with pairwise distinct supports. In this interpretation, the edges are the cycles of α (the n transpositions), the vertices are the cycles of ψ, and the faces are the cycles of $\alpha\psi$. The permutation ψ allows to define an ordering of the half-edges around each vertex. Figure 5 gives the relation between (α, ψ) and the drawing of a map.

Let us mention that another equivalent approach, that we consider also in chapter VI is to consider a genus g map as a gluing of polygons along their edges, such that the resulting surface is orientable, compact and has genus g.

The *size* of a map receives different meanings according to the model of random maps one considers. It can be defined as the number of vertices, as the number of edges, or as the number of faces. In chapter III, it is the number of vertices whereas in chapter IV and V, it is the number of faces.

Let us denote by $\mathbb{M}_g(n)$ the set of maps of genus g of size n, (for the suited definition of size). The *degree* of a vertex (respectively a face) is the number of edges adjacent to this vertex (resp. this face). If a map m has genus g, then the numbers of vertices, edges and faces satisfy Euler relation:

$$|\mathcal{V}(m)| - |\mathcal{E}(m)| + |\mathcal{F}(m)| = 2 - 2g = \chi(m). \tag{3.1}$$

$\chi(m)$ is the Euler characteristic of m. For a map m with n edges, defined by the permutations α and ψ like in definition 3.5, let us note $\mathrm{Aut}(m)$ the group of symmetries (or automorphisms) of m. It is a subgroup of $\mathfrak{S}_{2n}$, and consists of permutations of the half-edges that leave m unchanged in the following manner:

$$\mathrm{Aut}(m) = \{\phi \in \mathfrak{S}_{2n} | \alpha = \phi \circ \alpha \circ \phi^{-1} \, ; \, \psi = \phi \circ \psi \circ \phi^{-1}\}. \tag{3.2}$$

The cardinal $|\mathrm{Aut}(m)|$ is the *symmetry factor* of m. Obviously, the identity is an automorphism of any map, so $|\mathrm{Aut}(m)| \geq 1$. For a generic map, the symmetry factor is 1. The following example shows a case where the symmetry group is not trivial.

Example 3.1. Let us consider the map m with 6 edges (hence 12 half-edges), defined by the permutations:

$$\begin{cases} \psi = (1,2,3)(4,5,6)(7,8,9)(10,11,12) \\ \alpha = (1,12)(2,11)(3,4)(5,8)(6,7)(9,10). \end{cases} \tag{3.3}$$

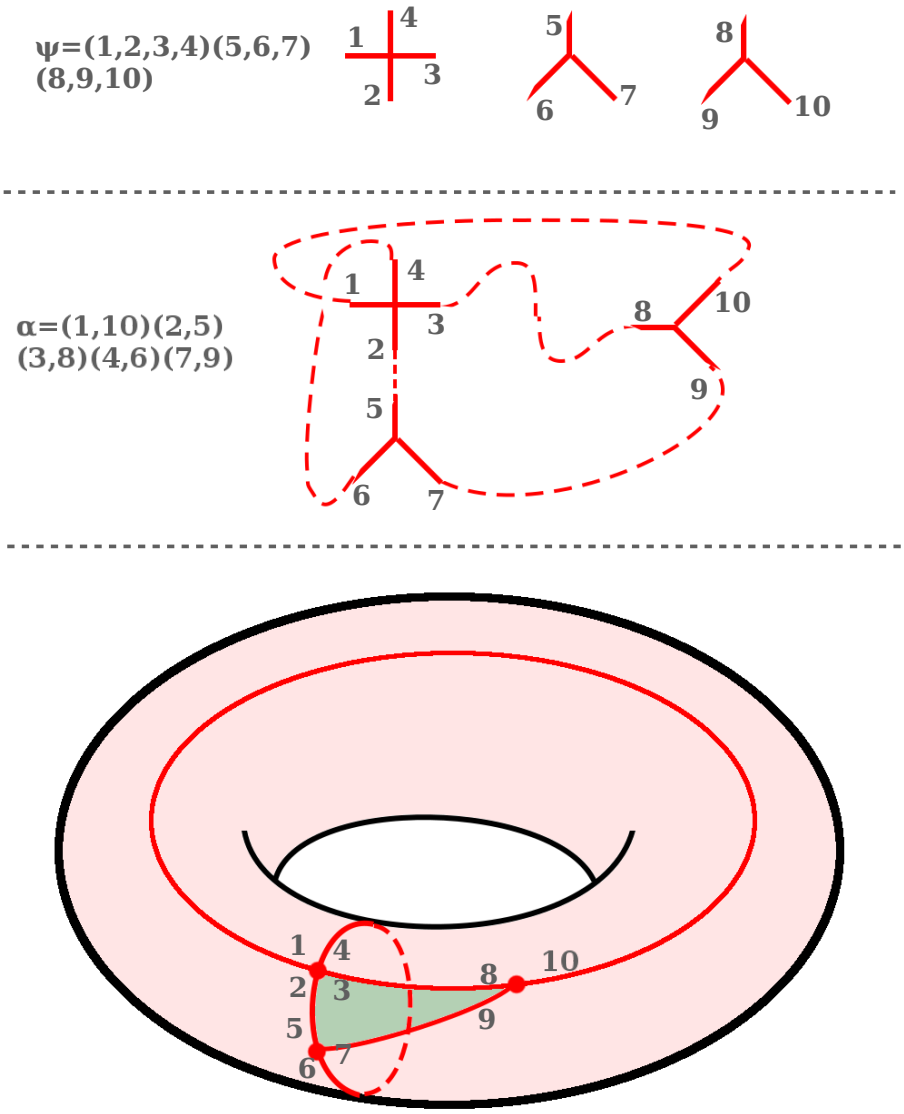

Figure 5: Construction of a map from 2 permutations ψ, α on a set of half-edges $\{1, \ldots, 10\}$. The permutation $\psi = (1,2,3,4)(5,6,7)(8,9,10)$ has 3 cycles and defines 3 vertices. $\alpha = (1,10)(2,5)(3,8)(4,6)(7,9)$ is a fixed-point free involution, which defines the edges on the map (we link the half edges i and j if they appear in α as a transposition (i,j). Last, we obtain a map, that we can embed in a torus. The faces of the map are the cycles of $\alpha\psi = (1,5,4,10,3,6,9)(2,8,7)$: the red face corresponds to the cycle $(1,5,4,10,3,6,9)$, while the green face corresponds to the cycle $(2,8,7)$.

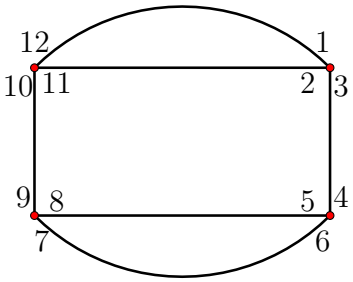

Figure 6: Map defined by the permutations $\psi = (1,2,3)(4,5,6)(7,8,9)(10,11,12)$ and $\alpha = (1,12)(2,11)(3,4)(5,8)(6,7)(9,10)$.

A proper embedding of this map is shown in figure 6. The symmetry group $\mathrm{Aut}(m)$ is generated by the two following automorphisms:

$$\begin{aligned} \phi_1 &= (1,7)(2,8)(3,9)(4,10)(5,11)(6,12) \\ \phi_2 &= (1,5)(2,6)(3,4)(7,11)(8,12)(9,10) \end{aligned} \tag{3.4}$$

So $\mathrm{Aut}(m) = \{\mathrm{Id}, \phi_1, \phi_2, \phi_1\phi_2\}$, and $|\mathrm{Aut}(m)| = 4$.

If a vertex $v^\bullet$ of m is marked, as well as an adjacent edge $e^\bullet$, then the map is *rooted*. We denote $\mathbb{M}_g^\bullet(n)$ the set of rooted maps of genus g and size n. A map m has k *boundaries* if k faces are labeled $(f_1, \ldots, f_k)$, and each labeled face has a marked oriented edge, such that the marked face is on the right hand side of the edge along its orientation. The degree ℓ_i of the boundary f_i is the *length* of the boundary. A map with $k \geq 1$ boundaries is rooted. The set of maps of size n, genus g with k boundaries is denoted $\mathbb{M}_{g,k}(n)$. See figures 7 and 8 for examples. The symmetry group of a map with $k \geq 1$ boundaries is trivial, so $|\mathrm{Aut}(m)| = 1$ for $m \in \mathbb{M}_{g,k}(n)$.

Maps are used as discretizations of surfaces, and as candidates to mimic matter fields coupled to gravity or pure gravity in 2d. In order to mimic, at a discretized level, a field (matter field or metric field), it is necessary to specify a class of maps, which we call here a *model* of maps. The 4 chapters of this thesis are dedicated to the study of 3 models of maps. Specifying a model of maps means that one shall restrain the set of maps $\mathbb{M}_g(n)$ by putting constraints, and shall add decorations to maps. There exist many ways to restrain and to decorate the set of maps, but the most convenient ways to do so are to put *local* constraints and decorations (as opposed to *global* ones). A constraint or a decoration on a map is local if it involves to know the structure of the map around one vertex (resp. one edge, one face) to enforce it, and not the knowledge of the whole structure of the map. Let us look at examples of constraints and decorations to get an idea of this locality condition.

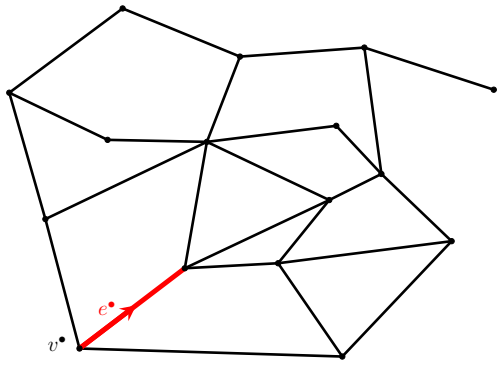

Figure 7: Example of a rooted map. The marked edge has a natural orientation, away from the marked vertex.

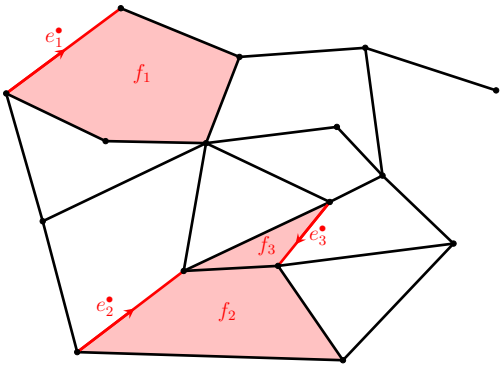

Figure 8: Example of a map with 3 boundaries of respective lengths 5, 4 and 3.The marked edge is oriented such that the boundaries have clockwise orientation.

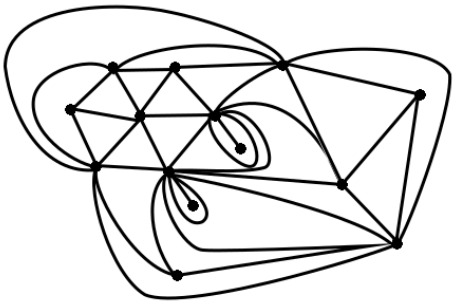

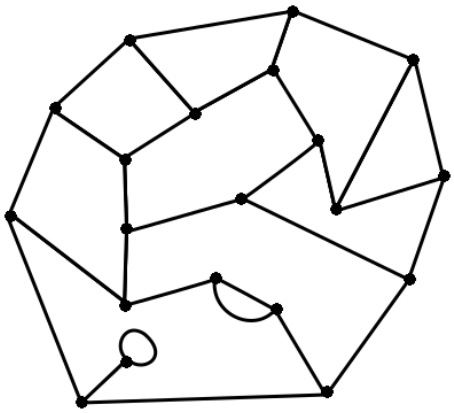

Figure 9: Examples of maps with constraints. On the left hand side, all the faces have degree 3 whereas on the right hand side, all the vertices have valency 3.

- **Examples of constraints:** one may restrict its study to the subset of $\mathbb{M}_g(n)$ composed of maps having faces of certain degrees. For instance, in chapter III, we allow uniquely maps with faces of degree 3, that is to say triangles. This constraint is local, since in order to check if it is satisfied, one has to look at each face individually. One can also restrict $\mathbb{M}_g(n)$ to maps having vertices of certain degrees, as it is the case of Strebel graphs in chapters IV and V, where we consider maps with trivalent vertices (of degree 3). See figure 9 for those examples.

- **Examples of decorations:** the intuitive idea is that if one considers planar maps without decorations, he may describe only the geometry of surfaces without matter on them. One of the aims of decorated maps is to add some matter

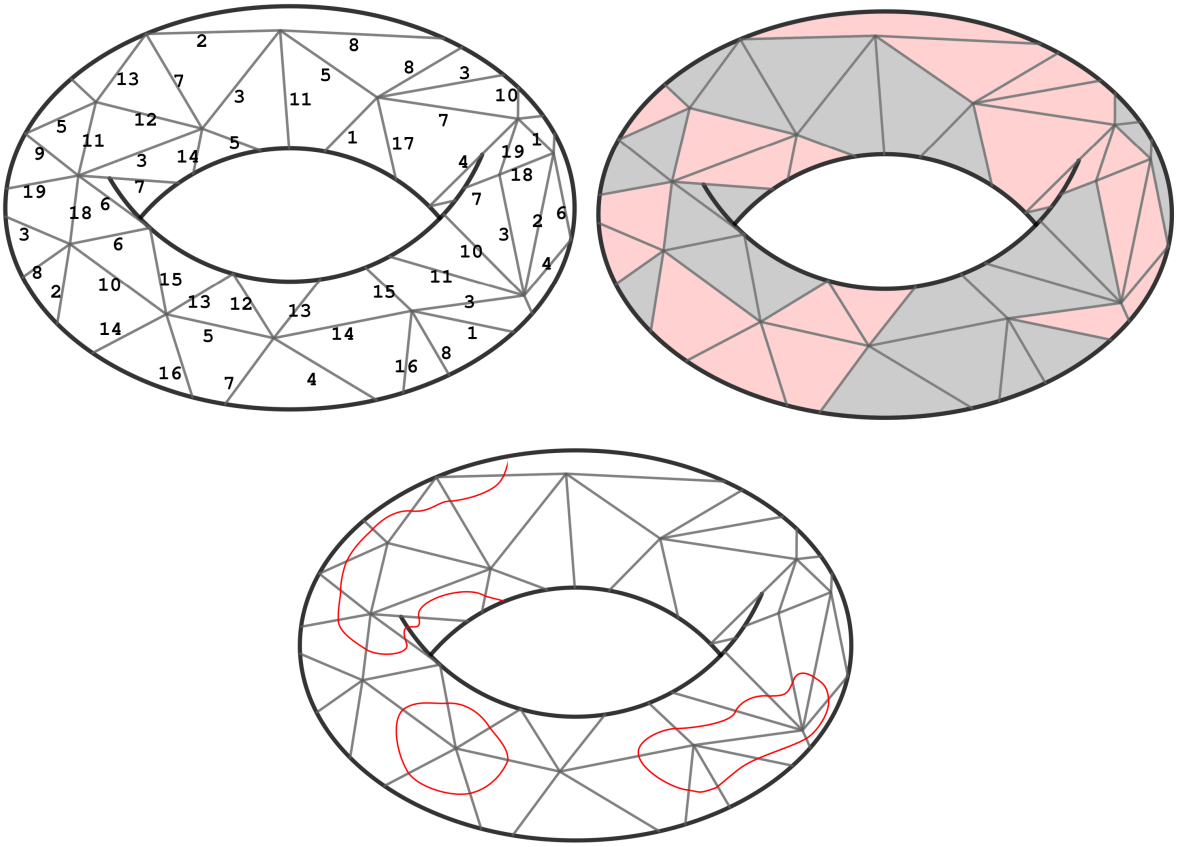

Figure 10: Three examples of decorations on a triangulation of the torus. In the first case, an integer (between 1 and 19) is associated to each edge, in the second case, each face has a color, and in the third case, a system of non intersecting (red) loops is drawn on the triangulation.

content at the discrete level, in order to hope for a description of matter coupled with gravity when one tends to the continuous limit (limit that we define later). As examples of decorations one can add (see figure 10), one can associate to each edge $e \in \mathcal{E}(m)$ a discrete or continuous parameter. It is the case of Delaunay triangulations (chapter III) and Strebel graphs (chapters IV and V). Labels can be associated to vertices of faces, making the maps labeled. One can also assign a classical spin (equivalently a color) to each face, or draw systems of non intersecting loops on triangulations. This non intersecting condition seems non local since it involves all the faces crossed by the loop, but it can be made local by forcing pieces of loops to cross the triangles in either of the two ways depicted in figure 11. In appendix E, we propose to construct a bi-colored quadrangulation on a torus with two boundaries.

By imposing constraints and decorating the maps, for each (g, n) we end up with a

Figure 11: The 2 ways of crossing a triangle for a loop coming from the upper left edge. This rule prevents loops from intersecting each other.

set of decorated maps $\widetilde{\mathbb{M}}_g(n)$. This set specifies the model of maps studied. Although the set $\mathbb{M}_g(n)$ is finite, the set $\widetilde{\mathbb{M}}_g(n)$ may be infinite (but of finite dimension), if the decorations involve continuous parameters. Now, we introduce some randomness in the set $\widetilde{\mathbb{M}}_g(n)$ by giving a weight to each of its elements. For a given model, we may want to focus on the specificities of this model: for instance, if maps are decorated with spins, one may want to study the statistics of spins on the maps. So for a given model, let us define a set of "interesting" local objects $\mathcal{LO}$ (trivalent vertices, quadrangles, spin +, loops etc.) of this model. For a local object $\ell o \in \mathcal{LO}$, define a *fugacity* $f_{\ell o} \in \mathbb{C}$. The fugacity is equivalent to the energy associated to a local configuration. For each $m \in \widetilde{\mathbb{M}}_g(n)$, one can count how many of each local object $\ell o \in \mathcal{LO}$ there is in m, and note $n_{\ell o}(m)$ this number. In order to give a weight to each map, we distinguish two case.

- The set $\widetilde{\mathbb{M}}_g(n)$ is finite or countable: the weight of a map $w(m)$ is given by:

$$w(m) = \prod_{\ell o \in \mathcal{LO}} f_{\ell o}^{n_{\ell o}(m)}. \tag{3.5}$$

  The set of fugacities is said *admissible* if the sum

$$Z_{g,n} = \sum_{m \in \widetilde{\mathbb{M}}_g(n)} \frac{1}{|\mathrm{Aut}(m)|} w(m) \tag{3.6}$$

  is finite.

- If the set $\widetilde{\mathbb{M}}_g(n)$ is also decorated with continuous parameters. For a map $m \in \widetilde{\mathbb{M}}_g(n)$, we distinguish between the decorations that are continuous parameters, and the others, called *countable* decorations (the name is not canonical). We call the $\mathbb{M}_g(n)^c$ the set of maps with countable decorations. Then $\widetilde{\mathbb{M}}_g(n)$ has a cellular decomposition $\widetilde{\mathbb{M}}_g(n) = \bigsqcup_{m^c \in \mathbb{M}_g(n)^c} \widetilde{\mathbb{M}}_g(n)^{m^c}$: to each map structure m^c decorated with countable decorations, is associated the continuous set $\widetilde{\mathbb{M}}_g(n)^{m^c}$ of all possible continuous decorations on this structure. Then, we give a weight $w(m^c)$ to the map structure by formula 3.5, and we put a measure $d\nu_{g,n}(m^c)$ on

the set $\widetilde{\mathbb{M}}_g(n)^{m^c}$ of continuous parameters. In the end, we get a measure on the whole set $\widetilde{\mathbb{M}}_g(n)$ by:

$$d\nu_{g,n}(m) = w(m^c)d\nu_{g,n}(m^c). \tag{3.7}$$

The set of fugacities along with the measure are *admissible* if

$$Z_{g,n} = \sum_{m^c \in \mathbb{M}_g(n)^c} \frac{1}{|\mathrm{Aut}(m)|} w(m^c) \int_{\widetilde{\mathbb{M}}_g(n)^{m^c}} d\nu_{g,n}(m^c) \tag{3.8}$$

is finite.

Whether it be in the countable or the uncountable case, if the fugacities and the measure are admissible, the quantity $Z_{g,n}$ is called the *partition function* of the model for genus g and size n maps. The weights and the measure allow to define probability distribution for maps of genus g and size n. To introduce the remaining notions, let us restrain to the countable case for clarity, examples for continuous parameters case are treated explicitly in chapters III and IV. We define the probability that one picks a map $m \in \widetilde{\mathbb{M}}_g(n)$ as:

$$\mathbb{P}(m) = \frac{1}{|\mathrm{Aut}(m)|} \frac{w(m)}{Z_{g,n}}. \tag{3.9}$$

An *observable* $\mathcal{O}$ of the model is a subset of $\widetilde{\mathbb{M}}_g(n)$. The *expectation value* of $\mathcal{O}$ is defined by:

$$\langle \mathcal{O} \rangle = \frac{1}{Z_{g,n}} \sum_{m \in \mathcal{O}} \frac{w(m)}{|\mathrm{Aut}(m)|}. \tag{3.10}$$

Often, the observable $\mathcal{O}$ is a subset defined by conditions of the type "faces (vertices) $1, \ldots, k$ have prescribed degrees (decorations)". This kind of observables are *correlation functions* between faces, and are also called *$k-$point functions*.
The partition function of the grand canonical ensemble for the maps of genus g is the following formal series in t:

$$Z_g = \sum_{n=0}^{+\infty} t^n Z_{g,n} \in \mathbb{C}[[t]], \tag{3.11}$$

t is the fugacity associated to the size of the maps. To recover the partition function of maps of genus g and size n, one must compute the coefficient of t^n. If the radius of convergence of the series is strictly positive, this coefficient is simply recovered by carrying out the residue:

$$Z_{g,n} = \operatorname*{Res}_{t \to 0} t^{-n-1} Z_g(t) dt. \tag{3.12}$$

The partition functions and the expectation values are generating functions with parameters t and the fugacities of the model. For instance, if one wants to compute the

(weighted) number of maps of genus g and size n having n_1 occurences of the local object $\ell o \in \mathcal{LO}$, this number is simply given by:

$$\operatorname*{Res}_{f_{\ell o}\to 0} f_{\ell o}^{-n_1-1} Z_{g,n} df_{\ell o}. \tag{3.13}$$

Therefore, one sees that the expectation value of an observable, as defined in equation 3.10, reduces to an enumeration problem. This is why models of random maps are often seen as combinatorial problems. The techniques to enumerate maps are diverse, we dwell on the formal matrix models methods in section 5 bellow. We can distinguish two types of approaches to enumerate maps:

- By solving equations "à la Tutte" [Tutte, 1962]. The principle of those equations, whose name is due to William Thomas Tutte, is to find a relation satisfied by the generating function of maps, by erasing an edge of the map.
- By bijective approaches, *i.e* by finding a bijection between the set of maps $\widetilde{\mathbb{M}}_g(n)$ and a set of better known objects (for which the enumeration has already been done or is trivial). For random maps, the most used bijections are Schaeffer bijection [Schaeffer, 1998] and a generalization, Bouttier, Di Francesco, Guitter bijection [Bouttier - Di Francesco - Guitter, 2004]. Those are bijections between bipartite maps and decorated trees.

The interest of discretization for 2d quantum gravity is that it allows, for each size n, to define properly the expectation values of observables. In order to recover the continuous theory of Liouville quantum gravity, one must make the size of the maps grow to infinity, so that the mesh formed by the embeddings of the maps on a fixed surface becomes denser and denser. In the end, the mesh shall be so dense as to mimic in itself a continuous surface. To give a sense to the limiting theory that can arise, one must define and study the large n limit of a model of random maps, also called the *continuous limit* of the model.

4 Continuous limit of random maps

The continuous limit of random maps has two main acceptations.

Convergence as probabilistic spaces The type of convergence we are studying in chapters III, IV and V the convergence of random maps models viewed as probabilistic spaces. For each model of random maps, we see that formula 3.9 allows to define a probability distribution on sets of maps, from the weights of maps (and the measure if continuous parameters are present). 2d quantum gravity (in the continuous aproach)

can be viewed as a probabilistic theory (the approach DKRV gives a rigorous meaning to this theory). Viewed as a stochastic space, the correlation functions of 2d quantum gravity one wants to compute are actually expectation values of observables. The measure $D\phi e^{-S_L^{\gamma,\mu}[\phi]}$ in the path-integral formalism on the fields ϕ has to be understood rather as a probability measure on a set of distributions.
The first way of defining the continuous limit is to study the convergence of the probability measure in the sense of distributions. For a given model of random maps, we are able to define probability measure $d\nu_{g,n}$ on the set $\widetilde{\mathbb{M}}_g(n)$ for every $n \in \mathbb{N}$, whether it be in the case where $\widetilde{\mathbb{M}}_g(n)$ is discrete or continuous. The questions to tackle in the case of 2d quantum gravity are:

- do the measures $d\nu_{g,n}$ converge in the sense of distributions towards a limiting measure $d\nu_{g,n} \xrightarrow{(d)} d\nu_g$ when the size grows to infinity $n \to \infty$?
- Does the limit measure $d\nu_g$ have the same properties as the one defined for continuous theories, such as DKRV's approach ?

In order to answer those questions, the convergence is studied here in two ways. The first way, which is the convergence of the measure in itself, is carried out for Delaunay triangulations: section 8 is dedicated to prove properties of the measure $d\nu_n$ itself. Those properties are preliminary steps to the possible study of the convergence of the measures in the continuous limit, in the sense of distributions.
The second way is weaker (for proving convergence), but more tractable. It consists in studying the convergence of expectation values of observables (equivalently random variables) when the size of the maps tend to infinity, so it amounts to studying the convergence of the measures $d\nu_{g,n}$ integrated against test functions. More precisely, choose an observable $\mathcal{O}$ that has a meaning for all the sets $\widetilde{\mathbb{M}}_g(n)$ with $n \geq n_0$, and call $\mathcal{O}_n$ the observable for the set $\widetilde{\mathbb{M}}_g(n)$. For instance, if the model of maps considered is the set of planar triangulations with labeled faces where the size is the number of faces, a possible choice of observable is $\mathcal{O} = \{\text{triangulations such that triangles } 2, 3, 4 \text{ share an edge with triangle } 1\}$. This observable supposes that $n \geq 4$, and has a meaning for all n. On the contrary, the observable $\mathcal{O} = \{\text{triangulations with 6 edges}\}$ is not eligible, because only triangulations of size 4 match the condition. Then, one looks at the convergence of the sequence $(\langle \mathcal{O}_n \rangle)_{n \geq n_0}$. By this way, we get a flavour of what is the limiting theory, but we cannot characterize entirely the latter. However, it is a legitimate way of tackling the study of 2d quantum gravity, since a physical theory is relevant if the quantities that we can compute from it, which are precisely expectation values of observables in a quantum theory, are coherent with the experiments. Of course, experiments do not exist for 2d quantum

gravity, but we can fix as a goal to recover the same expectation values as the one found in the path-integral formalism.

Convergence as metric spaces The second way is to view the sets $\widetilde{\mathbb{M}}_g(n)$ as metric spaces, by defining a suitable (with respect to the model) distance $d_m(v_1, v_2)$ on each map $m \in \widetilde{\mathbb{M}}_g(n)$ between any two vertices $v_1, v_2 \in \mathcal{V}(m)$. The study of random maps as metric spaces is not the purpose of this thesis, however throughout this manuscript, we mention natural graph metrics (for Delaunay triangulations in chapter III and Strebel graphs in chapter IV) that are eligible for a metric study of those models in further developments. We give here the meaning of a convergence in the continuous limit as a metric space for random maps, in order to justify the fact that we will insist on the fact that we have natural distances associated to our maps. Each map is a metric space, so in order to compare two metric spaces, one uses Gromov-Hausdorff topology. Gromov-Hausdorff topology is based on Gromov-Hausdorff distance $d_{GH}(X, Y)$ between two metric spaces X, Y:

Definition 4.1. *If X and Y are submetric spaces of a metric space M (with distance d), the* Hausdorff *distance d_H between X and Y is:*

$$d_H(X, Y) = \max\left(\inf_{x\in X} d(x, Y), \inf_{y\in Y} d(y, X)\right). \tag{4.1}$$

Then, the Gromov-Hausdorff *distance d_{GH} measures how two metric spaces X, Y are similar, by minimizing the Hausdorff distance on all isometries φ, ψ, embedding X and Y in the same space:*

$$d_{GH}(X, Y) = \inf_{\substack{M \text{ metric} \\ \varphi: X\to M \\ \psi: Y\to M \\ \text{isometries}}} d_H(\varphi(X), \psi(Y)). \tag{4.2}$$

The metric space $\widetilde{\mathbb{M}}_g = \cup_{n\in\mathbb{N}}\widetilde{\mathbb{M}}_g(n)$ equipped with Gromov-Hausdorff distance, can be completed to form $\overline{\mathbb{M}}_g$. The continuous limit of random maps must then be understood in the following way: it is the limit of a converging (in Gromov-Hausdorff sense) sequence of random maps $(m_n)_{n\in\mathbb{N}}$ with m_n of size n.
Actually, it is not necessary to compute the infimum of all possible isometries between graphs, and to prove that a sequence $(m_n)_{n\in\mathbb{N}}$ converges, it is enough to find a family of isometries $\varphi_n : m_n \to M$ for which the sequence $(\varphi(m_n))_{n\in\mathbb{N}}$ converges in the Hausdorff topology.
The convergence of metric spaces has been first solved for certain models of random maps in the works of Le Gall [Le Gall, 2013], Miermont [Miermont, 2013].

Universality There are various ways to define a model of random maps. The constraints imposed may be of different types (for instance the degrees of the faces, of the vertices), as well as the decorations, the weights of local objects, the measure on continuous parameters, and the distances on the maps. Therefore, it is legitimate to think that the continuous limits differ for two different models. It is actually the case, but for some close models, the continuous limits are almost the same. Let us illustrate more precisely this *universality* property, and let us consider the three following examples of random maps:

Example 4.1. *In the first model, we only put a constrain on the faces, which we force to have degree 3, and we mark an edge and a vertex, that is to say the set* $\widetilde{\mathbb{M}}_g(n) = \mathcal{T}_g^\bullet(n)$ *is the set of rooted triangulations with* n *vertices and genus* g*. The fugacity associated to a vertex is* $t^{\mathcal{T}}$*. The weight of a triangulation* $T \in \mathcal{T}_g^\bullet(n)$ *is* $w(T) = \left(t^{\mathcal{T}}\right)^n$*. The generating function of rooted triangulations of genus* g *has the following expression:*

$$F_g^{\mathcal{T}}(t^{\mathcal{T}}) = \sum_{n=0}^{\infty} \sum_{m \in \mathcal{T}_g^\bullet(n)} \frac{w(m)}{|\mathrm{Aut}|(m)}, \tag{4.3}$$

and it has the singular behaviour when $t^{\mathcal{T}}$ *reaches the critical value* $t_c^{\mathcal{T}} = \frac{1}{4\sqrt{27}}$ *[Eynard, 2016]:*

$$F_g^{\mathcal{T}} \underset{t^{\mathcal{T}} \to t_c^{\mathcal{T}}}{\sim} \left(1 - \frac{t^{\mathcal{T}}}{t_c^{\mathcal{T}}}\right)^{\frac{5}{2}(1-g)} (t_c^{\mathcal{T}})^{2-2g} \tilde{F}_g^{\mathcal{T}}, \tag{4.4}$$

where $\tilde{F}_g^{\mathcal{T}}$ *is independent of* $t^{\mathcal{T}}$*. One sees that for* $g \geq 2$*, the generating function diverges when the fugaticty of the vertices reaches the critical value. The critical exponent can be written in terms of the* string susceptibility exponent $\gamma_g^{\mathcal{T}}$*:* $\frac{5}{2}(1-g) = 2 - \gamma_g^{\mathcal{T}}$*. I gives the string susceptibility:* $\gamma_g^{\mathcal{T}} = \frac{5g-1}{2}$*. The large* n *limit of the model is related to the behaviour of the generating functions close to their critical points, so the string susceptibility is a feature of the continuous limit.*

Example 4.2. *Second, instead of looking at rooted triangulations, we consider rooted quadrangulations:* $\widetilde{\mathbb{M}}_g(n) = \mathcal{Q}_g^\bullet(n)$*, where* n *is still the number of vertices, whose fugacity is set to* $t^{\mathcal{Q}}$*. Again, the generating function of rooted quadrangulations of genus* g *is given by:*

$$F_g^{\mathcal{Q}}(t^{\mathcal{Q}}) = \sum_{n=0}^{\infty} \sum_{m \in \mathcal{Q}_g^\bullet(n)} \frac{w(m)}{|\mathrm{Aut}|(m)}, \tag{4.5}$$

which has the singular behaviour when $t^{\mathcal{Q}}$ *reaches the critical value* $t_c^{\mathcal{Q}} = \frac{1}{12}$ *[Eynard, 2016]:*

$$F_g^{\mathcal{Q}} \underset{t^{\mathcal{Q}} \to t_c^{\mathcal{Q}}}{\sim} \left(1 - \frac{t^{\mathcal{Q}}}{t_c^{\mathcal{Q}}}\right)^{\frac{5}{2}(1-g)} (t_c^{\mathcal{Q}})^{2-2g} \tilde{F}_g^{\mathcal{Q}}, \tag{4.6}$$

where $\tilde{F}_g^{\mathcal{Q}}$ is independent of $t^{\mathcal{Q}}$, and is actually equal to $\tilde{F}_g^{\mathcal{T}}$. Again, the string susceptibility is $\gamma_g^{\mathcal{Q}} = \frac{5g-1}{2}$.

Example 4.3. *Last, let us consider the set of rooted quadrangulations whose faces are decorated with spins. + spins correspond to red-colored quadrangles, and − spins to black quadrangles. We call $\mathcal{I}_g^\bullet(n)$ the set of colored and rooted quadrangulations of genus g with n vertices. The fugacities of the local objects are chosen to be:*

- *vertex: $t^{\mathcal{I}}$;*
- *edge separating two red faces, or two black faces: $\frac{4}{15}$;*
- *edge separating a red face and a black face: $\frac{1}{15}$.*

We see that the energy associated to a bi-colored edge (separating two faces of different colors), is greater than the energy associated to mono-colored edge. Therefore, the configurations where there are few interfaces between red and black faces are more likely to appear than the others. So we see in this example that for a given map, all the decorations do not have the same probability to appear, there is a coupling between matter (the color on the faces) and gravity (the structure of the map). The generating function of colored rooted quadrangulations of genus g is defined as:

$$F_g^{\mathcal{I}}(t^{\mathcal{I}}) = \sum_{n=0}^{\infty} \sum_{m \in \mathcal{I}_g^\bullet(n)} \frac{w(m)}{|\mathrm{Aut}(m)|}. \tag{4.7}$$

One can show [Eynard, 2016] that for $t^{\mathcal{I}} \sim t_c^{\mathcal{I}} = -\frac{10}{9}$ and $g \geq 2$, the generating function is singular and behaves like:

$$F_g^{\mathcal{I}} \underset{t^{\mathcal{I}} \to t_c^{\mathcal{I}}}{\sim} \left(1 - \frac{t^{\mathcal{I}}}{t_c^{\mathcal{I}}}\right)^{\frac{7}{3}(1-g)} (t_c^{\mathcal{I}})^{2-2g} \tilde{F}_g^{\mathcal{I}}, \tag{4.8}$$

where $\tilde{F}_g^{\mathcal{I}}$ is independent of $t^{\mathcal{I}}$, and differs from $\tilde{F}_g^{\mathcal{T}}$. The string susceptibilty is $\gamma_g^{\mathcal{I}} = \frac{7g-1}{3}$.

From those examples, one sees that, for the enumeration of triangulations or quadrangulations (examples 4.1 and 4.2), the generating functions $F_g^{\mathcal{T}}$ and $F_g^{\mathcal{Q}}$ show many similarities at their critical points, although their critical points are different $\frac{1}{4\sqrt{27}}$ and $\frac{1}{12}$ respectively. Actually, the string susceptibilities are equal, and the critical generating functions also:

$$\begin{cases} \gamma_g^{\mathcal{T}} = \gamma_g^{\mathcal{Q}} \\ \tilde{F}_g^{\mathcal{T}} = \tilde{F}_g^{\mathcal{Q}}. \end{cases} \tag{4.9}$$

This means that in the continuous limit, many of the features of random triangulations should be the same as the features of large random quadrangulations. If two models

show such similar features, such as common critical exponents, are said to sit in the same *universality class*, and their continuous limit shall be the same theory. The intuitive idea behind universality is that, if, in their definition, two models of random maps differ by features which seem to be details (irrelevant), those details should not be important in the continuous limit. For the previous examples, the fact that one looks at random maps with faces of degree 3 or 4 should not have a great influence on the continuous limit. On the contrary, some features of a model (decorations or constraints) may be crucial, as they can have an influence on the structures of the maps more likely to appear, so there is not only one universality class for random maps. For instance, the case of example 4.3 (which is the Ising model on random quadrangulations), shows very different behaviour at the critical point, whether it be for the value of the string susceptibility or the form of the function $\tilde{F}_g^{\mathcal{I}}$. This means that the continuous limit of this model is different from the continuous limit of the two others. In the Ising model, some colored configurations have a greater weight than others, and there is an interplay between the map structure and the decorations. Thus, in the continuous limit, the colored map shall mimic the interaction between a matter field and the metric (*i.e.* gravity), which is different from mimicking purely gravity. The model $\mathcal{I}_g^\bullet$ stands therefore in another universality class than $\mathcal{T}_g^\bullet$ and $\mathcal{Q}_g^\bullet$.
In chapters III and IV, we define models that we show to be in the universality class of 2d pure gravity, so in the continuous limit, they are supposed to converge to the same theory. The interest of looking at different models for a same continuous limit, is that the computation of expectation values of some observables is more convenient for certain models.

5 Formal matrix models

In many models of random maps, an instance of a map and its associated weight can be interpreted as a Feynman diagram and its amplitude of a zero-dimensional field theory of formal matrices. It is the case of Strebel graphs (in chapter IV), and of the Ising model (in chapter VI). We briefly describe here the relation between formal matrix models and random maps. This relation was noticed by 't Hooft ['t Hooft, 1974], and first used for the study of 2d quantum gravity by Brézin-Itzykson-Parisi-Zuber [Brézin et al., 1978]. The formalism of matrix models is powerful for finding equations satisfied by the generating functions (the loop equations), and very helpful to solve the enumeration of random maps and the computation of certain expectation values. This presentation is inspired by [Eynard, 2016] and [Di Francesco et al., 1995]. We restrain it to random Hermitian matrices, although other ensembles of matrices can be used.

5.1 Feynman graphs of matrix integrals

Let us consider the set H_N of Hermitian matrices of size N, and the Lebesgue measure on H_N:

$$dM = \prod_{i=1}^{N} dM_{i,i} \prod_{1 \leq i < j \leq N} dM_{i,j} d\overline{M}_{i,j}. \tag{5.1}$$

We note $\mathcal{Z}_0$ the Gaussian integral over H_N:

$$\mathcal{Z}_0 = \int_{H_N} dM e^{-\frac{N}{2} \operatorname{Tr} M^2} = 2^{\frac{N}{2}} \left(\frac{\pi}{N}\right)^{\frac{N^2}{2}}. \tag{5.2}$$

The "0" subscript stands for the fact that, as we will see in next subsection, this quantity corresponds to the partition function of a matrix model without potential. The expectation value of an observable $\mathcal{O}(M)$ is defined by:

$$\langle \mathcal{O}(M) \rangle_0 = \frac{1}{\mathcal{Z}_0} \int_{H_N} \mathcal{O}(M) dM e^{-\frac{N}{2} \operatorname{Tr} M^2}. \tag{5.3}$$

A fundamental piece of matrix models is the *propagator*:

$$\langle M_{ij} M_{kl} \rangle_0 = \frac{1}{N} \delta_{il} \delta_{jk}. \tag{5.4}$$

Let $v_1, \ldots, v_n \geq 1$ be n integers. Then, the following Gaussian integral has a diagrammatic interpretation:

$$\begin{aligned} \left\langle \prod_{i=1}^{n} N \frac{\operatorname{Tr} M^{v_i}}{v_i} \right\rangle_0 &= \frac{1}{\mathcal{Z}_0} \int_{H_N} dM \prod_{i=1}^{n} N \frac{\operatorname{Tr} M^{v_i}}{v_i} e^{-\frac{N}{2} \operatorname{Tr} M^2} \\ &= \frac{1}{\mathcal{Z}_0} \int_{H_N} dM \prod_{i=1}^{n} \left(\frac{N}{v_i} \sum_{j_1, \ldots, j_{v_i}=1}^{N} M_{j_1 j_2} M_{j_2 j_3} \ldots M_{j_{v_i} j_1} \right) e^{-\frac{N}{2} \operatorname{Tr} M^2} \end{aligned} \tag{5.5}$$

It is the correlation function of $\sum_{i=1}^{n} v_i$ matrix elements. As it is a Gaussian integral, it does not vanish only if $\sum_{i=1}^{n} v_i = 2k$ is even. The diagrammatic decomposition relies on *Wick*'s theorem and equation 5.4. Wick's theorem states that the expectation value (with a Gaussian measure) of a product of $2k$ matrix elements is the sum over all possible pairings of the propagators. A pairing of $2k$ elements is a fixed-point free involution $\sigma \in \mathfrak{S}_{2k}$. Such permutation can be written as a product of k transpositions with disjoint support $\sigma = (\ell_1, \sigma(\ell_1)) \ldots (\ell_k, \sigma(\ell_k))$. Wick's theorem is summarized in the following equation:

$$\langle M_{i_1, j_1} \ldots M_{i_{2k}, j_{2k}} \rangle_0 = \sum_{\sigma \text{ pairings}} \prod_{m=1}^{k} \left\langle M_{i_{\ell_m} j_{\ell_m}} M_{i_{\sigma(\ell_m)} j_{\sigma(\ell_m)}} \right\rangle_0. \tag{5.6}$$

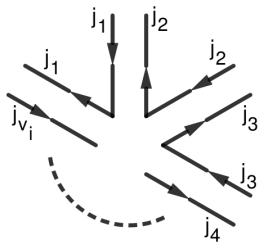

Figure 12: Vertex of a ribbon graph. The weight is $\frac{N}{v_i}$

For instance, Wick's theorem applied to the observable $N \operatorname{Tr} M^4$ gives:

$$\begin{aligned}
\left\langle N\frac{\operatorname{Tr} M^4}{4}\right\rangle_0 &= \sum_{i,j,k,l=1}^{N}\frac{N}{4}\left\langle M_{ij}M_{jk}M_{kl}M_{li}\right\rangle_0 \\
&\overset{\text{Wick}}{=} \frac{N}{4}\sum_{i,j,k,l=1}^{N}\Big(\left\langle M_{ij}M_{jk}\right\rangle_0\left\langle M_{kl}M_{li}\right\rangle_0+\left\langle M_{ij}M_{kl}\right\rangle_0\left\langle M_{jk}M_{li}\right\rangle_0 \\
&\quad +\left\langle M_{ij}M_{li}\right\rangle_0\left\langle M_{jk}M_{kl}\right\rangle_0\Big) \\
&\overset{\text{eq.5.4}}{=} \frac{N}{4}\sum_{i,j,k,l=1}^{N}\frac{1}{N^2}\left(\delta_{ik}\delta_{ki}+\delta_{il}\delta_{jk}\delta_{ji}\delta_{kl}+\delta_{jl}\delta_{lj}\right) \\
&= \frac{1}{4}(N^2+N^2+1)=\frac{N^2}{2}+\frac{1}{4}. \qquad (5.7)
\end{aligned}$$

The diagrammatic representation of the expectation value 5.5 works as follow:

- In the definition of the observable, to each trace $N\frac{\operatorname{Tr} M^{v_i}}{v_i}$, we associate a vertex of degree v_i, where each edge is fattened in order to carry 2 indices (that are the indices of the matrices). Each line of the fattened edge carries an orientation, and two lines are connected if their indices are equal and their orientations are consistent. On a diagram, a vertex of degree v_i carries a weight $\frac{N}{v_i}$. This rule is depicted in figure 12.

- For a given pairing $\sigma = (\ell_1, \sigma(\ell_1))\dots(\ell_k, \sigma(\ell_k))$, the integral 5.5 is the product of propagators. In the diagram, the propagator $\left\langle M_{ij}M_{kl}\right\rangle_0 = \frac{1}{N}\delta_{il}\delta_{jk}$ forces the lines having the indices i, j to carry the same indices as the lines carrying respectively the indices l, k. Diagrammatically, the edge i, j is connected to the edge l, k consistently with their orientations, forming a propagator (see figure 13). The weight associated to a propagator is $\frac{1}{N}$.

- In the end, one obtains a non necessarily connected graph with fat edges composed of 2 lines. Such graph is called a *ribbon* graph. All the lines are closed, and if one properly embeds the ribbon graph on a Riemann surface, each closed

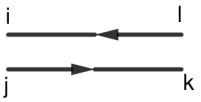

Figure 13: Propagator of a ribbon graph. The weight is $\frac{\delta_{il}\delta jk}{N}$.

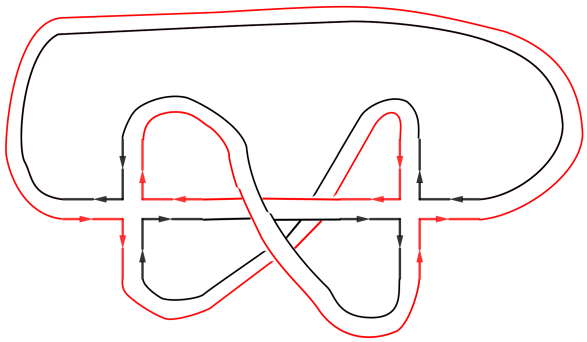

Figure 14: Example of a ribbon graph with 2 closed lines, one red and one black. In a proper embedding (on a torus), this graph has 2 faces.

line corresponds to a face (see figure 14). Each closed line carries a weight N (it corresponds to the summation over the index associated to the line).

In the end, the expectation value of equation (5.5) is a sum over ribbon graphs with n vertices. For a properly embedded ribbon graph G, note $|\mathcal{V}(G)|$, $|\mathcal{E}(G)|$, and $|\mathcal{F}(G)|$ respectively the number of vertices, the number of fat edges and the number of closed lines (faces) of G. The weight associated to G is:

$$w(G) = N^{|\mathcal{V}(G)|-|\mathcal{E}(G)|+|\mathcal{F}(G)|} \prod_{i=1}^{n} \frac{1}{v_i}. \tag{5.8}$$

For a connected ribbon graph, the power of N is the Euler characteristic $\chi(G)$ of the embedded graph G. Some ribbon graphs are equivalent as maps, as we can see in example 5.1.

Example 5.1. *Let us compute the expectation value* $\left\langle \left(N \frac{\mathrm{Tr}\, M^3}{3} \right)^2 \right\rangle_0$ *with the diagrammatic rules. In total, there are 15 connected ribbon graphs in the sum, that we can classify into three sets (see figures 15, 16 and 17). The first set comprises 9 graphs of genus 0 which have the form of "handcuffs", with 2 faces of length 1 and one face of length 4. The dual of each graph of this set is the map* m_1*. In the second set, the three graphs are also planar, with 3 faces of degree 2. The dual map corresponding to those ribbon graphs is denoted* m_2*. Last, in the third set, each of the three graphs has genus 1, with only one face of degree 6. The dual map is called* m_3*. The maps* m_i *are*

depicted in figure 18. The weight of each ribbon graph of genus 0 is $\frac{N^2}{9}$, and the weight of each ribbon graph of genus 1 is $\frac{N^0}{9}$. In the end, we get:

$$\begin{aligned}\left\langle \left(N\frac{\mathrm{Tr}\, M^3}{3}\right)^2 \right\rangle_0 &= 9\frac{N^2}{9} + 3\frac{N^2}{9} + 3\frac{N^0}{9} \\ &= \frac{4}{3}N^2 + \frac{1}{3}N^0. \end{aligned} \tag{5.9}$$

One can recover this formula by summing over the three maps m_1, m_2, m_3:

$$\begin{aligned}\left\langle \left(N\frac{\mathrm{Tr}\, M^3}{3}\right)^2 \right\rangle_0 &= \frac{N^2}{|\mathrm{Aut}(m_1)|} + \frac{N^2}{|\mathrm{Aut}(m_2)|} + \frac{N^0}{|\mathrm{Aut}(m_3)|} \\ &= \frac{N^2}{1} + \frac{N^2}{3} + \frac{N^0}{3}. \end{aligned} \tag{5.10}$$

Indeed, the group of automorphisms of m_1 is trivial whereas those of m_2 and m_3 have 3 elements.

The sum over ribbon graphs can be reduced to a sum over maps (where the edges are fattened):

Theorem 5.1. *[Brézin et al., 1978] The expectation value $\prod_{i=1}^{n} N\frac{\mathrm{Tr}\, M^{v_i}}{v_i}$ can be computed as a sum over (non necessarily connected) maps having n vertices of valencies $v_1, \ldots, v_n$:*

$$\left\langle \prod_{i=1}^{n} N\frac{\mathrm{Tr}\, M^{v_i}}{v_i} \right\rangle_0 = \sum_{m\,\mathrm{map}} \frac{N^{|\mathcal{V}(m)|-|\mathcal{E}(m)|+|\mathcal{F}(m)|}}{|\mathrm{Aut}(m)|}. \tag{5.11}$$

This theorem shows the relation between Gaussian matrix integrals and maps. The diagrammatic decomposition in theorem is exact in the sense that the integrals are convergent and the sum over maps is finite. The connected expectation value restrains the sum to connected maps:

$$\left\langle \prod_{i=1}^{n} N\frac{\mathrm{Tr}\, M^{v_i}}{v_i} \right\rangle_0^c = \sum_{\substack{m\,\mathrm{map} \\ \mathrm{connected}}} \frac{N^{|\mathcal{V}(m)|-|\mathcal{E}(m)|+|\mathcal{F}(m)|}}{|\mathrm{Aut}(m)|}. \tag{5.12}$$

The dual of a ribbon graph is a map (see figure 19), so when one carries out the sums over ribbon graphs, it is equivalent to carry out the sum over their duals. In the end, we have that:

$$\begin{aligned}\left\langle \prod_{i=1}^{n} N\frac{\mathrm{Tr}\, M^{v_i}}{v_i} \right\rangle_0 &= \sum_{G\,\mathrm{ribbon\,graph}} \frac{w(G)}{|\mathrm{Aut}(G)|} \\ &= \sum_{\substack{m\,\mathrm{map} \\ \mathrm{dual\,of}\, G}} \frac{N^{|\mathcal{V}(m)|-|\mathcal{E}(m)|+|\mathcal{F}(m)|}}{|\mathrm{Aut}(m)|}, \end{aligned} \tag{5.13}$$

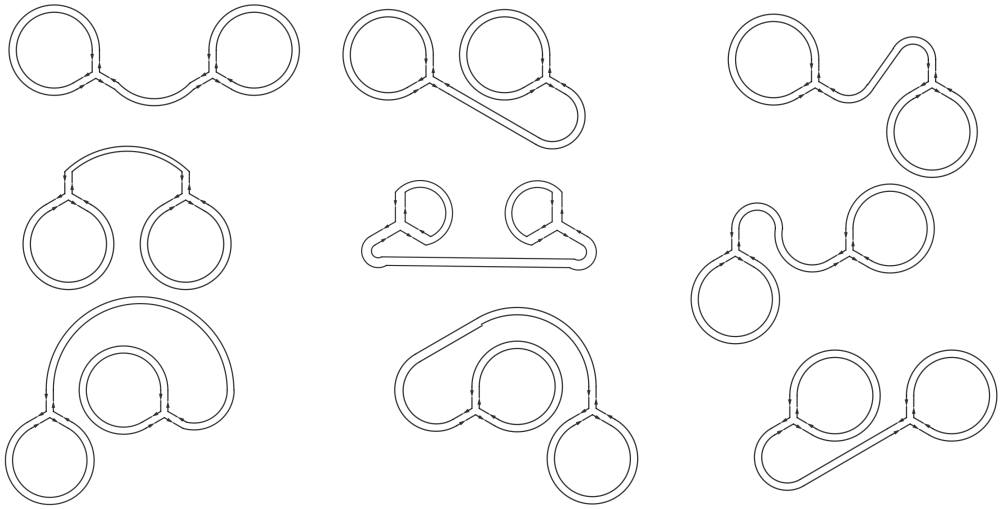

Figure 15: Ribbon graphs of the first set. The weight of each graph is $\frac{N^2}{9}$.

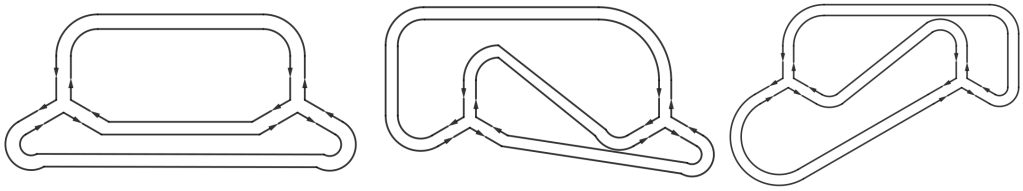

Figure 16: Ribbon graphs of the second set. The weight of each graph is $\frac{N^2}{9}$.

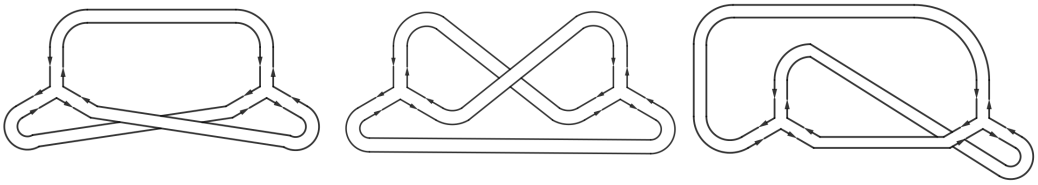

Figure 17: Ribbon graphs of the third set. The weight of each graph is $\frac{N^0}{9}$.

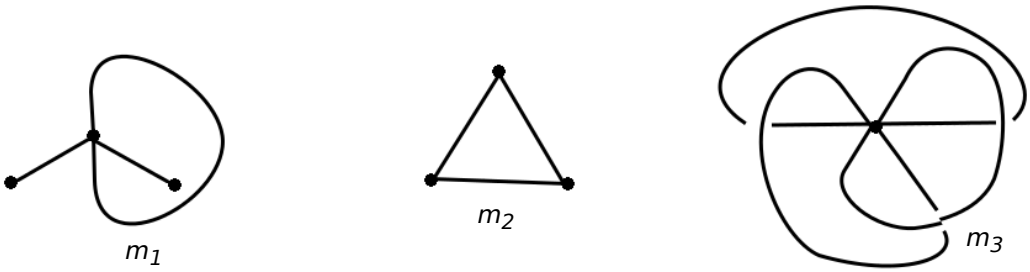

Figure 18: The maps m_1, m_2, m_3 corresponding to each set of ribbon graphs. Each map is the gluing of two triangles.

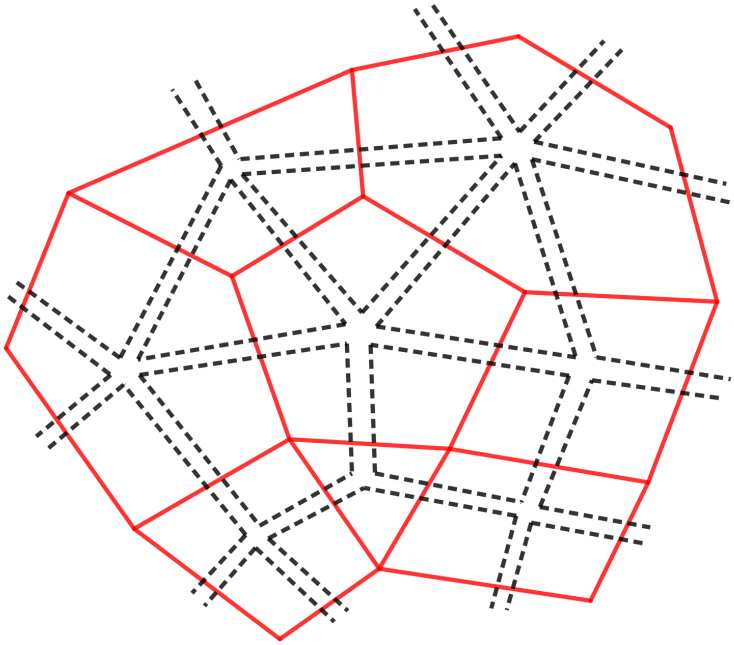

Figure 19: The dual of a ribbon graph is a map.

where we have, for $m = G^*$, $|\mathrm{Aut}(G)| = |\mathrm{Aut}(m)|$ (the group of automorphisms of a graph has the same cardinal as the group of automorphisms of its dual), and $w(G) = N^{\mathcal{V}(G)|-|\mathcal{E}(G)|+|\mathcal{F}(G)|} = N^{\mathcal{F}(m)|-|\mathcal{E}(m)|+|\mathcal{V}(m)|} = w(m)$ (the vertices, edges and faces of a graph correspond respectively to the faces, edges and vertices of its dual). We shall privilege this way of writing the expectation values, and in the following, when a sum over maps is written, the sum runs implicitly over the duals of ribbon graphs.

5.2 Formal matrix models

In the following, we interpret random maps models in terms of formal matrix models. We begin with generic one-matrix models, and extend to the case of 2-matrix models, as it is used in chapter VI.

One matrix model Define the following potential:

$$V(M) = \frac{M^2}{2} - \sum_{j=3}^{d} t_j \frac{M^j}{j}, \tag{5.14}$$

then the *partition function* of the formal matrix model associated to this potential is the formal integral:

$$\mathcal{Z} = \int_{\text{formal}} dM e^{-N \,\mathrm{Tr}\, V(M)}. \tag{5.15}$$

It has to be understood as a formal series in $t_3, \ldots, t_d$: $\mathcal{Z} \in \mathbb{Q}[[t3, \ldots, t_d]]$, where each coefficient is a sum of Gaussian integrals over H_N. The series is not convergent, and the study of formal matrix models is different from the study of convergent matrix models.

$$\mathcal{Z}(t_1, \ldots, t_d, N) = \sum_{n=0}^{\infty} \frac{1}{n!} \sum_{k_1,\ldots,k_n=3}^{d} \mathcal{Z}_0 \left\langle \prod_{i=1}^{n} N t_{k_i} \frac{M^{k_i}}{k_i} \right\rangle_0 . \tag{5.16}$$

By using the theorem 5.1 of the previous section, the partition function can be written as a formal series over (non necessarily connected) ribbon with vertices of degrees $3, \ldots, d$. It corresponds to a formal series over non connected maps with faces of degrees between 3 and d. For a map m, we note $n_i(m)$ the number of faces of degree i in m.

$$\begin{aligned} \mathcal{Z}(t_1, \ldots, t_d, N) &= \mathcal{Z}_0 \sum_{m \,\text{maps}} t_3^{n_3(m)} \ldots t_d^{n_d(m)} \frac{N^{|\mathcal{V}(m)|-|\mathcal{E}(m)|+|\mathcal{F}(m)|}}{|\mathrm{Aut}(m)|} \\ &= \mathcal{Z}_0 \sum_{m \,\text{maps}} N^{\chi(m)} \frac{w(m)}{|\mathrm{Aut}(m)|}. \end{aligned} \tag{5.17}$$

By this formula, we see that the partition function of a formal matrix model is a sum over maps m, each one carrying a weight $w(m)$. This weight is a product of fugacities. The power of N (the size of the matrices) accounts for the topology of the map through the Euler characteristic of the map. The fugacity associated to a face of degree k is t_k. We then have a model of random maps with faces constrained to have degrees $3, \ldots, d$. Therefore, the partition function of this formal matrix model is the partition function that enumerates not connected maps. The partition function of connected maps is the free energy of the model and is given by the logarithm of $\mathcal{Z}$; it is denoted F:

$$\begin{aligned} F(t_1, \ldots, t_d, N) &= \log \mathcal{Z}(t_1, \ldots, t_d, N) \\ &= \sum_{m \,\text{connected map}} N^{\chi(m)} \frac{w(m)(t_1, \ldots, t_d)}{|\mathrm{Aut}(m)|}. \end{aligned} \tag{5.18}$$

F is a formal series in t_j. Since the maps are connected, the Euler characteristic of a map $\chi(m)$ is simply expressed in terms of its genus: $\chi(m) = 2 - 2g$. If one views the free energy also as a formal series in N, then the coefficient F_g of N^{2-2g} is a formal series in $t_1, \ldots, t_d$, and it is the partition function of connected maps of genus g:

$$\begin{aligned} F(t_1, \ldots, t_d, N) &= \sum_{g=0}^{\infty} N^{2-2g} F_g(t_1, \ldots, t_d) \\ &= \sum_{g=0}^{\infty} N^{2-2g} \sum_{m \in \mathbb{M}_g} \frac{w(m)(t_1, \ldots, t_d)}{|\mathrm{Aut}(m)|}, \end{aligned} \tag{5.19}$$

where the set of maps $\mathbb{M}_g$ is restrained to the connected maps of genus g, of generic size, and with faces of valencies $3, \ldots, d$. When the size N of the matrices tends to

infinity, only the leading order term in N^2, which is the partition function of planar maps, survives.

The observables of interest for formal matrix models are

$$\prod_{i=1}^{\ell} \operatorname{Tr} M^{k_i}.$$

The expectation value of such observable is a formal series in the fugacities $t_1, \ldots, t_d$, and it is defined by the following formula:

$$\left\langle \prod_{i=1}^{\ell} \operatorname{Tr} M^{k_i} \right\rangle = \frac{1}{\mathcal{Z}} \int_{\text{formal}} dM e^{-N \operatorname{Tr} V(M)} \prod_{i=1}^{\ell} \operatorname{Tr} M^{k_i}. \tag{5.20}$$

It is worth noticing that both the numerator and the denominator are formal series. Translating this expectation value as a sum over maps, it is the partition function of connected maps having ℓ boundary faces of lengths $k_1, \ldots, k_\ell$. The non-connected maps are canceled out by the term $\frac{1}{\mathcal{Z}}$. The distinguished faces do not have fugacities, and can have lengths greater than d (the maximum length of the faces of the interior of the map).

$$\left\langle \prod_{i=1}^{\ell} \operatorname{Tr} M^{k_i} \right\rangle = \sum_{m \in \mathbb{M}_{g,k}} N^{2-2g} w(m). \tag{5.21}$$

(The automorphism group of a map with boundaries is trivial, so $|\mathrm{Aut}(m)| = 1$).

Two-matrix model A slight extension of the one-matrix model is the two-matrix model, first introduced by Kazakov [Kazakov, 1986] to study the Ising model on random maps. Let us look at two Hermitian matrices M_1 and M_2, and the potentials:

$$\begin{cases} V_1(M_1) = t_2 \frac{M_1^2}{2} - \sum_{i=3}^{d_1} t_i \frac{M_1^i}{i} \\ V_2(M_2) = \tilde{t}_2 \frac{M_2^2}{2} - \sum_{i=3}^{d_2} \tilde{t}_i \frac{M_2^i}{i}. \end{cases} \tag{5.22}$$

The partition function of the formal 2-matrix model we look at in chapter VI is:

$$\mathcal{Z}_2(t_2, \ldots, t_{d_1}; \tilde{t}_2, \ldots, \tilde{t}_{d_2}) = \int_{\text{formal}} e^{-N \operatorname{Tr}(V_1(M_1) + V_2(M_2) - c M_1 M_2)} dM_1 dM_2. \tag{5.23}$$

Again, this partition function has to be understood as a formal series in $t_3, \ldots, t_{d_1}, \tilde{t}_3, \ldots, \tilde{t}_{d_2}$. In the same manner as for the one matrix model, this partition function can be interpreted as a sum over ribbon graphs, or, looking at the dual, a sum over random maps. Let us first focus on the ribbon graph interpretation. When looking at a coefficient of the formal series, the typical integral to compute is:

$$\int_{H_N \times H_N} \prod_{i=1}^{\ell} t_{k_i} \frac{\operatorname{Tr} M_1^{k_i}}{k_i} \prod_{j=1}^{n} \tilde{t}_{\tilde{k}_j} \frac{\operatorname{Tr} M_2^{\tilde{k}_j}}{\tilde{k}_j} e^{-N \operatorname{Tr}\left(t_2 \frac{M_1^2}{2} + \tilde{t}_2 \frac{M_2^2}{2} - c M_1 M_2\right)} dM_1 \, dM_2. \tag{5.24}$$

Figure 20: The propagators of the bi-colored ribbon graphs. The weight of a red (resp. black) propagator is $\frac{1}{N}\frac{\tilde{t}_2}{t_2\tilde{t}_2-c^2}$ (resp. $\frac{1}{N}\frac{t_2}{t_2\tilde{t}_2-c^2}$). The weight of mixed propagators is $\frac{1}{N}\frac{c}{t_2\tilde{t}_2-c^2}$.

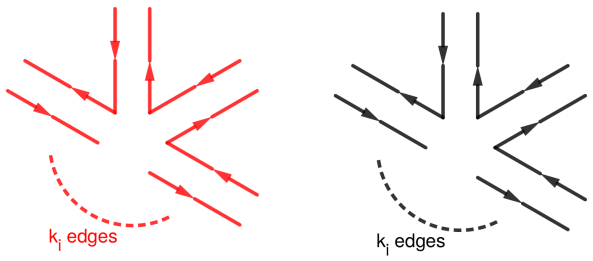

Figure 21: The vertices of the bi-colored ribbon graphs. The weight of a red (resp. black) vertex of degree k_i (resp. $\tilde{k}_i$) is $N\frac{t_{k_i}}{k_i}$ (resp. $N\frac{\tilde{t}_{\tilde{k}_i}}{\tilde{k}_i}$).

Applying Wick's theorem, this integral can be written as a sum over pairings of matrix coefficients. The crossed term cM_1M_2 in the Gaussian integral allows to pair coefficients of the matrix M_1 with coefficients of the matrix M_2. Each pairing corresponds to a bi-colored ribbon graph G, and given a ribbon graph G appearing in the sum, one computes its weight with the following rules:

- A fat edge of G is red when it carries the indices of the matrix M_1, it is black when it carries the indices of matrix M_2. Three types of propagators are allowed in the ribbon graph. The two first types are mono-colored propagators, which connect red (resp. black) fat edges to red (resp. black) fat edges. A red (resp.) propagator has weight $\frac{1}{N}\frac{\tilde{t}_2}{t_2\tilde{t}_2-c^2}$ (resp. $\frac{1}{N}\frac{t_2}{t_2\tilde{t}_2-c^2}$). The third type is mixed propagators, which connect red fat edges to black fat edges with a weight $\frac{1}{N}\frac{c}{t_2\tilde{t}_2-c^2}$. Figure 20 summarizes those weights.

- There are red and black vertices ; red vertices have valencies $k_1,\dots,k_m$ and black vertices have degrees $\tilde{k}_1,\dots,\tilde{k}_n$. A red vertex of degree k_i has weight $N\frac{t_{k_i}}{k_i}$, a black vertex of degree $\tilde{k}_i$ has weight $N\frac{t_{\tilde{k}_i}}{\tilde{k}_i}$, see figure 21.

- The lines of G are closed, but can change color. Each closed lines contributes to the weight of G with a factor N.

The weight of G is the product of the weights associated to the propagators, the vertices, and the closed lines. If one notes $n_{rr}(G)$, $n_{bb}(G)$ and $n_{rb}(G)$ respectively the

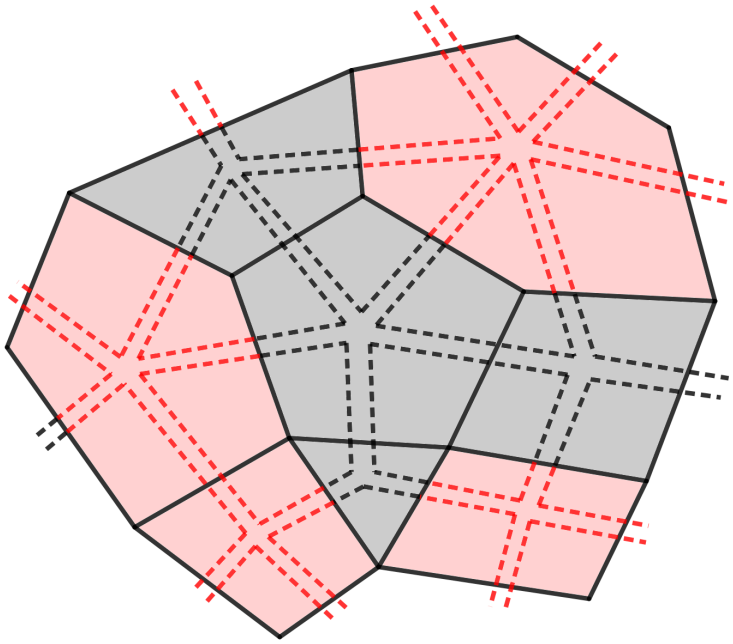

Figure 22: The dual of a bi-colored ribbon graph is a bi-colored map.

number of red, black, and mixed propagators of G, the integral 5.24 can be written as the following sum over non connected ribbon graphs with ℓ red vertices of degree $k_1, \dots, k_\ell$ and n black vertices of degree $\tilde{k}_1, \dots, \tilde{k}_n$:

$$\left(\int_{H_N \times H_N} e^{-N \operatorname{Tr}\left(t_2 \frac{M_1^2}{2} + \tilde{t}_2 \frac{M_2^2}{2} - c M_1 M_2\right)} dM_1\, dM_2\right) \prod_{i=1}^{\ell} \frac{t_{k_i}}{k_i} \prod_{j=1}^{n} \frac{\tilde{t}_{\tilde{k}_j}}{\tilde{k}_j} \times$$
$$\sum_{G \text{ ribbon graph}} N^{\chi(G)} \frac{1}{|\mathrm{Aut}(G)|} \left(\frac{\tilde{t}_2}{t_2 \tilde{t}_2 - c^2}\right)^{n_{rr}(G)} \left(\frac{t_2}{t_2 \tilde{t}_2 - c^2}\right)^{n_{bb}(G)} \left(\frac{c}{t_2 \tilde{t}_2 - c^2}\right)^{n_{rb}(G)} \quad (5.25)$$

Equivalently, this sum can be written as a sum over maps, by considering the dual of the bi-colored ribbon graphs (see figure 22). We obtain a sum over non connected maps which have ℓ red faces of degree $k_1, \dots, k_\ell$ and n black faces of degree $\tilde{k}_1, \dots, \tilde{k}_m$. The weight associated to a red (resp. black) face of degree k_i (resp. black) is $N \frac{t_{k_i}}{k_i}$ (resp. $N \frac{\tilde{t}_{\tilde{k}_i}}{\tilde{k}_i}$). The weight of an edge separating two red (resp. black) faces is $\frac{1}{N} \frac{\tilde{t}_2}{t_2 \tilde{t}_2 - c^2}$ (resp. $\frac{1}{N} \frac{t_2}{t_2 \tilde{t}_2 - c^2}$). The weight of an edge separating a red face and a black face is $\frac{1}{N} \frac{c}{t_2 \tilde{t}_2 - c^2}$. Last, a vertex contributes a factor N to the weight of the map. We note $n_{rr}(m)$, $n_{bb}(m)$ and $n_{rb}(m)$ respectively the number of red, black, and mixed edges of the non connected map m. Then the integral 5.24 is worth:

$$\left(\int_{H_N \times H_N} e^{-N \operatorname{Tr}\left(t_2 \frac{M_1^2}{2} + \tilde{t}_2 \frac{M_2^2}{2} - c M_1 M_2\right)} dM_1\, dM_2\right) \prod_{i=1}^{\ell} \frac{t_{k_i}}{k_i} \prod_{j=1}^{n} \frac{\tilde{t}_{\tilde{k}_j}}{\tilde{k}_j} \times$$

$$\sum_{\substack{m \text{ non connected} \\ \text{map}}} N^{\chi(m)} \frac{1}{|\mathrm{Aut}(m)|} \left(\frac{\tilde{t}_2}{t_2\tilde{t}_2 - c^2}\right)^{n_{rr}(m)} \left(\frac{t_2}{t_2\tilde{t}_2 - c^2}\right)^{n_{bb}(m)} \left(\frac{c}{t_2\tilde{t}_2 - c^2}\right)^{n_{rb}(m)} \quad (5.26)$$

The partition function $\mathcal{Z}_2$ enumerates non connected bi-colored and weighted maps with red faces of degrees between 3 and d_1, and black faces of degrees between 3 and d_2. The partition function of connected bi-colored maps is the following formal series:

$$\begin{aligned} F(t_2, \ldots, t_{d_1}; \tilde{t}_2, \ldots, \tilde{t}_{d_2}) &= \log \mathcal{Z}_2(t_2, \ldots, t_{d_1}; \tilde{t}_2, \ldots, \tilde{t}_{d_2}) \\ &= \sum_{g=0}^{\infty} N^{2-2g} F_g(t_2, \ldots, t_{d_1}; \tilde{t}_2, \ldots, \tilde{t}_{d_2}), \end{aligned} \quad (5.27)$$

Where the F_g's are the partition functions of connected bi-colored maps of genus g. The observables that one computes in the Ising model have the form:

$$\mathcal{O}(M_1, M_2) = \prod_{i=1}^{\ell} \mathrm{Tr}\, M_1^{k_i} \prod_{j=1}^{n} \mathrm{Tr}\, M_2^{\tilde{k}_j} \prod_{\alpha=1}^{p} \mathrm{Tr}\, (M_1^{k_{\alpha,1}} M_2^{\tilde{k}_{\alpha,1}} \ldots M_1^{k_{\alpha,\ell_\alpha}} M_2^{\tilde{k}_{\alpha,\ell_\alpha}}), \quad (5.28)$$

whose expectation value is the formal series:

$$\langle \mathcal{O}(M_1, M_2) \rangle = \frac{1}{\mathcal{Z}_2} \int_{\text{formal}} \mathcal{O}(M_1, M_2) e^{-N \mathrm{Tr}\, (V_1(M_1) + V_2(M_2) - cM_1M_2)} dM_1 dM_2. \quad (5.29)$$

It enumerates connected (thanks to the denominator $\mathcal{Z}_2$) bi-colored maps of any genus, with ℓ red boundaries of lengths $k_1, \ldots, k_\ell$, n black boundaries of lengths $\tilde{k}_1, \ldots, \tilde{k}_n$, and p mixed boundaries. The mixed boundary α is a boundary of length $\sum_{i=1}^{\ell_\alpha} k_{\alpha,i} + \tilde{k}_{\alpha,i}$, which has $k_{\alpha,1}$ consecutive red edges, followed by $k_{\alpha,2}$ consecutive black edges, and so on.

Example 5.2. The map showed in figure 23 has 3 boundaries:

- boundary 1 has length 8 and is uniformly red ;
- boundary 2 has length 9 and is uniformly black ;
- boundary 3 has length 11, with an alternating pattern of colors, there are 3 changes of colors.

This map appears in the moment

$$\left\langle \mathrm{Tr}(M_1^8) \mathrm{Tr}(M_2^9) \mathrm{Tr}(M_1^2 M_2^1 M_1^1 M_2^2 M_1^2 M_2^3) \right\rangle_c$$

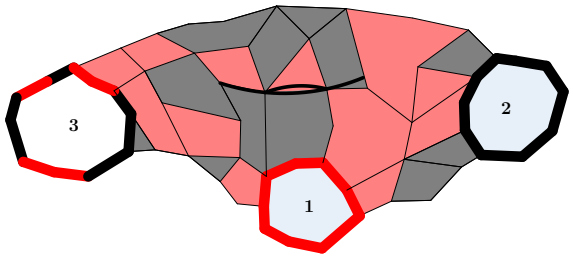

Figure 23: Example of a map with 3 boundaries.

5.3 Reduction of the integrals, orthogonal polynomials and loop equations

The matrix models allow to study a large range of random maps models. Although it is not the way we are tackling our models in this thesis, we use repeatedly results that come from formal matrix methods, especially in chapters V and VI. We expose here some techniques that allows to get the results that we use later, in the optics of clarity of this manuscript.

Separation between radial and angular parts of matrix integrals The first simplification of the matrix integrals is to separate it into integral over angular part and radial part. In the formal matrix models introduced above, the matrices are Hermitian. This entails that they are diagonalizable:

$$\forall M \in H_N,\ \exists U \in U(N),\ \lambda_1, \dots, \lambda_N \in \mathbb{R}\ s.t.\ M = U\Lambda U^\dagger, \tag{5.30}$$

where $\Lambda = \mathrm{Diag}(\lambda_1, \dots, \lambda_N)$. The matrix U is called the angular part of M, and the matrix Λ, which consists of the eigenvalues of M, is its radial part. The diagonalization property means that the map:

$$\begin{array}{rcl} U(N) \times \mathbb{R}^N & \longrightarrow & H_N \\ (U, \Lambda) & \longmapsto & U\Lambda U^\dagger \end{array} \tag{5.31}$$

is surjective. Carrying out the change of variable $M = U\Lambda U^\dagger$ in the matrix integrals of the one-matrix models, we get:

$$\int_{H_N} dM\, f(M) = C_N \int_{\mathbb{R}^N} d\lambda_1 \dots d\lambda_N \Delta^2(\lambda) \int_{U(N)} \mathcal{D}U\, f(U\,\Lambda\,U^\dagger), \tag{5.32}$$

where:

- $f(M)$ is a function of M
- C_N is a coefficient independent of U and Λ

- $\mathcal{D}U$ is the Haar measure – that is, invariant under the group structure – on $U(N)/U(1)^N$
- $\Delta(\lambda) = \prod_{1\leq i<j\leq N}(\lambda_j - \lambda_i) = \det_{1\leq i,j\leq N}(\lambda_i^{j-1})$ is the Vandermonde determinant of the eigenvalues λ_i.

This formula is a change of variable, and $C_N\Delta^2(\lambda)$ is the Jacobian of the reparametrization. If one applies this formula to the one-matrix model, it yields:

$$\begin{aligned}\mathcal{Z} &\overset{\text{formal}}{=} C_N \int_{\mathbb{R}^N} d\lambda_1 \dots d\lambda_N \Delta^2(\lambda) \int_{U(N)} \mathcal{D}U\, e^{-N \operatorname{Tr} V(U\,\Lambda\, U^\dagger)} \\ &\overset{\text{formal}}{=} C_N \int_{\mathbb{R}^N} d\lambda_1 \dots d\lambda_N \Delta^2(\lambda) \int_{U(N)} \mathcal{D}U\, e^{-N \operatorname{Tr} U\, V(\Lambda)\, U^\dagger} \\ &\overset{\text{formal}}{=} C_N \mathrm{Vol}(U(N)) \int_{\mathbb{R}^N} \Delta^2(\lambda) \prod_{i=1}^N d\lambda_i\, e^{-N \operatorname{Tr} V(\lambda_i)} \end{aligned} \tag{5.33}$$

Thanks to the cyclicity of the trace $\operatorname{Tr}(ABC) = \operatorname{Tr}(CAB)$, the one-matrix model is reduced to a N-dimensional integral over the radial part, since the angular part is traced out. The constant $C_N\mathrm{Vol}(U(N))$ is irrelevant for the computation of expectation values. The equalities above make sense as formal series, hence the term "formal" over the equality signs. The same simplification occurs for expectation values of observables implying traces of M, and one gets:

$$\langle \mathcal{O}(M) \rangle \overset{\text{formal}}{=} \frac{\int_{\mathbb{R}^N} \mathcal{O}(\Lambda)\Delta^2(\lambda) \prod_{i=1}^N d\lambda_i\, e^{-N \operatorname{Tr} V(\lambda_i)}}{\int_{\mathbb{R}^N} \Delta^2(\lambda) \prod_{i=1}^N d\lambda_i\, e^{-N \operatorname{Tr} V(\lambda_i)}}. \tag{5.34}$$

In the case of 2-matrix models, the matrices M_1 and M_2 are diagonalizable:

$$\begin{cases} M_1 = U_1 X U_1^\dagger \\ M_2 = U_2 Y U_2^\dagger. \end{cases} \tag{5.35}$$

Yet, since they do not commute (in general), the angular part of the integrals cannot be carried out so simply because of the crossed term $\operatorname{Tr} cM_1M_2$:

$$\begin{aligned} \operatorname{Tr} cM_1M_2 &= c \operatorname{Tr} U_1 X U_1^\dagger U_2 Y U_2^\dagger \\ &= c \operatorname{Tr} (U_1^\dagger U_2)^\dagger X U_1^\dagger U_2 Y. \end{aligned} \tag{5.36}$$

This entails that the partition function of the 2-matrix model takes this form:

$$\begin{aligned} \mathcal{Z}_2 &\overset{\text{formal}}{=} \int_{\mathbb{R}^N\times\mathbb{R}^N} \Delta^2(X)\Delta^2(Y) \prod_{i=1}^N dx_i\, e^{-N \operatorname{Tr} V_1(x_i)} \prod_{j=1}^N dy_j\, e^{-N \operatorname{Tr} V_2(y_j)} \int_{U(N)} \mathcal{D}U\, e^{cN \operatorname{Tr} UXU^\dagger Y} \\ &\overset{\text{formal}}{=} \int_{\mathbb{R}^N\times\mathbb{R}^N} dX\, dY\, \Delta^2(X)\Delta^2(Y) e^{-N \operatorname{Tr}(V_1(X)+V_2(Y))} \int_{U(N)} \mathcal{D}U\, e^{cN \operatorname{Tr} UXU^\dagger Y}. \end{aligned} \tag{5.37}$$

This transformation of the 2-matrix model is used in chapter VI.

Orthogonal polynomials Rewriting the one-matrix model as an integral over the eigenvalues of the Hermitian matrices opens the way for the technique of orthogonal polynomials. This technique is not applied in this thesis, but its consequences are, in the case of the continuous limit of planar Strebel graphs in chapter V. The technique of orthogonal polynomials relies on the fact that, since $\Delta(\lambda) = \det_{1\leq i,j\leq N} \lambda_i^{j-1}$, if one takes any family $(\pi_i)_{i\geq 0}$ of *monic polynomials*, that is:

$$\pi_i(\lambda) = \lambda^i + \text{lower degree terms},$$

then the following identity holds:

$$\Delta(\lambda) = \det_{1\leq i,j\leq N} \pi_{j-1}(\lambda_i). \tag{5.38}$$

From this identity and equation 5.33, one gets easily the determinantal formula for the partition function:

$$\mathcal{Z} \overset{\text{formal}}{=} C_N \text{Vol}(U(N)) \det_{1\leq i,j\leq N} \left[\int_{\mathbb{R}} d\lambda\, \pi_{i-1}(\lambda)\pi_{j-1}(\lambda) e^{-N\,V(\lambda)} \right]. \tag{5.39}$$

For a fixed N, we construct the monic polynomial family $(p_{k,N})_{k\geq 0}$, such that they are pairwise orthogonal with respect to the following scalar product:

$$\langle f|g\rangle_N = \int_{\mathbb{R}} d\lambda\, f(\lambda)g(\lambda)e^{-N\,V(\lambda)}. \tag{5.40}$$

In other terms, we can write:

$$\langle p_{i,N}|p_{j,N}\rangle_N = h_{i,N}\delta_{ij}, \tag{5.41}$$

and the partition function simplifies:

$$\begin{aligned} \mathcal{Z} &\overset{\text{formal}}{=} C_N \text{Vol}(U(N)) \det_{0\leq i,j\leq N-1} \langle p_{i,N}|p_{j,N}\rangle_N \\ &\overset{\text{formal}}{=} C_N \text{Vol}(U(N)) \prod_{i=0}^{N-1} h_{i,N}. \end{aligned} \tag{5.42}$$

From the orthogonal polynomials $p_{k,N}$ we define the functions $\psi_{k,N}$:

$$\psi_{k,N}(\lambda) = \frac{p_{k,N}(\lambda)}{\sqrt{h_{k,N}}} e^{-\frac{N}{2}V(\lambda)},$$

which are orthonormal for the scalar product $(f|g) = \int_{\mathbb{R}} d\lambda f(\lambda)g(\lambda)$:

$$(\psi_{k,N}|\psi_{k',N}) = \delta_{k,k'}.$$

Those orthonormal functions will appear indirectly in chapter V in the study of the continuous limit of Strebel graphs, via two operators $Q = x$, $P = \frac{d}{dx}$ acting on them. They act on the basis of orthonormal functions in this way:

$$\begin{cases} x\psi_{k,N}(x) = Q_{k,k+1}^{(N)}\psi_{k+1,N}(x) + Q_{k,k}^{(N)}\psi_{k,N}(x) + Q_{k,k-1}^{(N)}\psi_{k-1,N}(x) \\ \frac{d}{dx}\psi_{k,N}(x) = \sum_{j=0}^{k+d-1} P_{k,j}^{(N)}\psi_{j,N}(x), \end{cases} \tag{5.43}$$

where d is the degree of the potential V. Although the operators Q, P do not depend on the size N of the matrices, their coefficients in the basis $(\psi_{k,N})$ do, because the orthonormal functions depend on N. The operators P and Q satisfy the so-called *string equation*:

$$[P, Q] = \mathrm{Id}. \tag{5.44}$$

We will encounter this equation in the continuous limit of Strebel graphs. The continuous limit of a matrix model can be studied with the formalism of orthogonal polynomials, by taking the *double scaling limit*, which consists in letting N tend towards infinity while the parameters t_i of the potential tend to their critical value t_i^c with a rate depending on N:

$$\begin{cases} N \to \infty \\ t_i - t_i^c = N^{\alpha_i}\tilde{t}_i. \end{cases} \tag{5.45}$$

In this double scaling limit, we transform the family $(\psi_{k,N}(x))_{k\geq 0}$ into the function of two variables $u(s, x)$, with $s = \frac{k}{N}$. The operators P and Q are then differential operators in the variable s. Tuning the parameters of the matrix model in a specific way, we reach the so-called $(3, 2)$ minimal model, described in chapter V, and the operators take the form:

$$\begin{cases} Q = \partial_s^2 - 2v_0(s, N) \\ P = \partial_s^3 - 3v_1(s, N)\partial_s + v_2(s, N). \end{cases} \tag{5.46}$$

Those equations will be discussed later in the continuous limit of Strebel graphs.

Part III

Local properties of the random Delaunay triangulation model and topological models of 2D gravity

We stressed in the introductory part (see section 4), that there are several ways to study the continuous limit of maps, and our approach is to study the convergence of random maps as probabilistic spaces. For a given model of random maps and at the discrete level, *i.e.* for a given size of maps, the probabilistic space is constructed by putting a measure on the set of maps of given size. Then, a natural way to study the probabilistic space constructed on random maps is to study the measure. This is the aspect addressed in this part.
In order to do so, we introduce the model of Delaunay triangulations and the associated measure. This model has already been studied by David and Eynard [David and Eynard, 2014] and we recall some of their results that we shall use in the following. The results of this part are of two kinds. The first result relates the measure over Delaunay triangulations with the Weil-Petersson measure on the moduli space of punctured Riemann surfaces. The notion of moduli space is briefly reviewed to fit our purposes. This result allows to relate our combinatorial problem to a well studied problem of geometry. The second kind of results concerns more local properties of the measure, as preliminary steps to study the continuous limit of the measure. The results of this chapter are based on the article [II].

6 Delaunay triangulations

6.1 Circle patterns and Delaunay triangulations

Triangulations of the sphere are planar maps such that every face has degree 3. We restrict the set of triangulations to maps which do not contain any self loop or double edges (two edges joining the same vertices). For instance, the situation of figure 24 is forbidden. Let us call $\mathcal{T}_n$ this restriction of the set of triangulations of the sphere with n vertices. In this chapter, the size of a triangulation is the number of vertices. For $T \in \mathcal{T}_n$, let us note $\mathcal{V}(T)$, $\mathcal{E}(T)$ and $\mathcal{F}(T)$ respectively the sets of vertices, edges and faces of T. T is planar, so the Euler relation gives $|\mathcal{V}(T)| - |\mathcal{E}(T)| + |\mathcal{F}(T)| = 2$. As T is a triangulation, we also know that $|\mathcal{F}(T)| = 2|\mathcal{E}(T)|$. Then the sizes of those sets

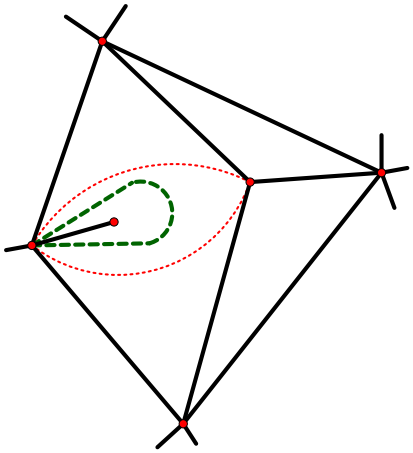

Figure 24: Part of a triangulation: all the faces are triangles (the dotted and dashed edges are taken into account). The green dashed edge is a self loop: the ends of the edge is a single vertex. The red dotted edges are double edges: they are adjacent to the same vertices.

are:

$$\begin{cases} |\mathcal{V}(T)| = n \\ |\mathcal{E}(T)| = 3n - 6 \\ |\mathcal{F}(T)| = 2n - 4. \end{cases} \tag{6.1}$$

A triangulation $T \in \mathcal{T}_n$ is an abstract triangulation, in the sense that it contains only information on the structure of the triangulation – the adjacency relations between vertices, the order of the half-edges –, and not on the embedding in the Riemann sphere $\mathbb{S}_2 = \mathbb{C} \cup \{\infty\} = \overline{\mathbb{C}}$ – that is to say the way to represent the map on the sphere. For a given triangulation, there are infinitely many ways to embed it in the sphere. In this chapter, two equivalent approaches are employed to describe the problem of Delaunay triangulations. The first one starts from an abstract triangulation, and by solving a circle pattern problem, embed it in the Riemann sphere. The second one takes a configuration of points as a support for drawing triangulations, and consists in finding a Delaunay triangulation.

6.1.1 Circle patterns

The circle packing problem, solved by Koebe [Koebe, 1936], is the following: let $T \in \mathcal{T}_n$, is there a way to embed T in a complex domain, such that to each vertex $v \in \mathcal{V}(T)$ is associated a circle $\mathscr{C}_v$, centered at v, tangent to all the neighboring circles $\mathscr{C}_{v'}$ with v' adjacent to v, and intersecting no other circle ? By Koebe-Andreev-Thurston theorem [Koebe, 1936], it is possible. Circle pattern problems are extensions of circle packing. In the one considered here, and solved by Rivin [Rivin, 1994], the circles

$\mathscr{C}_f$ are circumcircles of the faces f – that are triangles. Then, we endow each edge $e \in \mathcal{E}(T)$ with an angle $\theta(e) \in \mathbb{R}$, where $\theta : \mathcal{E}(T) \to \mathbb{R}$. Let us note $\tilde{T} = (T, \theta)$, and call the set $\boldsymbol{\theta} = \theta(e); e \in \mathcal{E}(T)$ the angle pattern. The problem is the following: is it possible to find an embedding of the triangulation, such that

- the interior of the circle $\mathscr{C}_f$ of a face does not contain any vertex of the triangulation ;
- the circles $\mathscr{C}_f$, $\mathscr{C}_{f'}$ of two adjacent faces separated by an edge e, intersect with an angle $\pi - \theta(e)$?

By Rivin's theorem [Rivin, 1994], the embedding exists and is unique up to Möbius transformations for admissible flat Euclidean triangulations. The proof relies on the minimization of a functional. We present this theorem hereafter. First, let us define the set of admissible flat Euclidean triangulations:

Definition 6.1. *An Euclidean triangulation $\tilde{T} = (T, \theta)$ is a triangulation T plus an associated edge angle pattern $\boldsymbol{\theta}$, such that*

$$0 \leq \theta(e) < \pi \ . \tag{6.2}$$

An Euclidean triangulation is flat *if for each vertex $v \in \mathcal{V}(T)$, the sum of the angles of the adjacent edges satisfy*

$$\sum_{e \to v} \theta(e) = 2\pi \tag{6.3}$$

A flat Euclidean triangulation is admissible *if for any closed oriented contour $\mathcal{C}^\star$ on the dual graph $T^\star$ of the triangulation T, the sum of the angles associated to the edges e dual (orthogonal) to the edges $e^\star$ of $\mathcal{C}^\star$ satisfy*

$$\sum_{e \perp \mathcal{C}^\star} \theta(e) \geq 2\pi \tag{6.4}$$

The set of admissible flat Euclidean triangulations of size n is denoted by $\widetilde{\mathcal{T}}_n^f$.

Those conditions are represented in figure 25. The flatness condition is not required for Rivin theorem, but it is the framework we use to study Delaunay triangulations. Allowing different sums around a vertex in equation 6.3, that is $\sum_{e \to v} = \Phi_v$, is equivalent to embed a triangulation on a sphere having conical singularities located at the vertices. This generalization will be discussed in the end of chapter IV. For the moment, we shall require equation 6.3 to hold. For a triangulation $\tilde{T} = (T, \theta) \in \widetilde{\mathcal{T}}_n^f$, we can distinguish the structure $T \in \mathcal{T}_n$ of $\tilde{T}$, and the angular part θ. For a given size n, there are finitely many structures of triangulations. Yet, for a given T, there are

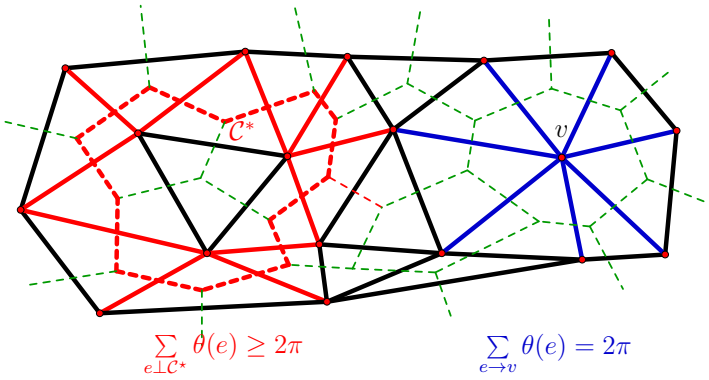

Figure 25: Part of a triangulation (plain lines), along with its dual graph (dashed lines). On the left hand side, the condition of equation 6.4 is shown. The contour $\mathcal{C}^*$ of the dual graph is in red thick dashed lines. The sum runs over the red plain edges that cross the contour. On the right hand side, the condition 6.3 concerns the sum over the blue plain edges around the vertex v.

infinitely many angle patterns which match equations 6.2, 6.3 and 6.4. Let us call $\widetilde{\mathcal{T}}_n^f(T_0) = \{\tilde{T} \in \widetilde{\mathcal{T}}_n^f, \tilde{T} = (T_0, \theta)\}$ the cell associated to the structure T. Then the set $\widetilde{\mathcal{T}}_n^f$ can be decomposed in cells, indexed by the structure of the triangulations:

$$\widetilde{\mathcal{T}}_n^f = \bigsqcup_{T\in\mathcal{T}_n} \widetilde{\mathcal{T}}_n^f(T) \tag{6.5}$$

Let us compute the dimension of each cell. For $\tilde{T} \in T \in \mathcal{T}_n(T)$, there are $|\mathcal{E}(T)| = 3n-6$ real angles $\theta(e)$ and $|\mathcal{V}(T)| = n$ constraints, so there are $2n-6$ free real angles. Therefore, $\dim_{\mathbb{R}}(\widetilde{\mathcal{T}}_n^f(T)) = 2n-6$.
The theorem of Rivin allows to solve the circle pattern problem:

Theorem 6.1. *[Rivin, 1994] There exist a unique embedding, up to Möbius transformations, of an admissible flat Euclidean triangulation $\tilde{T}$ in the compactified complex plane $\overline{\mathbb{C}}$, such that the circumcircles of adjacent faces f, f' separated by the edge e intersect with angle $\theta^*(e) = \pi - \theta(e)$, and such that the interior of any circumcircle $\mathscr{C}_f$ does not contain any vertex.*

Möbius transformations are the automorphisms of the Riemann sphere, they correspond to transformations:

$$z \mapsto \frac{az+b}{cz+d}, \qquad a,b,c,d \in \mathbb{C}, \qquad ad-bc = 1 \tag{6.6}$$

We identify (a,b,c,d) with $(-a,-b,-c,-d)$. A Möbius transformation is equivalent to the data of the matrix

$$m = \begin{pmatrix} a & b \\ c & d \end{pmatrix}, \qquad m \in PSL_2(\mathbb{C}), \tag{6.7}$$

so the group of Möbius transformations is identified with $PSL_2(\mathbb{C})$.

In figure 26, the angles $\theta(e)$, $\theta^*(e)$ associated to the edge e are shown in the embedding

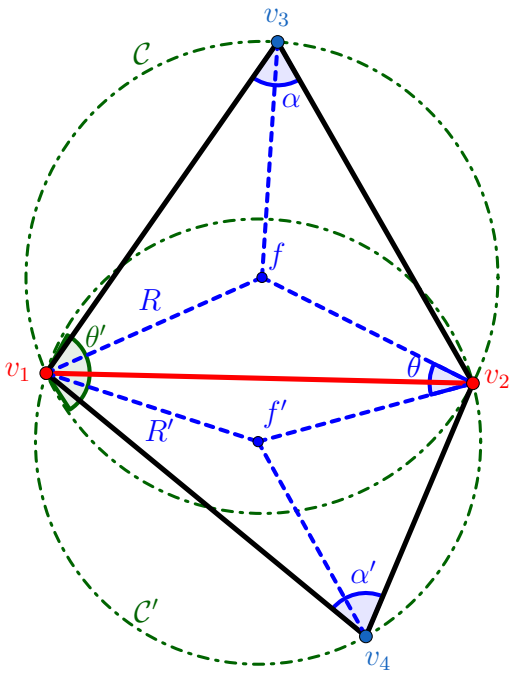

Figure 26: The triangles f and f', the circumcircles $\mathcal{C}$ and $\mathcal{C}'$ and angles θ and $\theta' = \pi - \theta$ associated to an edge $e = (v_1, v_2)$ of a Delaunay triangulation. Here, R and R' are the radii of $\mathcal{C}$ and $\mathcal{C}'$ respectively.

corresponding to the circle pattern.

Some care must be given to the notion of interior of a circle here. Indeed, in the Riemann sphere $\mathbb{C} \cup \{\infty\}$, the point at infinity is included. There are then two cases for the embedding chosen:

- either there is a vertex at infinity ;
- or ∞ belongs to a face of the triangulation.

It is always possible, by a Möbius transform, to be in the second case. Let us call f_∞ the face which contains ∞. Let us say that it is the face of the vertices v_1, v_2, v_3. If one draws the circumcircle of f_∞, then the interior is the domain of $\overline{\mathbb{C}}$ containing ∞. This means that all the vertices must be located in the disc defined by the circumcircle. The situation is depicted in figure 27.

A triangulation embedded in the compactified complex plane such that no vertex is located in the interior of any circumcircle is called a Delaunay triangulation. Such

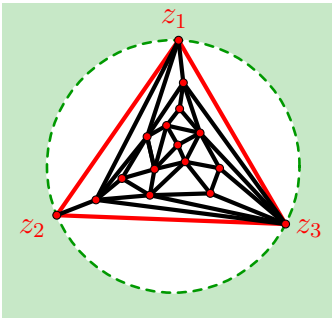

Figure 27: If the point at infinity is in the face (z_1, z_2, z_3), the interior of the circumcircle associated to this face (green dashed line), is the region shown in green.

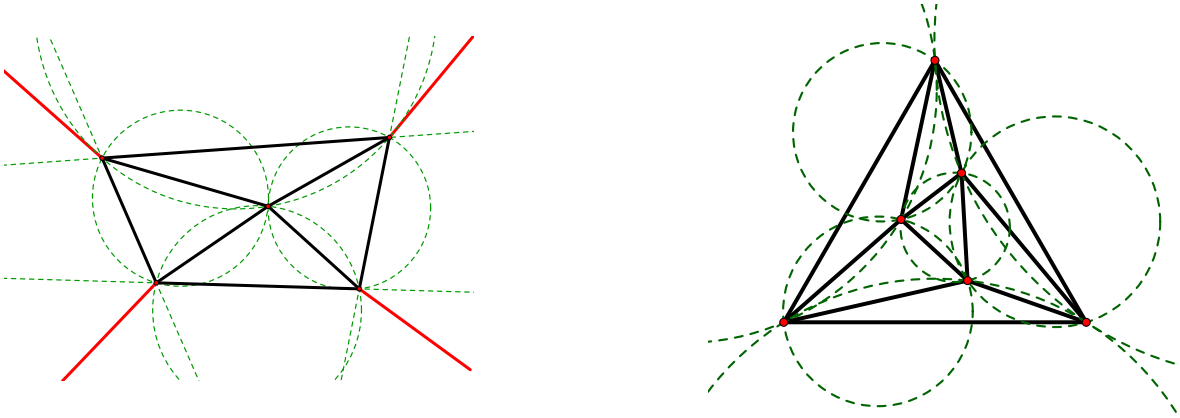

Figure 28: Two examples of Delaunay triangulations of size 6. In the first case, a point of the triangulation is at infinity, and is linked to four points by red edges. In the second case, the point at infinity is inside a face. The dashed circles are the circumcircles of the faces. No vertex belongs to the interior of a circumcircle.

triangulations are shown in figure 28 (the two cases for the point at infinity are represented).

As it was mentioned previously, the proof of Rivin theorem relies on a variational principle. We excluded self loops in triangulations, so every edge e separates two distinct faces f_1, f_2, so we may write $e = (f_1, f_2)$. For what follows, the ordering induced by the labels does not matter. Let us consider any embeddding – which does not match the conditions for the circle pattern problem a priori – of the triangulation $\tilde{T} \in \widetilde{\mathcal{T}}_n^f(T)$. This embedding is the data of the positions $\mathbf{z} = \{z_1, \dots, z_n\}$ of the vertices of the triangulation in the complex plane. For such a configuration of points, the radius of the circumcircle of face f is denoted by r_f. Then, the functional used by Bobenko and Springborn associates an energy to the embedding by the formula:

$$S((T,\theta);\mathbf{z}) = \sum_{e=(f_1,f_2)\in\mathcal{E}(T)} \left(\mathrm{ImLi}_2\left(\frac{r_{f_1}}{r_{f_2}}e^{\mathrm{i}\,\theta(e)}\right) + \mathrm{ImLi}_2\left(\frac{r_{f_2}}{r_{f_1}}e^{\mathrm{i}\theta(e)}\right) - (\pi-\theta(e))\ln(r_{f_1}r_{f_2})\right)$$

$$+2\pi \sum_{f \in \mathcal{F}(T)} \ln(r_f). \tag{6.8}$$

The function Li_2 is the dilogarithm, see appendix A for the definition. The fact that the order of the indices for the faces is irrelevant, is manifest in the formula. Bobenko and Springborn [Bobenko and Springborn, 2004] showed that the configurations of points $z_1, \ldots, z_n$ which solve the circle pattern problem exposed above are the minima of this functional. This formula shows that circle patterns minimize an energy involving the dilogarithm, a feature that we shall recognize later in this chapter.

6.1.2 Delaunay triangulations

The second equivalent approach consists in stating the problem in the reverse manner. Let us take $n \geq 3$ distinct points $z_1, \ldots, z_n \in \overline{\mathbb{C}}$. By a Möbius transform, we can fix $(z_1, z_2, z_3) = (0, 1, \infty)$. The problem is then the following: is there a Delaunay triangulation T^D whose vertices are $\{z_1, \ldots, z_n\}$? Indeed, for a generic triangulation T having $z_1, \ldots, z_n$ as vertices, there are vertices located inside the interior of some circumcircle, so it is not a Delaunay triangulation. However, it is always possible to construct a Delaunay triangulation out of a configuration of points on the Riemann sphere. There exist several algorithms to build the Delaunay triangulation of a configuration of points. As we will use one of these algorithms in this chapter, we describe it here, and it relies on the Lawson flip algorithm (LFA). The Delaunay algorithm is taken from [Brévilliers, 2008], and the Lawson flip algorithm was first described by Lawson [Lawson, 1972].

Initialization: first, draw the convex hull of the points $0, 1, z_4, \ldots, z_n$. Draw an edge between all the vertices belonging to the convex hull and the point at infinity. Then, draw a planar triangulation of the points $0, 1, z_4, \ldots, z_n$, such that the edges of the convex hull are edges of the triangulation (see figure 29). We obtain a triangulation T_0 of the points $0, 1, \infty, z_4, \ldots, z_n$, which is not a Delaunay triangulation in general. Consider an edge $e \in \mathcal{E}(T_0)$, which links the vertices v, w. It separates two faces f_1^e, f_2^e. The faces f_1^e, f_1^e are the triangles (v, w, x_1) and (v, w, x_2) respectively. One can draw the circumcircles $\mathscr{C}_{f_1^e}$, $\mathscr{C}_{f_2^e}$ of those faces. Then, the edge e is said *illegal* if x_1 is in the interior of $\mathscr{C}_{f_2^e}$, and x_2 is in the interior of $\mathscr{C}_{f_1^e}$. In the triangulation T_0, identify all the illegal edges. By construction, the edges adjacent to ∞, and the edges of the convex hull are not illegal. If there is no illegal edge, then T_0 is a Delaunay triangulation. Else, let us note $e_1, \ldots, e_m$ those illegal edges.

Steps of the algorithm: from the triangulation T_0, we construct successively the triangulations $T_1, \ldots, T_k = T^D$. The step $T_i \to T_{i+1}$ is described. Choose an illegal edge $e_i = (b^i, c^i) \in \mathcal{E}(T_i)$, separating the faces (a^i, b^i, c^i) and (d^i, b^i, c^i). Then, perform the Lawson flip for this edge (see figure 30). It transforms the edge $e_i = (b^i, c^i)$ into

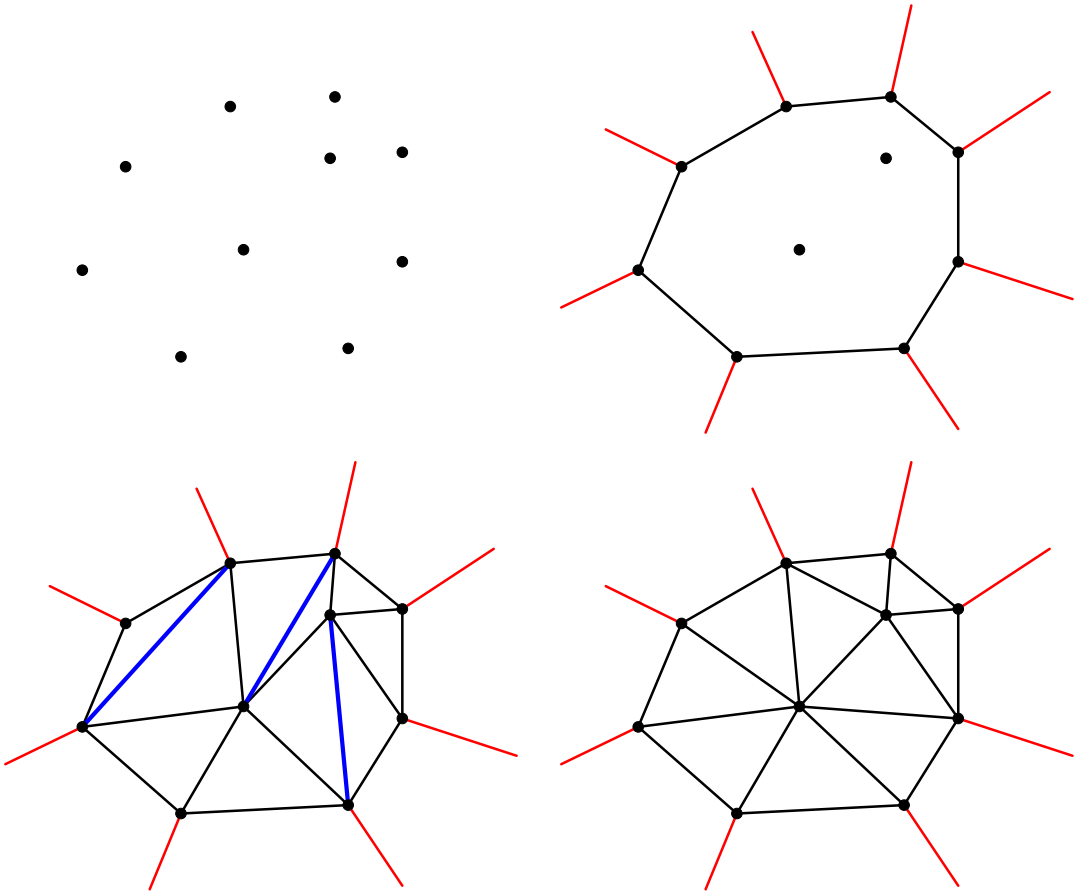

Figure 29: We begin with a configuration of 11 points (one is at ∞) in the plane (top left corner). We draw the convex hull of the points, and link the outer points to ∞ (red lines in the top right corner). Then, we draw a generic triangulation in the convex hull. The illegal edges are identified in blue (bottom left corner). In the end, the graph is a Delaunay triangulation (bottom right corner).

$e'_i(a^i, d^i)$, which is not illegal anymore. The triangulation T_{i+1} is the triangulation obtained after the flip (see [Brévilliers, 2008]).

Final step: in the end, one obtains a triangulation T_k which does not contain any illegal edge, and this triangulation is precisely the Delaunay triangulation T^D of the points $0, 1, \infty, z_4, \ldots, z_n$.

Once this Delaunay triangulation T^D is constructed, the angle $\theta^*(e) = \pi - \theta(e)$ associated to the edge $e \in \mathcal{E}(T^D)$ is the angle of intersection of the circumcircles of the adjacent faces (see figure 26). For a generic configuration of points, the Delaunay triangulation is unique. Yet, if four vertices a, b, c, d of the triangulation are cocyclic, there are two choices to define the Delaunay triangulation (see figure 31). In this special

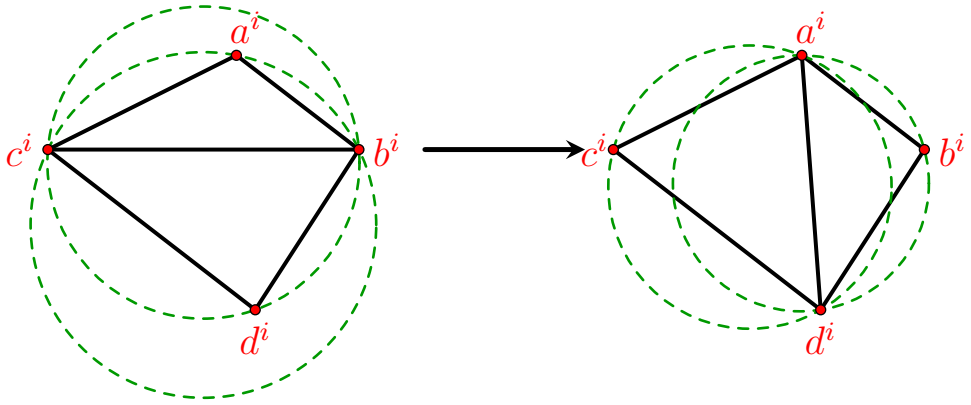

Figure 30: Effect of a flip at one step of the Lawson Flip Algorithm. The illegal edge is flipped.

case, the angle $\theta(e)$ associated to the internal edge is null. This situation is specific, so for the following reasoning, let us consider a generic set of points such that the Delaunay triangulation is unique. A configuration of distinct points $\mathbf{z} = \{0, 1, \infty, z_4, \dots, z_n\}$ determines a single Delaunay triangulation $T^D(\mathbf{z})$, from which we deduce an angle pattern $\boldsymbol{\theta}(\mathbf{z})$. Therefore, we started with an embedding, that is to say the points $\mathbf{z}$, and we ended with a triangulation $T^D(\mathbf{z})$ along with an angle pattern $\boldsymbol{\theta}(\mathbf{z})$. It is easy to check that this angle pattern satisfies conditions 6.2, 6.3 and 6.4. So we considered here the reverse problem of previous section. The free parameters in this approach are the positions of the points $z_4, \dots, z_n$. So there are $2(n-3) = 2n-6$ free real parameters. It corresponds to the dimension of a cell $\dim_{\mathbb{R}}(\widetilde{\mathcal{T}}_n^f(T))$ in the other approach, so it is consistent.
For $n \geq 3$, let us call $\mathfrak{D}_n = \{\{0, 1, \infty, z_4, \dots, z_n\} \in \mathbb{C}^n | z_i \neq z_j \text{ for } i \neq j\} \subset \mathbb{C}^{n-3}$ the set of Delaunay triangulations of the plane. In the end, there is a bijection:

$$\widetilde{\mathcal{T}}_n^f \leftrightarrow \mathfrak{D}_n.$$

When we refer to Delaunay triangulations, we equivalently consider elements of $\widetilde{\mathcal{T}}_n^f$ or $\mathfrak{D}_n$.
A Delaunay triangulation is dual to a Voronoï tessellation: given $\tilde{T} \in \widetilde{\mathcal{T}}_n^f$, whose embedding in the Riemann sphere has vertices at $z_1, \dots, z_n$. The centers of the circumcircles of the faces are noted $c_1, \dots, c_{2n-4}$. Then, the dual graph $\tilde{T}^*$ of the Delaunay triangulation, drawn with straight lines between the vertices c_i, is the Voronoï tessellation of the points $z_1, \dots, z_n$.

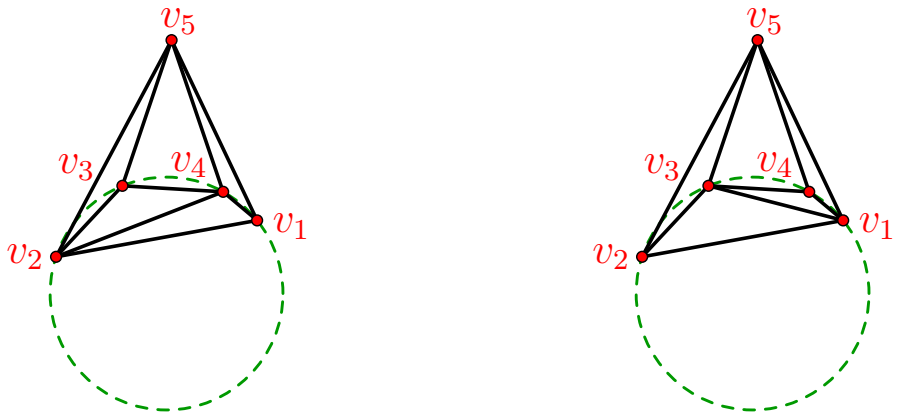

Figure 31: If 4 points of the triangulation are cocyclic (here v_1, v_2, v_3, v_4), there are two choices for the Delaunay triangulation: if one flips the edge (v_2, v_4) (left hand side) into (v_1, v_3) (right hand side), the graph remains a Delaunay triangulation.

6.2 Metric associated to a Delaunay triangulation

In the view of quantum gravity, a triangulation of the sphere of size n and its embedding represent an instance of a "discretized" metric. This discretized metric associated to a triangulation can be defined in various ways, one is discussed here. The term "discretized" used here does not mean that the metric must have discrete values on the triangulation. It means that it is defined on a discretized surface (a triangulation of size n), rendering the space of functions defined on this surface of finite dimension. Let us take $n \geq 3$.

To any Delaunay triangulation $\tilde{T}$ with n points on the complex plane, we can associate an explicit surface $\mathcal{S}$ with constant negative curvature and n punctures as follows. Let $\mathbb{H}_3 = \mathbb{C} \times \mathbb{R}_+^*$ be the upper half-space above $\mathbb{C}$, with coordinates (z, h) embodied with the Poincaré metric $ds^2 = (dzd\bar{z} + dh^2)/h^2$. It makes $\mathbb{H}_3$ the 3-dimensional hyperbolic space, with $\mathbb{C} \cup \{\infty\}$ its asymptotic boundary at infinity. Consider a triangle f_{123} with vertices $(1, 2, 3)$ (in counter clockwise order) with complex coordinates (z_1, z_2, z_3) in $\mathbb{C}$. Let $\mathcal{B}_{123}$ be the hemisphere in $\mathbb{H}_3$ whose center is the center of the circumcircle of f_{123} (in $\mathbb{C}$), and which contains the points $(1, 2, 3)$. $\mathcal{B}_{123}$, embodied with the restriction of the Poincaré metric ds^2 of $\mathbb{H}_3$, is isometric to the 2 dimensional hyperbolic disk $\mathbb{H}_2$. Let $\mathcal{L}_{12}$ be the intersection of $\mathcal{B}_{123}$ with the half plane orthogonal to $\mathbb{C}$ which contains the points 1 and 2, this is a semicircle orthogonal to $\mathbb{C}$. With a similar definition for (23) and (31), the semicircles $\mathcal{L}_{12}$, $\mathcal{L}_{23}$ and $\mathcal{L}_{31}$ delimit a spherical triangle $\mathcal{S}_{123}$ on the hemisphere in $\mathbb{H}_3$. The semicircles $\mathcal{L}_{12}$, $\mathcal{L}_{23}$ and $\mathcal{L}_{31}$ are geodesics in $\mathbb{H}_3$, hence in $\mathcal{B}_{123}$, so that $\mathcal{S}_{123}$ is an ideal triangle in $\mathbb{H}_2$. $\mathcal{S}_{123}$ is nothing but the face (123) of the ideal

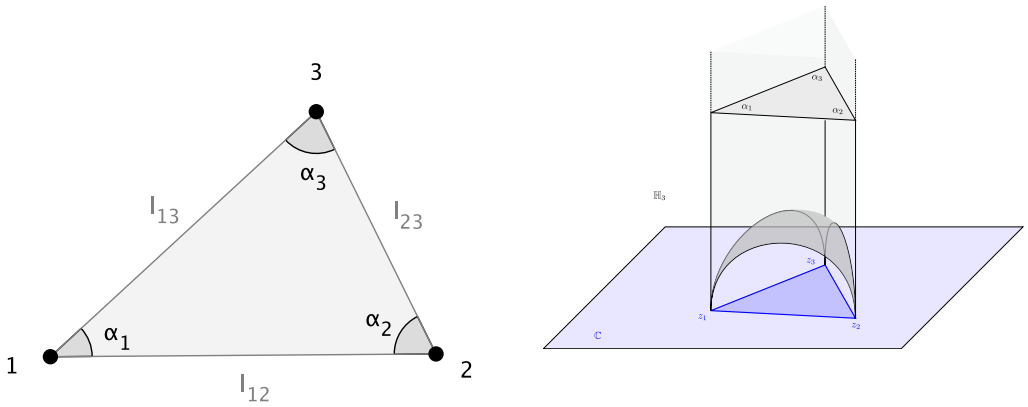

Figure 32: A triangle $f = (1, 2, 3)$ (left) and the associated ideal spherical triangle $\mathcal{S}_{123}$ in $\mathbb{H}_3$ (right).

tetraedra (z_1, z_2, z_3, ∞) in $\mathbb{H}_3$, see figure 32.

Now consider a Delaunay triangulation $\tilde{T}$ in the plane, with n points, and with one point at infinity for simplicity. The union of the ideal spherical triangles $\mathcal{S}_f$ associated to the faces f of $\tilde{T}$ form surface $\mathcal{S}$ in $\mathbb{H}_3$

$$\mathcal{S} = \bigcup_{f \in \mathcal{F}(T)} \mathcal{S}_f \tag{6.9}$$

See figure 33. The surface $\mathcal{S}$ embodied with the restriction of the Poincaré metric of $\mathbb{H}_3$, is a constant negative curvature surface. Indeed since the triangles $\mathcal{S}_f$ are glued along geodesics, no curvature is localized along the edges of these triangles. It is easy to see that the endpoints z_i of the triangulations are puncture curvature singularities of $\mathcal{S}$, i.e. points where the metric can be written (in local conformal coordinates with the puncture at the origin)

$$ds^2 = \frac{dw d\overline{w}}{|w|^2 |\log(1/|w|)|^2} \tag{6.10}$$

Through the orthogonal projection from $\mathcal{S}$ to the plane $\mathbb{C}$, the metric in each $\mathcal{S}_f$ become the standard Beltrami-Cayley-Klein hyperbolic metric in the triangle f. We recall that it is defined in the unit disk $\mathbb{D}_2 = \{z; |z| < 1\}$ in radial coordinates as

$$ds^2_{\mathscr{B}.} = \frac{dr^2 + r^2 d\theta^2}{(1 - r^2)} + \frac{(r\, dr)^2}{(1 - r^2)^2} \tag{6.11}$$

that it is not conformal, and is such that geodesics are straight lines in the disk. This is an example of continuous metrics defined by a triangulation, which has singularities at the vertices. It will be used to prove the link between the measure on the set

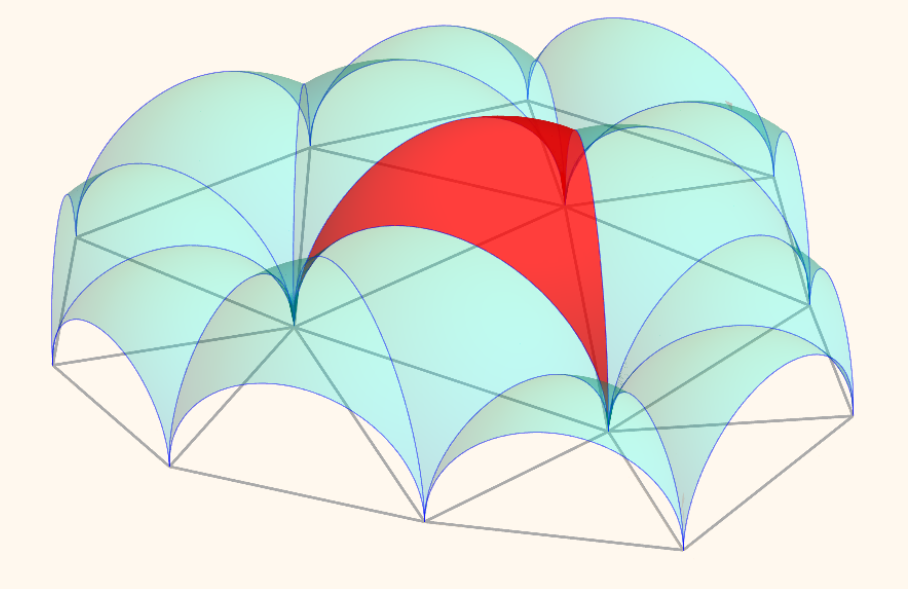

Figure 33: A triangulation and the associated punctured surface

of Delaunay triangulations, and the Weil-Petersson volume form on a moduli space. Having this natural metric allows also to define a natural distance on the dual of a Delaunay triangulation. This is discussed in section 6.4.

6.3 Measure on the Delaunay triangulations

Each discretized metric of size n – associated to a triangulation of size n – has a probability of apparition. Actually, the set of admissible flat Euclidean triangulations of size n has dimension $2n-6$, so we must give a probability distribution to the set of triangulations. This is the meaning of the measure $d\nu$ we put on $\widetilde{\mathcal{T}}_n^f$. As there are two approaches to describe the Delaunay triangulations, there are two equivalent measures $d\nu$ and $d\tilde{\nu}$ on $\widetilde{\mathcal{T}}_n^f$ and $\mathfrak{D}_n$ respectively, according to which approach we use.
Following the works of David and Eynard [David and Eynard, 2014], the measure on the set $\widetilde{\mathcal{T}}_n^f$ is given by:

$$d\nu_n(\widetilde{T}) = d\nu_n(T,\theta) = \text{uniform}(T) \prod_{e\in\mathcal{E}(T)} d\theta(e) \prod_{v\in\mathcal{V}(T)} \delta\Big(\sum_{e\mapsto v}\theta(e)-2\pi\Big) \prod_{\mathcal{C}^\star} \Theta\Big(\sum_{e\perp\mathcal{C}^\star}\theta(e)-2\pi\Big) \tag{6.12}$$

where, $\Theta(x) = \begin{cases} 1 \text{ if } x \geq 0 \\ 0 \text{ if } x < 0 \end{cases}$ is the Heaviside function, and the notation $e \to v$ means that the sum runs over the edges adjacent to vertex v. It is the flat Lebesgue measure on the admissible flat Euclidean triangulations. When expressed in terms of the configurations of points in $\mathfrak{D}_n$, this measure is not the Lebesgue measure on $\mathbb{C}^{n-3}$, but it

rather writes:

$$d\nu_n(T,\theta) = d\tilde{\nu}_n(\mathbf{z}) \quad = \quad \mathcal{D}^T_{\{i,j,k\}}(\mathbf{z}) \prod_{\substack{v=1 \\ v\neq i,j,k}}^{n} d^2 z_v, \tag{6.13}$$

where $\mathcal{D}^T_{\{i,j,k\}}(\mathbf{z})$ is the Jacobian to switch from the variables $\theta(e)$ to the points z_v of the embedding. The Jacobian depends on the structure of the triangulation T, hence the superscript ; and it depends on which points are fixed by a Möbius transform. Here, we consider that the points z_i, z_j, z_k are kept fixed, this is why the subscript is $\{i,j,k\}$.
The volume of $\widetilde{\mathcal{T}}^f_n$ computed with the measure $d\nu_n$ is finite, as it is bounded by $\pi^{3n-6} \times |\mathcal{T}_n|$, where the number of triangulations $|\mathcal{T}_n|$ is finite, so the measure $d\nu_n$ enables us to endorse $\widetilde{\mathcal{T}}^f_n$ with a probability distribution. Let us note $V_n^{\mathscr{D}} = \int_{\widetilde{\mathcal{T}}^f_n} d\nu_n(T,\theta)$ the volume of the set of admissible flat Euclidean triangulations of size n. The probability distribution of a triangulation $\tilde{T}_0 = (T_0, \theta_0) \in \widetilde{\mathcal{T}}^f_n$ is given by $\frac{d\nu_n(\tilde{T}_0)}{V_n^{\mathscr{D}}}$.
Let us stress the fact that, for fixed n, the measure $d\nu_n(T,\theta)$ is admissible. Indeed, for a given triangulation, if one integrates the volume $d\nu_n$ over the configurations of the parameters $\theta(e)$, it is obvious that:

$$\int_{T \text{ fixed}} d\nu_n(T,\theta) \leq \text{uniform}(T)\, \pi^{2n-6}. \tag{6.14}$$

As the number of simple triangulations of size n is finite, the volume of Delaunay triangulations measured with $d\nu_n$ is finite. Hence, the measure $d\nu_n$ is admissible.

6.4 Study of the measure

This chapter is dedicated to the study of the measures $d\nu_n(T,\theta) = d\tilde{\nu}_n(\mathbf{z})$. Along the computations we carry out, we may switch from one representation to another, according to their convenience. The study carried out here has two sides. On the one hand, we study the measure for n fixed, in order to relate it to a well-known formalism, which is the Weil-Petersson measure on the moduli space $\overline{\mathcal{M}}_{0,n}$ of Riemann surfaces. This result allows to compute explicitly the volume of $\widetilde{\mathcal{T}}^f_n$, and correlation functions of the Delaunay triangulations that depend only on the topology (and not on metric properties). On the other hand, the study addresses the properties of the measures when n changes. The ultimate goal is to study the continuous limit of the model, that is to say the limit $n \to \infty$ in one of the meanings given in the introduction. Since we saw two mathematical meanings for the concept of "continuous limit", let us briefly discuss those meanings in order to defuse the possible confusion.

Random metrics: One may first consider our model as a model of *random Riemannian metrics* on the plane. Indeed, if one looks at a configuration of distinct points $\{z_1, \dots, z_n\}$ on the Riemann sphere and adds progressively points $z_{n+1}, z_{n+2}, \dots$, we have seen in section 6.2 that at each step, one can embody each triangle of the Delaunay triangulation with its natural Beltrami hyperbolic metric. This will happen to be a useful tool to prove the relation with Weil Petersson measure. It gives a global metric which is hyperbolic but has puncture singularities at the points z_i (see equation 6.10). Since the punctures are at infinite distances, and the metric is not compact, there is clearly no hope, even with an ad hoc rescaling of the metric, that the space of triangulations equipped with the Beltrami metric has a limit in the Gromov-Hausdorff sense when $n \to \infty$.

However, in order to have a chance of convergence and by analogy with the random planar map model, one may rather consider random *discrete metrics spaces* constructed from the random triangulations. Here is an eligible example of discrete metric space associated to a Delaunay triangulation and using the Beltrami metric defined previously. Consider the random Voronoï graph $T^\star$, dual to the random Delaunay triangulation T, whose vertices are the centers (with coordinates ω_f) of the circumcircles to the faces (the triangles) f of the triangulation T. An edge $e^\star = (\omega_f, \omega_{f'})$ of $T^\star$ is dual to an edge of T, since it is the straight segment between the centers of two faces f and f' adjacents to an edge $e = (z_{v_1}, z_{v_2})$ of T (with the notations of figure 26). This dual edge $e^\star$ is in fact a geodesic in the global hyperbolic Beltrami metric, with length

$$\ell(e^\star) = \frac{1}{2} \log \left(\frac{(1+\sin(\theta_m))(1+\sin(\theta_s))}{(1-\sin(\theta_m))(1-\sin(\theta_s))} \right) \tag{6.15}$$

where $\theta_m = \mathrm{Arg}((w_f - z_{v1})/(z_{v_2} - z_{v_1}))$ is the angle between the vectors (v_1, v_2) and (v_1, f) while $\theta_s = \mathrm{Arg}((z_{v_2} - z_{v_1})/w_{f'} - z_{v_1}))$ is the angle between the vectors (v_1, f') and (v_1, v_2). This defines a distance function $d_{T^\star}$ on the Voronoï graph $T^\star$, and this mapping $T^\star \to d_{T^\star}$ is continuous on the space of Delaunay triangulations with n points, since it is continuons when one performs a flip. Indeed an edge e is flipped if $\theta(e) = \theta_m + \theta_s = 0$, hence when $l(e^\star) = 0$. The distance is defined between two vertices $\omega_1, \omega_2 \in \mathcal{V}(T^*)$ by the first passage percolation distance:

$$d_{T^*}(\omega_1, \omega_2) = \min_{\gamma \text{ path in } T^*} \sum_{e^* \in \mathcal{E}(\gamma)} l(e^*), \tag{6.16}$$

where the paths γ join the vertices ω_1 and ω_2. Other natural choices of edge lengths can be done for Delaunay triangulations. For instance, one can assign to an edge e^* the length:

$$\ell(e^*) = \theta(e), \tag{6.17}$$

defining this way another first passage percolation distance d'_{T^*}. The mapping $T^* \to d_{T^*}$ is still continuous on the space of Delaunay triangulations with n points, since an edge e is flipped when $\theta(e) = \ell(e^*) = 0$. A natural conjecture, is that for those metric spaces (for the distances d_{T^*} and d'_{T^*}), the large n limit makes sense and is in the same universality class as the random planar map model, namely that $(T^\star, n^{-1/4} d_{T^\star})$, considered as a random (discrete) metric space, converges in the Gromov-Hausdorff sense towards the Brownian map as in LeGall [Le Gall, 2013] and Miermont [Miermont, 2013]. However, this is not the convergence we are tackling in this chapter. We mention those natural discrete metrics for future developments.

Random (conformal) measures: Secondly, one may rather consider our model as a model of *random measures* on the plane, to study the convergence as probability space. This is the point of view developed in the introduction, that we use in this work, and this is the one relevant when discussing the relation between the continuum limit of our model, or of random maps, with the Liouville quantum gravity. Indeed, in the Liouville theory the Liouville field ϕ_L defines by its exponential $\exp(\gamma\phi_L)$ random measures with fascinating multifractal properties linked to multiplicative chaos theory (see for instance [David et al., 2015] and references therein), and conformal invariance. It is for instance expected that the moments of the *local density* of points $\rho(z)^\beta$ are related to the local vertex operators $\exp(\alpha\phi_L(z))$ in the Liouville theory.

For the rest of the chapter, we suppose that $n \geq 3$, so that the notion of Delaunay triangulation is well-defined, and so that the group of automorphisms of $(\overline{\mathbb{C}}; \{z_1, \dots, z_n\})$ is finite.

6.5 Known results

The results presented in this chapter are a continuation of the work of David and Eynard. They showed several properties of the measures $d\nu_n$, $d\tilde{\nu}_n$, that are useful in the proof of our results. We present them in this section, all the following theorems are from their article [David and Eynard, 2014]. The size of the triangulations is supposed to be greater than 3. The first three results concern the measure $d\tilde{\nu}_n$, that is to say the Delaunay triangulations viewed from configurations of points, whereas the last result deals with the angular form of the measure $d\nu_n$.
First, we define the *hyperbolic volume* of the face and the *prepotential*. $\mathcal{A}_T(\mathbf{z})$.

Definition 6.2. *For a triangle f with (counter clockwise oriented) vertices (z_a, z_b, z_c), the hyperbolic volume* $\mathrm{Vol}(f)$ *in the hyperbolic upper half space $\mathbb{H}^3$ of the ideal tetraedron*

with vertices (z_a, z_b, z_c, ∞) *on its boundary (see figure 32) is given by:*

$$\mathrm{Vol}(f) = \mathrm{ImLi}_2\left(\frac{z_c - z_a}{z_b - z_a}\right) + \ln\left|\frac{z_c - z_a}{z_b - z_a}\right| \mathrm{Arg}\left(\frac{\mathrm{z_c} - \mathrm{z_b}}{\mathrm{z_a} - \mathrm{z_b}}\right). \tag{6.18}$$

For a triangulation T *of the points* $\mathbf{z} = \{z_1, \ldots, z_n\}$*, the prepotential* $\mathcal{A}_T(\mathbf{z})$ *is the sum of the hyperbolic volumes associated to the faces:*

$$\mathcal{A}_T(\mathbf{z}) = -\sum_{f \in \mathcal{F}(T)} \mathrm{Vol}(f). \tag{6.19}$$

The prepotential is then the hyperbolic volume of the domain located above the surface $\mathcal{S}$ defined in equation 6.9 from the triangulation T. The reason for the calling $\mathcal{A}_T$ the prepotential comes from the following theorem, showing that the measure on the triangulations is a Kähler measure with prepotential $\mathcal{A}_T$.

Theorem 6.2. *The measure* $d\nu_n(T, \theta) = d\nu_n(\mathbf{z})$ *on* $\mathfrak{D}_n$ *is a Kähler measure of the local form*

$$d\tilde{\nu}_n(\mathbf{z}) = 2^{n-3} \det\left[D_{\{i,j,k\}}(T)\right] \prod_{\substack{v=1 \\ v \neq i,j,k}}^{n} d^2 z_v \tag{6.20}$$

where $D_{\{i,j,k\}}$ *is the restriction to the* $n-3$ *lines and columns* $u, v \in \{1, \ldots, n\} \backslash \{i, j, k\}$ *of the Kähler metric on* $\mathbb{C}^n$*:*

$$D_{u,v}(\mathbf{z}) = \frac{\partial}{\partial z_u} \frac{\partial}{\partial \overline{z}_v} \mathcal{A}_T(\mathbf{z}). \tag{6.21}$$

As a side remark, this theorem relates the jacobian $\mathcal{D}^T_{\{i,j,k\}}$ to the prepotential $\mathcal{A}_T$ which involves the dilogarithm. This special function already appeared in the functional allowing to embed the triangulation in the plane, so this function is central in the study of Delaunay triangulations.

Note that the Kähler metric D is also defined for generic triangulations (not necessarily Delaunay). The three following results show properties for generic triangulations. The Kähler metric can be expressed in terms of the matrices A and E:

Theorem 6.3.

$$D = \frac{1}{4\mathrm{i}} A E A^\dagger \tag{6.22}$$

with A *the* $n \times 3(n-2)$ *vertex-edge matrix*

$$A_{ue} = \begin{cases} \frac{1}{z_u - z_{u'}} & \text{if } u \text{ is an end point of the edge } e = (u, u') \text{ of } T, \\ 0 & \text{otherwise.} \end{cases} \tag{6.23}$$

and E *the* $3(n-2) \times 3(n-2)$ *antisymmetric matrix*

$$E_{ee'} = \begin{cases} +1 & \text{if } e \text{ and } e' \text{ consecutive edges of a face } f, \text{ in c.w. order,} \\ -1 & \text{if } e \text{ and } e' \text{ consecutive edges of a face } f, \text{ in c.c.w. order,} \\ 0 & \text{otherwise.} \end{cases} \tag{6.24}$$

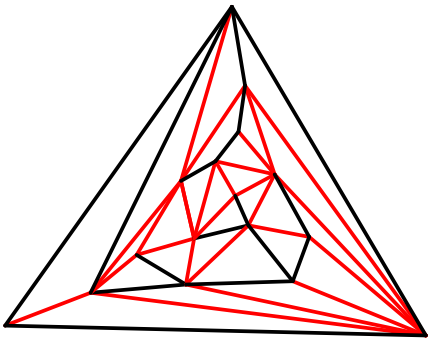

Figure 34: The red edges form a basis of edges of a triangulation of size 16. Their complementary (black edges) form a cycle-rooted spanning tree of the triangulation. The cycle is of length 3, and the cycle-rooted spanning tree has 16 edges.

The Kähler metric D is positive:

Lemma 6.1. *If the faces of a planar triangulation T are all positively oriented, the Hermitian for $D_{u,v}(T)$ is positive.*

The Jacobian $\mathcal{D}^T_{\{i,j,k\}}$ depends on the three points z_i, z_j, z_k chosen to be kept fixed, but the following lemma shows a covariance property with respect to the choice of the 3 points.

Lemma 6.2. *The quantity*

$$\frac{\mathcal{D}^T_{\{i,j,k\}}}{|\Delta_3(i,j,k)|^2} ,$$

with $\Delta_3(i,j,k) = (z_i - z_j)(z_i - z_k)(z_j - z_k)$, is independent of the choice of the three fixed points $\{z_i, z_j, z_k\}$.

It allows to change the three fixed points in a computation. For the last result, we switch to the other viewpoint for the measure. It allows the delta functions to get rid-off the measure.

Definition 6.3. *Given a triangulation $T \in \mathcal{T}_n$, a* cycle-rooted spanning tree *of T is a subgraph of T which contains all the vertices of T, and has n edges. It necessarily has a cycle. A set $\mathcal{E}_0 \subset \mathcal{E}(T)$ of $2n-6$ edges is a* basis *if its complementary $\mathcal{E}(T) \backslash \mathcal{E}_0$ is a cycle-rooted spanning tree of the triangulation T, where the cycle is of odd-length.*

For a same triangulation, several basis of edges exist. An example is shown in figure 34.

Theorem 6.4. *Let $T \in \mathcal{T}_n$ be a triangulation of size n, and note $\mathcal{E}_0$ a basis of edges. In the cell $\widetilde{\mathcal{T}}_n^f(T) \subset \widetilde{\mathcal{T}}_n^f$, the measure can be written in this ways:*

$$d\nu_n(T,\theta) = \frac{1}{2}\text{uniform}(T) \prod_{e\in\mathcal{E}_\prime} d\theta(e). \tag{6.25}$$

In particular, it is independent of the choice of basis $\mathcal{E}_0$.

This theorem will be useful for the simple case of a Delaunay triangulation of size 4.

7 Relation with Weil-Petersson metric

As was mentioned in previous section, David and Eynard [David and Eynard, 2014] showed that the flat measure on Delaunay triangulations can be expressed in terms of a Kähler metric D, defined in equation 6.21. We showed with David and Eynard [II] that this very Kähler metric D is related to the Weil-Petersson metric on the moduli space of decorated punctured surfaces. Hence, this result allows to use the known results on Weil-Petersson metric to study the model of Delaunay triangulations presented in the previous section. In the reverse manner, it also furnishes another way to realize the Weil-Petersson in a random map model. We first present briefly the moduli space of punctured surfaces decorated with horospheres, and give a formula for the Weil-Petersson 2-form $\Omega_{\mathscr{W}\mathscr{P}}$. Then, we relate the latter to a 2-form defined from the Kähler metric D. Last, we discuss the consequences of this relation.

7.1 Moduli space of decorated punctured surfaces

We briefly present the moduli space of marked Riemann surfaces, which will be useful in next chapter too, and Teichmüller space of marked surfaces. Then we decorate this moduli space with λ-lengths, and relate it to the Weil-Petersson measure on the moduli space.

Let $\mathcal{M}_{g,n}$ be the moduli space of compact Riemann surfaces of genus g, with n distinct marked points:

$$\mathcal{M}_{g,n} = \{(\Sigma_g, p_1, \dots, p_n)\}/\text{Iso} \tag{7.1}$$

where Σ_g is a Riemann surface of genus g and $p_1, \dots, p_n$ are n distinct and labeled marked points on Σ_g. Two marked Riemann surfaces $(\Sigma_g, p_1, \dots, p_n)$ and $(\tilde{\Sigma}_g, \tilde{p}_1, \dots, \tilde{p}_n)$ are isomorphic iff there exists an analytic bijection φ (whose inverse

φ^{-1} is also analytic) that maps one to the other, respecting the marked points:

$$\begin{cases} \varphi : \Sigma_g \to \tilde{\Sigma}_g \text{ analytic bijection} \\ \varphi^{-1} : \tilde{\Sigma}_g \to \Sigma_g \text{ analytic} \\ \forall i \in \{1, \dots, n\} \ \varphi(p_i) = \tilde{p}_i. \end{cases} \tag{7.2}$$

In this case the marked surfaces are equivalent: $(\Sigma_g, p_1, \dots, p_n) \sim (\tilde{\Sigma}_g, \tilde{p}_1, \dots, \tilde{p}_n)$, and in the moduli space $\mathcal{M}_{g,n}$, they are identified. The points of $\mathcal{M}_{g,n}$ are equivalence classes of marked Riemann surfaces, that are quotiented by the group of automorphisms (isomorphisms of $(\Sigma_g, p_1, \dots, p_n)$ onto itself). For instance, the identity is an automorphism. Therefore, the space $\mathcal{M}_{g,n}$ is an orbifold (locally a manifold quotiented by a group). It is well defined if its elements have finite automorphism groups ; in this case the elements are called stable marked surfaces. The following examples show an example of an unstable surface and two examples of stable surface.

Example 7.1. Let (Σ_0, p_1, p_2) be a Riemann surface of genus 0 with two distinct marked points. By Riemann uniformization theorem, Σ_0 is isomorphic to the Riemann sphere , i.e. the complex plane compactified by adding a point at ∞, and this is also the complex projective line, we write it

$$\overline{\mathbb{C}} = \mathbb{C} \cup \{\infty\} = \mathbb{C}P^1. \tag{7.3}$$

Therefore, $(\Sigma_0, p_1, p_2) \sim (\overline{\mathbb{C}}, z_1, z_2)$. By the isomorphism $z \mapsto \frac{z - z_1}{(z-z_1)\left(1+\frac{1}{z_1 - z_2}\right)+1}$, we even have $(\Sigma_0, p_1, p_2) \sim (\overline{\mathbb{C}}, 0, 1)$. The automorphisms of the Riemann sphere are Möbius transformations $z \to (az + b)/(cz + d)$ with $ad - bc = 1$. The automorphisms of the Riemann sphere with two marked points 0, 1 are Möbius transformations that have 0 and 1 as fixed points. They take the form $z \mapsto \frac{z}{z(1-d)+d}$, $\forall d \in \mathbb{C}^*$. This group is cleary infinite, so genus 0 surfaces with 2 marked points are unstable.

Example 7.2. If one considers a the Riemann sphere with $n \geq 3$ distinct marked points $(\overline{\mathbb{C}}, z_1, \dots, z_n)$, then there is a unique Möbius transformation which maps z_1, z_2, z_3 to respectively 0, 1, ∞. Therefore, $(\overline{\mathbb{C}}, z_1, \dots, z_n) \sim (\overline{\mathbb{C}}, 0, 1, \infty, p_4, \dots, p_n)$. The automorphisms of $(\overline{\mathbb{C}}, 0, 1, \infty, p_4, \dots, p_n)$ are Möbius transformations that must leave $0, 1, \infty$ unchanged, so the only automorphism of this marked sphere is the identity, so it is stable.
The moduli space of genus 0 compact Riemann surfaces with $n \geq 3$ marked points has the following description:

$$\mathcal{M}_{0,n} = \{(\overline{\mathbb{C}}, 0, 1, \infty, p_4, \dots, p_n) | p_i \neq p_j, 0, 1, \infty\}. \tag{7.4}$$

So $\dim_{\mathbb{R}}(\mathcal{M}_{0,n}) = 2(n - 3)$.

Example 7.3. Let Σ_g be an unmarked genus g surface, with $g \geq 2$. By Hurwitz's automorphism theorem:

$$|\mathrm{Aut}(\Sigma_g)| \leq 84(g-1), \tag{7.5}$$

so any surface of genus $g \geq 2$ is stable.

More generally, marked Riemann surfaces $(\Sigma_g, p_1, \ldots, p_n)$ are stable if $2-2g-n < 0$ (it is its Euler characteristic). For $2-2g-n < 0$, the orbifold $\mathcal{M}_{g,n}$ has real dimension

$$\dim_{\mathbb{R}} \mathcal{M}_{g,n} = 2(3g-3+n). \tag{7.6}$$

This means that it can be parametrized (locally) by $2(3g-3+n)$ real parameters, or also by $3g-3+n$ complex parameters.
Last, we will compute volumes of moduli spaces, so we need compact spaces. To do so, we use *Deligne-Mumford compactification* (see [Deligne and Mumford, 1969]), which, by adding nodal surfaces to the moduli spaces $\mathcal{M}_{g,n}$, is a procedure giving compact moduli spaces $\overline{\mathcal{M}}_{g,n}$.

Another useful space is the Teichmüller space of marked surfaces, defined as follows. Let Σ_g be a compact Riemann surface of genus g, and $P = \{p_1, \ldots, p_n\} \subset \Sigma_g$ be a set of n distinct points in Σ_g. Let φ_1, φ_2 be two diffeomorphisms: $\varphi_i : (\Sigma_g, P) \to (\Xi_i, Q_i)$, where Ξ_i are 2 Riemann surfaces and $Q_i \subset \Xi_i$ are marked points on those surfaces. φ_1 and φ_2 are said *equivalent* $\varphi_1 \approx \varphi_2$ if there exists a biholomorphic map $\Phi : (\Xi_1, Q_1) \leftrightarrow (\Xi_2, Q_2)$ such that $\Phi \circ \varphi_1$ is isotopic to φ_2, and where the diffeomorphisms preserve the set P (they can permute the points of P). Then the *Teichmüller* space $\mathcal{T}_{\Sigma_g,P}$ of a marked surfaces of genus g is composed of equivalence classes of diffeomorphisms. Equivalently, it is the equivalence classes of hyperbolic structures on (Σ_g, P):

$$\begin{aligned} \mathcal{T}_{\Sigma_g,P} &= \{\varphi : (\Sigma_g, P) \to (\Xi, Q)\}/\approx \\ &= \{\text{Hyperbolic structures on } (\Sigma_g, P)\}/\approx . \end{aligned} \tag{7.7}$$

The Teichmüller space $\mathcal{T}_{\Sigma_g,\{p_1,\ldots,p_n\}}$ of marked surfaces is related to the moduli space $\mathcal{M}_{g,n}$ of marked Riemann surfaces thanks to the *mapping class group* $MC(\Sigma_g, \{p_1, \ldots, p_n\})$, which is the group of isotopy classes of orientation-preserving homeomorphisms of $(\Sigma_g, \{p_1, \ldots, p_n\})$. Then we have the following:

$$\mathcal{M}_{g,n} = \mathcal{T}_{\Sigma_g,\{p_1,\ldots,p_n\}}/MC(\Sigma_g, \{p_1, \ldots, p_n\}). \tag{7.8}$$

The Teichmüller space of marked surfaces is the universal cover of the moduli space of Riemann surfaces.

Example 7.4. For compact genus 0 surfaces, the mapping class group of $(\Sigma_0, \{p_1, \ldots, p_n\})$ is the group of permutations $\mathfrak{S}_n$ of the marked points, so

$$\mathcal{M}_{0,n} = \mathcal{T}_{\Sigma_0,\{p_1,\ldots,p_n\}}/\mathfrak{S}_n.$$

Once those concepts are introduced, we relate them to our problem of Delaunay triangulations. We saw in section 6.2 that each Delaunay triangulation – modulo $PSL(2,\mathbb{C})$ transformations – gives explicitly a surface with constant negative curvature. So each Delaunay triangulation of size n represents a point in the moduli space $\mathcal{M}_{0,n}$. We want to compare the measure of Delaunay triangulations with a measure on moduli space of surfaces. To do so, we relate our Delaunay triangulations with *decorated* Teichmüller and moduli.Those are not decorated yet, in the sense that a point in $\mathcal{M}_{g,n}$ is simply a punctured surface. Following [Penner, 1987], we decorate surfaces by supplementing each puncture v by a horocycle $\mathfrak{h}_v$, i.e. a closed curve orthogonal to the geodesics emanating from v (in the constant curvature metric). Horocycles are uniquely characterized by their length ℓ_v. The moduli space of decorated punctured surfaces is simply

$$\tilde{\mathcal{M}}_{g,n} = \mathcal{M}_{g,n} \otimes \mathbb{R}_+^{\otimes_v} \tag{7.9}$$

A geodesic triangulation $\mathfrak{T}$ of the abstract surface $\mathcal{S}$ is a triangulation such that the edges are (infinite length) geodesics joining the punctures, and the triangles are oriented counter clockwise (and non-overlapping). For a decorated surface $\tilde{\mathcal{S}}$, for any geodesics $\mathfrak{e}$ joining two punctures u and v (generically one may have $u = v$), its λ-length $\Lambda_\mathfrak{e}(u,v)$ is defined from the (finite, algebraically defined) geodesic distance $d_\mathfrak{e}(u',v')$ along $\mathfrak{e}$ between the intersections u' and v' of e with the horocycles $\mathfrak{h}_u$ and $\mathfrak{h}_v$ by

$$\Lambda_\mathfrak{e}(u,v) = \exp(d_\mathfrak{e}(u',v')/2) \tag{7.10}$$

For a given triangulation $\mathfrak{T}$ (of a genus g surface with n punctures), it is known that the set of the independent λ-lengths $\Lambda_e \in \mathbb{R}_+$ for the $6g+3n-6$ edges of $\mathfrak{T}$ provide a complete set of coordinates for the decorated Teichmüller space $\tilde{\mathcal{T}}_{\Sigma_g,\{p_1,\dots,p_n\}}$. This parametrization is independent of the choice of triangulation, thanks to the Ptolemy's relations between lambda-lengths when one passes from a triangulation $\mathfrak{T}$ to another one $\mathfrak{T}'$ through a flip similar to the ones of figure 54, namely

$$\Lambda_{13}\Lambda_{24} = \Lambda_{12}\Lambda_{34} + \Lambda_{14}\Lambda_{23} \tag{7.11}$$

In this parametrization, the so-called Weil-Petersson 2-form on $\mathcal{M}_{g,n}$ (through its projection from $\tilde{\mathcal{T}}_{\Sigma_g,\{p_1,\dots,p_n\}}$) can be written simply as a sum over the $2(2g+n+2)$ oriented faces (triangles) $\mathfrak{f}$ of $\mathfrak{T}$, as

$$\Omega_{\mathscr{WP}} = -2 \sum_{\text{faces } \mathfrak{f}} d\log(\Lambda_{12}) \wedge d\log(\Lambda_{23}) + d\log(\Lambda_{23}) \wedge d\log(\Lambda_{31}) + d\log(\Lambda_{31}) \wedge d\log(\Lambda_{12}) \tag{7.12}$$

where (1,2,3) denote the vertices (punctures) $v_1(f)$, $v_2(f)$ and $v_3(f)$ (here in counter clockwise order) of the geodesic triangle $\mathfrak{f}$ of $\mathfrak{T}$, and the Λ_{ij} denote the λ-length of the edges of the triangle.

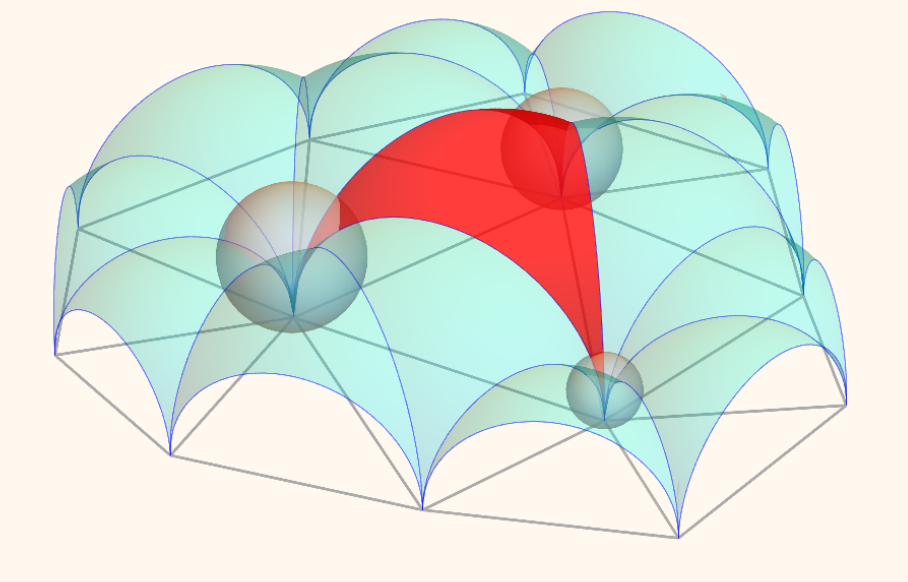

Figure 35: The punctured surface decorated with horospheres. Although this 3d representation looks non smooth at the edges, the intrinsic metric of the surface is indeed a smooth constant curvature metric.

In order to compare the 2-form $\Omega_{\mathscr{WP}}$ to a 2-form defined from a Delaunay triangulation, one simply has to look at horocycles and λ-lengths in Delaunay triangulations. We have an explicit representation of a point in $\mathcal{M}_{0,n}$ as the constant curvature surface $\mathcal{S}$ in $\mathbb{H}_3$ constructed above the Delaunay triangulation T for the set of points $\mathbf{z} = \{z_i\}_{i=1,n}$ in the complex plane. Horocycles are easily constructed by decorating each point (puncture) z_i by a horosphere $\mathcal{H}_i$, i.e. an Euclidean sphere in $\mathbb{R}^3$, tangent to the complex place $\mathbb{C}$ at the point z_i, and lying above z_i (i.e. in $\mathbb{H}_3$). The intersection (in $\mathbb{H}_3$) of the horosphere $\mathcal{H}_i$ with the union of the ideal spherical triangles $\mathcal{S}_f$ for the faces f which share the vertex i defines the horocircle $\mathfrak{h}_i$ associated to the puncture i of $\mathcal{S}$. It is depicted in figure 35.

Let R_i denote the Euclidean radius of the horosphere $\mathcal{H}_i$ above vertex i. The λ-length for the edge joining two vertices (i, j) of the triangulation is easily calculated (applying for instance the formula in the Poincaré half-plane in 2 dimensions) and is

$$\Lambda(i, j) = \frac{|z_i - z_j|}{\sqrt{4\, R_i\, R_j}} \tag{7.13}$$

where $|z_i - z_j|$ is the Euclidean distance between the points i and j in the plane $\mathbb{C}$. See figure 36.

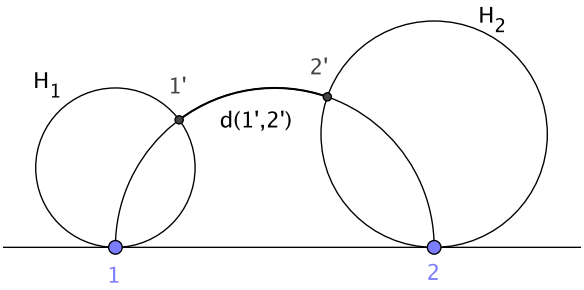

Figure 36: The geodesics between the horospheres H_1 and H_2 at points 1 and 2.

Incorporating this into 7.12, the Weil-Petersson 2-form 7.12 the takes the form:

$$\Omega_{\mathscr{WP}} = -2\sum_{\mathfrak{f}} \frac{d\,|z_1 - z_2]}{|z_1 - z_2|} \wedge \frac{d\,|z_2 - z_3]}{|z_2 - z_3|} + \frac{d\,|z_2 - z_3]}{|z_2 - z_3|} \wedge \frac{d\,|z_3 - z_1]}{|z_3 - z_1|} + \frac{d\,|z_3 - z_1]}{|z_3 - z_1|} \wedge \frac{d\,|z_1 - z_2]}{|z_1 - z_2|} \tag{7.14}$$

Let us remark that, although this formula refers to a given geodesic triangulation, the resulting 2-form $\Omega_{\mathscr{WP}}$ is known to be independent of the triangulation through the Ptolemy's relation. This 2-form is related to a 2-form associated to the Kähler metric of Delaunay triangulations, as shown in next section.

7.2 Kähler metric and Weil-Petersson 2-form

The set of Delaunay triangulations allows to define the *Delaunay Kähler 2-form*:

$$\Omega_{\mathscr{D}.}(\mathbf{z}) = \frac{1}{2\mathrm{i}} dz_u \wedge d\bar{z}_v \, D_{u,v}(\mathbf{z}), \tag{7.15}$$

where the Kähler metric D was defined in equation 6.21. Let us note that $\Omega_{\mathscr{D}.}$ is continuous across flips, so it is continuous on $\widetilde{\mathcal{T}}_n^f$. We show the following result:

Theorem 7.1.

$$\Omega_{\mathscr{D}.} = \frac{1}{2}\Omega_{\mathscr{WP}} \tag{7.16}$$

Proof. We use theorem 6.3 of David and Eynard [David and Eynard, 2014] to express the matrix D in the following form:

$$D = \frac{1}{4\mathrm{i}} AEA^\dagger. \tag{7.17}$$

With this factorization, the 2-form $\Omega_{\mathscr{D}.}$ takes a simple form, as a sum over faces (triangles) f of T. Let us denote (f_1, f_2, f_3) the vertices of a triangle f, in counter clockwise order (this is defined up to a cyclic permutation of the 3 vertices).

$$\Omega_{\mathscr{D}.}(\mathbf{z}) = \sum_{\text{faces } f} \omega_{\mathscr{D}.}(z_{f_1}, z_{f_2}, z_{f_3}) \tag{7.18}$$

with, for a face f with vertices labelled $(1,2,3)$ (for simplicity), and denoting $z_{ij} = z_j - z_i$

$$\omega_{\mathscr{D}.}(z_1,z_2,z_3) = \frac{1}{8}\begin{pmatrix} d\,\log(z_{23})\wedge d\,\log(\overline{z}_{31}) + d\,\log(\overline{z}_{23})\wedge d\,\log(z_{31}) \\ +d\,\log(z_{31})\wedge d\,\log(\overline{z}_{12}) + d\,\log(\overline{z}_{31})\wedge d\,\log(z_{12}) \\ +d\,\log(z_{12})\wedge d\,\log(\overline{z}_{23}) + d\,\log(\overline{z}_{12})\wedge d\,\log(z_{23}) \end{pmatrix} \tag{7.19}$$

Reexpressed in term of the log of the modulus and of the argument of the z_{ij}'s

$$\lambda_{ij} = \log(|z_j - z_i)|\ , \quad \vartheta_{ij} = \arg(z_j - z_i) \tag{7.20}$$

we obtain

$$\omega_{\mathscr{D}.} = \omega_{\text{length}} + \omega_{\text{angle}} \tag{7.21}$$

with the length contribution

$$\omega_{\text{length}} = \frac{1}{4}(d\,\lambda_{12}\wedge d\,\lambda_{23} + d\,\lambda_{23}\wedge d\,\lambda_{31} + d\,\lambda_{31}\wedge d\,\lambda_{12}) \tag{7.22}$$

and the angle contribution

$$\omega_{\text{angle}} = \frac{1}{4}(d\,\vartheta_{12}\wedge d\,\vartheta_{23} + d\,\vartheta_{23}\wedge d\,\vartheta_{31} + d\,\vartheta_{31}\wedge d\,\vartheta_{12}) \tag{7.23}$$

Reexpressed in terms of the angles α_1, α_2 and α_3 of the triangle $(1,2,3)$ (using $\alpha_1 = \vartheta_{13} - \vartheta_{12}$, etc.), and using $\alpha_1 + \alpha_2 + \alpha_3 = \pi$, one has

$$\omega_{\text{angle}} = \frac{1}{4}(d\,\alpha_1\wedge d\,\alpha_2) = \frac{1}{4}(d\,\alpha_2\wedge d\,\alpha_3) = \frac{1}{4}(d\,\alpha_3\wedge d\,\alpha_1) \tag{7.24}$$

Using the triangle relation

$$\frac{\sin(\alpha_1)}{\exp(\lambda_{23})} = \frac{\sin(\alpha_2)}{\exp(\lambda_{31})} = \frac{\sin(\alpha_3)}{\exp(\lambda_{12})} \tag{7.25}$$

one gets

$$\begin{aligned} d\alpha_1\cot\alpha_1 - d\lambda_{23} =& d\alpha_2\cot\alpha_2 - d\lambda_{31} = d\alpha_3\cot\alpha_3 - d\lambda_{12} \\ &= (d\alpha_1 + d\alpha_2)\frac{\cot\alpha_1\,\cot\alpha_2 - 1}{\cot\alpha_1 + \cot\alpha_2} - d\lambda_{12} \end{aligned} \tag{7.26}$$

which gives

$$d\alpha_1 = \frac{\csc^2\alpha_2}{\cot\alpha_1 + \cot\alpha_2}(d\lambda_{23} - d\lambda_{12}) + \frac{\cot\alpha_1\,\cot\alpha_2 - 1}{\cot\alpha_1 + \cot\alpha_2}(d\lambda_{31} - d\lambda_{12}) \tag{7.27}$$

$$d\alpha_2 = \frac{\cot\alpha_1\,\cot\alpha_2 - 1}{\cot\alpha_1 + \cot\alpha_2}(d\lambda_{23} - d\lambda_{12}) + \frac{\csc^2\alpha_1}{\cot\alpha_1 + \cot\alpha_2}(d\lambda_{31} - d\lambda_{12}) \tag{7.28}$$

which implies

$$d\,\alpha_1\wedge d\,\alpha_2 = d\,\lambda_{12}\wedge d\,\lambda_{23} + d\,\lambda_{23}\wedge d\,\lambda_{31} + d\,\lambda_{31}\wedge d\,\lambda_{12} \tag{7.29}$$

Hence $\omega_{\text{angle}} = \omega_{\text{length}}$. Therefore one has

$$\omega_{\mathscr{D}.} = \frac{1}{2}(d\,\lambda_{12} \wedge d\,\lambda_{23} + d\,\lambda_{23} \wedge d\,\lambda_{31} + d\,\lambda_{31} \wedge d\,\lambda_{12}). \tag{7.30}$$

This means that the Delaunay Kähler 2-form has the following expression:

$$\Omega_{\mathscr{D}.} = \frac{1}{2} \sum_{f \in \mathcal{F}(T)} \frac{d\,|z_1 - z_2]}{|z_1 - z_2|} \wedge \frac{d\,|z_2 - z_3]}{|z_2 - z_3|} + \frac{d\,|z_2 - z_3]}{|z_2 - z_3|} \wedge \frac{d\,|z_3 - z_1]}{|z_3 - z_1|} + \frac{d\,|z_3 - z_1]}{|z_3 - z_1|} \wedge \frac{d\,|z_1 - z_2]}{|z_1 - z_2|}. \tag{7.31}$$

This shows the theorem 7.1 of this section:

$$\Omega_{\mathscr{D}.} = \frac{1}{2}\Omega_{\mathscr{WP}}. \tag{7.32}$$

□

7.3 Consequences

This identity between the Weil-Petersson form and our form on the space of random triangulations shows that the random Delaunay triangulation model is equivalent to the more abstract topological Witten-Kontsevich intersection theory based on the Weil-Petersson measure on moduli spaces. The Weil-Petersson volume form $d\nu_n^{\mathscr{WP}}$ on $\overline{\mathcal{M}}_{0,n}$ is a $2n-6$ form, and is given by:

$$d\nu_n^{\mathscr{WP}} = \frac{1}{(n-3)!}\Omega_{\mathscr{WP}}^{n-3}. \tag{7.33}$$

Then, the Weil-Petersson volume of the moduli space $\overline{\mathcal{M}}_{0,n}$ of Riemann surfaces of genus 0 with n punctures is

$$\text{Vol}_{\mathscr{WP}}\left(\overline{\mathcal{M}}_{0,n}\right) = \int_{\overline{\mathcal{M}}_{0,n}} \frac{1}{(n-3)!}\Omega_{\mathscr{WP}}^{n-3}. \tag{7.34}$$

By theorem 6.2 of David and Eynard, the measure $d\tilde{\nu}_n(\mathbf{z})$ can in turn be expressed in terms of the two-form $\Omega_{\mathscr{D}}$:

$$d\tilde{\nu}_n(\mathbf{z}) = \frac{2^{n-3}}{(n-3)!}\Omega_{\mathscr{D}}^{n-3}. \tag{7.35}$$

Therefore, the previous result shows that the two following volumes are actually equal:

$$V_n^{\mathscr{D}} = \text{Vol}_{\mathscr{WP}}\left(\overline{\mathcal{M}}_{0,n}\right). \tag{7.36}$$

The total Weil-Petersson volume of the $\overline{\mathcal{M}}_{g,n}$ was computed by Zograf, Kaufmann, Manin, Zagier, and finally by Mirzakhani for all genera ([Zograf, 1993] [Kaufmann et al., 1996], [Manin and Zograf, 2000]). It behaves for large n as

$$\text{Vol}_{\mathscr{WP}}\left(\overline{\mathcal{M}}_{g,n}\right) \;=\; C^n\, n^{(5g-7)/2}\,(a_g + \mathcal{O}(1/n)) \tag{7.37}$$

C and the a_g are known positive constants. Note that we omit the $n!$ factor in the explicit result of Mirzakhani [Manin and Zograf, 2000]). This factor comes from the labelling of the punctures, while in our model the punctures are unlabelled. For planar Delaunay triangulations, we shall take $g = 0$ and mutiply by 2^{-n+3}. This result, in particular the explicit form of the "string exposent" $(5g-7)/2$ which is the same as for random maps, shows that the Random Delaunay model is in the universality class of pure two-dimensional gravity (Liouville theory with $\gamma = \sqrt{8/3}$ and $c_{\text{matter}} = 0$). For finite n, the volume $\text{Vol}_{\mathscr{WP}}\left(\overline{\mathcal{M}}_{0,n}\right)$ is given in the same references. We shall come back to those volumes in next chapter when we will compare the features of Delaunay triangulations volumes to the Strebel graph volumes (see section 13.2).

Apart from the volumes of the sets $\widetilde{\mathcal{T}}_n^f$, the identification of Delaunay triangulations with the Witten-Kontsevich intersection theory based allows to compute explicitly other generating functions on Delaunay triangulations, that are *topological* in the sense that they do not depend on the metric associated to a triangulation (whether it be a discrete metric or the Beltrami metric). Those accessible topological generating functions $Z_{n,k}^{\mathscr{D}}(\Theta_1, \ldots, \Theta_k)$ are briefly discussed in section 13 of next chapter, and are defined by analogy to the generating functions of Strebel graphs.

Note that it is possible to generalize the random Delaunay model from the planar case (genus $g = 0$) to the higher genus $g > 0$ case. Since the identification 7.32 between the Delaunay Kähler form and the Weil-Petersson form is local, it should also be valid for the $g > 0$ case. As it was visible in equation 7.37, the higher genera volumes are also known, and this makes the identification of the 2-forms an effective tools to compute volumes of Delaunay triangulations of any genus g.

Therefore, this identification of the measures shows very effective to compute generating functions and extend the model of Delaunay triangulations. However, is the study of Delaunay triangulations in the frame of quantum gravity worth to be continued if it seems contained in the Witten-Kontsevich intersection theory ? Actually, the random Delaunay model remains an interesting model of random two-dimensional geometry since it is an explicit model of a global conformal mapping of an abstract (or intrinsic) but continuous two-dimensional geometry model onto the complex plane. This mapping through Delaunay triangulations is different, and somehow simpler, than the general mapping provided by the Riemann uniformization theorem, which is usually considered. Indeed a local modification of the position of one vertex of the triangulation translates in a local modification of the associated Kähler form, since the Kähler potential $\mathcal{A}_T$ given by 6.19 is a sum over local terms (the hyperbolic volumes $\mathbf{V}(f)$ of the triangles). This is not the case for the uniformization mapping, which leads to a global Kähler potential (a classical Liouville action).

Therefore the model discussed here should allow to study the local properties of the conformal mapping of a random metric onto the plane, as we shall see in the next section where two preliminary local results are presented.

8 Local properties of the measure

In the previous part, we showed that the measure $d\nu_n = d\tilde{\nu}_n(\mathbf{z})$ on $\widetilde{\mathcal{T}}_n^f$ can be expressed locally in terms of the Weil-Petersson measure on $\overline{\mathcal{M}}_{0,n}$. Although this result allows to compute various correlation functions such as the volume of $\widetilde{\mathcal{T}}_n^f$, the study of finer observables (which depend on the metrics) is out of the reach of Weil-Petersson measure. In order to get more effective tools to study the convergence of the correlations functions (moments and cumulants) for this random measure in the complex plane (defined from Delaunay triangulations), it is necessary to know the *local properties* of this random measure, considered as a random point process in $\mathbb{C}$. In this section we present two first results on the properties of this measure.

8.1 Maximality property over the Delaunay triangulations

Looking at the measure $d\tilde{\nu}_n(\mathbf{z})$ on $\mathfrak{D}_n$ (the space of distributions of n points on the Riemann sphere), theorem 6.20 gives

$$d\tilde{\nu}_n(\mathbf{z}) = 2^{n-3} \ \det\left[D_{\{1,2,3\}}(\mathbf{z})\right] \prod_{v=4}^{n} d^2 z_v,$$

where, implicitely, the Kähler metric D is defined from the Delaunay triangulation T^D of the points $\{z_1, \ldots, z_n\}$. However, for a generic triangulation T of those points, the Kähler metric $D(T)$ is still well defined. A question on can legitimately ask is wether the Kähler metric has special properties when it is defined on Delaunay triangulations rather than generic ones. We prove here two properties on the metric when one varies the structure of the triangulations. The second one shows that, indeed, Delaunay triangulations are special for the Kähler metric. We use a short-hand notation in this section:

$$d_{(ijk)}(T) = \det\left[D_{\{i,j,k\}}(T)\right]. \tag{8.1}$$

In order to compare the metric of a generic triangulation T with the metric of a Delaunay triangulation T^D, we use the Lawson Flip Algorithm described in section 6.1.2. With this algorithm, two successive triangulation differ by an edge flip (see figure 37). A preliminary result concerns the variation of $d_{(ijk)}(T)$ when T undergoes a Lawson flip. The final triangulation is called T'. With the notations of figure 37,

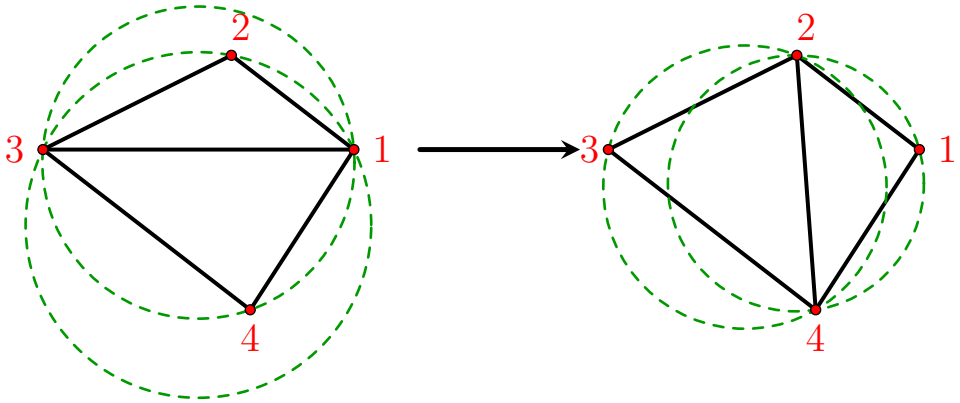

Figure 37: Lawson flip, the illegal edge (13) is flipped.

we consider that the edge (z_1, z_3) is flipped into (z_2, z_4), and note this flip $T \xrightarrow[(24)]{(13)} T'$. Through this flip the Kähler metric changes according to this lemma:

Lemma 8.1. *Denote f the triangle (124), and ω_f, R_f respectively the center and the radius of its circumcircle. Then*

$$d_{(124)}(T') - d_{(124)}(T) = \det\left[D_{\{1,2,3,4\}}(T)\right] \times \text{Area}(f) \frac{|z_3 - \omega_f|^2 - {R_f}^2}{|z_3 - z_1|^2 |z_3 - z_2|^2 |z_3 - z_4|^2}, \quad (8.2)$$

where $D_{\{1,2,3,4\}}$ means that we restrict the matrix $D_{u,v}$ to the indices $u, v \neq 1, 2, 3, 4$, and $\text{Area}(f)$ is the Euclidean area of the triangle f.

Proof. The proof of this lemma is given in appendix C. □

This preliminary result will appear useful to prove a maximality property specific to Delaunay triangulations:

Theorem 8.1. *Given n points $z_1, \ldots, z_n$ in $\mathbb{C}$, their Delaunay triangulation $T^D(\mathbf{z})$ is the one which maximizes $d_{(ijk)}(T)$ among all possible triangulations T:*

$$d_{(ijk)}(T^D(\mathbf{z})) = \max_{T \text{ triangulation of } \mathbf{z}} d_{(ijk)}(T). \quad (8.3)$$

Proof of the theorem 8.1. For the configuration of points $\{z_v\}$, take a generic triangulation T on this configuration, and note T^D the Delaunay triangulation of those points. We must prove that $d_{(123)}(T^D) \geq d_{(123)}(T)$.
The proof relies on the Lawson Flip Algorithm (LFA) described in section 6.1.2. It transforms the triangulation T into T^D by a sequence of edge flip. At each step of the

algorithm, the LFA applies a single edge flip. Note $(T_i)_{0\leq i\leq k}$ the sequence of successive triangulations obtained by the LFA, with $T_0 = T$ and $T_k = T^D(\{z_v\})$:

$$T_0 = T \xrightarrow[(a^1d^1)]{(b^1c^1)} T_1 \xrightarrow[(a^2d^2)]{(b^2c^2)} \dots \xrightarrow[(a^kd^k)]{(b^kc^k)} T_k = T^D(\{z_v\}). \tag{8.4}$$

At each step, the illegal edge (b^i, c^i) is flipped into the edge (a^i, d^i) (see figure 30 in section 6.1.2). It follows that for the two new faces (a^i, c^i, d^i) and (a^i, d^i, b^i), their circumcircles enclose respectively neither b^i nor c^i. We prove that:

$$d_{(a^i,c^i,d^i)}(T_{i+1}) - d_{(a^i,c^i,d^i)}(T_i) \geq 0.$$

Indeed, from lemma 8.1, this difference yields:

$$\begin{aligned} d_{(a^i,c^i,d^i)}(T_i) - d_{(a^i,c^i,d^i)}(T_{i-1}) &= \det\left[D_{\{a^i,b^i,c^i,d^i\}}(T_i)\right] \times \text{Area}(a^ic^id^i)\times \\ &\quad \frac{\left|b^i - \omega_{(a^ic^id^i)}\right|^2 - {R_{(a^ic^id^i)}}^2}{\left|b^i - a^i\right|^2 \left|b^i - c^i\right|^2 \left|b^i - d^i\right|^2}. \end{aligned} \tag{8.5}$$

As all the faces are positively oriented (we enforce it in our notations), lemma 6.1 states that the Hermitian for $D(T_i)$ is positive, so the principal minors of $D(T_i)$ are positive. Therefore,

$$\det\left[D_{\{a^i,b^i,c^i,d^i\}}(T_i)\right] \geq 0.$$

Then, the difference $d_{(a^i,c^i,d^i)}(T_i) - d_{(a^i,c^i,d^i)}(T_{i-1})$ is positive only if b^i is outside the circumcircle of $(a^ic^id^i)$. Precisely, the flip was done in order to satisfy this condition. So we have:

$$d_{(a^i,c^i,d^i)}(T_i) - d_{(a^i,c^i,d^i)}(T_{i-1}) \geq 0. \tag{8.6}$$

This is true at each step, and now, using the covariance property of the measure (see lemma 6.2), we have:

$$\frac{d_{(123)}}{|\Delta_3(1,2,3)|^2} = \frac{d_{(ijk)}}{|\Delta_3(i,j,k)|^2}. \tag{8.7}$$

Therefore, inequality 8.6 can propagate along the steps:

$$\begin{aligned} d_{(123)}(T^D) - d_{(123)}(T) &= \sum_{i=1}^{k} \left[d_{(123)}(T_i) - d_{(123)}(T_{i-1})\right] \\ &= |\Delta_3(1,2,3)|^2 \sum_{i=1}^{k} \left[\frac{d_{(a^i,c^i,d^i)}(T_i) - d_{(a^i,c^i,d^i)}(T_{i-1})}{|\Delta_3(a^i,c^i,d^i)|^2}\right] \\ &\geq 0. \end{aligned}$$

This ends the proof. □

The measure $d\tilde{\nu}_n(\mathbf{z})$ used is then maximal over the Delaunay triangulations.

8.2 Growth of the volume

The second result relates to the n dependence of the total volume

$$\begin{aligned} V_n^{\mathscr{D}} &= \int_{\widetilde{\mathcal{T}}_n^f} d\nu_n(T,\theta) \\ &= \int_{\mathfrak{D}_n} d\tilde{\nu}_n(\mathbf{z}). \end{aligned} \tag{8.8}$$

The space $\mathfrak{D}_n$ of configurations of n distinct points modulo Möbius tranformations in contained in $\mathbb{C}^{n-3}$. As the set $\mathbb{C}^{n-3}\backslash\mathfrak{D}_n$ is of measure 0 (with the measure $d\tilde{\nu}_n$), we can write:

$$V_n^{\mathscr{D}} = \int_{\mathbb{C}^{n-3}} 2^{n-3} \det\left[D_{\{1,2,3\}}(T^D(\{z_v\}))\right] \prod_{v=4}^{n} d^2 z_v \tag{8.9}$$

It is the volume of the space of Delaunay triangulations with n vertices with the measure $d\tilde{\nu}_n(\mathbf{z})$. A lower bound of the growth of the volume when the number of vertices increases is given by the following inequalities:

Theorem 8.2. *If we add a $n+1$'th point to a given triangulation and integrate over its position, the following inequality holds:*

$$\begin{aligned} &\int_{\mathbb{C}} d^2 z_{n+1} \det\left[D_{\{1,2,3\}}(T^D(\{z_1,\ldots,z_{n+1}\}))\right] \\ &\geq (n-2)\frac{\pi^2}{8} \det\left[D_{\{1,2,3\}}(T^D(\{z_1,\ldots,z_n\}))\right] \end{aligned} \tag{8.10}$$

It involves the inequality for the total volumes

$$V_{n+1}^{\mathscr{D}} \geq (n-2)\frac{\pi^2}{8} V_n^{\mathscr{D}}. \tag{8.11}$$

Before proving the theorem, let us stress that this growth property is global with respect to the last point z_{n+1}. The result gives more information than the inequality 8.11 on the volumes, which is of little interest once we know from last section that it is a volume of Weil-Petersson. The inequality 8.10 is local in the variables $z_1,\ldots,z_n$, and this is the interesting feature for this result.
A similar inequality does not stand locally for the measure $\det\left[D_{\{1,2,3\}}(T^D(\{z_v\}))\right]$ when one adds a vertex at a fixed position to an existing Delaunay triangulation. This has been checked numerically.

Proof. We first focus on the inequality 8.10. The proof follows the following procedure:

- Fix n points $\{z_1,\ldots,z_n\}$ in $\mathbb{C}$, and note $T^D(\{z_v\})$ the Delaunay triangulation constructed on this configuration.

- Pave the Riemann sphere with regions $\mathcal{R}(f)$ (defined bellow) associated with the faces f of the triangulation.
- Then add a point z_{n+1} in $\mathbb{C}$ to this triangulation. Depending on the region $\mathcal{R}(f)$ where it stands, transform the triangulation to include the new point and compute the measure associated with this triangulation.
- Integrate over z_{n+1}, find a lower bound on of the integral, and compare the result with the measure associated with $T^D(\{z_1, \ldots, z_n\})$.

For the Delaunay triangulation constructed over $\{z_1, \ldots z_n\}$, the Riemann sphere can be conformally paved with regions $\mathcal{R}(f)$ associated to each face in the following way. Let us look at the edge e whose neighboring faces are f and f'. The circumcircles of f and f' meet at the vertices located at the ends of e with an angle $\theta'(e) = (\pi - \theta(e))$. Define $\mathcal{C}_e$ the arc of a circle joining the ends of e, and making an angle $\theta'(e)/2 = (\pi - \theta(e))/2$ with each of the circumcircles of f and f' at the vertices of e. See figure 38. The region $\mathcal{R}(f)$ is now defined as the domain enclosed in the three arcs of a circle $\mathcal{C}_{e_1}, \mathcal{C}_{e_2}, \mathcal{C}_{e_3}$ corresponding to the three edges e_1, e_2, e_3 surrounding f (see figure 39). This domain is now transformed covariantly under a Möbius transformation.

We add the point z_{n+1} in the Riemann sphere. If $z_{n+1} \in \mathcal{R}(f)$, we construct

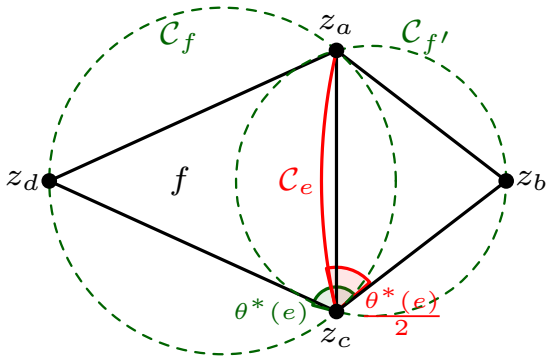

Figure 38: Definition of the arc $\mathcal{C}_e$.

the triangulation $T_f^D(\{z_1, \ldots, z_n\}, z_{n+1})$ by joining the vertex z_{n+1} to the vertices a, b and c of the face f. The triangulation $T_f^D(\{z_1, \ldots, z_n\}, z_{n+1})$ is in general different from the Delaunay triangulation $T^D(\{z_1, \ldots, z_{n+1}\})$. Yet it is still possible to define the measure $\det D_{\{1,2,3\}}(T_f^D(\{z_v\}, z_{n+1}))$, which is still a positive quantity, and which, from theorem 8.1, satisfies:

$$\det \left[D_{\{1,2,3\}}(T_f^D(\{z_v\}, z_{n+1}))\right] \leq \det \left[D_{\{1,2,3\}}(T^D(\{z_1, \ldots, z_{n+1}\}))\right] \tag{8.12}$$

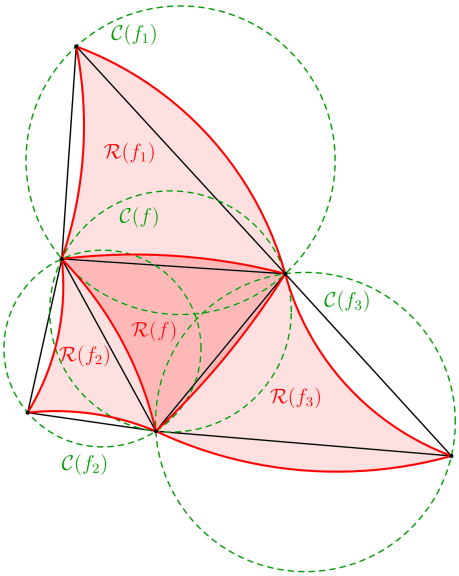

Figure 39: The region $\mathcal{R}(f)$ is enclosed in the bissector arcs.

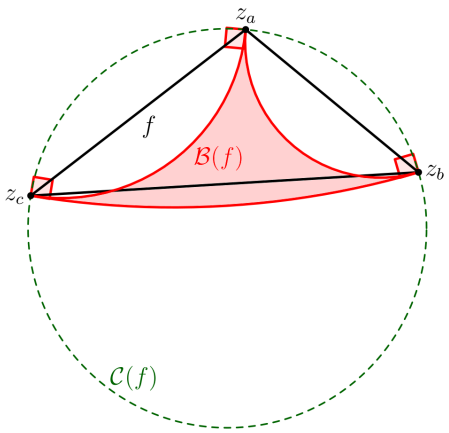

Figure 40: The region $\mathcal{B}(f)$ associated with a face f.

The aim is to find a lower bound to the integral over each region $\mathcal{R}(f)$. The interesting result is that we found a lower bound that does not depend on the region, although the shapes of the regions depend on the angle $\theta(e)$ between two neighboring circumcircles. We take this dependence out by integrating over smaller regions $\mathcal{B}(f) \subseteq \mathcal{R}(f)$. for the face f, $\mathcal{B}(f)$ is the region enclosed by the three arcs of circle that pass through two of the vertices of f and that are orthogonal to the circumcircle of f (see figure 40).

The integration over z_{n+1} thus decomposes in the following way:

$$\begin{aligned}
&\int_{\mathbb{C}} d^2 z_{n+1} \, \det\left[D_{\{1,2,3\}}(T^D(\{z_1,\ldots,z_{n+1}\}))\right] \\
&\qquad = \sum_f \int_{\mathcal{R}(f)} d^2 z_{n+1} \det\left[D_{\{1,2,3\}}(T^D(\{z_1,\ldots,z_{n+1}\}))\right] \\
&\qquad \geq \sum_f \int_{\mathcal{R}(f)} d^2 z_{n+1} \det\left[D_{\{1,2,3\}}(T_f^D(\{z_v\},z_{n+1}))\right] \\
&\qquad \geq \sum_f \int_{\mathcal{B}(f)} d^2 z_{n+1} \det\left[D_{\{1,2,3\}}(T_f^D(\{z_v\},z_{n+1}))\right] \qquad (8.13)
\end{aligned}$$

In the last line, the integral can be computed explicitly. If $z_{n+1} \in \mathcal{B}(f)$ with $f = (abc)$,

one can compute the integration on $\mathcal{B}(f)$ using lemma 6.2:

$$\int_{\mathcal{B}(f)} d^2 z_{n+1} \ \det\left[D_{\{1,2,3\}}(T_f^D(\{z_v\}, z_{n+1}))\right] = \frac{\Delta_3(z_1, z_2, z_3)}{\Delta_3(a, b, c)} \int_{\mathcal{B}(f)} d^2 z_{n+1} \det\left[D_{\{a,b,c\}}(T_f^D(\{z_v\}, z_{n+1}))\right]. \tag{8.14}$$

Then the right term factorizes nicely thanks to the shape of the triangulation around z_{n+1}:

$$\int_{\mathcal{B}(f)} d^2 z_{n+1} \ \det\left[D_{\{a,b,c\}}(T_f^D(\{z_v\}, z_{n+1}))\right] = \int_{\mathcal{B}(f)} d^2 z_{n+1} \det\left[D_{\{a,b,c\}}(T^D(\{z_v\}))\right] \times \det\left[D_{\{a,b,c\}}(T^D(\{a, b, c, z_{n+1}\}))\right]. \tag{8.15}$$

In the integrand, the term depending on z_{n+1} is the second determinant, so we need to estimate:

$$I = \int_{\mathcal{B}(f)} d^2 z_{n+1} \det\left[D_{\{a,b,c\}}(T^D(\{a, b, c, z_{n+1}\}))\right]. \tag{8.16}$$

It is the integral of the measure on the Delaunay triangulation made of the 4 points a, b, c and z_{n+1}, where z_{n+1} crosses the region $\mathcal{B}(f)$ (see figure 41):

$$I = \int_{\mathcal{B}(f)} d\tilde{\nu}_4(\{a, b, c, z_{n+1}\}). \tag{8.17}$$

The integral is computable if one switches the approach and considers the measure $d\nu_4$ in terms of the angles. Using the theorem 6.4, we express the measure $d\nu_4$ in terms of a basis of two angles θ_1, θ_2 (they are depicted in figure 41):

$$I = \frac{1}{2} \int_{z_{n+1} \in \mathcal{B}(f)} d\theta_1 d\theta_2 \tag{8.18}$$

The point z_{n+1} belongs to the region $\mathcal{B}(f)$ if $\theta_i^{\min} \leq \theta_i \leq \theta_i^{\min} + \frac{\pi}{2}$ for $i = 1, 2, 3$. $\theta_i^{\min}$ corresponds to the angle θ_i for which the point z_{n+1} is on the boundary arc of $\mathcal{B}(f)$ associated with the edge i.
We also have $\theta_1 + \theta_2 + \theta_3 = \pi$ and $\theta_1^{\min} + \theta_2^{\min} + \theta_3^{\min} = \frac{\pi}{2}$, so eventually, $z_{n+1} \in \mathcal{B}(f)$ if:

$$\theta_1^{\min} \leq \theta_1 \leq \theta_1^{\min} + \frac{\pi}{2} \tag{8.19}$$

$$\theta_2^{\min} \leq \theta_2 \leq \theta_2^{\min} + \frac{\pi}{2} \tag{8.20}$$

$$\theta_1^{\min} + \theta_2^{\min} \leq \theta_1 + \theta_2 \leq \theta_1^{\min} + \theta_2^{\min} + \frac{\pi}{2} \tag{8.21}$$

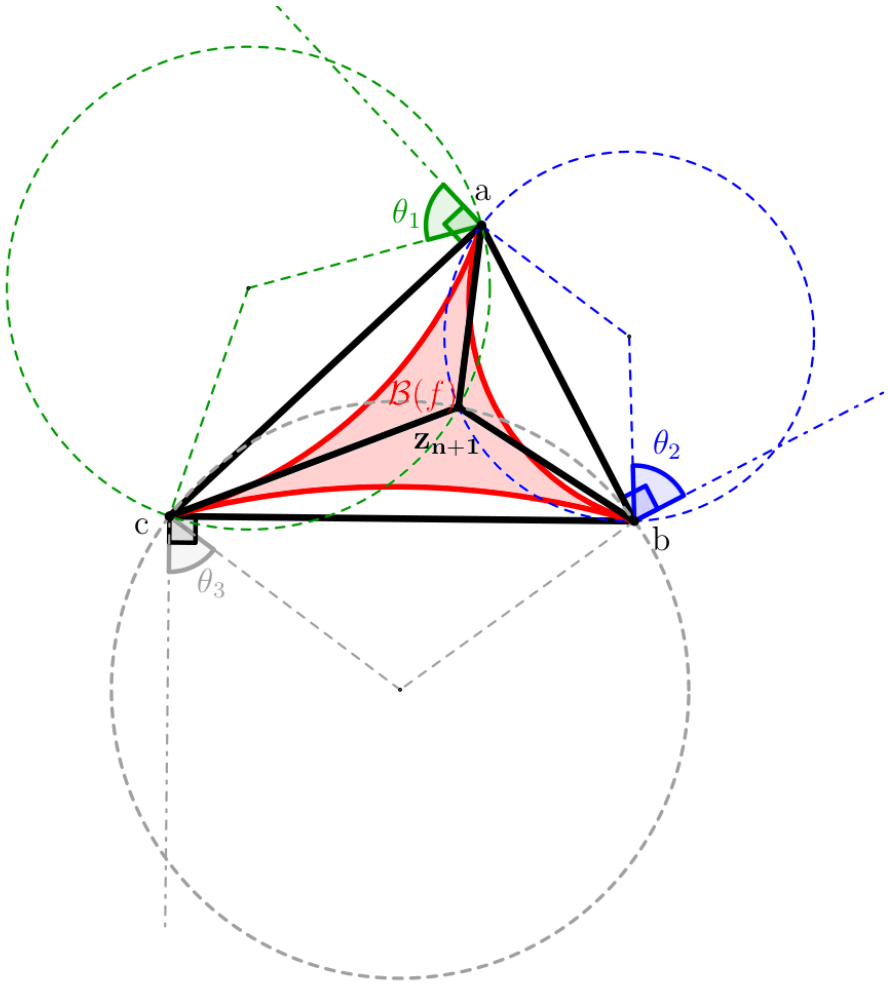

Figure 41: The Delaunay triangulation (in black) with the associated circumcircles. The center of the external face is at ∞.

From these conditions we immediately obtain that $I = \frac{1}{2}\left[\frac{1}{2}\left(\frac{\pi}{2}\right)^2\right] = \frac{\pi^2}{16}$. Then, one gets in equation 8.15:

$$\begin{aligned}\int_{\mathcal{B}(f)} d^2 z_{n+1}\ \det\left[D_{\{a,b,c\}}(T_f^D(\{z_v\}, z_{n+1}))\right] \\ &= \frac{\pi^2}{16}\det\left[D_{\{a,b,c\}}(T^D(\{z_1,\dots,z_n\}))\right] \\ &= \frac{\pi^2}{16}\frac{\Delta_3(a,b,c)}{\Delta_3(z_1,z_2,z_3)}\det\left[D_{\{1,2,3\}}(T^D(\{z_1,\dots,z_n\}))\right] \qquad (8.22)\end{aligned}$$

So in the end:

$$\begin{aligned}\int_{\mathbb{C}} d^2 z_{n+1}\ \det\left[D_{\{1,2,3\}}(T^D(\{z_1,\dots,z_{n+1}\}))\right] \\ &\geq \sum_{f\in\mathcal{F}(T^D)}\frac{\pi^2}{16}\det\left[D_{\{1,2,3\}}(T^D(\{z_1,\dots,z_n\}))\right] \\ &\geq (n-2)\frac{\pi^2}{8}\det\left[D_{\{1,2,3\}}(T^D(\{z_1,\dots,z_n\}))\right], \qquad (8.23)\end{aligned}$$

which is the inequality 8.10. A corollary is:

$$V_{n+1}^{\mathscr{D}} \geq (n-2)\frac{\pi^2}{8}V_n^{\mathscr{D}} \qquad (8.24)$$

□

The previous result gives a lower bound which does not depend on the shape of the triangle, by integrating over a restrained region $\mathcal{B}(f)$. If we do the same calculation and keep the region $\mathcal{R}(f)$, then the lower bound is more accurate, but not universal any more (it depends on the triangulation of size n). In this case, we then get a refined result:

Theorem 8.3.

$$\begin{aligned}\int_{\mathbb{C}} d^2 z_{n+1}\ \det\left[D_{\{1,2,3\}}(T^D(\{z_1,\dots,z_{n+1}\}))\right] \\ &\geq \left[(n-2)\frac{\pi^2}{8} + \frac{1}{8}\sum_{e\in\mathcal{E}(T^D)}\theta(e)(2\pi-\theta(e))\right]\det\left[D_{\{1,2,3\}}(T^D(\{z_1,\dots,z_n\}))\right] \qquad (8.25)\end{aligned}$$

(See appendix D for a proof). We see that the angles associated to the triangulation appear. This angle-dependent term should be related to the kinetic term of the Liouville action in the continuum limit.

Part IV

Convergence of correlation functions: the case of iso-perimetric planar Strebel graphs

In previous chapter, a model of random maps – namely Delaunay triangulations – was studied through a measure defined on the set of random maps. Therefore, all the results proven for Delaunay triangulations address directly the properties of the measure. Another way to characterize the measure, and to get a flavor of the continuous limit of the model is to define observables on the random maps model whose expectation value with respect to the measure are computable explicitly. This is equivalent to studying the measure through its moments, so it is less complete mathematically than directly studying the measure. However, this approach makes sense physically. Indeed, the only way to know about a physical system is by its interactions : for instance, a particle cannot be detected if it does not interact with an instrument. A physical system can only be characterized by the quantity one is able to *observe*, that is by the expectation values of observables. It cannot be known intrinsically from scratch. Another image is that of the definition of tangent spaces of differentiable manifolds in mathematics. The tangent space of a manifold at a point is defined thanks to the way functions defined on the manifold vary around this point: in order to know the tangent space, it is necessary to "test" the manifold with functions, and to see how they behave. In a similar manner, in order to know the physical system defined by a random map model, it is necessary to test it with observables, and look at their behaviour when the maps vary.

We adopt this paradigm here, so the aspect studied in this chapter is the computation of observables. In order to do so, we introduce a different map model, isoperimetric planar Strebel graphs which looks very alike duals of Delaunay triangulations, we embody them with a measure, and we define observables. The model defined may look very special as the constraints may look fancy and arbitrary. However, they are justified by the fact that they allow to compute explicitly the expectation values of many observables, thanks to a theorem of Kontsevich. This theorem supposes to introduce Chern classes, which we do. The result will show that Bessel functions play a primordial role. We analyze the continuous limit of the one-point function with different scalings for the perimeters, in order to spot how the large Strebel graphs behave when one face has a different perimeter. Last, we dwell on the similarities and the differences

between Strebel graphs and Delaunay triangulations. It appears that Bessel functions also appears in expectation values of observables of Delaunay triangulations, and that the Strebel graphs constitute a source of inspiration for defining observable of Delaunay triangulations. The articles [I] (for the Strebel graphs) and [II] (for the result on Delaunay) cover the problems addressed in this part.

9 Presentation of Strebel graphs

The Strebel graphs are ribbon graphs, with trivalent vertice Let us first define formally the Strebel graphs:

Definition 9.1. *A Strebel graph of genus g with n faces, is a connected* ribbon graph*, that can be embedded on a surface of genus g, with* trivalent vertices*, whose n faces are labeled topological discs (it is a* cellular graph*), and which is* metric*: the edges e carry a real positive number called the edge length $\ell_e \geq 0$. n is the size of the graph, and we denote by $\mathscr{S}_{g,n}$ the set of Strebel graphs of genus g and size n.*

In the same fashion as in the previous part, if $\Gamma \in \mathscr{S}_{g,n}$, we call $\mathcal{F}(\Gamma) = \{f_1, \ldots, f_n\}$, $\mathcal{E}(\Gamma)$ and $\mathcal{V}(\Gamma)$ respectively the set of faces, edges and vertices of Γ. The Euler relation stands:

$$|\mathcal{F}(\Gamma)| - |\mathcal{E}(\Gamma)| + |\mathcal{V}(\Gamma)| = 2 - 2g, \tag{9.1}$$

and as the vertices are trivalent, we have the constrain $2|\mathcal{E}(\Gamma)| = 3|\mathcal{V}(\Gamma)|$, so in the end:

$$\begin{aligned} |\mathcal{F}(\Gamma)| &= n & (9.2)\\ |\mathcal{E}(\Gamma)| &= 3n - 6 + 6g & (9.3)\\ |\mathcal{V}(\Gamma)| &= 2n - 4 + 4g. & (9.4) \end{aligned}$$

Example 9.1. In figure 42, a planar (that is to say, $g = 0$) Strebel graph of size 20 is shown. It is an element of $\mathscr{S}_{0,20}$

As the faces are bounded by edges carrying lengths, one can define the perimeter P_f of the face f:

$$P_f = \sum_{e \to f} \ell_e \tag{9.5}$$

where the notation $e \to f$ means that the sum runs over the edges adjacent to the face f. Then, one denotes by $\mathscr{S}_{g,n}(L_1, \ldots, L_n)$ the subset of $\mathscr{S}_{g,n}$ such that, for all $i \in \{1, \ldots, n\}$ the face i has perimeter L_i: $P_i = L_i$, $\forall i$. It is a stratum of $\mathscr{S}_{g,n}$ In example 9.1, the graph belongs to $\mathscr{S}_{0,20}(10)$. The sets $\mathscr{S}$ and $\mathscr{S}_{0,n}(P_1, \ldots, P_n)$ have

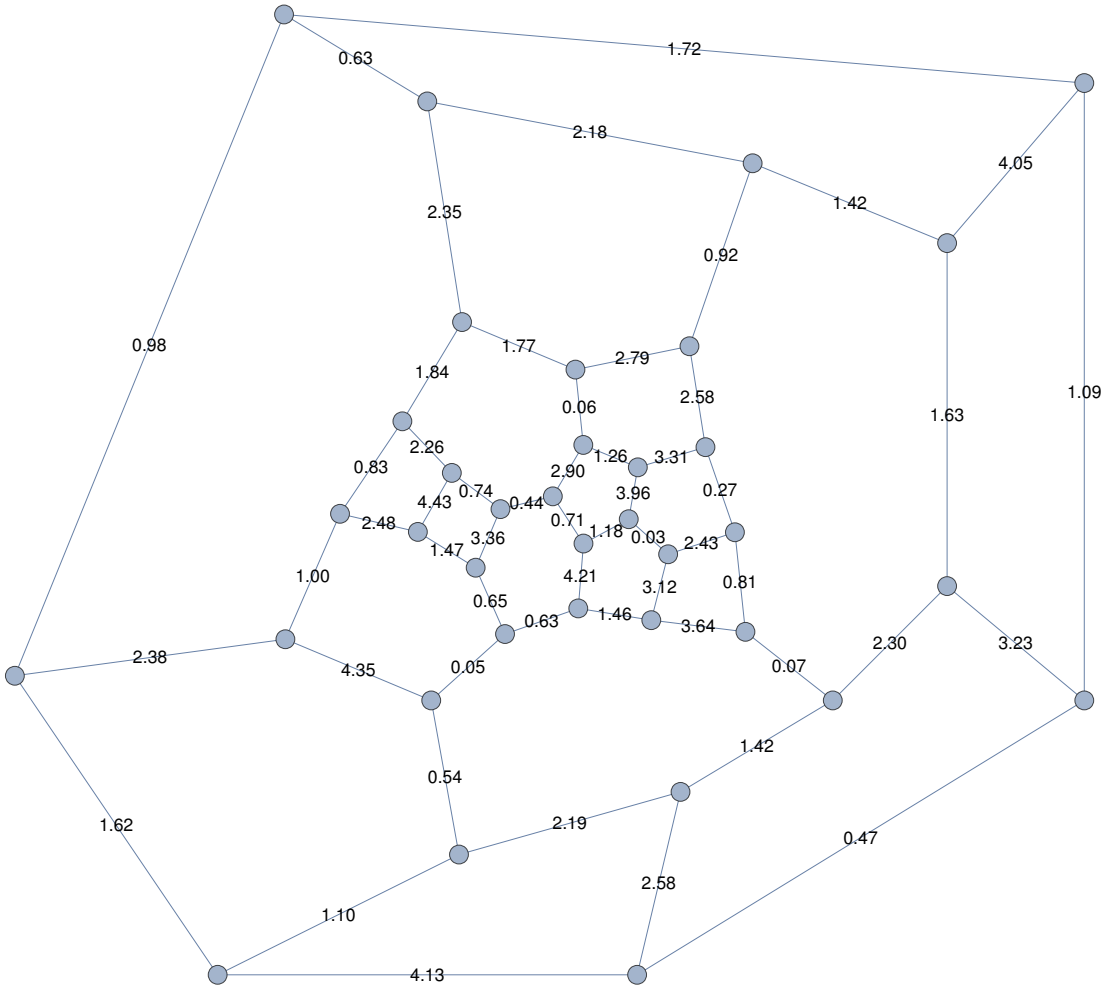

Figure 42: Example of a planar isoperimetric Strebel graph of size 20. Each face has perimeter 10 (± 0.05). It belongs to the set $\mathscr{S}_{0,20}(10)$

cellular decompositions, where each cell is indexed by a graph structure. A (g,n)-graph structure $\Gamma_{g,n}$ is a cellular trivalent connected graph of genus g and size n. Then the following holds:

$$\begin{aligned} \mathscr{S}_{g,n} &= \bigcup_{\Gamma_{g,n}} \{(\Gamma_{g,n}, \ell_1, \ldots, \ell_{3n-6+6g}) | \ell_i \in \mathbb{R}_+\} \\ \mathscr{S}_{g,n}(L_1, \ldots, L_n) &= \bigcup_{\Gamma_{g,n}} \{(\Gamma_{g,n}, \ell_1, \ldots, \ell_{3n-6+6g}) | \ell_i \in \mathbb{R}_+,\ P_f = L_f\} \end{aligned} \tag{9.6}$$

For g and n given, there are finitely many cells, but each cell is uncountable. For $\mathscr{S}_{g,n}$, the real dimension of a cell is the number of edges, that is $3n-6+6g$, and the lengths $\ell_1, \ldots, \ell_{3n-6+6g}$ are local coordinates.

A standard way to study distances (see the review of Miermont for a summary of results [Miermont, 2009]) for the study of random maps as metric spaces is to take the graph distance (each edge is considered to be of length 1), that is to say, the distance between two vertices $v_1,\ v_2 \in \mathcal{V}(\Gamma)$ is:

$$d(v_1, v_2) = \min_{l \text{ path from } v_1 \text{ to } v_2} |l|. \tag{9.7}$$

For Strebel graphs, the natural distance to consider on the graph is the first passage percolation distance, that takes the lengths of the edges into account (a similar distance was shown in previous chapter):

$$d(v_1, v_2) = \min_{l \text{ path from } v_1 \text{ to } v_2} \sum_{e \in l} \ell_e. \tag{9.8}$$

Actually, a great asset of Strebel graphs is that from the combinatorial data of a graph $\Gamma \in \mathscr{S}_{g,n}(L_1, \ldots, L_n)$ with $2-2g-n<0$, it is possible to construct a metric ω on a Riemann surface of genus g with n punctures, such that Γ is composed of geodesics of ω, and such that the lengths ℓ_e of the Strebel graphs are the lengths of the geodesics measured with the metric ω. Therefore, one can extend the notion of distance from the graph to a whole surface of genus g by using the metric ω. The way to construct ω from Γ is described hereafter, and it needs quadratic differentials.

9.1 Strebel differentials on Riemann surfaces

From marked Riemann surfaces to Strebel graphs: Strebel's theorem
Let Σ_g be a compact Riemann surface of genus g ; $p_1, \ldots, p_n \in \Sigma_g$, n labeled marked points ; and $P_1, \ldots, P_n \in \mathbb{R}_+$, n positive real numbers. Let $\{U_\alpha, \varphi_\alpha\}$ be an atlas of Σ_g. In the following, the local coordinate inherited from φ_α on U_α will be denoted by z_α
A meromorphic quadratic differential is a meromorphic section

$$\Omega : \Sigma_g \to K^2_{\Sigma_g},$$

where K_{Σ_g} is the canonical bundle of Σ_g and $K^2_{\Sigma_g}$ the symmetric square of the canonical bundle. Locally, we say that Ω is a meromorphic quadratic differential, if for all chart U_α, Ω can be written in the form:

$$\Omega(z_\alpha) = f_\alpha(z_\alpha)\,(dz_\alpha)^2\,, \tag{9.9}$$

with f_α a meromorphic function on U_α. If $p \in U_\alpha \cap U_\beta$ lays in the intersection of two charts, the local functions f_α and f_β must satisfy:

$$f_\alpha(z_\alpha(p)) = f_\beta(z_\beta(p)) \left(\frac{dz_\beta}{dz_\alpha}(p)\right)^2 \tag{9.10}$$

Strebel differentials are quadratic differentials, with contraints. Let us specify them in the following, and state Strebel's theorem. First, the poles of a Strebel differential Ω must be of order 2: let $p \in U_\alpha$ (we note $p_\alpha = z_\alpha(p)$) be a pole of Ω, then the admissible poles for a Strebel differential are double poles of this form:

$$\Omega(z_\alpha) \underset{z_\alpha \to p_\alpha}{=} \frac{-R^2}{(z_\alpha - p_\alpha)^2}(1 + O(z_\alpha - p_\alpha))(dz_\alpha)^2, \tag{9.11}$$

with $R \in \mathbb{R}_+$. According to the rule 9.10, the coefficient $-R^2$ does not depend on the local coordinate. It is the residue of Ω, for the following reason: if $\mathscr{C}_p$ is a small simple loop circling around p, then $\sqrt{\Omega}$ is well defined on $\mathscr{C}_p$ and one has:

$$\oint_{\mathscr{C}_p} \sqrt{\Omega} = \oint_{p_\alpha} \mathrm{i}R \frac{dz_\alpha}{(z_\alpha - p_\alpha)} \sqrt{1 + O(z_\alpha - p_\alpha)} = -2\pi R \tag{9.12}$$

(modulo the sign). Second, a Strebel differential allows to define horizontal and vertical trajectories:

Definition 9.2. *Let us consider $\gamma : [0,1] \to \Sigma_g$ a C^1 parametric curve. Let us suppose without loss of generality that $\gamma([0,1]) \subset U_\alpha$. Then γ is said to be:*

- *a horizontal trajectory, if $\forall t \in [0,1]$, $f_\alpha(z_\alpha(\gamma(t)))\left(\frac{dz_\alpha(\gamma(t))}{dt}\right)^2 > 0$.*
- *a vertical trajectory, if $\forall t \in [0,1]$, $f_\alpha(z_\alpha(\gamma(t)))\left(\frac{dz_\alpha(\gamma(t))}{dt}\right)^2 < 0$.*

Horizontal (resp. vertical) trajectories correspond to lines for which $\mathrm{Im}(\int^{\gamma(t)} \sqrt{\Omega}) =$ constant (resp. $\mathrm{Re}(\int^{\gamma(t)} \sqrt{\Omega}) =$ constant). Near a pole p of Ω with residue R, there exists a local coordinate z such that $z(p) = 0$ and Ω can be written as $\Omega = -R^2 \frac{dz^2}{z^2}$. The horizontal trajectories satisfy:

$$-R^2 \left(\frac{d\ln(z)}{dt}\right)^2 > 0, \tag{9.13}$$

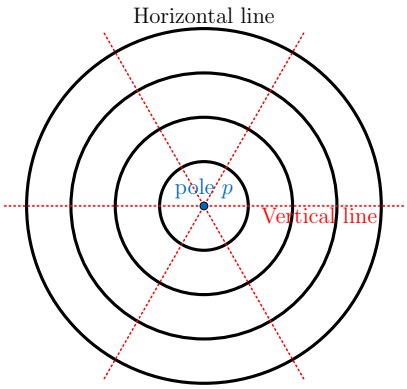

Figure 43: Horizontal trajectories (black plain circles) and vertical trajectories (red dashed rays) around a pole p.

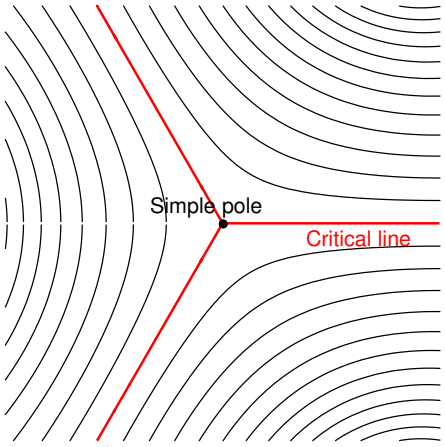

Figure 44: Horizontal lines around a simple zero. The thick red rays are critical lines.

that is to say, if we are close enough to p, $\operatorname{Re}\ln(z) = \text{constant}$, so the horizontal trajectories near p in the coordinate z are circles of center p. The vertical trajectories must satisfy $\operatorname{Im}\ln(z) = \text{constant}$, so they are rays stemming from p. Figure 43 shows the horizontal and vertical trajectories in the vicinity of p. Near a zero $a \in U_\alpha$ of Ω of order $k > 0$, take a local coordinate z such that $z(a) = 0$ and such that the Strebel differential has the local behaviour:

$$\Omega \underset{z\sim 0}{=} \frac{(k+2)^2}{4} z^k (dz)^2. \tag{9.14}$$

The horizontal and vertical trajectories obey respectively:

$$\begin{aligned} \left(\frac{d}{dt} z^{\frac{k+2}{2}}\right)^2 &> 0 \\ \left(\frac{d}{dt} z^{\frac{k+2}{2}}\right)^2 &< 0 \end{aligned} \tag{9.15}$$

Therefore, in the coordinate z, $k+2$ horizontal lines and vertical lines meet at 0 with angle $\frac{2\pi}{k+2}$ (see figure 44). For a simple zero, 3 horizontal lines meet with an angle $\frac{2\pi}{3}$. Among the horizontal trajectories of a generic quadratic differential with double poles satisfying equation 9.11, we distinguish the *critical* trajectories, which are the horizontal trajectories that arrive at a zero of Ω. Note that generically, the horizontal trajectories that emerge from a zero of Ω are not compact and can wind a infinite times around a domain. In that case, the critical trajectories are the accumulation points of the horizontal trajectories. It is now possible to define Strebel differentials:

Definition 9.3. *A Strebel differential on Σ_g Ω with poles $p_1, \ldots, p_n$ and residues $-P_1^2, \ldots, -P_n^2$ is a meromorphic quadratic differential, having the behaviour of equa-*

tion 9.11 with residue P_i around the pole p_i, and such that the critical trajectories form a connected cellular graph.

The set of critical trajectories form a connected graph of genus g. The vertices a_j are the zeros of Ω, and for a Strebel differential with simple zeros, the vertices are trivalent. The pole p_i of Ω sits in the center of the face f_i.
The critical trajectory $\mathscr{C}_{a_1,a_2}$ linking a_1 and a_2 is the edge e between the vertices a_1 and a_2. On $\mathscr{C}_{a_1,a_2}$, we have $\int_{a_1}^{z}\sqrt{\Omega}>0$ uniformly or $\int_{a_1}^{z}\sqrt{\Omega}<0$ uniformly. We define the length of e as:

$$\ell_e=\frac{1}{2\pi}\left|\int_{\mathscr{C}_{a_1,a_2}}\sqrt{\Omega}\right|. \tag{9.16}$$

What is more, the perimeter of the face f_i is simply the residue P_i of Ω at the pole p_i:

$$\sum_{e\to f_i}\ell_e=\frac{1}{2\pi}\left|\oint_{\mathscr{C}_{p_i}}\sqrt{\Omega}\right|=P_i. \tag{9.17}$$

Therefore, a Strebel differential of genus g with simple zeros and residues $P_1,\dots,P_n$ at the poles $p_1,\dots,p_n$, defines naturally a Strebel graph of genus g, size n, with perimeters $P_1,\dots,P_n$. Strebel's theorem allows to make a one-to-one correspondence between Strebel differentials and marked compact Riemann surfaces with perimeters:

Theorem 9.1. *Strebel [Strebel, 1984] For $g\geq 0$, $n\geq 1$ and $2g+n-2>0$, let Σ_g be a compact Riemann surface of genus g, $p_1,\dots,p_n$ be n marked points on Σ_g, and $P_1,\dots,P_n\in\mathbb{R}_+$. Then, there exists a unique Strebel differential on Σ_g whose only poles are $p_1,\dots,p_n$ with respective residues $-P_1^2,\dots,-P_n^2$.*

Example 9.2. In figure 45, a representation of horizontal lines of a Strebel differential of genus 0 with 4 poles is shown, as well as the Strebel graph corresponding to it. It belongs to $\mathscr{S}_{0,4}(1,1,1,1)$.

The metric associated to a Strebel differential Ω is then

$$\begin{aligned}\omega &= \frac{1}{2\pi}\sqrt{\Omega}\times\sqrt{\overline{\Omega}}\\ &= \frac{1}{2\pi}|f_\alpha(z_\alpha)|dz_\alpha d\overline{z}_\alpha\end{aligned} \tag{9.18}$$

A face f of the Strebel graph obtained from a Strebel differential Ω, endowed with the metric ω is a semi-infinite cylinder of perimeter P_f. Indeed, near a pole p_i, one can use the local coordinate z_i such that $z_i(p_i)=0$ and such that $\Omega=-P_i^2\frac{(dz_i)^2}{z_i^2}$. If one uses the coordinate $x_i=\ln(z_i)$ for $z_i\notin\mathbb{R}_-$, the coordinate x_i is defined on a strip (see figure 46). If one identifies the sides of the strip, x_i is defined on a cylinder. In this local

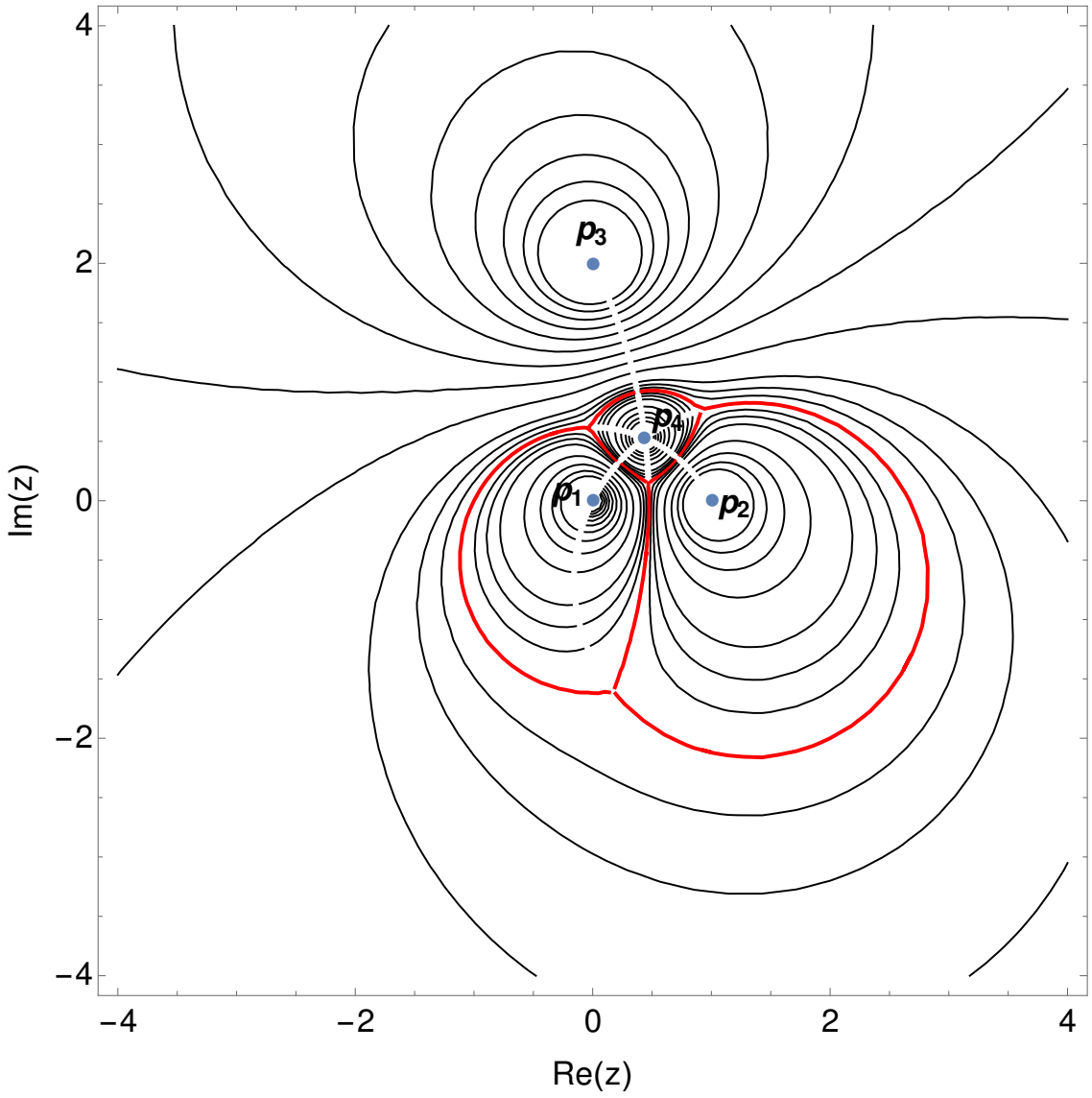

Figure 45: Horisontal lines of a Strebel differential of genus 0 with four poles $(p_1, p_2, p_3, p_4) = (0, 1, 2\mathrm{i}, \frac{1}{e^{-\frac{\mathrm{i}\pi}{6}}+2e^{-\frac{\mathrm{i}\pi}{3}}})$. The critical lines (red and thick) form an isoperimetric Strebel graph. In this example, each edge is of length $\frac{1}{3}$ so that the graph is in $\mathscr{S}_{0,4}(1,1,1,1)$. The white pieces of circles cutting the horizontal lines are due to the cut coming from the square roots in computing the integral $\int^z \sqrt{\Omega}$.

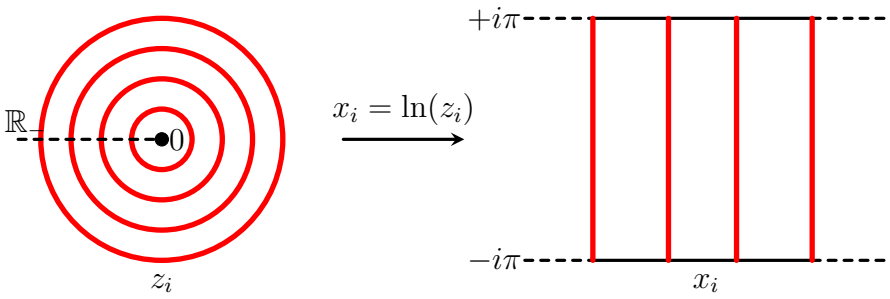

Figure 46: The change of coordinates from z_i to x_i transforms the circles in straight vertical lines in a strip, where the lines $\mathrm{Im}(x_i) = \pm i\pi$ are identified.

coordinate, the metric is just $\omega = P_i^2 dx_i d\overline{x}_i$: it is a flat metric, defined on a cylinder. The perimeter of the cylinder is just the width of the strip, that is P_i. Globally, the surface Σ_g endowed with the metric ω is a punctured surface with singularities at the marked points p_i, and which is a gluing of semi-infinite cylinders (see figure 47 for a 3 dimensional view of this gluing).

From Strebel graphs to marked Riemann surfaces In what precedes, Strebel graphs arise as critical curves on Riemann surface. The critical curves are defined through a quadratic differential Ω, that allows to define a metric $\frac{1}{2\pi}|\Omega|$ on the whole surface. The converse problem is the following: given a Strebel graph, that is, the combinatorial data of a metric cellular trivalent ribbon graph, is it possible to construct the differential Ω ? The answer is yes, and we describe the procedure to locally (that is, in a system of charts) construct Ω. Given a Strebel graph Γ, there is a canonical way to describe it as the critical graph of a Strebel differential, so there is a canonical way to associate a metric to a Strebel graph. We show here a local description (that is, in a system of charts) of the Strebel differential, inspired from Mulase and Penkava [Mulase and Penkava, 1998]. The set of charts is divided in three sets

$$\bigcup_{v\in\mathcal{V}(\Gamma)} U_v \bigcup_{e\in\mathcal{E}(\Gamma)} U_e \bigcup_{f\in\mathcal{F}(\Gamma)} U_f. \tag{9.19}$$

The chart U_v (respectively U_e, U_f) is defined in the neighborhood of the vertex v (resp. center of edge e, center of face f), and containing no other vertex (resp. edge, face). We describe the charts and the local coordinates, the Strebel differential and the transition functions between the charts.

Charts associated to the vertices Radius l_min. The coordinate z_v chosen around vertex v is such that the half-edges meeting at v are straight rays meeting at 0 (see figure 48) with an angle $\frac{2\pi}{3}$. Then, Strebel differential has the form :

$$\Omega = \frac{9}{4} z_v (dz_v)^2 \tag{9.20}$$

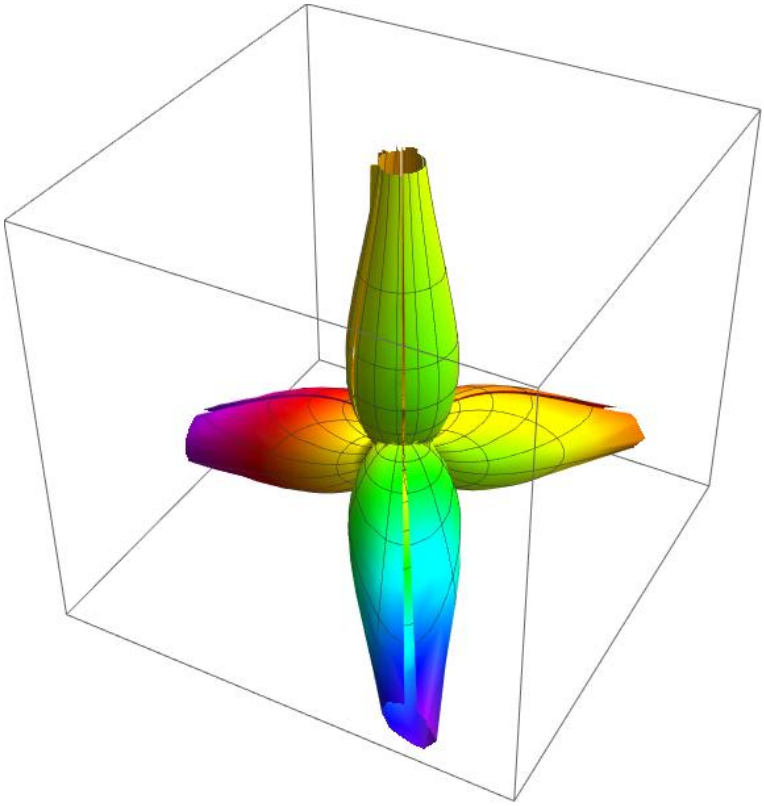

Figure 47: In this plot, the Riemann sphere is the unit sphere $\mathbb{S}^2 = \{(\cos\theta\sin\varphi, \sin\theta\sin\varphi, \cos\varphi),\ (\theta,\varphi) \in [0, 2\pi[\times[0, \frac{\pi}{2}]\}$. The surface depicts the radial view of $\left|\mathrm{Re}\int^z \sqrt{\Omega}\right|$ above $\mathbb{S}^2$: the distance between the origin and the surface in a direction (θ,φ) (above the point $z = (\cos\theta\sin\varphi, \sin\theta\sin\varphi, \cos\varphi)$) is equal to the value $1 + \left|\mathrm{Re}\int^z \sqrt{\Omega}\right|$. The picture emphasizes the fact that a Strebel Differential corresponds to a gluing of cylinders.

With this local coordinate, the chart U_v is a disk of radius $\frac{l_{min}}{2}$.

Charts associated to the edges Close to an edge e of length l_e, the coordinate z_e

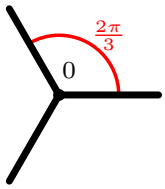

Figure 48: Critical lines meeting at 0 in the chart U_v with the local coordinate z_v.

chosen is such that the edge is the segment $[0, 2\pi]$ and such that Strebel differential is

$$\Omega = (dz_v)^2 \tag{9.21}$$

In this system of coordinates, the chart U_e is an infinite strip $\{z_e \in \mathbb{C}, 0 < \mathrm{Re}(z_e) < l_e\}$.

Charts associated to the faces The perimeter of face f is P_f, so we choose z_f such that:

$$\Omega = -\frac{P_f^2}{4\pi^2}\frac{(dz_f)^2}{z_f^2} \tag{9.22}$$

And in this system of coordinates, the chart U_f is a disk.

Transition functions

- If $p \in U_v \cap U_e$, then the transition relation between local coordinates is:

$$z_v(p) = c z_e(p)^{\frac{2}{3}} \tag{9.23}$$

  where c is a 3^{rd} root of unity.

- If $p \in U_e \cap U_f$, one has:

$$z_f(p) = e^{\frac{2\pi \mathrm{i} z_e(p)}{P_f}} e^{\frac{2\pi \mathrm{i}}{P_f}\sum_{e'<e}\ell_{e'}} \tag{9.24}$$

  where one choses arbitrarily an edge of reference e_1 on the face f, and assign a label to the edges in counterclockwise order.

- If $p \in U_v \cap U_f$, the transition is given by:

$$z_f(p) = \gamma e^{\frac{-2\pi z_v(p)^{\frac{3}{2}}}{P_f}} \tag{9.25}$$

  where γ is a constant of integration.

In the end, the data of a Strebel graph allows to define a metric on a whole punctured sphere. At the level of quantum gravity, as it was mentioned in previous chapter for Delaunay triangulations, there is no hope that, when the number of faces grows to infinity, that is to say, the number of punctures grows to infinity, the metrics converge toward a meaningful limiting metric. Yet, the interest of endorsing a graph with a metric on the whole surface, is that one is able to study naturally the distances in the graphs, without invoking the discrete graph metric. Strebel graphs considered as discrete metric spaces with the natural distances have chances to converge to a limiting metric space in the continuous limit.

10 Definition of the correlation functions

We specialize the model of Strebel graphs by adding two constraints: first, we consider planar graphs (g=0). Second, let $L > 0$, we consider isoperimetric Strebel graph, by requiring all the perimeters to satisfy $P_i = L$. Therefore, the set of interest is $\mathscr{S}_{0,n}(L,\dots,L)$, that is denoted $\mathscr{S}_{0,n}(L)$. In figure 42 is shown a example where $L = 10$. As in the case of Delaunay triangulations, the Lebesgue measure $d\nu_n^{L_1,\dots,L_n}$ of a stratum $\mathscr{S}_{0,n}(L_1,\dots,L_n)$ of $\mathscr{S}_{0,n}$ allows to define a probability distribution over $\mathscr{S}_{0,n}(P_1,\dots,P_n)$. Let $\Gamma_{g,n}$ be a (g,n)-graph structure. Then locally, that is to say for a given graph structure) , the measure can be expressed in terms of the edge lengths:

$$d\nu_n^{L_1,\dots,L_n}(\Gamma_{g,n}) = \prod_{e\in\mathcal{E}(\Gamma_{g,n})} d\ell_e \prod_{f\in\mathcal{F}(\Gamma_{g,n})} \delta(P_f - L_f). \tag{10.1}$$

For isoperimetric Strebel graphs, the measure is:

$$d\nu_n^{L}(\Gamma_{g,n}) = \prod_{e\in\mathcal{E}(\Gamma_{g,n})} d\ell_e \prod_{f\in\mathcal{F}(\Gamma_{g,n})} \delta(P_f - L). \tag{10.2}$$

As for the measure defined on Delaunay triangulations, this one is also admissible. Indeed, for a given graph structure $\Gamma_{g,n}$, the integral of the measure over the parameters ℓ_e has an obvious upper bound:

$$\int_{[0,L]^{3n-6+6g}} d\nu_n^{L}(\Gamma_{g,n}) \leq L^{2n-6+6g}. \tag{10.3}$$

Moreover, the number of graph structures for g, n fixed is finite, so the total volume:

$$\sum_{\substack{\Gamma_{g,n}\text{ graph}\\ \text{structure}}} \int_{[0,L]^{3n-6+6g}} d\nu_n^{L}(\Gamma_{g,n}) \tag{10.4}$$

is finite. Therefore, the measure is admissible.
The reference sets under study are the strata $\mathscr{S}_{0,n}(L)$, for $n \geq 3$. The aim is to

characterize $\mathscr{S}_{0,n}(L)$ with the measure $d\nu_n^L$ when $n \to \infty$. For a fixed large n and $k \geq 0$ bounded (in the limit $n \to \infty$, $k \ll n$), it is useful to study deformations of the stratum $\mathscr{S}_{0,n+k}(L)$, by letting k perimeters to be different from L. In other words, the strata $\mathscr{S}_{0,n+k}(L; L_1, \ldots, L_k) = \{\Gamma \in \mathscr{S}_{0,n+k} | P_1 = \cdots = P_n = L,\ P_{n+i} = L_i\}$, that are deformations of the stratum $\mathscr{S}_{0,n+k}(L)$, will allow to define correlation functions of the model. The k faces for which the perimeters may vary are similar to k sensors on $\mathscr{S}_{0,n+k}(L)$, allowing to study the sensibility of the set $\mathscr{S}_{0,n+k}(L)$ to a change of perimeter.

Definition 10.1. *Let $n \geq 3$ and $k \geq 0$. The correlation functions of Strebel graphs are defined as follows:*

- *The volume of $\mathscr{S}_{0,n+k}(L)$:*

$$V_{n+k}(L) = \sum_{\Gamma_{0,n+k} \text{ graph structure}} \int_{[0,L]^{3(n+k)-6}} d\nu_{n+k}^L(\Gamma_{0,n+k}) \tag{10.5}$$

- *The k-point function:*

$$Z_{n,k}(L; L_1, \ldots, L_k) = \sum_{\Gamma_{0,n+k} \text{ graph structure}} \int_{[0,L]^{3(n+k)-6}} d\nu_{n+k}^{L;L_1,\ldots,L_k}(\Gamma_{0,n+k}). \tag{10.6}$$

  It is the volume of $\mathscr{S}_{0,n+k}(L; L_1, \ldots, L_k)$.

Those correlation functions are encoded in the generating functions $\mathcal{V}(\mu, L)$ and $\mathcal{Z}_k(\mu, L; L_1, \ldots, L_k)$:

$$\begin{aligned} \mathcal{V}(\mu, L) &= \sum_{n=3}^{+\infty} \frac{\mu^n}{n!} V_n(L) \\ \mathcal{Z}_k(\mu, L; L_1, \ldots, L_k) &= \sum_{n=3}^{+\infty} \frac{\mu^n}{n!} Z_{n,k}(L; L_1, \ldots, L_k) \end{aligned} \tag{10.7}$$

Those generating functions are series in μ defined for μ close to 0. If one knows $\mathcal{V}(\mu, L)$ and if it is analytic in a neighborhood of 0, it is possible to recover any volume $V_n(L)$ for $n \geq 3$:

$$V_n(L) = n! \operatorname*{Res}_{\mu \to 0} \frac{\mathcal{V}(\mu, L)}{\mu^{n+1}} d\mu. \tag{10.8}$$

From the generating functions $\mathcal{Z}_k$ one can define the Legendre transform $\mathcal{U}_k$ and the Laplace transform $\mathcal{F}_k$:

$$\mathcal{U}_k(\mu, L; d_1, \ldots, d_k) = \frac{1}{(\mu L^2)^k} \int^{\mu} d\mu_{k-4} \int^{\mu_{k-4}} d\mu_{k-5} \cdots \int^{\mu_1} d\mu_0 \operatorname*{Res}_{L_k \to 0} \frac{d_k! 2^{2d_k}}{L_k^{2d_k+1}} dL_k \ldots$$

$$\begin{aligned}
& \operatorname*{Res}_{L_1\to 0} \frac{d_1! 2^{2d_1}}{L_1^{2d_1+1}} dL_1 \; \mathcal{Z}_k(\mu_0, L; L_1, \dots, L_k) \\
\mathcal{F}_k(\mu, L; z_1, \dots, z_k) &= \int_0^\infty dL_1 \cdots \int_0^\infty dL_k e^{-\sum_{i=1}^k z_i L_i} \mathcal{Z}_k(\mu, L; L_1, \dots, L_k) \qquad (10.9)
\end{aligned}$$

Those auxiliary functions are redundant with $\mathcal{Z}_k$, yet in chapter V, we shall see that the Laplace transform plays an important role. In this chapter, except for section 15, the Strebel graphs of interest are planar. This is why, for convenience, there is no mention of the genus in the correlation functions defined above. Yet, it will be useful, in chapter V, to consider correlation functions of generic genus. For generic $g \geq 0$:

$$\begin{aligned}
\mathcal{V}^g(\mu, L) &= \sum_{n=1}^\infty \frac{\mu^n}{n!} \mathrm{Vol}(\mathscr{S}_{g,n}(L)) \\
\mathcal{Z}_k^g(\mu, L; L_1, \dots, L_k) &= \sum_{n=1}^\infty \frac{\mu^n}{n!} \mathrm{Vol}(\mathscr{S}_{g,n+k}(L; L_1, \dots, L_k)) \\
\mathcal{F}_{g,k}(\mu, L; z_1, \dots, z_k) &= \int_0^\infty dL_1 \cdots \int_0^\infty dL_k e^{-\sum_{i=1}^k z_i L_i} \mathcal{Z}_k^g(\mu, L; L_1, \dots, L_k) \qquad (10.10)
\end{aligned}$$

Now that the correlation functions are defined, the tools to compute them are presented in next section.

Remark 10.1. *Strebel graphs, and more precisely their duals, Kontsevich graphs, are encoded in a matrix model. Let $\Lambda = \mathrm{diag}(\lambda_1, \dots, \lambda_N)$ be a real diagonal matrix of size N, and $V_\Lambda(M)$ be the following potential on the Hermitian matrices:*

$$V_\Lambda(M) = \Lambda M^2 - \frac{M^3}{3}. \qquad (10.11)$$

The the matrix model encoding Kontsevich graphs is encoded in the partition function:

$$\begin{aligned}
\mathcal{Z}_K &\overset{\text{formal}}{=} \frac{\int_{H_N} dM\, e^{-N \operatorname{Tr} V_\Lambda(M)}}{\int_{H_N} dM e^{-N \operatorname{Tr} \Lambda M^2}} \\
&\overset{\text{formal}}{=} \frac{\int_{H_N} dM\, e^{-N \operatorname{Tr} \Lambda M^2 - \frac{M^3}{3}}}{\int_{H_N} dM e^{-N \operatorname{Tr} \Lambda M^2}}. \qquad (10.12)
\end{aligned}$$

In this matrix model, the vertices of the ribbon graphs are trivalent, and the propagators now have weights:

$$\langle M_{ij} M_{kl} \rangle = \frac{1}{N} \frac{1}{\lambda_i + \lambda_j} \delta_{il} \delta_{jk}. \qquad (10.13)$$

Each face – or closed line – of the ribbon graph then carries an index j, and a parameter $\lambda_j \in \mathbb{R}$. The parameters λ_j of the ribbon graphs correspond to the parameters introduced if one makes the laplace transform of the perimeters of a Strebel graphs. Indeed, let us take a Strebel graphs of size n with perimeters $L_1, \dots, L_n$. If one fattens every edge of

the graph into a ribbon bordered by 2 lines, and then associate the index i to the line in face i, and if one carries out the Laplace transform $\int_{\mathbb{R}} dL_i e^{-\lambda_i L_i}$ of the perimeters to replace them by λ_i, then we end up with a ribbon graph that appears in the diagrammatic expansion of the partition function 10.12.

11 Moduli space, Kontsevich theorem and intersection numbers

As was advertised in the introduction of the chapter, there is a practical interest for defining the specific model of isoperimetric Strebel graphs with the correlation functions V_n and $Z_{n,k}$, being that those are explicitly computable by applying Kontsevich's theorem. This theorem relates the sets Strebel graphs and moduli spaces of Riemann surfaces. After a brief presentation of decorated moduli space of Riemann surfaces and of the Chern classes and intersection numbers, Kontsevich's theorem is stated. The moduli space of marked Riemann surfaces was introduced in section 7.1 of previous chapter. In order to relate the moduli space $\mathcal{M}_{g,n}$ to the set of Strebel graphs $\mathscr{S}_{g,n}$, we decorate each marked point p_i of a Riemann surface with a positive real number L_i, which plays the role of perimeters in the case of Strebel graphs. In other words, we consider the extension:

$$\tilde{\mathcal{M}}_{g,n} = \mathcal{M}_{g,n} \times \mathbb{R}_+^n. \tag{11.1}$$

Its dimension is

$$\dim_{\mathbb{R}} \tilde{\mathcal{M}}_{g,n} = 3n + 6g - 6. \tag{11.2}$$

It has the same dimension as $\mathscr{S}_{g,n}$, and by Strebel's theorem (theorem 9.1) [Strebel, 1984], and the works of Penner [Penner, 1988], Harer, Zagier [Harer - Zagier, 1986], Kontsevich [Kontsevich, 1992], there exists an orbifold-isomorphism, i.e. respecting the quotients by automorphism groups on both sides:

$$\tilde{\mathcal{M}}_{g,n} \sim \mathscr{S}_{g,n}. \tag{11.3}$$

A point of $\tilde{\mathcal{M}}_{g,n}$, is therefore uniquely represented by a Strebel graph, and the edge lengths provide a set of real coordinates. The interest of this isomorphism is that the measure $d\nu_n^{L_1,\dots,L_n}$ defined on the set of planar Strebel graphs can be pulled back to a measure on the moduli space genus 0 surfaces, which requires the introduction of Chern classes.

11.1 Chern classes over $\mathcal{M}_{g,n}$

Let us first recall the notion of cohomological class. Let U be a manifold and $\Omega^k(U)$ the set of differential k-forms. For each k, the exterior derivative d maps a k form to

a $k+1$ form:

$$\Omega^0(U) \xrightarrow{d} \Omega^1(U) \xrightarrow{d} \dots \Omega^k(U) \xrightarrow{d} \Omega^{k+1}(U) \xrightarrow{d} \dots . \tag{11.4}$$

A k-form $\omega \in \Omega^k(U)$ is *closed* if $d\omega = 0$, that is to say if:

$$\omega \in \ker(d) \qquad d : \Omega^k(U) \longrightarrow \Omega^{k+1}(U). \tag{11.5}$$

It is *exact* if there exists $\alpha \in \Omega^{k-1}(U)$ such that $\omega = d\alpha$, *i.e.* :

$$\omega \in \mathrm{Im}(d) \qquad d : \Omega^{k-1}(U) \longrightarrow \Omega^k(U). \tag{11.6}$$

The set of closed (respectively exact) k-forms is denoted $Z^k(U)$ (respectively $B^k(U)$). Since $d \circ d = 0$, every exact form is closed: $B^k(U) \subset Z^k(U) \subset \Omega^k(U)$. The quotient space $Z^k(U)/B^k(U)$ is denoted $H^k(U)$, and it is the *kth cohomology group of* U. The elements of $[\omega] \in H^k(U)$ are *cohomology classes*, and any two elements ω_1, ω_2 of a same class differ by an exact form $\omega_1 - \omega_2 = d\alpha$.
For instance, if $U = \mathbb{R}^2 \backslash \{0\}$ with canonical coordinates x, y. The following one-form $\alpha \in \Omega^1(U)$:

$$\alpha = \frac{xdy - ydx}{x^2 + y^2} \tag{11.7}$$

is closed $d\alpha = 0$, but not exact, so $[\alpha] \neq 0$.
Chern classes are cohomology classes, that are defined on fiber bundles. Let $\mathcal{L}$ be a complex vector bundle over the complex manifold U, whose fibers are of complex dimension r: $\mathbb{C}^r$. U is covered by a set of charts U_i, and locally, the fiber bundle can be trivialized as $U_i \times \mathbb{C}^r$. The coordinates on U_i are denoted x_μ. Then, let us choose a connection one-form $\omega \in \Omega^1(\mathcal{L}) \otimes \mathrm{End}(\mathbb{C}^r)$, whose expression in local coordinates takes the form

$$\omega = (\partial^\mu - A^\mu) dx_\mu. \tag{11.8}$$

The term A^μ is a matrix of size r, which acts on the fibers of the bundle. The curvature F of the connection is an element of $\Omega^2(\mathcal{L}) \otimes \mathrm{End}(\mathbb{C}^r)$, and has the following local expression:

$$F = (\partial^\mu A^\nu - \partial^\nu A^\mu) dx_\mu \wedge dx_\nu. \tag{11.9}$$

Chern classes are defined from the matrix value 2-form F.

Definition 11.1. *Given a complex vector bundle $\mathcal{L}$ over the complex manifold U with fibers $\mathbb{C}^r$ and F the curvature of a connection on $\mathcal{L}$, the Chern classes $c_0, \dots, c_r$ are the coefficients of the characteristic polynomial of F.*

$$\det_{r \times r}(y - F) = \sum_{k=0}^{r} (-1)^k c_k y^{r-k}. \tag{11.10}$$

The cohomology class $c_k(\mathcal{L})$ is the k^{th} Chern class of $\mathcal{L}$, it belongs to $H^k(U)$.

The 0^{th} Chern class is just a trivial constant function. In the case of a line bundle ($r = 1$), the only non trivial Chern class is the first Chern class $c_1(\mathcal{L})$, which is an element of $H^2(U)$: it is the cohomology class of the curvature $c_1(\mathcal{L}) = [F]$.
The Chern classes are independent of the choice of connection on $\mathcal{L}$, and are topological invariants of $\mathcal{L}$. Note that for any trivial line bundle $\mathcal{L}$ over U, $c_1(\mathcal{L}) = 0$. In the case of the moduli space $\mathcal{M}_{g,n}$, the line bundles $\mathcal{L}_1, \dots, \mathcal{L}_n$ over $\mathcal{M}_{g,n}$ are respectively the bundles whose fibers over $(\Sigma_g, p_1, \dots, p_n)$ are the cotangent spaces $T^*_{p_1}\Sigma_g, \dots, T^*_{p_n}\Sigma_g$ of the Riemann surface at the marked points $p_1, \dots, p_n$. In the same fashion, n line bundles $\tilde{\mathcal{L}}_1, \dots, \tilde{\mathcal{L}}_n$ are defined over $\tilde{\mathcal{M}}_{g,n}$:

$$\begin{array}{rcl} \mathcal{L}_i & \stackrel{\pi}{\to} & \mathcal{M}_{g,n} \\ (\Sigma_g, p_1, \dots, p_n, T^*_{p_i}\Sigma_g) & \mapsto & (\Sigma_g, p_1, \dots, p_n) \end{array} \tag{11.11}$$

and

$$\begin{array}{rcl} \tilde{\mathcal{L}}_i & \stackrel{\tilde{\pi}}{\to} & \tilde{\mathcal{M}}_{g,n} \\ (\Sigma_g, p_1, \dots, p_n, L_1, \dots, L_n, T^*_{p_i}\Sigma_g) & \mapsto & (\Sigma_g, p_1, \dots, p_n, L_1, \dots, L_n). \end{array} \tag{11.12}$$

The first Chern classes of those bundles are denoted:

$$\psi_i = c_1(\mathcal{L}_i) \quad \text{and} \quad \tilde{\psi}_i = c_1(\tilde{\mathcal{L}}_i). \tag{11.13}$$

Since $\tilde{\mathcal{M}}_{g,n} = \mathcal{M}_{g,n} \times \mathbb{R}^n_+$ is a product bundle, the Chern classes add, and since $\mathbb{R}^n_+$ is a trivial bundle its Chern class vanishes, so that, by misuse of notations, the two objects

$$\psi_i \quad \text{and} \quad \tilde{\psi}_i \tag{11.14}$$

will be denoted the same way. The class ψ_i is a 2-form, so $\left(\sum_{i=1}^n L_i^2 \psi_i\right)^{n-3+3g}$ is a $2n - 6 + 6g$ form, which is the dimension of $\mathcal{M}_{g,n}$, so it is a volume form on $\mathcal{M}_{g,n}$. As it was mentioned in section 7.1, the volume of $\mathcal{M}_{g,n}$ measured with this volume form makes sense if one compactifies $\mathcal{M}_{g,n}$. By Deligne-Mumford compactification procedure, $\overline{\mathcal{M}}_{g,n}$ is a compact space, and the following volume:

$$\int_{\overline{\mathcal{M}}_{g,n}} \left(\sum_{i=1}^n L_i^2 \psi_i\right)^{n-3+3g} \tag{11.15}$$

is well-defined. Thus, Chern classes allow to define a measure over the moduli spaces $\mathcal{M}_{g,n}$. Kontsevich's theorem relates this measure to a measure over Strebel graphs.

11.2 Kontsevich's theorem

Kontsevich used the isomorphism between $\tilde{\mathcal{M}}_{g,n}$ and $\mathscr{S}_{g,n}$ to express the Chern classes ψ_i in terms of edge lengths ℓ_e and perimeters. Then, he related the measure $\left(\sum_{i=1}^n L_i^2 \psi_i\right)^{n-3+3g} \prod_{i=1}^n dL_i$ over $\tilde{\mathcal{M}}_{g,n}$ to the Lebesgue measure over Strebel graphs.

Theorem 11.1. *Kontsevich [Kontsevich, 1992] Using the edge length coordinates induced by the isomorphism $\tilde{\mathcal{M}}_{g,n} \sim \mathscr{S}_{g,n}$ (for a point $(\Sigma_g, p_1, \ldots, p_n, L_1, \ldots, L_n)$ corresponding to a graph $\Gamma_{g,n} \in \mathscr{S}_{g,n}(L_1, \ldots, L_n)$), the Chern class takes locally the form*

$$\psi_i = \sum_{e<e' \text{ , adjacent to } p_i} d\left(\frac{\ell_e}{L_i}\right) \wedge d\left(\frac{\ell_{e'}}{L_i}\right) \qquad , \quad L_i = P_{f_i}, \tag{11.16}$$

where the e's adjacent to the vertex z_i are labelled in counterclockwise order. With this convention, the notation "$e < e'$ adjacent to z_i" means that the sum runs on the pairs of edges e, e' adjacent to the vertex z_i and such that their labels satisfy $e < e'$. What is more,

$$\prod_{e \in \mathcal{E}(\Gamma_{g,n})} d\ell_e = \frac{2^{5-5g-2n}}{(n-3+3g)!} \left(\sum_{i=1}^n L_i^2 \psi_i\right)^{n-3+3g} \prod_{i=1}^n dL_i. \tag{11.17}$$

11.3 Genus 0 case and intersection numbers

From now on, we shall focus on the planar case $g = 0$, and require that the number of marked points be $n \geq 3$ (see example 7.2). The previous result applied to $g = 0$ allows to reexpress the correlation functions of Strebel graphs as integrals over moduli spaces. Namely, for $k \geq 0$:

$$\begin{aligned} V_{n+k}(L) &= \frac{2^{5-2(n+k)}}{(n+k-3)!} \int_{\overline{\mathcal{M}}_{0,n+k} \times \mathbb{R}_+^{3(n+k)-6}} \left(\sum_{i=1}^{n+k} P_i^2 \psi_i\right)^{n+k-3} \prod_{i=1}^{n+k} dP_i \\ &\quad \prod_{j=1}^{n+k} \delta(P_j - L) \end{aligned} \tag{11.18}$$

$$\begin{aligned} Z_{n,k}(L; L_1, \ldots, L_k) &= \frac{2^{5-2(n+k)}}{(n+k-3)!} \int_{\overline{\mathcal{M}}_{0,n+k} \times \mathbb{R}_+^{3(n+k)-6}} \left(\sum_{i=1}^{n+k} P_i^2 \psi_i\right)^{n+k-3} \prod_{i=1}^{n+k} dP_i \\ &\quad \prod_{j=1}^{n} \delta(P_j - L) \prod_{m=1}^{k} \delta(P_{m+n} - L_m) \end{aligned} \tag{11.19}$$

The integrals over P_i are easily done:

$$V_{n+k}(L) = \frac{2^{5-2(n+k)}}{(n+k-3)!} \int_{\overline{\mathcal{M}}_{0,n+k}} \left(\sum_{i=1}^{n+k} L^2 \psi_i\right)^{n+k-3} \tag{11.20}$$

$$Z_{n,k}(L; L_1, \ldots, L_k) = \frac{2^{5-2(n+k)}}{(n+k-3)!} \int_{\overline{\mathcal{M}}_{0,n+k}} \left(\sum_{i=1}^{n} L^2 \psi_i + \sum_{i=1}^{k} L_i^2 \psi_{n+i}\right)^{n+k-3} \tag{11.21}$$

For all the correlation functions, it remains integrals over moduli spaces of marked Riemann spheres. If one develops the powers of the sums, it entails that the correlation

functions defined for Strebel graphs are combinations of terms of this form:

$$\int_{\overline{\mathcal{M}}_{0,n+k}} \psi_1^{d_1} \dots \psi_{n+k}^{d_{n+k}}. \tag{11.22}$$

These called are intersection numbers of $\mathcal{M}_{0,n+k}$, and noted:

$$\int_{\overline{\mathcal{M}}_{0,n+k}} \psi_1^{d_1} \dots \psi_{n+k}^{d_{n+k}} = \langle \psi_1^{d_1} \dots \psi_{n+k}^{d_{n+k}} \rangle_{0,n+k} = \langle \tau_{d_1} \dots \tau_{d_{n+k}} \rangle_0. \tag{11.23}$$

With this notation, the Legendre transform $\mathcal{U}_k$ of $\mathcal{Z}_k$ takes the form

$$\mathcal{U}_k(\mu, L; d_1, \dots, d_k) = \frac{1}{2} \sum_{n=0}^{\infty} \frac{\mu^n}{2^{2n}(n+k)!} \int_{\overline{\mathcal{M}}_{0,n+k+3}} \left(\sum_{d=0}^{\infty} \frac{L^{2d}}{d!} \tau_d \right)^{n+3} \prod_{i=1}^{k} (2L)^{2d_i-2} \psi_{n+3+i}^{d_i}. \tag{11.24}$$

The term *intersection* comes from the notion of intersection of cycles on a manifold. Let us look at an example with 2 oriented cycles γ_1 and γ_2 drawn on an oriented surface M (that has real dimension 2). γ_2 can cross γ_1 in two ways: either the crossing is direct with respect to the orientation of the surface, in which case one associates the number $+1$ to the crossing, or it is indirect and the crossing bears a -1 (see figure 49). The intersection number $\gamma_1 \cap \gamma_2$ is the sum of the crossing numbers of γ_2 intersecting γ_1. It is anti-symmetric: $\gamma_1 \cap \gamma_2 = -\gamma_2 \cap \gamma_1$. In figure 49, we have $\gamma_1 \cap \gamma_2 = +1$. The intersection number is invariant under a homotopic change of γ_1 and γ_2, so actually it is defined for *homology classes* $[\gamma_1], [\gamma_2] \in H_1(M, \mathbb{R})$, that are linear combinations of cycles (the addition of two classes is the concatenation of the cycles), seen up to homotopy. The elements of $H_1(M, \mathbb{R})$ are generalized cycles that have the form $\sum_i \alpha_i [\gamma_i]$, where γ_i are cycles and $\alpha_i \in \mathbb{R}$. The intersection number is a bilinear map, so $(\alpha_1[\gamma_1] + \alpha_2[\gamma_2]) \cap [\gamma_3] = \alpha_1[\gamma_1] \cap [\gamma_3] + \alpha_2[\gamma_2] \cap [\gamma_3]$. This example covers only the case of a surface of real dimension 2, with two paths that have dimension 1.

Let us extend the intersection of cycles to a more general case, where now M is an orientable manifold of dimension r, $[\gamma_1] \in H_k(M)$ is a homology class of order k (that has co-dimension $r-k$), and $[\gamma_2] \in H_{r-k}(M)$. Note that the co-dimensions of γ_1, γ_2 must sum up to give r, the dimension of the manifold. In order to define $\gamma_1 \cap \gamma_2$, we resort to Poincaré duality theorem: it allows to define a form-cycle duality, by associating to a homology class (a generalized cycle) $[\gamma] \in H_k(M, \mathbb{R})$, a cohomology class (a form) $[\gamma^*] \in H^{r-k}(M, \mathbb{R})$. Then, the intersection number is defined by:

$$\begin{aligned} [\gamma_1] \cap [\gamma_2] &= \int_{\gamma_1} \gamma_2^* \\ &= -\int_{\gamma_2} \gamma_1^* \end{aligned}$$

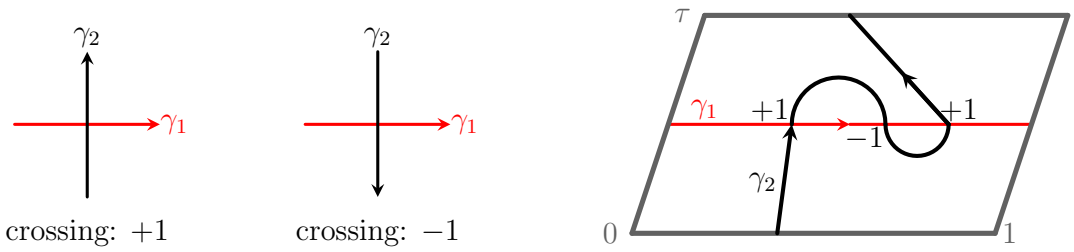

Figure 49: On the left hand side, the types of crossings of two oriented cycles with their crossing numbers ; on the right hand side, an example of two intersecting cycles on a torus with intersection number $\gamma_1 \cap \gamma_2 = 1 - 1 + 1 = +1$.

$$= \int_M \gamma_1^* \wedge \gamma_2^*. \tag{11.25}$$

The intersection number of two cycles defined on a manifold is an integer, so the integral $\int_M \gamma_1^* \wedge \gamma_2^* \in \mathbb{Z}$ in this case.
In our case, the integral of Chern classes $\int_{\overline{\mathcal{M}}_{0,n+k}} \psi_1^{d_1} \dots \psi_{n+k}^{d_{n+k}}$ is the intersection of the homology classes

$$[\psi_1^{d_1}]^* \cap \dots \cap [\psi_{n+k}^{d_{n+k}}]^* \in \mathbb{Q}.$$

These intersection numbers are not integers (except for $g = 0$) but rather rational numbers because $\overline{\mathcal{M}}_{g,n}$ is an orbifold and not a manifold.
If the set of Strebel graphs has been specialized to planar graphs in this study, it is because the intersection numbers in genus 0 are known:

$$\langle \tau_{d_1} \dots \tau_{d_{n+k}} \rangle_0 = \begin{cases} \frac{(n+k-3)!}{d_1! \dots d_{n+k}!} & \text{if } d_1 + \dots + d_{n+k} = n + k - 3 \\ 0 \quad \text{otherwise.} \end{cases} \tag{11.26}$$

12 Computation of the correlation functions and Bessel functions

The correlation functions are now computed, the whole section relies on formula 11.26. The modified Bessel function will arise naturally from the generating functions.

12.1 Volumes of Strebel graphs

It is easier to compute the 3rd derivative of the volume generating function. Using 11.26, we get:

$$\frac{\partial^3}{\partial \mu^3} \mathcal{V}(\mu, L) \quad = \quad \sum_{n=0}^{\infty} \frac{\mu^n}{n!} V_{n+3}(L)$$

$$
\begin{aligned}
&= \frac{1}{2}\sum_{n=0}^{\infty}\frac{\mu^n}{2^{2n}\ n!}\sum_{d_1+\cdots+d_{n+3}=n}\frac{L^{2n}}{\prod_{i=1}^{n+3}d_i!}\left\langle\prod_{i=1}^{n+3}\tau_{d_i}\right\rangle_0\\
&= \frac{1}{2}\sum_{n=0}^{\infty}\frac{\mu^n}{2^{2n}\ n!}\sum_{d_1+\cdots+d_{n+3}=n}\frac{L^{2n}}{\prod_{i=1}^{n+3}d_i!}\ \frac{n!}{\prod_{i=1}^{n+3}d_i!}\\
&= \frac{1}{2}\sum_{n=0}^{\infty}\mu^n L^{2n}\sum_{d_1+\cdots+d_{n+3}=n}\frac{1}{\prod_{i=1}^{n+3}2^{2d_i}d_i!^2}
\end{aligned}
\tag{12.1}
$$

Let us consider the first kind modified Bessel function $I_0(z)$:

$$
I_0(z)=\sum_{d=0}^{\infty}\frac{z^{2d}}{2^{2d}\,d!^2}. \tag{12.2}
$$

We have

$$
\sum_{d_1+\cdots+d_{n+3}=n}\frac{1}{\prod_i 2^{2d_i}d_i!^2}=[z^{2n}]I_0(z)^{n+3}=\mathrm{Res}_{z\to 0}\,\frac{dz}{z^{2n+1}}I_0(z)^{n+3}, \tag{12.3}
$$

where $[z^k]f(z)$ stands for the coefficient of z^k in the expansion of f around 0. Therefore

$$
\begin{aligned}
\frac{\partial^3}{\partial\mu^3}\mathcal{V}(\mu,L) &= \frac{1}{2}\sum_{n=0}^{\infty}\operatorname*{Res}_{z\to 0}\frac{dz}{z^{2n+1}}I_0(z)^{n+3}(\mu L^2)^n\\
&= \frac{1}{4\pi\mathrm{i}}\oint_{\mathcal{C}}\frac{dz}{z}\,\frac{I_0(z)^3}{1-\mu L^2 I_0(z)/z^2}
\end{aligned}
\tag{12.4}
$$

where $\mathcal{C}$ is the integration contour of fig.51 below. Indeed, the residue $\operatorname*{Res}_{z\to 0}f(z)dz$ is an integral over a contour $\mathcal{C}$ encircling 0, and no other pole of $f(z)$: $\operatorname*{Res}_{z\to 0}f(z)dz=\frac{1}{2\pi\mathrm{i}}\oint_{\mathcal{C}}f(z)dz$. The size of the contour is fixed after exchanging the sum and the residue. Once they are formally exchanged, one ends up with $\frac{1}{2\pi\mathrm{i}}\oint_{\mathcal{C}}dz\sum_n\frac{1}{z^{2n+1}}I_0(z)^{n+3}(\mu L^2)^n$. The sum is convergent iff $\left|\frac{z^2}{I_0(z)}\right|>\mu L^2$, so the contour $\mathcal{C}$ has to surround $\pm u(\mu L^2)$, defined as the $O(\mu)$ solutions of

$$
\mu L^2=\frac{u^2}{I_0(u)}. \tag{12.5}
$$

The function $u^2/I_0(u)$ is plotted in fig.50. As one sees on the plot, the $O(\mu)$ solutions of equation 12.5 cease to make sense when $|u|\geq u_c\approx 2.58$. This value is critical, and the study of its neighborhood is crucial to get the large n limit of volumes.

The contour integral can be evaluated; it consists of residues of the 2 poles at $z=\pm u(\mu L^2)$:

$$
\frac{\partial^3}{\partial\mu^3}\mathcal{V}(\mu,L) = \frac{1}{\mu L^2 u}\ \frac{I_0(u)^3}{2I_0(u)/u^3-I_0'(u)/u^2}
$$

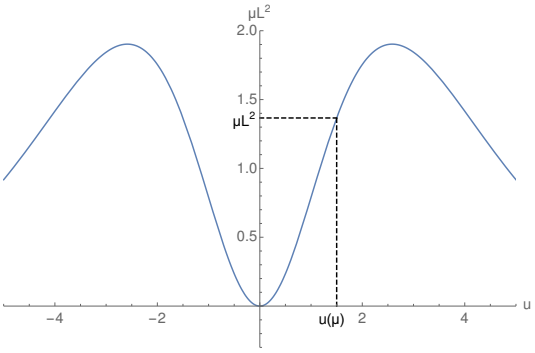

Figure 50: Plot of the function $\frac{u^2}{I_0(u)}$.

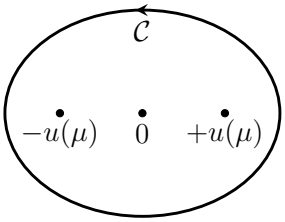

Figure 51: Contour of integration

$$= \frac{I_0(u)^4}{2I_0(u) - uI_0'(u)} \tag{12.6}$$

The derivative of the Bessel function I_0 is the Bessel function I_1 (see appendix A), thus

$$\frac{\partial^3}{\partial\mu^3}\mathcal{V}(\mu, L) = \frac{I_0(u)^3}{2 - uI_1(u)/I_0(u)} = \frac{uI_0(u)^2}{L^2}\,\frac{du}{d\mu}. \tag{12.7}$$

Using $I_1'(u) = I_0(u) - I_1(u)/u$, we can integrate:

$$\frac{\partial^2}{\partial\mu^2}\mathcal{V}(\mu, L) = \frac{u^2(I_0(u)^2 - I_1(u)^2)}{2L^2}. \tag{12.8}$$

Further integration is not doable explicitly, but this formula fits for our purpose of getting the behaviour of the large n volumes (see section 14).

12.2 k-point functions

Let us fix $d_1, \ldots, d_k$, and note $D \stackrel{\text{def}}{=} \sum_{i=1}^k (d_i - 1)$. We begin with the auxiliary generating function $\mathcal{U}$. In the same manner as for the volumes, we introduce the Bessel function $I_0(z)$ and we have:

$$\begin{aligned}\mathcal{U}_k(\mu, L; d_1, \ldots, d_k) &= \frac{1}{2}\sum_n \frac{\mu^n L^{2n}}{\prod_{i=1}^k d_i!}\,\mathrm{Res}_{z\to 0}\,\frac{dz}{z^{1+2(n-D)}} I_0(z)^{n+3} \\ &= \frac{1}{4\pi\mathrm{i}}\,\frac{1}{\prod_i d_i!}\oint_C \frac{z^{2D}dz}{z}\,\frac{I_0(z)^3}{1 - \mu L^2 I_0(z)/z^2}\end{aligned} \tag{12.9}$$

The residues at the two poles $z = \pm u(\mu L^2)$ can be evaluated easily. Besides, if $D < 0$, there can be another pole at $z = 0$. We have

$$\mathcal{U}_k(\mu, L; d_1, \ldots, d_k) = \overbrace{\frac{1}{\prod_i d_i!}\,\frac{u^{2D}\,I_0(u)^4}{2I_0(u) - uI_1(u)}}^{\text{Res at } \pm u}$$

$$
\begin{aligned}
& + \underbrace{\frac{1}{2}\frac{1}{\prod_i d_i!}\,\mathrm{Res}_{z\to 0}\, z^{2D+1}dz\,\frac{I_0(z)^3}{z^2-\mu L^2 I_0(z)}}_{\text{Res at } 0 \text{ if } D<0} \\
= \quad & \frac{1}{\prod_i d_i!}\,\frac{u^{2D}\,I_0(u)^4}{2I_0(u)-uI_1(u)} \\
& -\frac{1}{2}\frac{1}{\prod_i d_i!}\sum_{j=1}^{-D}\frac{1}{(\mu L^2)^j}\,\mathrm{Res}_{z\to 0}\, z^{2(D+j)-1}dz\, I_0(z)^{3-j}.
\end{aligned}
\tag{12.10}
$$

If $D<0$, the first term, proportional to u^{2D} is a Laurent formal series of μL^2, starting with a negative power, whereas the last term contributing only if $D<0$, is a polynomial of $1/\mu L^2$. Since the whole result should be a power series of μL^2 with only positive powers, we understand that the last term just cancels the negative part of the first. We thus may write:

$$
\mathcal{U}_k(\mu, L; d_1, \ldots, d_k) = \frac{1}{\prod_i d_i!}\left(\frac{u^{2D}\,I_0(u)^4}{2I_0(u)-uI_1(u)}\right)_+ \tag{12.11}
$$

meaning that we keep only positive powers of μL^2 in the Laurent expansion. We observe that upon multiplying by $\prod_i d_i!$, the right hand side depends only on D and u, we write it

$$
\mathcal{U}_k(\mu, L; d_1, \ldots, d_k) = \frac{1}{\prod_i d_i!}\, f_D(u) \quad , \quad f_D(u) = \left(\frac{u^{2D}\,I_0(u)^4}{2I_0(u)-uI_1(u)}\right)_+ . \tag{12.12}
$$

The relationship to our previously defined generating functions is

$$
\mathcal{Z}_k(\mu, L; L_1, \ldots, L_k) \quad = \quad L^{2k}\sum_{d_1,\ldots,d_k=0}^{\infty}\prod_{i=1}^{k}\frac{L_i^{2d_i}L^{-2d_i}}{2^{2d_i}d_i!}\;\partial_\mu^{k-3}\left(\mu^k \mathcal{U}_k(\mu, L; d_1, \ldots, d_k)\right) \tag{12.13}
$$

So

$$
\begin{aligned}
& \mathcal{Z}_k(\mu, L; L_1, \ldots, L_k) \\
= \quad & L^{2k}\sum_{d_1,\ldots,d_k}\prod_{i=1}^{k}\frac{L_i^{2d_i}L^{-2d_i}}{2^{2d_i}d_i!^2}\;\partial_\mu^{k-3}\left(\mu^k f_D(u(\mu L^2))\right) \\
= \quad & \partial_\mu^{k-3}\left(\mu^k L^{2k}\sum_D f_D(u(\mu L^2))\sum_{d_1+\cdots+d_k=D+k}\prod_{i=1}^{k}\frac{L_i^{2d_i}L^{-2d_i}}{2^{2d_i}d_i!^2}\right) \\
= \quad & \partial_\mu^{k-3}\left(\mu^k L^{2k}\sum_D f_D(u(\mu L^2))\,\mathrm{Res}_{z\to 0}\frac{dz}{z^{1+2(D+k)}}\prod_{i=1}^{k} I_0(zL_i/L)\right) \\
= \quad & \partial_\mu^{k-3}\left(\mu^k L^{2k}\,\mathrm{Res}_{z\to 0}\frac{dz}{z^{1+2k}}\prod_{i=1}^{k} I_0(zL_i/L)\sum_{D=-k}^{\infty} z^{-2D}\, f_D(u(\mu L^2))\right)
\end{aligned}
$$

(12.14)

Carrying out the sum over D is possible if we impose $|z| > |u|$, so enforcing this condition, one gets:

$$\frac{1}{z^{1+2k}} \sum_{D=-k}^{+\infty} \frac{f_D(u(\mu L^2))}{z^{2D}} = \left(\frac{1}{u^{2k}} \frac{z}{z^2-u^2} \frac{I_0(u)^4}{2I_0(u) - uI_1(u)} \right)_+ \tag{12.15}$$

Then we can rewrite $\mathcal{Z}_k$ in the following way:

$$\begin{aligned} \mathcal{Z}_k(\mu, L; L_1, \ldots, L_k) &= \frac{1}{2\pi \mathrm{i}} \partial_\mu^{k-3} \left(\mu^k L^{2k} \left[\frac{1}{u^{2k}} \frac{I_0(u)^4}{2I_0(u) - uI_1(u)} \times \right. \right. \\ &\quad \left. \left. \oint_C \frac{z dz}{z^2-u^2} \prod_{i=1}^{k} I_0(zL_i/L) \right]_+ \right) \\ &= \partial_\mu^{k-3} \left(\mu^k L^{2k} \left[\frac{1}{u^{2k}} \frac{I_0(u)^4}{2I_0(u) - uI_1(u)} \prod_{i=1}^{k} I_0(uL_i/L) \right]_+ \right) \end{aligned} \tag{12.16}$$

The contour integral is now $\mathcal{C}$ (see figure 51), because, though the residue is around 0, we imposed $|z| > |u|$, in order to sum over D. Its Laplace transform is

$$\mathcal{F}_k(\mu, L; z_1, \ldots, z_k) = \partial_\mu^{k-3} \left(\mu^k L^{2k} \left[\frac{1}{u^{2k}} \frac{I_0(u)^4}{2I_0(u) - uI_1(u)} \prod_{i=1}^{k} (z_i^2 - u^2/L^2)^{-1/2} \right]_+ \right). \tag{12.17}$$

Again, note that the third derivative simplifies the result:

$$\partial_\mu^3 \mathcal{F}_k(\mu, L; z_1, \ldots, z_k) = \partial_\mu^k \left(\frac{\mu^k L^{2k}}{u^{2k}} \frac{I_0(u)^4}{2I_0(u) - uI_1(u)} \prod_{i=1}^{k} (z_i^2 - u^2/L^2)^{-1/2} \right). \tag{12.18}$$

In the end, we see that we can compute all the k-point functions we defined. More generally, for the set $\mathscr{S}_{0,n}(L)$ we can compute all the correlation functions expressible in terms of Chern classes $\psi_1, \ldots, \psi_n$. Therefore, we can compute n independent correlation functions (that is to say observables depending on n independent sets of edge lengths). The number of independent observables one can compute is the number of independent edge lengths in $\mathscr{S}_{0,n}(L)$, which is $2n-6$. Hence we are able to compute approximately half of the possible independent correlation functions. Among the correlation functions that are not computed here, there is the correlation function that compute the average distance (on the graph) between two vertices for instance.

13 Link with Delaunay triangulations

Strebel graphs and Delaunay triangulations are very close to be dual sets, that is, Strebel graphs and Voronoï tessellations look alike. Indeed, consider a Delaunay triangulation with $n \geq 3$ vertices $T \in \mathcal{T}_n$. To each edge $e \in \mathcal{E}(T)$ is associated the angle θ_e. At each vertex $v \in \mathcal{V}(T)$, the constraint

$$\sum_{e \to v} \theta_e = 2\pi \tag{13.1}$$

holds. T has $3n-6$ edges. Now, consider the dual T^* of T. It is a Voronoï tessellation with n faces, $3n-6$ edges, and trivalent vertices (as the faces of T are triangles). The label ℓ_{e^*} of an edge $e^* \in \mathcal{E}(T^*)$ dual to the edge $e \in \mathcal{E}(T)$ is simply the angle θ_e associated to e: $\ell_{e^*} = \theta_e$ The constraint 13.1 becomes

$$\sum_{e^* \to f^*} \ell_{e^*} = 2\pi \tag{13.2}$$

for any $f^* \in \mathcal{F}(T^*)$. Therefore, T^* is an isoperimetric Strebel graph of size n: $T^* \in \mathscr{S}_{0,n}(2\pi)$. The inclusion $\mathcal{T}_n^* \subset \mathscr{S}_{0,n}$ may incite to use the results obtained for Strebel graphs in previous section to Delaunay triangulations. Yet, many discrepancies appear when looking at the details of the models, preventing from making a strict correspondence between the models. Still, it is possible to compute correlation functions of Delaunay triangulations using cohomology classes, and the common feature of Bessel functions appears. Hereafter I stress on the differences and the similarities of the models.

13.1 Differences between Strebel graphs and Delaunay triangulations

First, the dual set of Delaunay triangulations is a strict subset of isoperimetric Strebel graphs. Indeed, consider the Strebel graph depicted in figure 52. It belongs to $\mathscr{S}_{0,5}(2\pi)$ and yet, its dual (depicted in dashed lines), although it is a triangulation, does not have the structure of a Delaunay triangulation, because of the edge $\tilde{e}$ linking the vertex v_1 to itself: Delaunay triangulations are simple graphs.

Second, once one knows that $\mathcal{T}_n^* \subsetneq \mathscr{S}_{0,n}(2\pi)$, one may still want to use the local expression of Chern classes (see theorem 11.1) and transpose the volumes of Delaunay triangulations in terms of intersection numbers of Chern classes, by integrating the cohomology classes on a subset of $\overline{\mathcal{M}}_{0,n}$. It happens that this is doomed to fail, for the following argument, that we developed in [II].

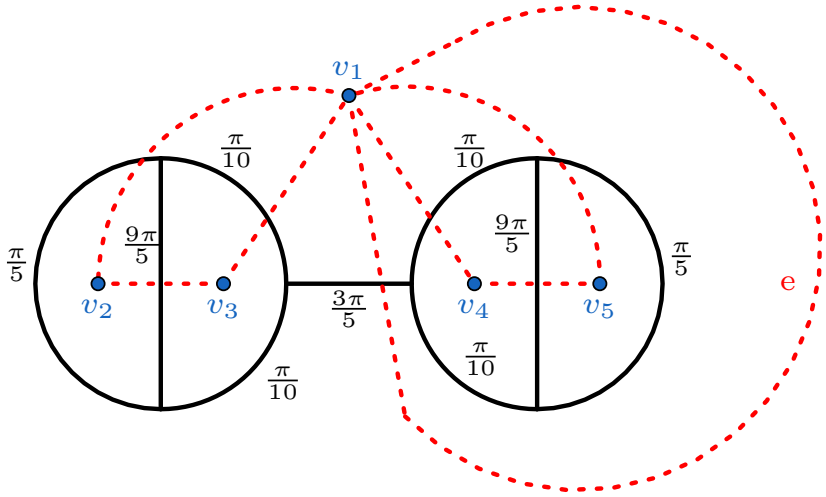

Figure 52: Example of an isoperimetric Strebel graph (black, plain lines) in $\mathscr{S}_{0,5}(2\pi)$ whose dual (red, dashed lines) is a triangulation, but cannot be a Delaunay triangulation.

Relation with topological Witten-Kontsevich intersection theory For a Delaunay triangulation $T \in \mathcal{T}_n,\ n \geq 3$ with n vertices, the formula 11.16 defining locally the Chern class ψ_i for each face i in the Strebel graphs case, can be transposed in order to define a cohomology class ψ_v for each vertex $v \in \mathcal{V}(T)$, provided that one replaces ℓ_e by θ_e, and L_i by 2π:

$$\psi_v = \frac{1}{(2\pi)^2} \sum_{e' < e \to v} d\left(\frac{\theta_e}{2\pi}\right) \wedge d\left(\frac{\theta'_e}{2\pi}\right), \tag{13.3}$$

with the same counterclockwise orientation of the edges as in formula 11.16. This idea of applying the local definition of Chern classes to the case of Delaunay triangulations was introduced in [David and Eynard, 2014]. The authors showed that indeed, the measure on Delaunay triangulations satisfies:

$$d\nu_n(T,\theta) = \frac{2^{2n-5}}{(n-3)!} \left(\sum_{v \in \mathcal{V}(T)} (2\pi)^2 \psi_v \right)^{n-3}. \tag{13.4}$$

Also, there is a one-to-one correspondence between the set $\mathcal{T}_n$ and the moduli space $\mathcal{M}_{0,n}$ of conformal structures of the sphere with n marked points, so we identify $\mathcal{T}_n$ with $\mathcal{M}_{0,n}$. Thus, it seems that the class ψ_v is a Chern class of a U(1) line bundle $\mathcal{L}_v \to \mathcal{M}_{0,n}$ attached to the vertex v, in the same manner as $\psi_i = c_1(\mathcal{L}_i)$. Yet, in order to be a Chern class over the set of Delaunay triangulations, the class ψ_v has

to be the curvature of a global connection. In the same paper of David and Eynard [David and Eynard, 2014], the 2-form ψ_v was defined explicitly as the curvature du_v of the U(1) connection

$$u_v = \frac{1}{(2\pi)^2} \sum_{f \to v} \theta(f_+)\, d\gamma_v(f) \tag{13.5}$$

In 13.5 the sum runs over the faces f adjacent to the vertex v. $\gamma_v(f)$ is the angle between a reference half-line γ_v with endpoint v and the half line starting from v and passing through the center of the (circumcircle of the) face f. f_+ is the leftmost edge of f adjacent to v (see figure 53). This connection is locally continuous inside each cell

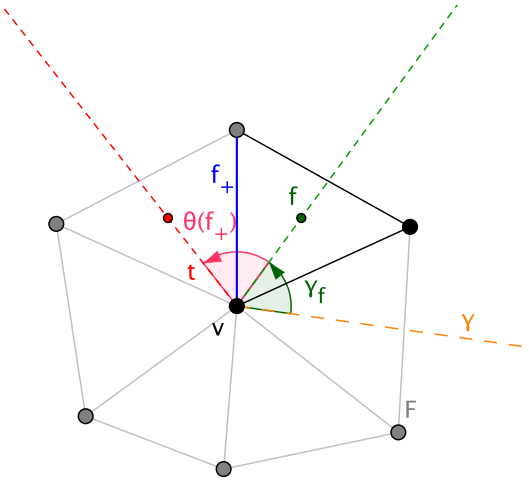

Figure 53: Construction of the connection u_v

(a cell corresponds to a triangulation structure T), but, as is shown in next paragraph, not continuous at the boundaries of the cells. Hence, the cohomology class is not a Chern class.

Discontinuities of the connection The total cohomology class of interest through 13.4 on Delaunay trinagulations is

$$\psi(T, \{d\theta\}) = \sum_{v \in \mathcal{V}(T)} \psi_v. \tag{13.6}$$

Inside a cell, that is for a triangulation structure T, the following equality holds

$$\psi(T, \{d\theta\}) = du(T, \{d\theta\}) \ , \quad u = \sum_{v \in \mathcal{V}(T)} u_v. \tag{13.7}$$

The curvature 2-form ψ and the 1-form u (the global U(1) connection) depend implicitly on a choice of triangulation T of the marked sphere, which is supposed to be kept fixed, but the final measure μ and its integral over the moduli space does not depend on the choice of triangulation.

In our formulation, the moduli space $\mathcal{M}_{0,n}$ is the closure of the union of disjoint domains $\mathcal{M}_n^{(T)}$ where the triangulation T is combinatorially a given structure of Delaunay triangulation. Two domains $\mathcal{M}_n^{(T)}$ and $\mathcal{M}_n^{(T')}$ meet along a face (of codimension 1) where the four vertices of two faces sharing an edge are cocyclic, so that one passes from T to T' by a flip, as depicted on Fig. 54. Hence, more generally, the 2-form ψ can be written in this form:

$$\psi = \sum_{\substack{T \text{ triangulation} \\ \text{structure}}} \chi_{(T)}\, du(T, \{d\theta\}) \tag{13.8}$$

where $\chi_{(T)}$ is the indicator function (hence a 0-form) of the domain $\mathcal{M}^{(T)}$ and $u(T, \{d\theta\})$ the 1-form for the triangulation T. David and Eynard [David and Eynard, 2014] showed that this measure is continuous at the boundary between two adjacent domains $\mathcal{M}_n^{(T)}$ and $\mathcal{M}_n^{(T')}$, so that the definition 13.8 is global.
The total class ψ is a Chern class if it is the curvature of a connection. Let us define

$$\tilde{u} = \sum_{\substack{T \text{ triangulation} \\ \text{structure}}} \chi_{(T)}\, u(T, \{d\theta\}). \tag{13.9}$$

Then $\tilde{u}$ is a global U(1) connection, and its curvature is

$$\begin{aligned} d\tilde{u} &= \sum_{\substack{T \text{ triangulation} \\ \text{structure}}} \chi_{(T)}\, du(T, \{d\theta\}) + d\chi_{(T)} \wedge u(T, \{d\theta\}) \\ &= \psi + \sum_{\substack{T \text{ triangulation} \\ \text{structure}}} d\chi_{(T)} \wedge u(T, \{d\theta\}) \end{aligned} \tag{13.10}$$

Therefore, ψ is a Chern class if the last sum vanishes. Inside a cell, one has obviously $d\chi_{(T)} = 0$, but on the boundary, if u is not continuous along a flip, ψ might not be exact. In this case, the measure over the Delaunay triangulation would be different from the measure over the moduli space of marked Riemann spheres.

Let us therefore compare the 1-form u for a triangulation T and the corresponding 1-form u' for the triangulation T' obtained from T by the flip $(2,4) \to (1,3)$ depicted on Fig. 54. The angles θ of the edges of T and θ' of the edges of T' are a priori different for the five edges depicted here (when the points 1, 2, 3 an 4 are not cocyclic) but only six among the ten angles are independent, since they satisfy the relation at vertex 1

$$\theta_{12} + \theta_{14} = \theta'_{12} + \theta'_{13} + \theta'_{14} \tag{13.11}$$

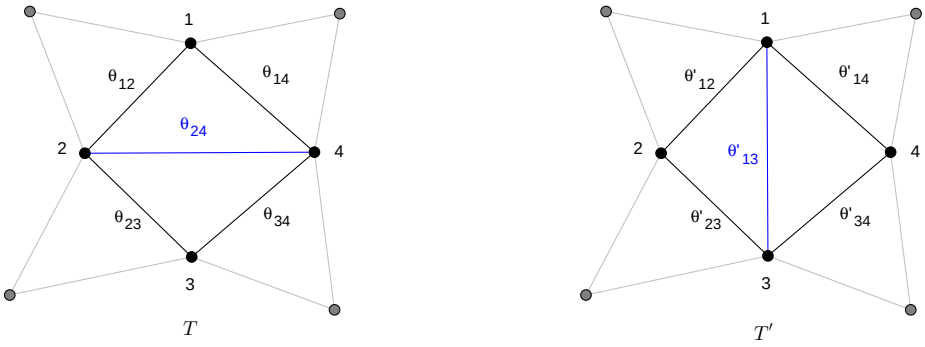

Figure 54

and the three similar relations for vertex 2, 3 and 4. These relations involve for instance that $\theta_{24}+\theta'_{13}=0$. From the definition 13.5 of the 1-forms u and u' one computes easily $u-u'$ (which depends a priori on the choice of section angles $\gamma_1, \dots \gamma_4$). However we are interested at the difference at the flip between the Delaunay triangulations T and T', i.e when the 4 points are cocyclic. Then $\theta_{12}=\theta'_{12}$, $\theta_{14}=\theta'_{14}$, $\theta_{23}=\theta'_{23}$, $\theta_{34}=\theta'_{34}$ and $\theta_{24}=\theta_{13}=0$ and we get

$$u(T,\{d\theta\})-u'(T',\{d\theta'\})|_{\text{flip}}=(\theta_{14}+\theta_{23}-\theta_{12}-\theta_{34})(d\theta_{12}-d\theta'_{12})+(\theta_{14}+\theta_{23})d\theta_{24}. \tag{13.12}$$

Despite of the apparent dihedral symmetry breaking of formula 13.12, it is actually symmetric, and using the relations holding at the vertices, it is equivalent to:

$$\begin{aligned} u(T,\{d\theta\})-u'(T',\{d\theta'\})|_{\text{flip}} &= \frac{1}{2}\left((\theta_{12}+\theta_{34})(d\theta'_{12}-d\theta_{12}+d\theta'_{34}-d\theta_{34})\right. \\ &\left.+(\theta_{14}+\theta_{23})(d\theta'_{14}-d\theta_{14}+d\theta'_{23}-d\theta_{23})\right) \end{aligned} \tag{13.13}$$

Therefore the 1-form u is not continuous on the boundary of a cell T. This means that ψ fails to be the curvature of a connection at the boundaries of the domains $\mathcal{M}_n^{(T)}$, so it is not a Chern class.

13.2 Common features of the models.

Despite the class ψ is not a Chern class, we showed (see chapter 85) that the measure over Delaunay triangulations of size n is the Weil-Petersson measure over $\overline{\mathcal{M}}_{0,n}$ – up to a factor $\frac{1}{2^{n-3}}$. Therefore, the volume

$$V_n^{\mathscr{D}}=\text{Vol}(\widetilde{\mathcal{T}}_n^f)=\sum_{\substack{T\in\mathcal{T}_n\\ \text{triangulation}\\ \text{structure}}}\int_{\widetilde{\mathcal{T}}_n^f(T)}d\nu_n(T,\theta) \tag{13.14}$$

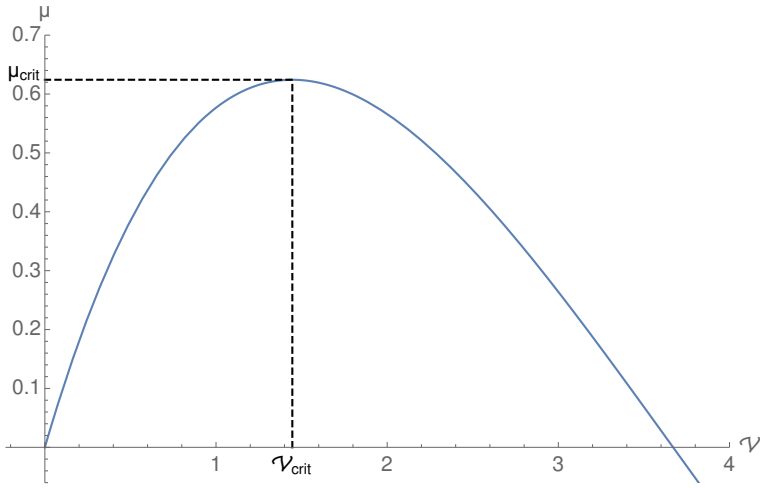

Figure 55: Plot of the function $\mu = \sqrt{\mathcal{V}^{\mathscr{D}}} J_1(2\sqrt{\mathcal{V}^{\mathscr{D}}})$. The relation is valid for $\mathcal{V}^{\mathscr{D}} \in [0, \mathcal{V}_{crit}]$.

of Delaunay triangulations of size n is equal to the Weil-Petersson volume $V_n^{\mathscr{W}\mathscr{P}} = \text{Vol}_{\mathscr{W}\mathscr{P}}(\overline{\mathcal{M}}_{0,n})$ of the moduli space $\mathcal{M}_{0,n}$: $V_n^{\mathscr{D}} = V_n^{\mathscr{W}\mathscr{P}}$. $V_n^{\mathscr{W}\mathscr{P}}$ was computed by Zograf [Zograf, 1993], Kaufmann, Manin and Zagier [Kaufmann et al., 1996], Manin and Zograf [Manin and Zograf, 2000], and more generally by Mirzakhani [Mirzakhani, 2007], who extended the formula for higher genus cases. In the same manner as for the volumes of Strebel graphs, one can encode the volumes $V_n^{\mathscr{D}}$ Weil-Petersson volumes in a generating function:

$$\begin{aligned} \mathcal{V}^{\mathscr{D}}(\mu) &= \sum_{n=3}^{\infty} \frac{\mu^{n-2}}{(n-2)!(n-3)!} V_n^{\mathscr{D}} \\ &= \sum_{n=3}^{\infty} \frac{\mu^{n-2}}{(n-2)!(n-3)!} V_n^{\mathscr{W}\mathscr{P}}. \end{aligned} \tag{13.15}$$

The generating function is defined for μ close to 0. Kaufmann, Manin and Zagier [Kaufmann et al., 1996] showed that this generating function satisfies the relation:

$$\begin{aligned} \mu &= \sum_{m=1}^{\infty} \frac{(-1)^{m-1}}{m!(m-1)!} \left(\mathcal{V}^{\mathscr{D}}(\mu)\right)^m \\ &= \sqrt{\mathcal{V}^{\mathscr{D}}} J_1(2\sqrt{\mathcal{V}^{\mathscr{D}}}) \end{aligned} \tag{13.16}$$

where $J_1(z) = \frac{z}{2} \sum_{m=0}^{+\infty} \frac{(-1)^m}{m!(m+1)!} \left(\frac{z^2}{4}\right)^m$ is a Bessel function of the first kind. It is related to $I_1(z)$ by $J_1(\mathrm{i}z) = \mathrm{i}I_1(z)$. Equation 13.16 is valid for μ close to 0. In figure 55 is plotted the function $\mu(\mathcal{V}^{\mathscr{D}})$. As for Strebel graphs, there is a critical value $\mu_c \approx 0.312115$ above which equation 13.16 is not valid anymore. Hence, a common feature between Strebel graphs and Delaunay triangulations is the presence of Bessel functions for the generating functions of the volumes.

This common features incites us to define k-point functions for Delaunay triangulations in a similar fashion as for Strebel graphs. Let us consider a Delaunay triangulation with $n+k$ vertices ($n \geq 3$, $k \geq 0$), for which one allows k vertices $v_{n+1}, \ldots, v_{n+k}$ to have respective conical singularities $\Theta_1, \ldots, \Theta_k \in \mathbb{R}_+$, that is, at those vertices, the condition 13.1 transforms into:

$$\sum_{e \to v_{n+i}} \theta_e = \Theta_i, \quad \forall i \in \{1, \ldots, k\}. \tag{13.17}$$

It is equivalent to allowing some perimeters L_i to be different from L in the case of isoperimetric Strebel graphs. Let us note $\widetilde{\mathcal{T}}_{n+k}(\Theta_1, \ldots, \Theta_k)$ the set of Delaunay triangulations with k vertices satisfying the condition 13.17. Note that Delaunay triangulations have unlabeled vertices, so the k vertices can be any of the $n+k$ vertices of the triangulation. Allowing k vertices to have some default angles enables to test the sensibility of Delaunay triangulations to the change of constraints. Then, in the same manner as for Strebel graphs, the k-point function $Z^{\mathscr{D}}_{n,k}(\Theta_1, \ldots, \Theta_k)$ is the volume of the stratum

$$\begin{aligned} Z^{\mathscr{D}}_{n,k}(\Theta_1, \ldots, \Theta_k) &= \mathrm{Vol}(\widetilde{\mathcal{T}}_{n+k}(\Theta_1, \ldots, \Theta_k)) \\ &= \sum_{\substack{T \text{ triangulation} \\ \text{structure}}} \int d\nu_{n+k}(T, \theta, \Theta_i). \end{aligned} \tag{13.18}$$

Those correlation functions are expressible in terms of Weil-Petersson volumes, and a similar analysis as for the volumes stands. Therefore, the study of Strebel graphs has allowed us to define computable correlation functions for Delaunay triangulations.

14 Asymptotic behaviour of the volume and the one-point function

It remains to study the large N behaviour of the observables. Since $n+k$ is the number of faces of the Strebel graph (number of vertices of the dual triangulation), the large n limit should be the continuum limit of large maps. It should tend towards the Brownian map (according to [Le Gall, 2013]-[Miermont, 2013]) and it is expected to converge towards Liouville theory.

Large n expansions are controlled by the singularities of the generating functions, that is to say we have to study the behavior as $\mu L^2 \to \mu_c L^2$, where μ_c is a point (closest to 0) at which the generating functions are not analytic.

Volume and correlation functions large n asymptotics are then related to the singular behavior of their respective generating functions when approaching the critical point μ_c.

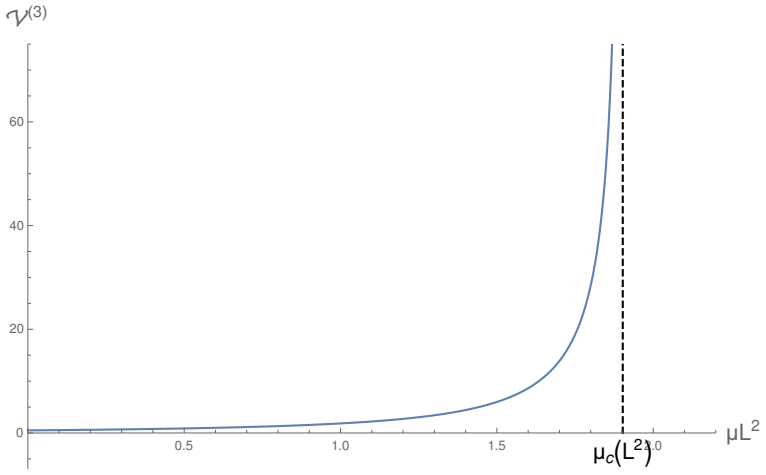

Figure 56: Plot of the third derivative of the generating function of the volumes $\partial_\mu \mathcal{V}$ in terms of μL^2. The generating function diverges at $\mu_c L^2$.

We first focuse on asymptotics of the volume, using the explicit computation we did in the second part. In order to compute the one point function at large N, we enforce the saddle point method in a second time. This allows us to identify a typical length scale for large maps. Last, we use Topological Recursion results and the critical Spectral curve to compute n-point functions.

14.1 Asymptotics of the volume

The third derivative of the generating function for the volume is given by formula 12.7 of section 12.1:

$$\partial_\mu^3 \mathcal{V}(\mu, L) = \frac{I_0(u)^4}{2I_0(u) - uI_1(u)} \tag{14.1}$$

A plot of this generating function is given in figure 56. It diverges at the critical point μ_c, for which $2I_0(u(\mu_c)) - u(\mu_c)I_1(u(\mu_c)) = 0$. This critical value is precisely the one for which $\frac{u(\mu)^2}{I_0(u(\mu))}$ is maximal (see figure 50).

If μ is close to μ_c, i.e. u is close to u_c, we have:

$$\frac{\mu}{\mu_c} = 1 - \frac{u_c^2 - 4}{2u_c^2}(u_c - u)^2 + O\left((u_c - u)^3\right) \qquad , \qquad \frac{u_c^2 - 4}{2u_c^2} = 0.2005...$$

i.e.

$$u_c - u \sim \sqrt{\frac{2u_c^2}{u_c^2 - 4}} \sqrt{1 - \frac{\mu}{\mu_c}} \left(1 + O(\sqrt{1 - \mu/\mu_c})\right) \qquad , \qquad \sqrt{\frac{2u_c^2}{u_c^2 - 4}} = 2.23... \tag{14.2}$$

So we get:

$$\partial_\mu^3 \mathcal{V}(\mu, L) \underset{\mu \to \mu_c}{\sim} \frac{C}{\sqrt{1 - \frac{\mu}{\mu_c}}} + O(1) \qquad , \qquad C = \frac{1}{\sqrt{2}} \frac{I_0(u_c)^3}{\sqrt{u_c^2 - 4}} = 18.69... \tag{14.3}$$

$\partial_\mu^3 \mathcal{V}(\mu, L)$ behaves as $(1-\mu/\mu_c)^{-1/2}$, so $\mathcal{V}(\mu, L)$ has a $(1-\mu/\mu_c)^{5/2}$ singularity. Writing that

$$\frac{C}{\sqrt{1-\frac{\mu}{\mu_c}}} = \sum_{n\geq 0} \frac{\mu^n}{n!} \frac{C(2n-1)!!}{2^n \mu_c^n}, \tag{14.4}$$

and comparing with:

$$\partial_\mu^3 \mathcal{V}(\mu, L) = \sum_{n=3}^{\infty} \frac{\mu^{n-3}}{(n-3)!} V_n(L), \tag{14.5}$$

we find the large n behavior of the volume

$$\begin{aligned} V_n(L) &\underset{n\to\infty}{\sim} C\,\frac{(2n-7)!!}{2^n \mu_c^n} = C\,\frac{(2n-7)!!\,L^{2n}}{2^n(\mu_c L^2)^n} \qquad , \qquad \mu_c L^2 = 1.902... \\ &\underset{n\to\infty}{\sim} C\,n!\,A(L)^n\,n^{-\frac{7}{2}} \end{aligned}$$

with $A(L) = \frac{L^2}{2\mu_c L^2}$. The exponent $-\frac{7}{2}$ is the same as the one for the large n volumes of Delaunay triangulations. It is a universal feature of pure gravity random map models, so this confirms that Strebel graphs lay in this universality class.

14.2 One-point function – Saddle point method

We want to study the large n limit of the one-point function:

$$\begin{aligned} f_n\left(L, \frac{L_1}{L}\right) &\overset{\text{def}}{=} Z_{n,1}(L, L_1) \\ &= \dots \qquad (14.6) \\ &= \frac{(n-2)!L^{2n-4}}{2} \operatorname*{Res}_{z\to 0} \frac{dz}{z} I_0(z)^2 e^{(n-2)(\ln I_0(z) - 2\ln z + \frac{1}{n-2}\ln I_0(zL_1/L))} \qquad (14.7) \end{aligned}$$

The detail of the computation has been transferred to appendix B for readability, as the calculus is close to the one for the volume. Let us define

$$S_n(z) = \ln I_0(z) - 2\ln z + \frac{1}{n-2}\ln I_0\left(\frac{L_1}{L} z\right) \tag{14.8}$$

S_n is an even function. In the large n limit, we use the saddle point approximation to compute the residue, hence we have to find the saddle point of S_n. First, let us

compute its derivatives.

$$\frac{\partial}{\partial y}S_n(x+iy) = i\left[\frac{I_1(x+iy)}{I_0(x+iy)} - \frac{2}{x+iy} + \frac{1}{n-2}\frac{L_1}{L}\frac{I_1\left(\frac{L_1}{L}(x+iy)\right)}{I_0\left(\frac{L_1}{L}(x+iy)\right)}\right] \tag{14.9}$$

$$\frac{\partial^2}{\partial y^2}S_n(x+iy) = -1 + \frac{I_1(x+iy)}{(x+iy)I_0(x+iy)} + \frac{I_1^2(x+iy)}{I_0^2(x+iy)} - \frac{2}{(x+iy)^2} - \tag{14.10}$$

$$\frac{1}{n-2}\left(\frac{L_1}{L}\right)^2\left(1 - \frac{I_1\left(\frac{L_1}{L}(x+iy)\right)}{\frac{L_1}{L}(x+iy)I_0\left(\frac{L_1}{L}(x+iy)\right)} - \frac{I_1^2\left(\frac{L_1}{L}(x+iy)\right)}{I_0^2\left(\frac{L_1}{L}(x+iy)\right)}\right) \tag{14.11}$$

$$\tag{14.12}$$

We distinguish three regimes for the behaviour of L_1 at large n. For each regime, we may compute the saddle points and carry out the residue. Let us note in all the regimes $l = \frac{L_1}{nL}$.

Regime 1: $l \to 0$ when $n \to \infty$ In this regime, the term $\frac{1}{n-2}\ln I_0\left(\frac{L_1}{L}z\right)$ is negligible, the saddle point is the saddle point of $\ln I_0(z) - 2\ln z$, it is independent of L_1/L, and it is worth $z = \pm u_c$. This gives

$$f_n\left(L, \frac{L_1}{L}\right) \underset{n\to\infty}{\sim} I_0\left(\frac{L_1}{L}u_c\right)\frac{I_0(u_c)^n}{u_c^{2n-4}}\frac{\sqrt{2\pi}}{\sqrt{u_c^2-4}}(n-2)!L^{2n-4} \tag{14.13}$$

$$Z_{n,1}(L;L_1) \underset{n\to\infty}{\sim} C\,n!\,\left[L^2A_1(l)\right]^n n^{-2}\,I_0\left(n\,l\,u_c\right) \tag{14.14}$$

$$\tag{14.15}$$

with $A_1(l) = \frac{I_0(u_c)}{u_c^2}$ (it is independent of l, but the parameter is kept to uniformize the notations with the other regimes).

Regime 2: $l = O(1)$ when $n \to \infty$ We use the asymptotics:

$$I_0(x) \underset{x\to\infty}{=} \frac{e^x}{\sqrt{2\pi x}}(1 + O\left(\frac{1}{x}\right)) \tag{14.16}$$

which gives:

$$S_n(z) = \ln\left(\frac{I_0(z)}{z^2}\right) + lz + O\left(\frac{\ln n}{n}\right) \tag{14.17}$$

By the same argument as in the first regime, there are two saddle points $x_0(l)$, $x_1(l) = -x_0(l)$ situated on the real axis. Again, let x_0 be the positive one. The equation $S_n'(x_0) = 0$ gives:

$$x_0 I_1(x_0) - (2 - lx_0)\,I_0(x_0) = 0 \tag{14.18}$$

At the point $x_0(l)$:

$$S_n(x_0) = \ln I_0(x_0) - 2\ln x_0 + l x_0 + o(1) \tag{14.19}$$

$$\frac{\partial^2}{\partial y^2} S_n(x_0) = -\left(1 + \frac{4l}{x_0} - \frac{4}{x_0^2} - l^2\right) + o(1) \tag{14.20}$$

$$= -1 + \left(l - \frac{2}{x_0}\right)^2 + o(1) \tag{14.21}$$

$$= O(1) \tag{14.22}$$

We then have:

$$f_n\left(L, \frac{L_1}{L}\right) = (n-2)! L^{2n-4} \frac{I_0(x_0(l))^n}{x_0(l)^{2n-4}} \frac{e^{(n-2)l x_0(l)}}{\sqrt{2\pi(n-2) l x_0(l)}} \frac{\sqrt{2\pi}}{\sqrt{(l^2+1)x_0(l)^2 + 5x_0(l) - 4}} \tag{14.23}$$

Of course, the factors 2π simplify, but in this form, we see that f_n in the second regime is matching the one of the first regime. Indeed, as $\frac{L_1}{L} \sim nl$, we have:

$$I_0\left(\frac{L_1}{L} x_0(l)\right) \underset{n\to\infty}{\sim} \frac{e^{n l x_0(l)}}{\sqrt{2\pi n l x_0(l)}} \tag{14.24}$$

What is more, if $l = 0$, the last fraction is equal to $\frac{\sqrt{2\pi}}{\sqrt{u_c^2 - 4}}$. So we recover the first regime in this limit, and more generally, in this regime:

$$Z_{n,1}(L; L_1) \underset{n\to\infty}{\sim} C\, n!\, \left[L^2 A_2(l)\right]^n n^{-2}\, I_0(n\, l\, x_0(l))$$

with $A_2(l) = \frac{I_0(x_0(l))}{x_0(l)^2}$.

Regime 3: $l \to \infty$ when $n \to \infty$ In this regime, $l \gg 1$. We can show that in this regime, we have necessarily, for the saddle point x_0:

$$x_0 \underset{n\to\infty}{\to} 0 \tag{14.25}$$

$$\frac{L_1}{L} x_0 \underset{n\to\infty}{\to} +\infty \tag{14.26}$$

We can then expand x_0 as a series of $n^\alpha \left(\frac{L_1}{L}\right)^\beta$. We find:

$$x_0(l) = \frac{2}{l} + \frac{2}{5}\frac{1}{nl} + O\left(\frac{1}{n^2 l}\right) \tag{14.27}$$

We then get:

$$\frac{\partial^2 S}{\partial y^2}(x_0(l)) = -\frac{l^2}{2}\left(1 + O\left(\frac{1}{n}\right)\right) \tag{14.28}$$

and

$$S_n(x_0(l)) = \ln I_0\left(\frac{2}{l}\right) - 2\ln\frac{2}{l} + \frac{1}{n-2}\ln I_0(2n-4)) \tag{14.29}$$

In the end, we obtain:

$$f_n\left(L, \frac{L_1}{L}\right) = n! L^{2n-4}\left[I_0\left(\frac{2}{l}\right)\right]^n \left(\frac{l}{2}\right)^{2n-4} n^{-2}\sqrt{\pi} I_0(2n-4), \tag{14.30}$$

so in the third regime:

$$Z_{n,1}(L; L_1) \underset{n\to\infty}{\sim} C\, n!\, \left[L^2 A_3(l)\right]^n n^{-2} I_0(2n)$$

with $A_3(l) = \frac{l^2}{4} I_0\left(\frac{2}{l}\right)$.

To summarize, for large n (for which $\ln n$ is negligible compared to n), the one-point function has the following behaviour :

$$\begin{aligned} \frac{1}{n}\ln\frac{Z_{n,1}(L; L_1)}{n! L^{2n} n^{-2}} &= \frac{\ln C}{n} + \ln A_i(l) + \frac{\ln I_0(nl x_0(l))}{n} \\ &\approx \ln A_i(l) + l x_0(l). \end{aligned} \tag{14.31}$$

The plot of this function is displayed in figure 57. The domain of validity of each regime is shown on the plot. One sees that in regime 1, the one-point function does-not depend on l, as it is nearly constant, so the coupling between the small face and the rest of the graph does not appear at the leading order ; in regime 3, the dependence becomes linear, so again, the face with a large perimeter decouples from the rest of the graph. Last, in regime 2, for which $L_1 \sim nL$, one sees a transition phase and a non trivial dependence of the one-point function. Therefore, the face with perimeter L_1 shows a strong coupling with the rest of the graph when L_1 scales as n.

15 Extension to genus 1

What makes all the previous computations possible is the fact that intersection numbers of Chern classes in genus 0 are known in a closed formula. This crucial fact is also true for genus 1:

$$\langle \tau_{d_1} \dots \tau_{d_n} \rangle_1 = \frac{1}{24}\frac{n!}{d_1! \dots d_n!}\, \delta\left(n - \sum_{i=1}^n d_i\right). \tag{15.1}$$

Following exactly the same steps as for genus 0, we end-up with the explicit formulas for those functions:

$$\begin{aligned} \mathcal{V}^1(\mu, L) &= \frac{1}{24}\frac{2I_0(u)}{2I_0(u) - uI_1(u)} \\ \mathcal{Z}_k^1(\mu, L; L_1, \dots, L_k) &= \frac{1}{24}\frac{d^k}{d\mu^k}\sum_{n=0}^{\infty}(\mu L^2)^{n+k}\, [z^{2n}]\left(I_0(z)^n \prod_{j=1}^k I_0\left(\frac{L_j}{L} z\right)\right) \end{aligned}$$

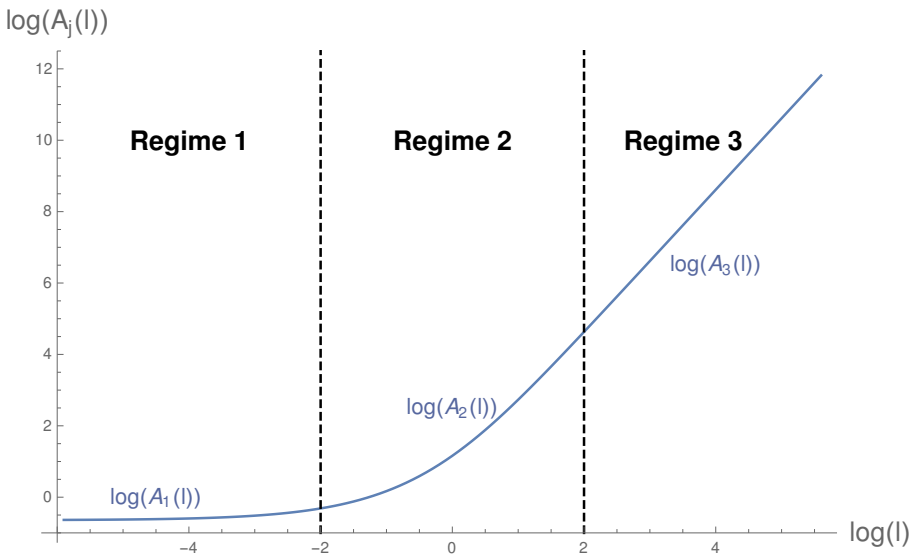

Figure 57: Plot of the dependence of the one-point function in terms of $\ln l$

$$= \frac{1}{24}\frac{d^k}{d\mu^k}\left((\mu L^2)^k\left[\frac{1}{u^{2k}}\frac{2I_0(u)}{2I_0(u)-uI_1(u)}\prod_{j=1}^{k} I_0\left(\frac{L_j}{L}z\right)\right]\right). \tag{15.2}$$

The results are very similar to the genus 0 case: instead of having $I_0(u)^4$ at the numerator, we get $I_0(u)$, and the order of the derivative with respect to μ changes also. Therefore, the combinatorics of isoperimetric Strebel graphs for genera 0 and 1 are very similar.

Part V

Spectral curve and topological recursion for Strebel graphs

The expectation values of the observables defined on isoperimetric planar Strebel graphs are explicitly known from previous chapter. Taking advantage of this result, it is possible to study the continuous limit of any k-point function $Z_{n,k}$. However, as we see in the case of the one-point function, whose continuous limit was approached via saddle point approximation, the computations are rather long, and for k-point functions with $k \geq 2$, the saddle point approximation is way subtler than for the 1-point function. Moreover, the continuous limit has to be derived for each correlation function, which means that, for the moment, we do not have a global view of what happens in the continuous limit, and hard to identify towards which theory it converges, if it does. It is therefore useful to be able to derive those correlation functions, encoded in generating functions, in a more systematic way. This way, in our case, is topological recursion, which is a procedure to compute certain class of generating functions of combinatorial models (among others), from the data of a spectral curve.

This chapter treats the same aspect of random maps as the previous one, that is, the computation of expectation values of observables, and it is realized thanks to topological recursion applied to the same model as the previous part, isoperimetric Strebel graphs. First, we introduce the procedure of topological recursion, developed by Eynard and Orantin [Eynard and Orantin, 2007]. Then, to apply it to Strebel graphs, we compute the spectral curve in our case. It allows to compute the generating functions of correlation functions defined previously, and also to generalize the computation to higher genera (and not only to planar correlation functions). As we will see, the continuous limit of Strebel graphs corresponds to critical point of the spectral curve, found by tuning the parameter μ of the model to a critical value μ_c. We exhibit the critical spectral curve and the scalings when the parameter μ is close to μ_c. Once the critical spectral curve and the different scalings are identified, there are two consequences. First we can determine to which theory the continuous limit of Strebel graphs is eligible to converge. We show that in the continuous limit, the model of Strebel graphs should be equivalent to the (3,2) minimal model, that we define briefly, dressed with gravity. This (3,2) minimal model corresponds to a conformal field theory with central charge $c = 0$, known to describe pure quantum gravity once dressed with Liouville theory. Second we are able to compute easily the behaviour of the correlation functions in the large n limit (the continuous limit).

The results proven in this section may make appear the one-point function analysis with the saddle-point machinery of previous chapter completely obsolete. Yet, this pedestrian study was necessary in order to spot the "interesting" regime for the marked perimeters $L_1, \dots, L_k$ (for which the behaviour of the generating functions is non-trivial). Indeed, we will use here the regime $L_i \sim nL$ found in chapter IV. This chapter is based on the article [I].

16 Spectral curve and topological recursion

Topological recursion was developed by Eynard and Orantin [Eynard and Orantin, 2007]. It is a procedure that allows, from the data of a spectral curve $\mathcal{S}$, to compute recursively invariants $\omega_{g,k}(z_1, \dots, z_k)$, which are meromorphic forms on a Riemann surface Σ, where $g, k \in \mathbb{N}$. The recursion is on the quantity $2 - 2g - k$, which is the Euler characteristic $\chi_{g,k}$ of a compact Riemann surface of genus g with k boundaries, and Eynard proved [Eynard, 2011] that the invariant $\omega_{g,k}$ is related to integrals over the moduli space $\mathcal{M}_{g,k}$ of Riemann surfaces of genus g with k boundaries, hence the name for "topological recursion". Let us give the definitions of the spectral curve and of topological recursion.
First, let us precise the notation: given a Riemann surface Σ, we note $\mathscr{M}^1(\Sigma)$ the set of meromorphic 1-forms on Σ. In the following, the meromorphic k-forms we refer to are not exterior k-forms but rather elements of $\underbrace{\mathscr{M}^1(\Sigma) \otimes \cdots \otimes \mathscr{M}^1(\Sigma)}_{k \text{ times}}$.
A spectral curve $\mathcal{S} = (\Sigma, \mathbb{C}, x, y, \omega_{0,2})$ is the data of

- a Riemann surface Σ (not necessarily connected nor compact) ;
- a base curve Σ_0, which is also a Riemann surface, we consider here that $\Sigma_0 = \mathbb{C}$;
- two meromorphic maps x, $y : \Sigma \to \mathbb{C}$;
- a symmetric meromorphic 2-form $\omega_{0,2} \in \mathscr{M}^1(\Sigma) \otimes^{\text{sym}} \mathscr{M}^1(\Sigma)$ whose only poles are double poles at coinciding points with this behaviour $\omega_{0,2}(z_1, z_2) \underset{z_1 \to z_2}{\sim} \frac{dz_1 \otimes dz_2}{(z_1 - z_2)^2} +$ analytic.

Figure 58 allows to visualize the curve Σ, the base curve Σ_0 and the map x. In an equivalent way, if we define the 1-form $\omega_{0,1}(z) = y(z)dx(z)$, the spectral curve is also the data of $(\Sigma, \mathbb{C}, x, \omega_{0,1}, \omega_{0,2})$. In an abuse of notation, later we shall identify the map x with the variable $x(p)$ for $p \in \Sigma$, and treat x as a variable on the base curve $\Sigma_0 = \mathbb{C}$. The maps x and y allow to embed the curve Σ in the space $\mathbb{C} \times \mathbb{C}$.
The recursive formula defining the $\omega_{g,k}$ requires the introduction of the branchpoints of $\mathcal{S}$, the involution σ_a, and the kernel $K_a(z; z_1)$.

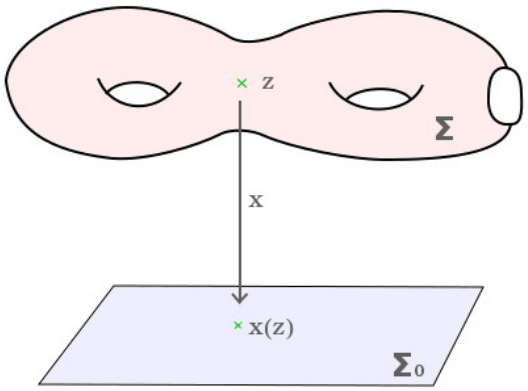

Figure 58: Representation of a spectral curve, with the elements Σ, $\Sigma_0 = \mathbb{C}$ and x.

- A branchpoint $a \in \Sigma$ of is a point of the curve such that $dx(a) = 0$. Generically, the branchpoints are simple, that is, the zero of dx in a is simple. A branchpoint a of order m is a zero of order m of $dx(z)$.
- In a neighborhood U_a of a simple branchpoint a (in this manuscript, all the branchpoints are simple), there exists an analytic involution $\sigma_a : U_a \to U_a$, $\sigma_a \neq \mathrm{Id}$, such that $x(z) = x(\sigma_a(z))$.
- The kernel $K_a(z, z_1)$ associated to a simple branchpoint a is given by the formula:

$$K_a(z; z_1) = \frac{1}{2} \frac{\int_{s=\sigma_a(z)}^{z} \omega_{0,2}(z_1, s)}{\omega_{0,1}(z) - \omega_{0,1}(\sigma_a(z))}, \tag{16.1}$$

  it is a 1-form in z_1, and $\frac{1}{K_a(z;z_1)}$ is a 1-form in z.

The formula of topological recursion for $k \geq 1$, $g \in \mathbb{N}$, $2 - 2g - k < 0$ is:

$$\begin{aligned} \omega_{g,k}(z_1, \ldots, z_k) \quad = \quad & \sum_{\substack{a \\ dx(a)=0}} \operatorname*{Res}_{z \to a} K_a(z; z_1) \Big[\omega_{g-1,k+1}(z, \sigma(z), z_2, \ldots, z_k) \\ & + \sum_{\substack{g_1+g_2=g \\ I_1 \sqcup I_2 = \{z_2, \ldots, z_k\}}}{}' \omega_{g_1, 1+|I_1|}(z, I_1) \omega_{g_2, 1+|I_2|}(\sigma(z), I_2) \Big] \end{aligned} \tag{16.2}$$

where $\sum'$ means that the sum excludes the pairs $(g_i, I_i) = (0, \varnothing)$. On the right hand side, the invariants $\omega_{g',k'}$ satisfy $2 - 2g' - k' > 2 - 2g - k$, therefore this formula is a recursive formula on $2 - 2g - k$. For all g, k, $\omega_{g,k}$ is a meromorphic k-form on Σ.
The so-called *free energies* F_g with $g > 1$ are computed from those invariants through:

$$F_g = \frac{1}{2 - 2g} \sum_{\substack{a \\ dx(a)=0}} \operatorname*{Res}_{z \to a} \Phi(z) \omega_{g,1}(z), \tag{16.3}$$

where Φ is a primitive of ydx, that is, once a base point $o \in \Sigma$ is chosen:

$$\Phi(z) = \int_o^z ydx. \tag{16.4}$$

There exist other formulations of topological recursion (see Kontsevich-Soibelman [Kontsevich and Soibelman, 2017], [Andersen - Borot - Chekhov - Orantin, 2017]), but this one fits for our purposes. This recursion relation is a type B-model, that is to say it defines invariants $\omega_{g,n}$ from a complex curve $\mathcal{S}$. In section 18, we shall see that a theorem from Eynard [Eynard, 2011] relates those invariants computed from a specific spectral curve (found in next section) to the problem of enumerating isoperimetric Strebel graphs. Problems of enumerative geometry are type A models. The interest of topological recursion for us is the correspondence between a type A model and a type B. This correspondence is the *mirror symmetry*.

An important property is that the invariants $\omega_{g,k}$ are unchanged under a reparametrization of the spectral curve. What is more, if one adds to y a polynomial in x, the kernel $K_a(z; z_1)$ remains unchanged. Indeed, if one adds a monomial x^m, then

$$\begin{aligned} \omega_{0,1}(z) - \omega_{0,1}(\sigma_a(z)) &= y(z)dx(z) - y(\sigma_a(z))dx(\sigma_a(z)) \\ &\quad + x(z)^m dx(z) - x(\sigma_a(z))^m dx(\sigma_a(z)) \\ &= y(z)dx(z) - y(\sigma_a(z))dx(\sigma_a(z)). \end{aligned} \tag{16.5}$$

Therefore, the invariants $\omega_{g,k}$ remain unchanged under $y \to y + x^m$.

17 Spectral curve for Strebel graphs

The spectral curve of the planar isoperimetric Strebel graphs derives from results shown by Eynard in [Eynard, 2007], [Eynard, 2011]. We have two parameters μ, L in our model, so actually, we need to determine the family of spectral curves $\mathcal{S}(\mu, L)$ indexed by those parameters. In order to express them, let us transform the formula for the generating function of the volumes in terms of times t_k. We showed in chapter IV, using a theorem by Kontsevich, that the generating function of the volumes $\mathcal{V}(\mu, L)$ can be expressed in terms of Chern classes. More precisely, if one looks at equation 12.1:

$$\begin{aligned} \mathcal{V}(\mu, L) &= \frac{1}{2} \sum_{n=3}^{\infty} \frac{2^3}{2^n} \frac{\mu^n}{n!} \sum_{d_1 + \cdots + d_n = n-3} \left\langle \prod_{i=1}^{n} \frac{L^{2d_i}}{2^{d_i} d_i!} \tau_{d_i} \right\rangle_0 \\ &= 4 \sum_{n=0}^{\infty} \frac{\mu^n}{2^n n!} \left\langle \left(\sum_{d=0}^{\infty} \frac{L^{2d}}{2^d d!} \tau_d \right)^n \right\rangle_0 \end{aligned}$$

$$= \quad 4 \left\langle e^{\frac{1}{2}\sum_{d=0}^{\infty} \mu \frac{L^{2d}}{2^d d!} \tau_d} \right\rangle_0 \tag{17.1}$$

where, to pass from the first line to the second line, we used the convention $\langle \tau_{d_1} \dots \tau_{d_n} \rangle_0 = 0$ if $n < 3$ or $d_1 + \dots d_n \neq n - 3$. We shall write it in the following form:

$$\mathcal{V}(\mu, L) = 4 \left\langle e^{\frac{1}{2}\sum_{d=0}^{\infty} (2d-1)!! t_{2d+1}(\mu,L)\tau_d} \right\rangle_0, \tag{17.2}$$

with the times $t_{2d+1}(\mu, L) = \frac{\mu L^{2d}}{(2d)!}$. We can define the even times – which do not appear here thus one can choose them arbitrarily – to be $t_{2d}(\mu, L) = \frac{\mu L^{2d-1}}{(2d-1)!}$, so that in general for $d \geq 0$

$$t_{d+1}(\mu, L) = \frac{\mu L^d}{d!}. \tag{17.3}$$

For a given (μ, L), the spectral curve $\mathcal{S}(\mu, L)$ of isoperimetric planar Strebel graphs is defined by the times $t(\mu, L) = (t_1(\mu, L), t_2(\mu, L), t_3(\mu, L), \dots)$. They are functions of μ and L, in the following we may drop the out (μ, L) in the formulas to get more readable expressions. Once $\mathcal{S}(\mu, L)$ is found, Topological Recursion allows to compute the quantities

$$F_g(\mu, L) = \left\langle e^{\frac{1}{2}\sum_{d=0}^{\infty} (2d-1)!! t_{2d+1}\tau_d} \right\rangle_g \quad \text{for } g \geq 2, \tag{17.4}$$

which are the generating functions of the volumes of isoperimetric Strebel graphs of genus g:

$$F_g(\mu, L) = \sum_{n=0}^{\infty} \frac{\mu^n}{n!} \mathrm{Vol}(\mathscr{S}_{g,n}(L)). \tag{17.5}$$

It has been shown (see *e.g.* [Eynard, 2011]) that for $g \geq 2$, one can express the free energies F_g in terms of Chern classes τ_d with $d > 0$:

$$F_g(\mu, L) = \left\langle e^{\frac{1}{2}\sum_{d=1}^{\infty} (2d-1)!! \check{t}_{2d+1}(\mu,L)\tau_d} \right\rangle_g \tag{17.6}$$

provided that the family of times $\check{t}(\mu, L) = (\check{t}_1(\mu, L), \check{t}_2(\mu, L), \check{t}_3(\mu, L), \dots)$ are related to t by

$$\check{t}_1 = \sum_{j=0}^{\infty} \frac{(2j-1)!!}{2^j j!} \check{t}_1^j t_{2j+1} \qquad , \qquad \check{t}_{2k+3} = \sum_{j=0}^{\infty} \frac{(2k+2j+1)!!}{(2k+1)!!\, 2^j j!} \check{t}_1^j t_{2k+2j+3}. \tag{17.7}$$

It is necessary to have $g \geq 1$ for the equality 17.6 to hold. Indeed, for genus 0, we saw that $\langle \tau_{d_1} \dots \tau_{d_n} \rangle_0 = 0$ if $d_1 + \dots + d_n \neq n - 3$. But if $d_i > 0$, we must have $d_1 + \dots + d_n \geq n$, so

$$\left\langle e^{\frac{1}{2}\sum_{d=1}^{\infty} (2d-1)!! \check{t}_{2d+1}\tau_d} \right\rangle_0 = 0. \tag{17.8}$$

Still, the spectral curve associated to the invariants F_g must be the spectral curve associated to $\mathcal{V}$, because the times t are the same. Eynard showed in [Eynard, 2007]

and [Eynard, 2011] that the spectral curve $\mathcal{S}(\mu, L)$ for the invariants $F_g(\mu, L)$ is:

$$\mathcal{S}(\mu, L) = \left(\overline{\mathbb{C}}, \mathbb{C}, x(\mu, L), y(\mu, L), \frac{dz_1 \otimes dz_2}{(z_1 - z_2)^2}\right)$$
$$\begin{cases} x(\mu, L; z) = z^2 + \check{t}_1 \\ y(\mu, L; z) = z - \frac{1}{2}\sum_{k=0}^{+\infty} \check{t}_{2k+3} z^{2k+1} \end{cases} \tag{17.9}$$

Therefore the Riemann surface is $\Sigma = \overline{\mathbb{C}}$, the base space is $\Sigma_0 = \mathbb{C}$, and the Bergman kernel is $B(z_1, z_2) = \frac{dz_1 \otimes dz_2}{(z_1 - z_2)^2}$. Those three objects are independent of the parameters μ, L. In order to get explicit formulas for the functions x and y, we simply need to compute the times $\check{t}(\mu, L)$, defined by equations 17.7 in terms of the times $t(\mu, L)$.

Time $\check{t}_1(\mu, L)$

The equation determining $\check{t}_1(\mu, L)$ is

$$\check{t}_1(\mu, L) = \mu \sum_{j=0}^{\infty} \frac{1}{2^{2j} j! j!} \check{t}_1^j L^{2j} = \mu I_0(L\sqrt{\check{t}_1(\mu, L)}), \tag{17.10}$$

That is to say:

$$\frac{\check{t}_1(\mu, L) L^2}{I_0(\sqrt{\check{t}_1(\mu, L) L^2})} = \mu L^2, \tag{17.11}$$

which is precisely the equation defining $u(\mu L^2)$. This means that actually $\check{t}_1(\mu, L) = \frac{u(\mu L^2)^2}{L^2}$.

Times $\check{t}_{2k+3}(\mu, L)$

Once the time $\check{t}_1$ found, the derivation of times $\check{t}_{2k+3}$ is straightforward, by application of formula 17.7. For $k \geq 0$

$$\begin{aligned} \check{t}_{2k+3}(\mu, L) &= \sum_{j=0}^{\infty} \frac{(2k + 2j + 1)!!}{(2k+1)!!\, 2^j j!} \check{t}_1^j t_{2k+2j+3} \\ &= \frac{\mu L^{2k+2}}{(2k+1)!!} \sum_{j=0}^{\infty} \frac{1}{2^{2j+k+1}(k+1+j)! j!} \check{t}_1^j L^{2j} \\ &= \frac{\mu L^{2k+2}}{(2k+1)!! u (\mu L^2)^{k+1}} \sum_{j=0}^{\infty} \frac{u^{2j+k+1}}{2^{2j+k+1}(k+1+j)! j!} \\ &= \frac{\mu L^{2k+2}}{(2k+1)!! u (\mu L^2)^{k+1}} I_{k+1}(u), \end{aligned} \tag{17.12}$$

where I_k is the k^{th} modified Bessel function of the first kind (see appendix A). Hence, the functions x and y can be expanded in terms of Bessel functions of $u(\mu L^2)$.

$$\mathcal{S}(\mu, L) = \left(\mathbb{C}, \mathbb{C}, x(\mu, L), y(\mu, L), \frac{dz_1 \otimes dz_2}{(z_1 - z_2)^2}\right)$$
$$\begin{cases} x(\mu, L; z) = z^2 + \frac{u(\mu L^2)^2}{L^2} \\ y(\mu, L; z) = z - \frac{\mu L^2}{2u} \sum_{k=0}^{+\infty} \frac{L^{2k} I_{k+1}(u)}{(2k+1)!! u^k} z^{2k+1}. \end{cases} \tag{17.13}$$

The functions x and y allow to embed the spectral curve in $\overline{\mathbb{C}} \times \overline{\mathbb{C}}$. In figure 59 are depicted the intersection of this embedding with $\mathbb{R} \times \mathbb{R}$ of the spectral curve for different values of the parameter μL^2. The generic case corresponds to the first plot. In order to run topological recursion, it is necessary to identify the branchpoints, the involutions σ_a and the kernels $K_a(z; z_1)$.

- There is one branchpoint: $dx(a) = 0$ for $a = 0$, it is a simple branchpoint.
- The associated involution is simply $\sigma_a(z) = \sigma_0(z) = -z$.
- As we see in the formula 16.1 for the kernel $K_a(z; z_1)$, a more fundamental object than the function y is the one form $\omega_{0,1}(\mu, L; z) = y(\mu, L; z)dx(\mu, L; z)$. Indeed, the invariants computed through topological recursion are differential forms $\omega_{g,n}$, that can be deduced from $\omega_{0,1}$ and $\omega_{0,2}$. It follows immediately from the description of $\mathcal{S}(\mu, L)$ that

$$\omega_{0,1}(\mu, L; z) = \left(2z^2 - \frac{\mu L^2}{u} \sum_{k=0}^{+\infty} \frac{L^{2k} I_{k+1}(u)}{(2k+1)!! u^k} z^{2k+2} \right) dz \tag{17.14}$$

  So the kernel is:

$$K_0(z; z_1) = \frac{1}{2} \frac{z}{z_1^2 - z^2} \frac{dz_1}{\omega_{0,1}(\mu, L; z)}. \tag{17.15}$$

The spectral curve depends on the parameters μ and L, but actually, the parameter L, which is the perimeter of the faces of the Strebel graphs, is just there to fix the scale of lengths. In the following, we may fix L, and then vary μ, so the spectral curves $\mathcal{S}(\mu, L)$ depend on one parameter μ.

18 topological recursion for strebel graphs of any genus

In this section, as a corollary of a result proved by Eynard in [Eynard, 2011], we see that topological recursion implemented on the spectral curve $\mathcal{S}(\mu, L)$ allows to compute the Laplace transform of correlation functions of isoperimetric Strebel graphs. Therefore, the correlation functions $\mathcal{Z}_{g,k}$ of isoperimetric Strebel graphs – which is an A-model –, can be deduced from the invariants $\omega_{g,k}$ computed through topological recursion on $\mathcal{S}(\mu, L)$ – B-model invariants. The following theorem is the

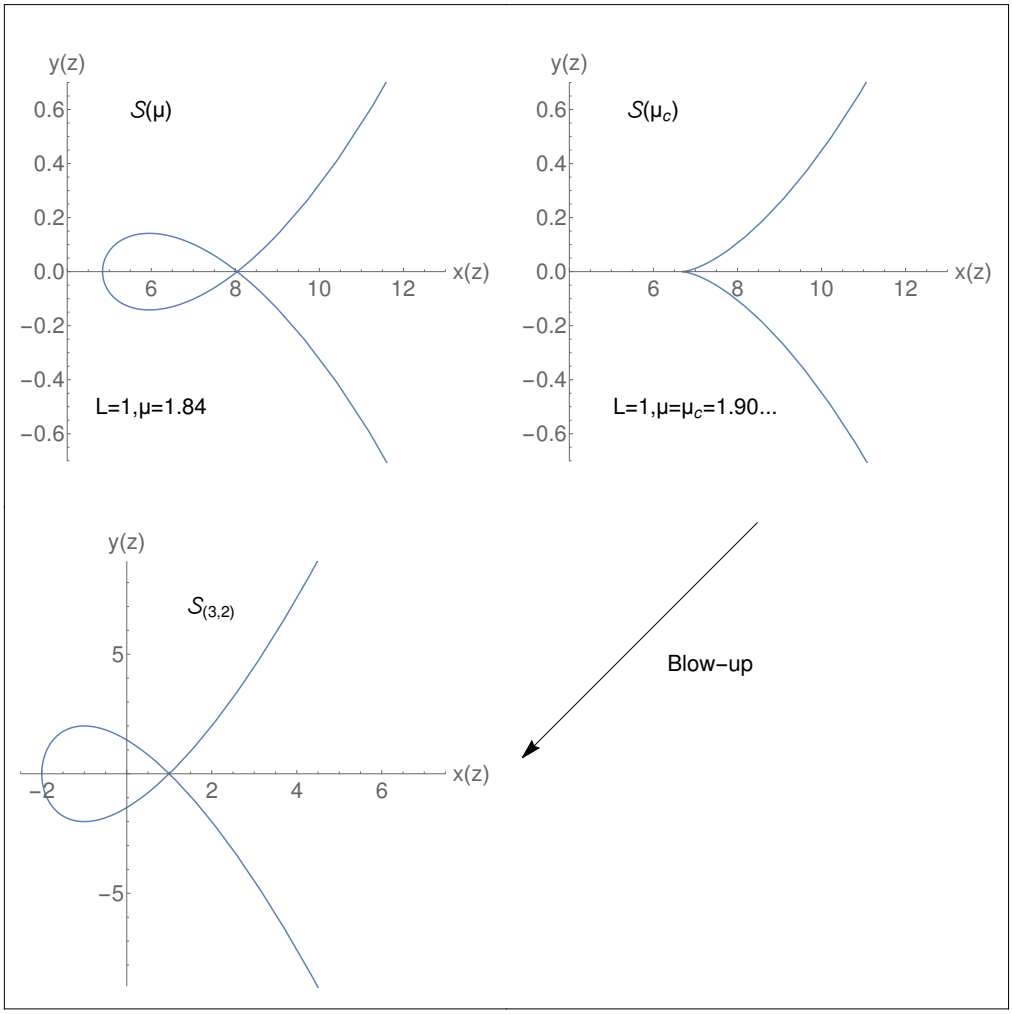

Figure 59: Intersections with $\mathbb{R}^2$ of the embedding of the spectral curves in $\overline{\mathbb{C}}^2$. The firs plot corresponds to a generic value of the parameter μL^2, the second plot corresponds to the critical value $\mu_c L^2$, for which the curve is singular and has a cusp. The third curve is the critical spectral curve, which happens to be the spectral curve of the (3,2) minimal model. For an animation of the variation of the embedding between the first plot (generic μL^2) and the second one (at the critical value), see the flipbook animation in the bottom right hand side corner along this chapter.

Theorem 18.1. *[Eynard, 2011] The invariants $d_{z_1}\dots d_{z_k}\mathcal{F}_{g,k}(\lambda;z_1,\dots,z_k)$ defined for generic times $t(\lambda)$ as:*

$$2^{2-2g-k}\sum_{\substack{d_1,\dots,d_k\\=0}}^{+\infty}\prod_{i=1}^{k}-\frac{(2d_i+1)!!dz_i}{z_i^{2d_i+2}}\left\langle e^{\frac{1}{2}\sum_{d=0}^{\infty}(2d-1)!!t_{2d+1}(\lambda)\tau_d}\prod_{i=1}^{k}\tau_{d_i}\right\rangle_g$$
$$= d_{z_1}\dots d_{z_k}\mathcal{F}_{g,k}(\lambda;z_1,\dots,z_k) \quad (18.1)$$

are the Eynard-Orantin invariants $\omega_{g,k}(\lambda;z_1,\dots,z_k)$ for the spectral curve $\mathcal{S}(\lambda)$ deduced from the times t.

As one looks at the expression on left hand side for genus 0, we see that these are precisely the Laplace transforms $\mathcal{F}_{0,k}(\mu,L;z_1,\dots,z_k)$ of the generating functions $\mathcal{Z}_k(\mu,L;L_1,\dots,L_k)$, if we specialize the times t to be $t_{2d+1}(\mu,L)=\frac{\mu L^{2d}}{(2d)!}$. We shall note those invariants in the following way $\mathcal{F}_{g,k}(\mathcal{S}(\mu,L);z_1,\dots,z_k)$ to emphasize the fact that they are computable from the spectral curve. The theorem is true for genus 0 invariants, provided that $k\geq 3$. Therefore, the recursion for the $\mathcal{F}_{g,k}$ is (we drop the dependence on $\mathcal{S}(\mu,L)$ for readability):

$$\begin{aligned} d_{z_1}\dots d_{z_k}\mathcal{F}_{g,k}(z_1,\dots,z_k) \quad = \quad & \operatorname*{Res}_{z\to 0}\frac{1}{2}\frac{1}{z^2-z_1^2}\frac{dz_1}{y(\mu,L;z)dz}\times \\ & [d_z d_{-z} d_{z_2}\dots d_{z_k}\mathcal{F}_{g-1,k+1}(z,-z,z_2\dots,z_k) \\ & + {\sum_{\substack{g_1+g_2=g\\ I_1\sqcup I_2=\{z_2,\dots,z_k\}}}}' d_z d_{z_{I_1}}\mathcal{F}_{g_1,1+|I_1|}(z,I_1)\times \\ & d_{-z}d_{z_{I_2}}\mathcal{F}_{g_2,1+|I_2|}(-z,I_2)\big]\,. \end{aligned} \quad (18.2)$$

As an example of application, let us compute the Laplace transform of the 3-point function.

Example 18.1. The invariant $\omega_{0,3}$ worthes:

$$\begin{aligned} \omega_{0,3}(z_1,z_2,z_3) &= d_{z_1}d_{z_2}d_{z_3}\mathcal{F}_{0,3}(\mathcal{S}(\mu,L);z_1,z_2,z_3) \\ &= \frac{1}{2}\operatorname*{Res}_{z\to 0}\frac{1}{z_1^2-z^2}\frac{dz_1}{y(\mu,L;z)dz}(\omega_{0,2}(z,z_2)\omega_{0,2}(-z,z_3) \\ &\quad +\omega_{0,2}(z,z_3)\omega_{0,2}(-z,z_2)) \\ &= \frac{1}{2}\operatorname*{Res}_{z\to 0}\frac{dz}{z^2-z_1^2}\frac{dz_1dz_2dz_3}{y(\mu,L;z)}\left(\frac{1}{(z-z_2)^2(z+z_3)^2}+\frac{1}{(z-z_3)^2(z+z_2)^2}\right) \\ &= -\frac{dz_1dz_2dz_3}{z_1^2z_2^2z_3^2}\operatorname*{Res}_{z\to 0}\frac{dz}{y(z)} \\ &= -\frac{2I_0(u)}{2I_0(u)-uI_1(u)}\frac{dz_1dz_2dz_3}{z_1^2z_2^2z_3^2}. \end{aligned} \quad (18.3)$$

From $\omega_{0,3}$ we deduce $\mathcal{F}_{0,3}$:

$$\mathcal{F}_{0,3}(\mathcal{S}(\mu,L);z_1,z_2,z_3)=\frac{2I_0(u)}{2I_0(u)-uI_1(u)}\frac{1}{z_1z_2z_3}. \tag{18.4}$$

19 Critical point and (3,2) minimal model

In previous chapter, we saw that the parameter μL^2 has a critical value, which allows to study the large n limit of correlation functions and volumes. What motivates the study of the large n limit (or continuum limit) of correlation functions is the study of correlation functions in a conformal field theory coupled with Liouville theory. This is equivalent to study correlation functions of a matter field (which abides by the CFT laws) dressed by gravity (the dressing corresponds to the coupling with Liouville theory). Conformal field theories are indexed by their central charge c. The question one may ask when studying a particular model of random maps is: to which gravity dressed conformal field theory does the model converge ? If one knows the family of spectral curves $\mathcal{S}(\lambda)$ spectral curve of a family of models of random maps indexed by the set of parameters λ, the continuum limit of the random maps is related to a critical spectral curve $\mathcal{S}_c$, corresponding to critical values of the set of parameters λ_c. Then, the conformal field theory, towards which the model random maps converges in the large n limit, can be deduced from the critical spectral curve. This section is dedicated to the critical spectral cure of isoperimetric Strebel graphs, that we find to be the spectral curve of the (3,2) minimal model dressed by gravity, corresponding to a conformal field theory of central charge 0 coupled with gravity, also known as a pure gravity. Thus, we prove that in the continuum limit, the model of isoperimetric Strebel graphs mimic pure (that is to say, with no content of matter) quantum gravity in 2d. The procedure to find a critical goes as what follows. To each parameters μ, L is associated a spectral curve $\mathcal{S}(\mu,L)$. For generic μ and L, the spectral curve is regular, that is to say, for all $z\in\Sigma=\overline{\mathbb{C}}$, $(dx(\mu,L;z),dy(\mu,L;z))\neq(0,0)$. Yet, μ and L can be tuned to critical values μ_c,L_c in order to get, at some $z_0\in\overline{\mathbb{C}}$:

$$dx(\mu_c,L_c;z_0)=dy(\mu_c,L_c;z_0)=0.$$

At that point, the spectral curve is singular, and its embedding in $\overline{\mathbb{C}}\times\overline{\mathbb{C}}$ has a cusp. By rescaling $x(\lambda;z)$ and $y(\lambda;z)$ close to $(\lambda_c;z_0)$ by powers of $\lambda-\lambda_c$, it is possible to resolve the singularity, to obtain a critical spectral curve

$$\begin{aligned}\tilde{\mathcal{S}} \;=\; \lim_{\lambda\to\lambda_c} \;&\Big(\overline{\mathbb{C}},\overline{\mathbb{C}},(\lambda-\lambda_c)^{-q\nu}x(\lambda;z_0+(\lambda-\lambda_c)^{\nu}(z-z_0)),\\ &(\lambda-\lambda_c)^{-p\nu}y(\lambda;z_0+(\lambda-\lambda_c)^{\nu}(z-z_0)),\frac{dz_1\otimes dz_2}{(z_1-z_2)^2}\Big)\end{aligned}$$

$$= \qquad \left(\overline{\mathbb{C}}, \overline{\mathbb{C}}, \tilde{x}(\xi), \tilde{y}(\xi), \frac{d\xi_1 \otimes d\xi_2}{(\xi_1 - \xi_2)^2}\right). \tag{19.1}$$

In the case of Strebel graphs, Eynard showed in [Eynard, 2007] and [Eynard, 2011] that for any times t:

$$\left\langle e^{\frac{1}{2}\sum_{d=0}^{\infty}(2d-1)!!t_{2d+1}\tau_d} \right\rangle_{all\ genera} = e^{\sum_{g=0}^{\infty} F_g}. \tag{19.2}$$

Kontsevich proved that precisely the left hand side is a KdV tau function evaluated at times t:

$$\left\langle e^{\frac{1}{2}\sum_{d=0}^{\infty}(2d-1)!!t_{2d+1}\tau_d} \right\rangle_{all\ genera} = \tau_{KdV}\left(\frac{1}{2}(2d-1)!!t_{2d+1}\right) \tag{19.3}$$

(the KdV hierarchy is independent of even times). Therefore, for isoperimetric Strebel graphs, we specialize the times to $t_{d+1} = \frac{\mu L^{2d}}{(2d)!}$, and the invariants F_g are linked to a KdV tau function. Thus, the critical spectral curve of isoperimetric Strebel graphs is related to a "critical" KdV tau function. This critical KdV tau function is related to a minimal model $M_{p,q}$. Once the minimal model of the critical spectral curve is identified and the rescaling exponents known, the continuum limit of correlation functions and of the model are known.

Let us apply this procedure to our spectral curve. The parameters of the model are $\lambda = (\mu, L)$. In what follows, the notation u_c implicitly means $u((\mu L^2)_c)$. The equations for getting a singular curve are:

$$\begin{cases} 2z_0 dz_0 = 0 \\ \left(1 - \frac{\mu_c L_c^2}{2u_c}\sum_{k=0}^{+\infty}\frac{L_c^{2k} I_{k+1}(u_c)}{(2k-1)!!u_c^k} z_0^{2k}\right) dz_0 = 0 \end{cases} \tag{19.4}$$

From which we deduce the critical parameters:

$$z_0 = 0 \qquad ; \qquad \frac{(\mu L^2)_c}{2u_c} I_1(u_c) = 1 \tag{19.5}$$

Actually, the second equation is an equation for μL^2. This means that we obtain a family of critical parameters ; to each perimeter $L > 0$ there exists one critical value μ_c such that the spectral curve is singular. If one recalls that $\mu L^2 = u^2/I_0(u)$, the second equation is simply equivalent to

$$\left.\frac{d}{du}\,\frac{u^2}{I_0(u)}\right|_{u_c} = 0. \tag{19.6}$$

That is to say, the critical parameter u_c is precisely the point for which μL^2 is maximal (see the plot of figure 50). There are two solutions for u_c to this equation, both of them corresponding to the same critical parameter $\mu_c L^2$:

$$u_c = \pm 2.5844\ldots \qquad ; \qquad \mu_c L^2 = 1.902\ldots. \tag{19.7}$$

The spectral curve is thus critical when the parameters are equal to the critical values found in the previous chapter. This is not surprising as in both cases, we search for parameters eligible for a study of large n maps. Let us consider – without loss of generality – the critical $u_c > 0$. In figure 59, the second plot, which is the intersection of the singular spectral curve with the plane $\mathbb{R}^2$, shows a cusp. This means that for $z - z_0 = (\mu_c L^2 - \mu L^2)^\nu \zeta$, the functions x and y scale as

$$\begin{aligned} x(\mu, L; z) - x(\mu_c, L; z_0) &\sim (\mu_c L^2 - \mu L^2)^{q\nu} \\ y(\mu, L; z) - y(\mu_c, L; z_0) &\sim (\mu_c L^2 - \mu L^2)^{p\nu}. \end{aligned} \tag{19.8}$$

Rescaling z, x, y respectively by $(\mu_c L^2 - \mu L^2)^{-\nu}$, $(\mu_c L^2 - \mu L^2)^{-q\nu}$ and $(\mu_c L^2 - \mu L^2)^{-p\nu}$ allows to desingularize the curve and to define the critical spectral curve $\tilde{\mathcal{S}}$.
In our case:

$$\begin{aligned} x(\mu, L; z) - x(\mu_c, L; z_0) &= (\mu_c L^2 - \mu L^2)^{2\nu} \zeta^2 \\ y(\mu, L; z) - y(\mu_c, L; z_0) &= (\mu_c L^2 - \mu L^2)^{\nu + \frac{1}{2}} \zeta \sqrt{I_0(u_c) \frac{u_c^2 - 4}{2u_c^2}} \\ &\quad - (\mu_c L^2 - \mu L^2)^{3\nu} \zeta^3 \frac{u_c^2 - 4}{2u_c^2} \\ &\quad + O((\mu_c L^2 - \mu L^2)^{5\nu}). \end{aligned} \tag{19.9}$$

One sees that for $\nu = \frac{1}{4}$, the function y scales as $(\mu_c L^2 - \mu L^2)^{\frac{3}{4}}(b\zeta^3 + c\zeta)$, so we choose this value for ν. Then, after a reparametrization of ζ:

$$\begin{aligned} z &= (\mu_c L^2 - \mu L^2)^{\frac{1}{4}} \zeta = (\mu_c L^2 - \mu L^2)^{\frac{1}{4}} \left(\frac{2u_c^2 I_0(u_c)}{9(u_c^2 - 4)} \right)^{\frac{1}{4}} \xi \\ x(\mu, L; z) &= x_0 + A(\mu_c L^2 - \mu L^2)^{\frac{1}{2}}(\xi^2 - 2) + O((\mu_c L^2 - \mu L^2)^{\frac{3}{4}}) \\ y(\mu, L; z) &= B(\mu_c L^2 - \mu L^2)^{\frac{3}{4}}(\xi^3 - 3\xi) + O((\mu_c L^2 - \mu L^2)) \end{aligned} \tag{19.10}$$

with $x_0 = \frac{u_c^2}{L^2}$, $A = \frac{u_c}{L^2}\sqrt{\frac{2I_0(u_c)}{u_c^2 - 4}}$ and $B = (u_c^2 - 4)^{\frac{1}{4}} \frac{(2I_0(u_c))^{\frac{3}{4}}}{6L\sqrt{u_c}}$. Therefore, the exponents are known : $\nu = \frac{1}{4}$, $q = 2$, $p = 3$, and we can take the following limits:

$$\begin{aligned} \lim_{\mu \to \mu_c} \frac{x(\mu, L; z) - x_0}{A(\mu_c L^2 - \mu L^2)^{\frac{1}{2}}} &= \xi^2 - 2 = \tilde{x}(\xi) \\ \lim_{\mu \to \mu_c} \frac{y(\mu, L; z)}{B(\mu_c L^2 - \mu L^2)^{\frac{3}{4}}} &= \xi^3 - 3\xi = \tilde{y}(\xi). \end{aligned} \tag{19.11}$$

The critical spectral curve is then:

$$\tilde{\mathcal{S}} = \left(\overline{\mathbb{C}}, \overline{\mathbb{C}}, \tilde{x}, \tilde{y}, \frac{d\xi_1 \otimes d\xi_2}{(\xi_1 - \xi_2)^2} \right) \quad \begin{cases} \tilde{x}(\xi) = \xi^2 - 2 \\ \tilde{y}(\xi) = \xi^3 - 3\xi \end{cases} \tag{19.12}$$

This critical spectral curve, whose intersection with $\mathbb{R}^2$ of its embedding into $\overline{\mathbb{C}}^2$ is displayed in the third plot of figure 59, is the spectral curve of the first reduction of the Korteweg-De-Vries (KdV) hierarchy. This reduction is also known as the minimal model $M_{3,2}$; Douglas [Douglas, 1990], studying the critical points of chain matrix models, formulated it in terms of differential operators. The generic minimal model $M_{3,2}$ is the data of 2 differential operators P and Q which statisfy the equations:

$$\begin{aligned} [P,Q] &= Id \\ Q &= \partial^2 - 2v_0(s,N) \\ P &= \partial^3 - 3v_1(s,N)\partial + v_2(s,N) \end{aligned} \tag{19.13}$$

where s, N are two additional parameters, and $\partial = \frac{1}{N}\frac{d}{ds}$. Those equations are obtained by considering the operators P, Q that act on orthogonal polynomials of a matrix model when the parameters of the potential of the matrix model are tuned. The operators P, Q and the orthogonal polynomials were briefly covered in section 5.3. In the frame of integrable systems, N is a parameter linked to the genus of the correlation one computes. It is, in the matrix model formalism, the size of the matrices. Therefore, the powers of N introduce a grading in the correlation functions. As far as we are concerned here, we are looking for genus 0 correlation functions, so in the following, we will select the leading order in N. The parameter s is related to a position in the integrable models, but for Strebel graphs, we will work at s fixed, and there is no specific interpretation for this parameter in the continuum limit of Strebel graphs. The first equation is the so-called "string equation" ; the derivation operator is a derivation with respect to s, $\partial = \frac{1}{N}\frac{d}{ds}$; and v_0, v_1, v_2 are functions to be determined by the string equation.
Solving the string equation leads to the following solution:

$$\begin{aligned} Q &= \partial^2 - 2v(s) \\ P &= \partial^3 + (\alpha - 3v(s))\partial - \frac{3}{2N}\dot{v}(s) = \left(Q^{\frac{3}{2}}\right)_+ + \alpha\left(Q^{\frac{1}{2}}\right)_+, \end{aligned} \tag{19.14}$$

under the condition that v satisfies the constraint:

$$\alpha R_1(v(s)) + R_2(v(s)) = s. \tag{19.15}$$

R_1 and R_2 are Gelfand-Dikii polynomials, which are worth:

$$\begin{cases} R_1(v) = -2v \\ R_2(v) = 3v^2 - \frac{\ddot{v}}{2N^2}. \end{cases} \tag{19.16}$$

Therefore the constraint 19.15 in the minimal model $M_{3,2}$ reduces to Painlevé I equation:

$$3v(s)^2 - \frac{\ddot{v}(s)}{2N^2} - 2\alpha v(s) = s \tag{19.17}$$

The critical spectral curve we found corresponds to operators $P = \partial^3 - 3\partial$, $Q = \partial^2 - 2$. It is a planar solution of the string equation (*i.e.* we take the limit $N \to \infty$ to get only the leading order), with $\alpha = 0$, and v evaluated at s_0 such that $v(s_0) = 1$. In this case, the planar solution of Painlevé I is $v(s) = \frac{\sqrt{3}}{3}\sqrt{s}$, so $s_0 = 3$. Therefore, we see that the large n limit of Strebel graphs is related to an integrable system. This integrability allows to determine the correlation functions in the limit. In order to relate the critical spectral curve with a conformal field theory coupled to Liouville theory, it is useful to keep the function $v(s) = \frac{\sqrt{3}}{3}\sqrt{s}$ generic, and specialize it to 1 in the end by evaluating it at $s_0 = 3$. The link between minimal models $M_{p,q}$ and amplitudes of a conformal field theory dressed by gravity – equivalently, coupled with Liouville theory– has been done by Di Francesco and Kutasov in [Di Francesco and Kutasov, 1990]. They related the partition function and certain correlation functions derived from the minimal model $M_{p,q}$ with amplitudes of a Liouville conformal field theory, provided that its central charge is given by:

$$c = 1 - \frac{6(p-q)^2}{pq}. \tag{19.18}$$

For the minimal model $M_{3,2}$, this corresponds to a central charge $c = 0$.
For generic minimal model $M_{p,q}$, the amplitudes of the conformal field theory one can recover by their method does not span the whole possible amplitudes. Yet, we know that for a null central charge, there is only one operator in the CFT, the identity. The primary field corresponding to the identity operator is $\phi_{(1,1)}$. The amplitudes that we can compute in this CFT are then the dressed k point functions:

$$\left\langle \phi_{(1,1)}(x_1)\phi_{(1,1)}(x_2)\dots\phi_{(1,1)}(x_k)\right\rangle.$$

Those amplitudes can be computed from the operators P, Q of the minimal model. First, let L be a pseudo-differential operator such that, for all $k \geq 0$, $Q^k = \left(L^{2k}\right)_+$. In our model,$L = \partial - v\partial^{-1} + \dots$. For a minimal model $M_{p,q}$, one can construct the operators:

$$R_{r,s} = L^{pr-qs}, \qquad 1 \leq s \leq r \leq q-1 \tag{19.19}$$

For $M_{3,2}$, there is one operator $R_{1,1} = L$. Then, Di Francesco and Kutasov showed [Di Francesco and Kutasov, 1990]:

$$\left\langle \phi_{(1,1)}(x_1)\phi_{(1,1)}(x_2)\dots\phi_{(1,1)}(x_k)\right\rangle = -2(\text{ Res } L)^{(k)}, \tag{19.20}$$

with Res L being the coefficient of ∂^{-1} in L, which is $-v(s)$. This involves that the dressed k-point functions for a generic s is:

$$\left\langle \phi_{(1,1)}(x_1)\phi_{(1,1)}(x_2)\dots\phi_{(1,1)}(x_k)\right\rangle = \frac{1}{(-4)^{k-1}}\frac{(2k-1)!}{(k-1)!}s^{-k+\frac{1}{2}}. \tag{19.21}$$

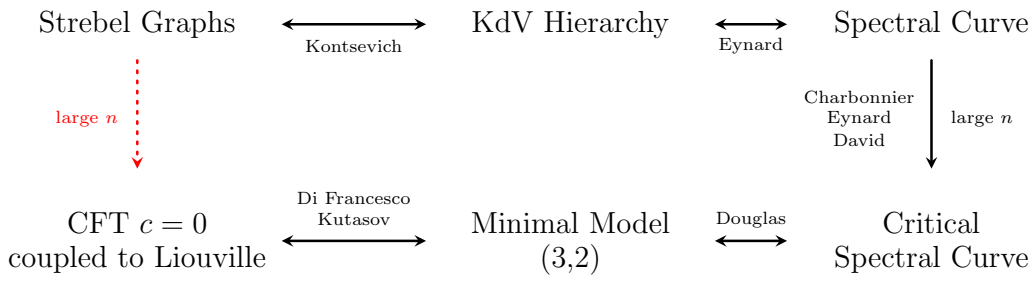

Figure 60: Summary of the reasoning for the large n limit of isoperimetric Strebel graphs and pure gravity.

At s_0, it worthes:

$$\left\langle \phi_{(1,1)}(x_1)\phi_{(1,1)}(x_2)\dots\phi_{(1,1)}(x_k)\right\rangle = \frac{1}{(-4)^{k-1}}\frac{(2k-1)!}{(k-1)!}3^{-k+\frac{1}{2}}. \tag{19.22}$$

It turns out that they are trivial (there is no dependence in the x_i's), which is the feature of the correlation of the identity operator.

In the end, the correlation functions of large isoperimetric Strebel graphs are computed from a critical spectral curve. This spectral curve is the one of a Liouville conformal field theory with $c = 0$, therefore the correlation functions we compute for Strebel graphs must be linear combination of amplitudes of a CFT dressed by gravity with central charge 0. This liouville CFT is called pure gravity, as there is no matter field, and just a trivial operator – the identity – in the matter content.The scheme 60 sums up the reasoning for this section.

20 Large n asymptotics of k-point functions

We saw in last chapter that we are able to compute explicitly the k-point generating functions $\mathcal{Z}_k$ and the large n limit of $Z_{n,1}(\mu, L; L_1)$. Yet, we needed to use the saddle point approximation, which is efficient for computing one point functions, but hard to handle for k point functions with $k \geq 2$. Hence, having a more generic results is necessary to get the continuous limit of generic correlation functions. As was stated in the previous section, the knowledge of $\tilde{\mathcal{S}}$, ν, q, and p allows to compute the large n limit of correlation functions. This is due to two results, from Eynard [Eynard, 2011] and Eynard and Orantin [Eynard and Orantin, 2007]. The first one is theorem 18.1, seen in section 18, states that the Laplace transforms $\mathcal{F}_k(\mu, L; z_1, \dots, z_k)$ are topological recursion invariants of the spectral curve $\mathcal{S}(\mu, L)$ found in this chapter. The second theorem gives the scalings of the invariants

$\mathcal{F}_{g,k}$. Let us state the latter, and apply the two results to our model. Our main result is to transform the scaling of the Laplace transforms $\mathcal{F}_{g,k}$ into the large n limit of any k point function, provided that the marked faces have large perimeters. As an application of this result, we apply it to the cases of 3 and 4 point functions.

Theorem 20.1. *[Eynard and Orantin, 2007] Let us consider a family of spectral curves $\mathcal{S}(\lambda)$ near a critical parameter λ_c, having those scalings:*

$$\begin{aligned} z - z_0 &= (\lambda_c - \lambda)^\nu \xi \\ x(\lambda; z) &= x(\lambda_c; z_0) + (\lambda_c - \lambda)^{q\nu} \tilde{x}(\xi) \\ y(\lambda; z) &= y(\lambda_c; z_0) + (\lambda_c - \lambda)^{p\nu} \tilde{y}(\xi). \end{aligned} \tag{20.1}$$

The critical spectral curve is noted $\tilde{\mathcal{S}}$. Note $\mathcal{F}_{g,k}(\mathcal{S}(\lambda); z_1, \dots, z_k)$ and $\tilde{\mathcal{F}}_{g,k}(\tilde{\mathcal{S}}; \xi_1, \dots, \xi_k)$ the invariants computed from the spectral curves $\mathcal{S}(\lambda)$ and $\tilde{\mathcal{S}}$ respectively. Then, for $2 - 2g - k < 0$:

$$\lim_{\lambda \to \lambda_c} (\lambda_c - \lambda)^{\gamma_{g,k}^{p,q,\nu}} \mathcal{F}_{g,k}(\mathcal{S}(\lambda); z_1, \dots, z_k) = \tilde{\mathcal{F}}_{g,k}(\tilde{\mathcal{S}}; \xi_1, \dots, \xi_k), \tag{20.2}$$

where $\gamma_{g,k}^{p,q,\nu} = (2 - 2g - k)(p + q)\nu$.

Let us apply those result to isoperimetric planar Strebel graphs, that is with the parameter $\lambda = \mu$ and scaling exponents $(\nu, p, q) = (\frac{1}{4}, 3, 2)$ for $k \geq 3$ point functions in genus $g = 0$. Then $2 - 2g - k = 2 - k < 0$, so we can apply the results. The critical spectral curve $\tilde{\mathcal{S}}$ is the one of the minimal model $M_{3,2}$.

$$\lim_{\mu \to \mu_c} (\mu_c - \mu)^{-\frac{5}{4}(2-k)} \mathcal{F}_{0,k}(\mathcal{S}(\mu, L); z_1, \dots, z_k) = C(L)^{2-k} \tilde{\mathcal{F}}_{0,k}(\tilde{S}; \xi_1, \dots, \xi_k) \tag{20.3}$$

where $C(L) = \left(\frac{2I_0(u_c)}{u_c^2 - 4}\right)^{\frac{5}{4}} \sqrt{\frac{u_c}{L}} \frac{u_c^2 - 4}{6}$ is global coefficient depending only on L.

Example 20.1. Let us look at the 3-point functions and 4-point functions. The invariants $\tilde{\mathcal{F}}_{0,3}(\tilde{\mathcal{S}}; \xi_1, \xi_2, \xi_3)$ and $\tilde{\mathcal{F}}_{0,4}(\tilde{\mathcal{S}}; \xi_1, \xi_2, \xi_3, \xi_4)$ have the following expressions [Eynard, 2016]:

$$\tilde{\mathcal{F}}_{0,3}(\tilde{\mathcal{S}}; \xi_1, \xi_2, \xi_3) = \frac{1}{6\xi_1\xi_2\xi_3} \tag{20.4}$$

$$\tilde{\mathcal{F}}_{0,4}(\tilde{\mathcal{S}}; \xi_1, \xi_2, \xi_3, \xi_4) = -\frac{1}{36\xi_1\xi_2\xi_3\xi_4} \left[1 + \frac{1}{\xi_1^2} + \frac{1}{\xi_2^2} + \frac{1}{\xi_3^2} + \frac{1}{\xi_4^2}\right]. \tag{20.5}$$

So the scalings are the following close to the critical parameter μ_c:

$$\mathcal{F}_{0,3}(\mathcal{S}(\mu, L); z_1, z_2, z_3) \underset{\mu \to \mu_c}{\sim} \frac{1}{(\mu_c - \mu)^{\frac{5}{4}} C(L)} \frac{1}{6\xi_1\xi_2\xi_3}$$

$$\mathcal{F}_{0,4}(\mathcal{S}(\mu,L);z_1,z_2,z_3,z_4) \underset{\mu\to\mu_c}{\sim} \frac{-1}{(\mu_c-\mu)^{\frac{5}{2}}C(L)^2} \frac{1}{36\xi_1\xi_2\xi_3\xi_4}\left[1+\frac{1}{\xi_1^2}+\frac{1}{\xi_2^2}+\frac{1}{\xi_3^2}+\frac{1}{\xi_4^2}\right]. \quad (20.6)$$

The expression for $\tilde{\mathcal{F}}_{0,3}$ is consistent with the one found in formula 18.4 for the invariant $\mathcal{F}_{0,3}$ at a generic value of the parameter μ. Also, the scaling deduced from the theorem of Eynard and Orantin, is consistent with the one we would find if we let μ tend to μ_c in equation 18.4.

Yet, with these results, we only get the scaling of the Laplace transforms of the original generating functions $\mathcal{Z}_k$. Therefore, we still do not have access to the large n limit of correlation functions $Z_{n,k}$. It remains to perform the inverse Laplace transform with respect to the variables ξ_i to get the asymptotics of correlation functions. One has to be careful in carrying out the inverse Laplace transform to be sure to take into account all the poles. This is the purpose of the following computations, whose result is stated in:

Theorem 20.2. *For $k\geq 3$, if $L_1,\dots,L_k$ scale as $L(\mu_c-\mu)^{-\frac{1}{2}}$, the k-point generating function $\mathcal{Z}_k(\mu,L;L_1,\dots,L_k)$ has the following behaviour:*

$$\mathcal{Z}_k(\mu,L;L_i) \underset{\mu\to\mu_c}{\sim} \frac{2^k}{i^k\pi^k}(\mu_c-\mu)^{\frac{5}{2}-\frac{3}{4}k}A^kC(L)^{2-k}\frac{L^k}{u_c^k}\int_{-\infty}^{+\infty}d\zeta_1\cdots\int_{-\infty}^{+\infty}d\zeta_k \prod_{i=1}^k e^{u\frac{L_i}{L}}\prod_{j=1}^k e^{-\frac{1}{2}\frac{L_j}{L}(u_c-u)\zeta_j^2}\zeta_j\tilde{\mathcal{F}}_{0,k}(\tilde{\mathcal{S}};i\zeta_j)(1+O(\sqrt{\mu_c-\mu})) \quad (20.7)$$

with $A=\frac{u_c}{L^2}\sqrt{\frac{2I_0(u_c)}{u_c^2-4}}$ and $C(L)=\left(\frac{2I_0(u_c)}{u_c^2-4}\right)^{\frac{5}{4}}\sqrt{\frac{u_c}{L}}\frac{u_c^2-4}{6}$, that are global coefficients depending only on the choice of perimeter L.

Indeed, for $k\geq 3$, we have:

$$2^{2-k}\prod_{i=1}^k(2d_i-1)!!\left\langle e^{\frac{\mu}{2}\sum_{d=0}^\infty\frac{L^{2d}}{2^d d!}\tau_d}\prod_{i=1}^k\tau_{d_i}\right\rangle_0 = \operatorname*{Res}_{z_i\to\infty}\prod_{i=1}^k z_i^{2d_i}dz_i\mathcal{F}_{0,k}(\mathcal{S}(\mu,L);z_1,\dots,z_k). \quad (20.8)$$

The quantity we are interested in is $\mathcal{Z}_k(\mu,L;L_1,\dots,L_k)$ and we want to recover it from the previous expression. The left hand side is equal to:

$$\text{l.h.s.} = 2^{-\sum_{i=1}^k d_i}L^{-2D}\prod_{i=1}^k(2d_i-1)!!\frac{\partial^{k-3}}{\partial\mu^{k-3}}[\mu^k\mathcal{U}_k(\mu,L,d_1,\dots,d_k)] \quad (20.9)$$

Hence, in order to recover $\mathcal{Z}_k$, we have to carry out the following sum:

$$\mathcal{Z}_k(\mu, L; L_1, \dots, L_k) = \sum_{d_1 \dots d_k} \prod_{i=1}^{k} \frac{L_i^{2d_i}}{2^{d_i}(2d_i-1)!!d_i!} \times \text{l.h.s.} \tag{20.10}$$

$$= \sum_{d_1 \dots d_k} \prod_{i=1}^{k} \frac{L_i^{2d_i}}{(2d_i)!} \times \operatorname*{Res}_{z_i \to \infty} \prod_{i=1}^{k} z_i^{2d_i} dz_i \mathcal{F}_{0,k}(\mathcal{S}(\mu, L); z_i) \tag{20.11}$$

The functions $\mathcal{F}_{0,k}(\mathcal{S}(\mu, L); z_i)$ are entire functions of the $\frac{1}{z_i}$'s. By the following change of coordinates : $z_i = \sqrt{\tilde{z}_i^2 + \frac{u^2}{L^2}}$, the functions $\mathcal{F}_{0,k}(\mathcal{S}(\mu, L); \tilde{z}_i)$ become polynomials in the $\frac{1}{\tilde{z}_i}$. Indeed, if $\tilde{z}_i \in \mathbb{C}$, the variables $\tilde{z}_i^2 + \frac{u^2}{L^2}$ are the x_i's, living on the base space Σ_0, and are then more 'canonical' than the z_i's. So we have:

$$\mathcal{Z}_k(\mu, L; L_i) = \sum_{d_1 \dots d_k} \prod_{i=1}^{k} \frac{L_i^{2d_i}}{(2d_i)!} \operatorname*{Res}_{\tilde{z}_i \to \infty} \prod_{i=1}^{k} \left(\tilde{z}_i^2 + \frac{u^2}{L^2} \right)^{d_i - \frac{1}{2}} 2\tilde{z}_i d\tilde{z}_i \mathcal{F}_{0,k}(\mathcal{S}(\mu, L); \tilde{z}_i). \tag{20.12}$$

The residue is taken at infinity, and we want to deform its contour of integration. The function $\mathcal{F}_{0,k}(\mathcal{S}(\mu, L); \tilde{z}_i)$ has poles only around $\tilde{z}_i = 0$; the term $\left(\tilde{z}_i^2 + \frac{u^2}{L^2} \right)^{d_i - \frac{1}{2}}$ has a cut on the segment $\left[-i\frac{u}{L}; +i\frac{u}{L} \right]$ (the branch cut for $\sqrt{}$ is $-i\mathbb{R}$). Hence, we can deform the contour of integration into the one described in figure 61. The contour surrounds the segment $\left[-i\frac{u}{L}; +i\frac{u}{L} \right]$, and the pole at 0.

Now it is possible to exchange $\sum$ and Res, because the contour is no longer at infinity. This gives:

$$\mathcal{Z}_k(\mu, L; L_i) = \sum_{d_1 \dots d_k} \operatorname*{Res}_{\tilde{z}_i \to \infty} \prod_{i=1}^{k} \frac{L_i^{d_i}}{d_i!} \sqrt{\tilde{z}_i^2 + \frac{u^2}{L^2}}^{d_i} \frac{2\tilde{z}_i \mathcal{F}_{0,k}(\mathcal{S}(\mu, L); \tilde{z}_i)}{\sqrt{\tilde{z}_i^2 + \frac{u^2}{L^2}}} d\tilde{z}_i \tag{20.13}$$

$$= 2^k \operatorname*{Res}_{\tilde{z}_i \to \infty} \prod_{i=1}^{k} e^{L_i \sqrt{\tilde{z}_i^2 + \frac{u^2}{L^2}}} \frac{\tilde{z}_i \mathcal{F}_{0,k}(\mathcal{S}(\mu, L); \tilde{z}_i)}{\sqrt{\tilde{z}_i^2 + \frac{u^2}{L^2}}} d\tilde{z}_i \tag{20.14}$$

We want the asymptotic behaviour ($n \to \infty$) of the Strebel Graph volumes with k marked faces, which corresponds to looking at the limit $\mu \to \mu_c$ in the function $\mathcal{Z}_k$. In that limit, the contour can be divided into two regions (see figure 61): region 1 corresponds to the parts of the contour which are close to the pole ($\tilde{z}_i = 0$) of $\mathcal{F}_{0,k}$, region 2 corresponds to the rest of the contour.
The contour integral over region 2 remains finite (of order 1) when $\mu \to \mu_c$. As we may see in the following, on the contrary, the integral over region 1 diverges as $\mu \to \mu_c$.
Region 1 is the part of the integral close to 0. Let us define:

$$\tilde{z}_i = -\sqrt{u_c - u} \frac{\sqrt{u}}{L} \xi_i \tag{20.15}$$

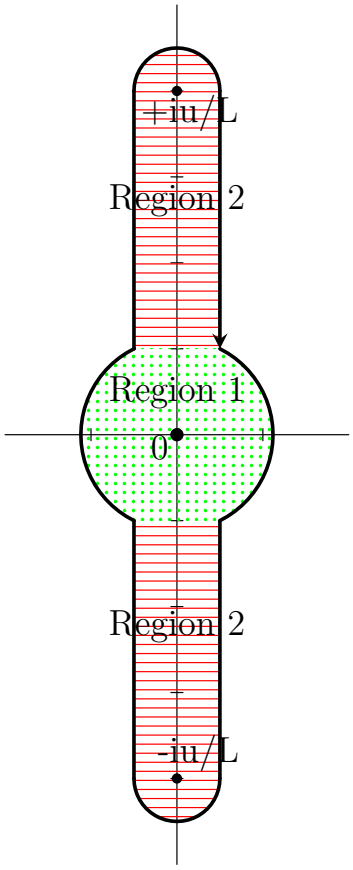

Figure 61: The contour of integration of $\underset{\infty}{\text{Res}}$ is deformed and encloses a cut.

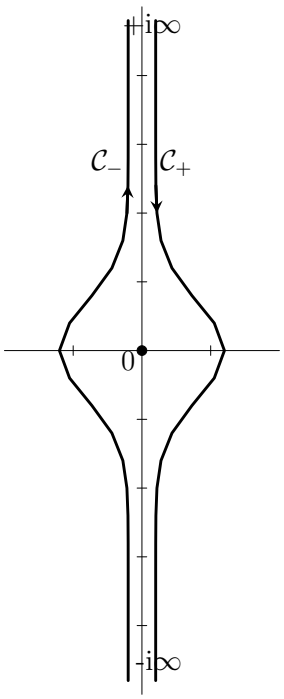

Figure 62: Contour of the region 1 in the variable ξ_i.

From the scaling of formula 20.3, we can replace $\mathcal{F}_{0,k}$ by its scaling, expressed in terms of the minimal model $M_{3,2}$ invariants. $\mathcal{F}_{0,k}$ behaves like $(\mu_c - \mu)^{\frac{5}{4}(2-k)}$, so, as $k \geq 3$, it is divergent when $\mu \to \mu_c$.
In order to get the dominant order in the large n limit, we may then focus our attention on the region 1. In the variables ξ_i, we have to carry out the integration over the contours $\mathscr{C}_+$, $\mathscr{C}_-$ (see figure 62). $\mathscr{C}_+$ is going from $+i\infty$ to $-i\infty$, with $Re(\xi_i) > 0$; $\mathscr{C}_-$ is going from $-i\infty$ to $+i\infty$, with $Re(\xi_i) < 0$.

We look at the expansion in $\mu_c - \mu$, so we re-express the square root as:

$$\sqrt{\tilde{z}_i^2 + \frac{u^2}{L^2}} = \sqrt{\frac{u_c^2}{L^2} + (u_c - u)\frac{u_c}{L^2}(\xi_i^2 - 2) + O((u_c - u)^2)} \tag{20.16}$$

$$= \frac{u_c}{L}\sqrt{1 + \frac{u_c - u}{u_c}(\xi_i^2 - 2) + O((u_c - u)^2)} \tag{20.17}$$

$$= \frac{u_c}{L} + \frac{1}{2}\frac{u_c - u}{L}(\xi_i^2 - 2) + O((u_c - u)^2) \tag{20.18}$$

We are also looking at a regime where $\frac{L_i}{L} \to \infty$ as $\mu \to \mu_c$. From the previous expansion, we see that the argument of the exponential contains $\frac{L_i}{L}(u_c - u)(\xi_i^2 - 2)$, which, at ξ_i fixed, remains of order 1 if $\frac{L_i}{L} \sim (u_c - u)^{-1} \sim (\mu_c - \mu)^{-\frac{1}{2}}$. This corresponds to a regime where $\frac{L_i}{L} \sim \sqrt{n}$.
The function to integrate is odd, but $\mathscr{C}_+$ and $\mathscr{C}_-$ have opposite orientations, so we can

restrict to the integration over $\mathscr{C}_+$:

$$\begin{aligned}
\mathcal{Z}_k(\mu, L; L_i) \quad &\underset{\mu\to\mu_c}{\sim} \quad 2^k(\mu_c-\mu)^{\frac{5}{4}(2-k)}C(L)^{2-k}\frac{2}{2i\pi}\int_{+i\infty}^{-i\infty}d\xi_1\dots\frac{2}{2i\pi}\int_{+i\infty}^{-i\infty}d\xi_k \\
&\prod_{i=1}^{k} e^{u_c\frac{L_i}{L}+\frac{1}{2}\frac{L_i}{L}(u_c-u)(\xi_i^2-2)}(u_c-u)\frac{u}{L^2}\frac{\xi_i}{\frac{u_c}{L}+\frac{1}{2}\frac{u_c-u}{L}(\xi_i^2-2)}\times \\
&\tilde{\mathcal{F}}_{0,k}(\tilde{\mathcal{S}};\xi_i)(1+O((\mu_c-\mu))) \\
&\underset{\mu\to\mu_c}{\sim} \quad \frac{2^{2k}}{(2i\pi)^k}(\mu_c-\mu)^{\frac{5}{2}-\frac{3}{4}k}A^k\tilde{C}(L)^{2-k}\left(\int_{+i\infty}^{-i\infty}d\xi_1\cdots\int_{+i\infty}^{-i\infty}d\xi_k\right) \\
&\prod_{i=1}^{k} e^{u_c\frac{L_i}{L}+\frac{1}{2}\frac{L_i}{L}(u_c-u)(\xi_i^2-2)}\frac{\xi_i}{\frac{u_c}{L}}\tilde{\mathcal{F}}_{0,k}(\tilde{\mathcal{S}};\xi_i)(1+O(\mu_c-\mu)^{\frac{1}{2}})
\end{aligned} \tag{20.19}$$

with $A=\frac{u_c}{L^2}\sqrt{\frac{2I_0(u_c)}{u_c^2-4}}$. We carry out the change of variable $\xi_i=i\zeta_i$, and in the end:

$$\begin{aligned}
\mathcal{Z}_k(\mu, L; L_i) \quad &\underset{\mu\to\mu_c}{\sim} \quad \frac{2^k}{\mathrm{i}^k\pi^k}(\mu_c-\mu)^{\frac{5}{2}-\frac{3}{4}k}A^kC(L)^{2-k}\frac{L^k}{u_c^k}\int_{+\infty}^{-\infty}id\zeta_1\cdots\int_{+\infty}^{-\infty}id\zeta_k \\
&\prod_{i=1}^{k} e^{u\frac{L_i}{L}}\prod_{j=1}^{k} e^{-\frac{1}{2}\frac{L_j}{L}(u_c-u)\zeta_j^2}i\zeta_j\tilde{\mathcal{F}}_{0,k}(\tilde{\mathcal{S}};\mathrm{i}\zeta_j)(1+O(\sqrt{\mu_c-\mu})) \\
&\underset{\mu\to\mu_c}{\sim} \quad \frac{2^k}{i^k\pi^k}(\mu_c-\mu)^{\frac{5}{2}-\frac{3}{4}k}A^kC(L)^{2-k}\frac{L^k}{u_c^k}\int_{-\infty}^{+\infty}d\zeta_1\cdots\int_{-\infty}^{+\infty}d\zeta_k \\
&\prod_{i=1}^{k} e^{u\frac{L_i}{L}}\prod_{j=1}^{k} e^{-\frac{1}{2}\frac{L_j}{L}(u_c-u)\zeta_j^2}\zeta_j\tilde{\mathcal{F}}_{0,k}(\tilde{\mathcal{S}};i\zeta_j)(1+O(\sqrt{\mu_c-\mu})).
\end{aligned} \tag{20.20}$$

This is the result announced in theorem 20.2. Let us apply it to the 3-point and the 4-point functions.

Example 20.2. 3-point function and 4-point function in the large n limit
Applying the result of formula 20.20, we obtain:

$$\mathcal{Z}_3(\mu, L; L_i) \underset{\mu\to\mu_c}{\sim} 8\left(\frac{2}{\pi}\right)^{\frac{3}{2}}\frac{L^4}{u_c^{\frac{5}{2}}(u_c^2-4)}(u_c-u)^{\frac{1}{2}}\prod_{i=1}^{3}\frac{e^{u_c\frac{L_i}{L}}}{\sqrt{\frac{L_i}{L}(u_c-u)}} \tag{20.21}$$

It may seem that this quantity is not divergent, but remember that, in the exponentials, we have $\frac{L_i}{L}\sim(u_c-u)^{-1}\sim(\mu_c-\mu)^{-\frac{1}{2}}$.
For the 4-point function:

$$\mathcal{Z}_4(\mu, L; L_i) \underset{\mu\to\mu_c}{\sim} \frac{64}{\pi^2}\frac{L^6}{u_c^3}\frac{1}{(u_c^2-4)^2}(u_c-u)^{-1}\left(1+\sum_{i=1}^{4}\frac{L_i}{L}(u_c-u)\right)\prod_{i=1}^{4}\frac{e^{u_c\frac{L_i}{L}}}{\sqrt{\frac{L_i}{L}(u_c-u)}} \tag{20.22}$$

Here, the divergence is clear. We want to underline that the terms $\sum_i \frac{L_i}{L}(u_c - u)$ are not subdominant, but of order 1, so we have to take them into account.

Part VI
Symmetries of correlation functions

The three preceding parts addressed the random maps as probabilistic spaces that need to be characterized, and whose continuous limit needs to be identified. This chapter is dedicated to another aspect of random maps, and does not concern the potential continuous limit of a model, but rather the symmetries arising in the enumeration of maps. In a model of maps, the maps that satisfy certain conditions, such as having k boundaries and genus g for instance, can often be enumerated, and the numbers of maps, called correlation functions, are encoded in generating functions. Those generating functions depend on a set of variables, and they inherit symmetry properties under certain permutations of variables from the symmetries of the random maps. Actually, random maps are a source of motivation and of intuition for such symmetries, but we shall progressively consider the problem of symmetries of expectation values for generic correlation functions, whether they be defined from random maps models or not. Those symmetries of correlation functions, defined independently of the underlying random maps, allow to put strong additional constraints on the correlation functions. It is then tempting to consider the correlation functions as amplitudes of states of an effective theory on the boundaries of the random maps, which is reminiscent of a kind of AdS/CFT duality between the theory in the bulk (the enumeration of random maps on surfaces with boundaries) and the theory on the boundaries. The constraints on the correlation functions are a clue that the enumeration of random maps can be related to integrable systems.

In this chapter, we show symmetry properties of correlation functions computed from the Ising model on random maps. First we review some symmetry properties inherited from the topological recursion. Second, we introduce the Ising model on random maps, the correlation functions that encode the combinatorics of such maps, the matrix model formulation of the model, and we give the recursive relation which presides over the computation of correlation functions, which was proven by Eynard and Orantin [Eynard and Orantin, 2008]. In this very section, we define the transformation that maps can undergo, and the possible symmetries of the correlation functions that we can hope to stand for the correlation functions. The recursion formula shows to be similar to the topological recursion in some of its aspects, but has also fundamental differences that prevent us from deducing symmetry properties. In the third section, we state the precise problem that we tackle, we give the already known results that we use after in our proofs, and we state the main theorem of the chapter. This result shows that certain planar correlation functions computed from the recursive relation

satisfy another recursion – which involves *link patterns* –, and as a corollary, they are also invariant under rotation and inversion transformations. We also give the first form a some kind of "forgetful map" for removing a change of color in the correlation functions. We then, in the fourth section, investigate some of the consequences of the main theorem. We show, using the work of Eynard [Eynard, 2016], that the correlation functions satisfy strong constraints, it is a first step for relating the correlation functions to an integrable system on the boundaries of the maps. We have only an inkling of this relation to integrable systems for the moment, and we still investigate at the time of writing this manuscript. Section 25 is dedicated to the quite technical proof of the theorem, and the sixth and last section addresses the future extensions of the theorem.

21 Introduction

21.1 Symmetries in Topological Recursion

Let us consider a spectral curve $\mathcal{S}$. We saw in chapter V the formula of topological recursion (equation 16.2), allowing to define invariants $\omega_{g,k}(z_1,\dots,z_k)$ from the knowledge of $\mathcal{S}$. In this formula, the variable z_1 plays a specific role with regards to $z_2,\dots,z_k$, as it appears in the kernel of recursion $K_a(z;z_1)$ and not in the invariants $\omega_{g',k'}$ present in the remaining part. This apparent lack of symmetry should naturally lead to invariants $\omega_{g,k}$ that are not symmetric under the exchange of variables $z_1 \leftrightarrow z_j$. Yet, for some spectral curves, the invariant $\omega_{g,k}$ is related to the enumeration of random maps drawn on a genus g surface with k boundaries. In the perspective of the combinatorial model, exchanging two boundaries do not affect the combinatorics: it amounts to apply a homeomorphism to the underlying surface, which has no effect on the enumeration of random maps (they are unchanged under such homeomorphisms). Therefore, for those spectral curves, it is obvious, from the combinatorial model, that the invariants $\omega_{g,k}$ are symmetric under a exchange of variables. Hence the legitimate question: is this symmetry attributable to the specificity of the spectral curves deduced from random maps models, or a systematic property of topological recursion ?
The answer, given by Eynard and Orantin [Eynard and Orantin, 2008], is that the invariants $\omega_{g,k}(z_1,\dots,z_k)$ are symmetric under the exchange of variables, no matter which spectral curve is used:

Lemma 21.1. *For any spectral curve $\mathcal{S}$, the invariants $\omega_{g,k}$ computed through topological recursion are symmetric:*

$$\forall \sigma \in \mathfrak{S}_k,\ \omega_{g,k}(z_1,\dots,z_k) = \omega_{g,k}(z_{\sigma(1)},\dots,z_{\sigma(k)}). \tag{21.1}$$

The proof is carried out by an easy recursion on $2g+k$. Hence, although the formulation of topological recursion is not symmetric, it defines symmetric invariants. This statement sums up the general idea of this chapter: we prove properties of symmetry for invariants computed from a recursion that is not symmetric in its formulation.

21.2 Forgetful map

Topological recursion allows to compute invariants $\omega_{g,k}$ from $\omega_{0,1}$ anf $\omega_{0,2}$ by recurrence on $2-2g-k$. The knowledge of the invariants $\omega_{g',k'}$ with $2g'+k' < 2g+k$ allows to determine $\omega_{g,k}$. The inverse question is the following: if one knows $\omega_{g,k}$, is it possible to recover $\omega_{g,k-1}$ (provided that $k \geq 2$) ? The answer is yes, and the operator carrying out the deletion of a boundary is the forgetful map $\mathcal{O}_k^{TR}$. It is valid for invariants computed by topological recursion. We introduce it here, following the results of Eynard and Orantin [Eynard and Orantin, 2007].
The root of the one-form $y(z)dx(z)$ is defined as:

$$\Phi(\tilde{z}) = \int_o^{\tilde{z}} y(z)dx(z), \tag{21.2}$$

where $o \in \Sigma$ is any base point on the spectral curve. Let us fix $k \geq 2$. The operator $\mathcal{O}_k^{TR} : \bigotimes^k \mathscr{M}^1(\Sigma) \to \bigotimes^{k-1} \mathscr{M}^1(\Sigma)$ is defined as:

$$\mathcal{O}_k^{TR} f(z_1, \ldots, z_k) = \begin{cases} \operatorname*{Res}_{z_2 \to z_1} \Phi(z_2) f(z_1, z_2) & \text{if } k = 2 \\ \frac{1}{2g+k-3} \sum_{a \text{ branchpoint}} \operatorname*{Res}_{z_k \to a} \Phi(z_k) f(z_1, \ldots, z_k) & \text{if } k > 2, \end{cases} \tag{21.3}$$

where f is a meromorphic k-form. Eynard and Orantin showed in [Eynard and Orantin, 2007], that the operator $\mathcal{O}_k^{TR}$ erases the last boundary in the invariant ω_k, that is:

$$\mathcal{O}_k^{TR} \omega_{g,k}(z_1, \ldots, z_k) = \omega_{g,k-1}(z_1, \ldots, z_{k-1}). \tag{21.4}$$

As we will define a forgetful map in this chapter, let us stress an important feature of the operator $\mathcal{O}_k^{TR}$, that we will want to impose to our operator: except for $k = 2$, $\mathcal{O}_k^{TR}$ is independent of the other variables $z_1, \ldots, z_{k-1}$, and depends only on the spectral curve (through the branchpoints and the root). We will show an operator in section 23.4.3 that matches this generic requirement.

22 Ising model on random maps

As was mentioned in the previous section, we shall prove properties of a recursion formula (equation 22.12 below), no matter what the underlying physical and combinatorial model – from which it comes from – is. However, it is useful to describe first this

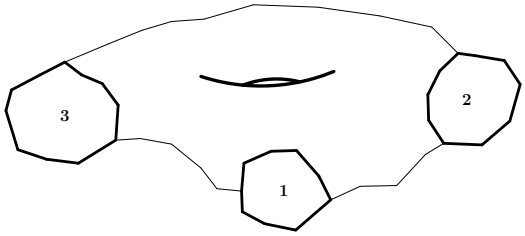

Figure 63: Riemann surface $\Sigma_{1,3}$ of genus 1 with 3 boundaries

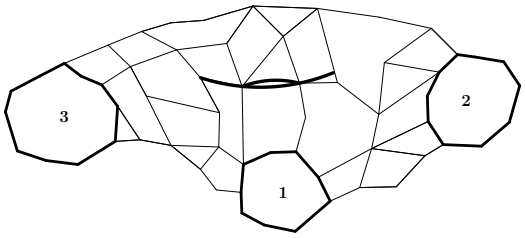

Figure 64: Random map on $\Sigma_{1,3}$

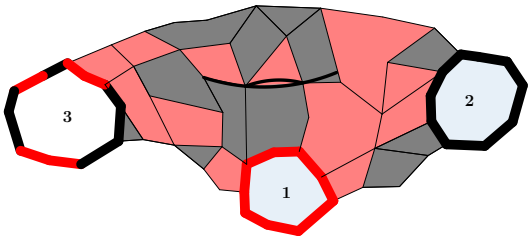

Figure 65: Ising model on $\Sigma_{1,3}$

very model, in order to understand how the properties translate in the physical side, and which are the consequences of such symmetries. This section briefly describes the Ising model on random maps, and the invariants $H^{(g)}_{\mathbf{k_L};m;n}$ that enumerate the maps.

22.1 Combinatorics of the Ising model

Consider an orientable surface $\Sigma_{g,K}$ of genus g with K labeled boundaries (figure 63), and a map $\mathcal{M}$ embedded in $\Sigma_{g,K}$, having faces of degree smaller than $d_{\max}$ (see figure 64). We assign a color (red or black) to every face of the map (see figure 65). Three types of boundaries can arise: uniform red boundaries (boundary 1 in figure 65), corresponding to boundaries having only red edges ; uniform black boundaries (*e.g.* boundary 2, figure 65) , whose edges are black ; and mixed boundaries (boundary 3), having both red and black edges. We give a type to every boundary edge of the map (see figure 66):

- For the edges belonging to a uniform (red or black) face, their type is the label of the face.
- For the mixed boundary i, we define

$$k_i = \#\text{connected sets of red edges of the boundary.}$$

  For instance, in figure 66, $k_i = 4$. The edges are labeled in the following manner. One chooses arbitrarily a connected part of red edges on the boundary (this part

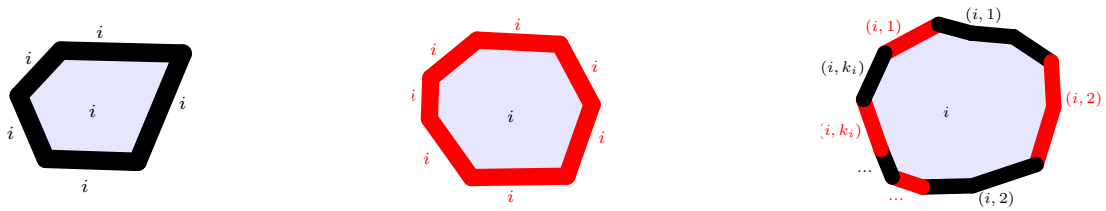

Figure 66: Ways to assign a type to any boundary edge according to the boundary type.

must be neighboured by black edges), and assigns to these edges the type $(i, 1)$. Then, the black edges part following clockwisely is given the same type $(i, 1)$. The next (in the clockwise order around the boundary) set of red edges then has label $(i, 2)$, etc. In the end, the edges of the mixed boundary i have types $(i, 1), \dots, (i, k_i)$.

Definition 22.1. *We define* $\mathbb{M}^{(g)}_{\mathbf{k_L};m;n}$ *as the set of connected random maps of genus* g *with* L *mixed boundaries with* $\mathbf{k_L} = \{k_1, \dots, k_L\}$ *changes of colors,* m *uniform red boundaries and* n *uniform black boundaries.*

In appendix E, the map we propose to build is a quadrangulation belonging to $\mathbb{M}^{(1)}_{3,3;0;0}$.
In order to assign a Boltzmann weight to a map $\mathcal{M} \in \mathbb{M}^{(g)}_{\mathbf{k_L};m;n}$, we assign a weight to local objects composing $\mathcal{M}$: The weight of $\mathcal{M}$ is then

$$\mathcal{W}(\mathcal{M}) = \prod_{k=1}^{d_{\max}} \prod_{\substack{I,J \\ \text{types of edges}}} \frac{t_k^{n_k} \tilde{t}_k^{\tilde{n}_k}}{x_I^{l_I+1} y_J^{\tilde{l}_J+1}} c_{rr}^{n_{rr}} c_{bb}^{n_{bb}} c_{br}^{n_{br}}. \tag{22.1}$$

The invariants of interest in this article are the partition functions of $\mathbb{M}^{(g)}_{\mathbf{k_L};m;n}$ for all $(g, \mathbf{k_L}, m, n)$. They are then computed by enumerating the weighted maps $\mathcal{M} \in \mathbb{M}^{(g)}_{\mathbf{k_L};m;n}$.

Definition 22.2. *The generating function of the set* $\mathbb{M}^{(g)}_{\mathbf{k_L};m;n}$ *is denoted by* $H^{(g)}_{\mathbf{k_L};m;n}$. *It is given by:*

$$H^{(g)}_{\mathbf{k_L};m;n} = \sum_{\mathcal{M} \in \mathbb{M}^{(g)}_{\mathbf{k_L};m;n}} \mathcal{W}(\mathcal{M}). \tag{22.2}$$

Those partition functions also called the correlation functions, generating functions, invariants, observables *or* amplitudes *of the Ising model on random maps with boundary conditions, depending on the context.*

Object	Description	Boltzmann weight	number in $\mathcal{M}$
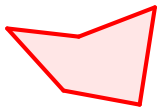	Red k-gone ($k \geq 3$)	t_k	n_k
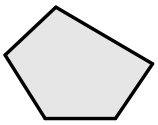	Black k-gone ($k \geq 3$)	$\tilde{t}_k$	$\tilde{n}_k$
	Edge between 2 red faces	$c_{rr} = \frac{\tilde{t}_2}{t_2\tilde{t}_2 - c^2}$	n_{rr}
	Edge between 2 black faces	$c_{bb} = \frac{t_2}{t_2\tilde{t}_2 - c^2}$	n_{bb}
	Edge between a red face and a black face	$c_{br} = \frac{c}{t_2\tilde{t}_2 - c^2}$	n_{br}
	Red boundary edge of type J	x_J	l_J
	Black boundary edge of type J'	$y_{J'}$	$\tilde{l}_{J'}$

The generating functions depend on the complex fugacities x_J and $y_{J'}$. Namely:

$$H^{(g)}_{\mathbf{k_L};m;n}\left((x_{1,1}, y_{1,1}, \ldots, x_{1,k_1}, y_{1,k_1}), \ldots, (x_{L,1}, \ldots, y_{L,k_L}); x_1, \ldots, x_m; y_1, \ldots, y_n\right).$$

The generating functions $H^{(g)}_{\mathbf{k_L};m;n}$ are formal power series in the times t_k, $\tilde{t}_k$ ($k \geq 3$), in the weights c_{rr}, c_{bb}, c_{br}, and in the variables $1/x_J$, $1/y_{J'}$, but as it was shown in [Eynard and Orantin, 2008], they are actually algebraic functions of the times t_k, $\tilde{t}_k$, of the weights c_{rr}, c_{bb}, c_{br}, and of the variables x_J, $y_{J'}$.

Physically, assigning a Boltzmann weight to a colored random map with boundaries, is equivalent to assigning an energy to a configuration of spins on the random map. Indeed, if red faces corresponds to faces of classical spin $+$, and black faces are faces of classical spin $-$, then the weights c_{rr}, c_{br}, c_{bb} are the energies of interaction between respectively 2 neighboring $+/+$ faces, 2 neighboring $+/-$ faces, and two neighboring $-/-$ faces. This is the reason why this model is called the Ising model. The hope, in the quantum gravity frame, is that when the number of faces increases toward infinity, the configuration of spins mimic a matter field of spin $\frac{1}{2}$, coupled with the geometry of the surface. This coupling means that the matter field interacts with the geometry, and therefore with gravity. At the level of finite random maps, the coupling between

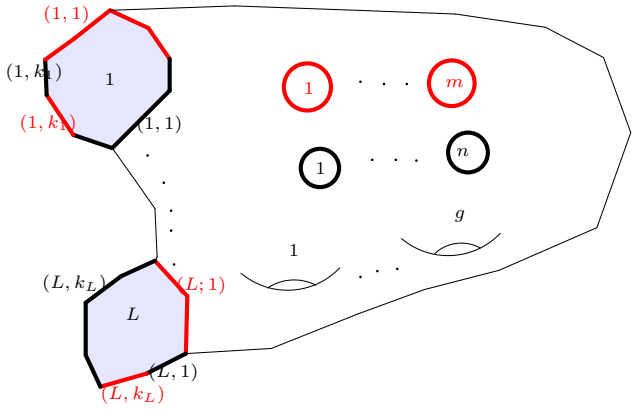

Figure 67: Representation of a map of genus g with m uniform red boundaries, n uniform black boundaries, and L mixed boundaries with $\{k_1, \dots, k_L\}$ changes of colors.

the spins and the geometry is visible in the Boltzmann weights. Indeed, the energy of a configuration depends on the structure of the random maps, that is to say the neighboring relations between the faces.
Graphically, we represent the generating function $H^{(g)}_{\mathbf{k_L};m;n}$ as in figure 67.

An alternative way to encode the correlation functions is to interpret them as expectation values in a random matrix model, introduced by Kazakov [Kazakov, 1986], as we saw in section 5. This 2-matrix model has a partition function that is expressible in terms of a formal integral over Hermitian matrices of size N:

$$\mathcal{Z} = \int_{\text{formal}} dM_1 dM_2 e^{-N\text{Tr}(V_1(M_1)+V_2(M_2)-cM_1M_2)}, \tag{22.3}$$

where V_1 and V_2 are the following polynomials:

$$\begin{cases} V_1(x) = t_2\frac{x^2}{2} - \sum_{k=3}^{d_1+1} t_k \frac{x^k}{k} \\ V_2(x) = \tilde{t}_2\frac{x^2}{2} - \sum_{k=3}^{d_2+1} \tilde{t}_k \frac{x^k}{k}. \end{cases} \tag{22.4}$$

The partition function enumerates (not necessarily connected) colored random maps, each random map being given the Boltzmann weight defined in what precedes. In the matrix model, the expectation value of an observable $\mathcal{O}(M_1, M_2)$ depending on the hermitian matrices M_1 and M_2 is given by the formula:

$$\langle \mathcal{O}(M_1, M_2) \rangle = \frac{1}{\mathcal{Z}} \int_{\text{formal}} dM_1 dM_2 \mathcal{O}(M_1, M_2) e^{-N\text{Tr}(V_1(M_1)+V_2(M_2)-cM_1M_2)}. \tag{22.5}$$

For instance, the moment $\langle \text{Tr} M_1^k \rangle$ is the generating function of maps of any genus, having one red boundary of length k. Yet, in this enumeration, the boundary edges

have weight 1. Those maps are not connected in general. The moment which enumerates the connected maps only, is denoted $\left\langle \mathrm{Tr} M_1^k \right\rangle_c$. Similarly, the moments $\left\langle \mathrm{Tr}(M_2^\ell) \right\rangle_c$, $\left\langle \mathrm{Tr}(M_1^k M_2^\ell) \right\rangle_c$ count connected maps of any genera, with respectively one black boundary of length ℓ, and one mixed boundary with k consecutive red edges and ℓ consecutive black edges.

Example 22.1. The map showed in figure 65 has 3 boundaries:

- boundary 1 has length 8 and is uniformly red ;
- boundary 2 has length 9 and is uniformly black ;
- boundary 3 has length 11, with an alternating pattern of colors, there are 3 changes of colors.

This map appears in the moment

$$\left\langle \mathrm{Tr}(M_1^8)\mathrm{Tr}(M_2^9)\mathrm{Tr}(M_1^2 M_2^1 M_1^1 M_2^2 M_1^2 M_2^3) \right\rangle_c$$

In order to integrate the fugacities of the boundary edges in the counting, we use the following notation:

$$\left\langle \mathrm{Tr} \frac{1}{x - M} \right\rangle = \sum_{k=0}^{+\infty} \frac{\left\langle \mathrm{Tr} M^k \right\rangle}{x^{k+1}}. \tag{22.6}$$

Example 22.2. The map of figure 65 will appear in the moment:

$$\left\langle \mathrm{Tr} \frac{1}{x_1 - M_1} \mathrm{Tr} \frac{1}{x_2 - M_2} \mathrm{Tr} \frac{1}{x_{1,1} - M_1} \frac{1}{y_{1,1} - M_2} \frac{1}{x_{1,2} - M_1} \frac{1}{y_{1,2} - M_2} \frac{1}{x_{1,3} - M_1} \frac{1}{y_{1,3} - M_2} \right\rangle_c$$

For the generating functions of generic random maps, if $l \geq 1$ – we are interested in maps having at least one mixed boundary –, the invariants H are defined in the following way:

$$H_{\mathbf{k_L};m;n}(\mathbf{S_L}; x_1, \ldots, x_m; y_1, \ldots, y_n) = \left\langle \prod_{i=1}^{l} \mathrm{Tr} \left(N\delta_{1,k_i} + \prod_{j=1}^{k_i} \frac{1}{x_{i,j} - M_1} \frac{1}{y_{i,j} - M_2} \right) \prod_{s=1}^{m} \mathrm{Tr} \left(\frac{1}{x_r - M_1} \right) \prod_{t=1}^{n} \mathrm{Tr} \left(\frac{1}{y_t - M_2} \right) \right\rangle_c \tag{22.7}$$

It enumerates connected maps of any genus with the boundary conditions of figure 67. It admits a topological expansion, that is, at large N:

$$H_{\mathbf{k_L};m;n} = \sum_{g=0}^{+\infty} N^{2-2g-l-m-n} H^{(g)}_{\mathbf{k_L};m;n}.$$

In this expansion, the term $H^{(g)}_{\mathbf{k_L};m;n}$ enumerates uniquely connected maps of genus g. This description of the generating functions in terms of a matrix model will be useful for deriving the consequences of the symmetries in the following.

In the article [Eynard and Orantin, 2008], Eynard and Orantin showed that the generating functions are computable by a recurrence relation. This recurrence relation differs from topological recursion in its expression but the principle is the same, as all the generating functions defined are encoded in a spectral curve $\mathcal{S} = (\Sigma, \Sigma_0, x, y, B)$ (see chapter V for the definition of the spectral curve). The meromorphic functions x and y are related by an algebraic equation $E(x(z), y(z)) = 0$, $\forall z \in \Sigma$. In the Ising model, the spectral curve is rational. That is to say, it has the following form:

- the surfaces Σ and Σ_0 are both the Riemann sphere $\overline{\mathbb{C}}$.
- The meromorphic functions x and y admit a rational parametrization:

$$\begin{cases} x(p) = \gamma p + \sum_{k=0}^{d_1} \alpha_k p^{-k} \\ y(q) = \gamma q^{-1} + \sum_{k=0}^{d_2} \beta_k q^k. \end{cases} \tag{22.8}$$

  In this case, the algebraic equation $E(x(z), y(z)) = 0$, $\forall z \in \overline{\mathbb{C}}$ is a polynomial in x and y of respective degrees d_1 and d_2.

- As the curve Σ is of genus 0, the Bergman kernel is simply:

$$B(p_1, p_2) = \frac{dp_1 \otimes dp_2}{(p_1 - p_2)^2}. \tag{22.9}$$

In what follows, let us consider generic spectral curves, that are not necessarily related to the combinatorics of Ising model. For given x, $y \in \Sigma_0$, there are respectively $d_1 + 1$ and $d_2 + 1$ preimages in Σ. We note them in this way:

$$\begin{cases} p^{0,0}, p^{1,0}, \dots, p^{d_1,0} \text{ such that } x(p^{i,0}) = x, \\ p^{0,0}, p^{0,1}, \dots, p^{0,d_2} \text{ such that } y(p^{0,j}) = y \end{cases} \tag{22.10}$$

(we take $p^{0,0} = p$). More generally,

$$\forall i = 0, \dots, d_1,\ \forall j = 0, \dots, d_2,\ \ y(p^{i,j}) = y(p^{i,0})$$

$$\forall i = 0, \dots, d_1,\ \forall j = 0, \dots, d_2,\ \ x(p^{i,j}) = x(p^{0,j}).$$

Actually, the boundary edges fugacities $x_{i,j}$ and $y_{i',j'}$ are the images $x(p_{i,j})$, $y(q_{i',j'})$ of $p_{i,j}$ and $q_{i',j'}$. The generating functions defined in equation 22.2 in terms of the fugacities $x_{i,j}$, $y_{i',j'} \in \Sigma_0$, are meromorphic functions of the variables $p_{i,j}$, $q_{i',j'} \in \Sigma$:

$$H^{(g)}_{\mathbf{k_L};m;n}\left((p_{1,1}, q_{1,1}, \dots, p_{1,k_1}, q_{1,k_1}), \dots, (p_{L,1}, \dots, q_{L,k_L}); p_1, \dots, p_m; q_1, \dots, q_n\right).$$

This statement deserves to be analysed. If one replaces the variable $p_{i,j}$ (resp. $q_{i,j}$) by $p_{i,j}^{k,0}$ with $k \neq 0$ (resp. $q_{i,j}^{0,k}$), then the value of $H^{(g)}_{\mathbf{k_L};m;n}$ changes. In this case, we have replaced $x_{i,j} = x(p_{i,j})$ (resp. $y_{i,j} = y(q_{i,j})$) by $x(p_{i,j}^{k,0}) = x(p_{i,j}) = x_{i,j}$ (resp. $y(q_{i,j}^{k,0}) = y(q_{i,j}) = y_{i,j}$): the fugacities are not changed. Therefore, it states that the original generating functions, defined in equation 22.2, with fugacities living in the base space Σ_0 is actually a multivalued function. It is monovalued only if one restrict the curve Σ to the so-called "physical sheet", which corresponds for the variable p – parameter of x – to the branch of Σ in the vicinity of ∞, and for the variable q – parameter of y – to the branch of Σ in the vicinity of 0. If p and q are in their respective physical sheets, let us denote:

$$X(y) = x(q)$$

and

$$Y(x) = y(p).$$

The generating function of the Ising model on planar maps having one mixed boundary with 1 change of color has been computed in [Eynard and Orantin, 2005], and is worth:

$$H^{(0)}_{1;0;0}(p,q) = \frac{E(x(p), y(q))}{(x(p) - x(q))(y(q) - y(p))} \tag{22.11}$$

An important property of this function is that it has only a pole at $p \to q$. If one considers a generic spectral curve, this equation stands as a definition for the invariant.

22.2 Recurrence relation

In order to make expressions more compact, we introduce the notations:

- $S_i = (p_{i,1}, q_{i,1}, p_{i,2}, q_{i,2}, \ldots, p_{i,k_i}, q_{i,k_i})$. It represents the variables associated to the i^{th} mixed boundary.

- $S_i(r) = (r, q_{i,1}, p_{i,2}, q_{i,2}, \ldots, p_{i,k_i}, q_{i,k_i})$: the first variable of the boundary is replaced by r.

Topological recursion [Eynard and Orantin, 2007] allows to compute the uniform invariants $\omega_{g,m}(p_1, \ldots, p_m) = H^{(g)}_{0;m;0}(p_1, \ldots, p_m)dx(p_1)\ldots dx(p_m)$, $\tilde{\omega}_{g,n}(q_1, \ldots, q_n) = H^{(g)}_{0;0;n}(q_1, \ldots, q_n)dy(q_1)\ldots dy(q_m)$, and $H^{(g)}_{0;m;n}(p_1, \ldots, p_m; q_1, \ldots, q_n)$. The generating function $H^{(0)}_{1;0,0}(p,q)$ is also known, by formula 22.11. Once those invariants are known, it remains therefore to compute the generating functions with mixed boundaries. A re-

cursion allowing to determine them was found to be (see [Eynard and Orantin, 2008]):

$$H^{(g)}_{\mathbf{k_L};m;n}(\mathbf{S_L};p_1,\dots,p_m;q_1,\dots,q_n) =$$
$$\operatorname*{Res}_{r\to p_{1,1},p_{i,\alpha},p_j,q^{0,j}_{1,k_1}} \frac{H^{(0)}_{1;0;0}(p_{1,1},q_{1,k_1})dx(r)}{(x(p_{1,1})-x(r))(y(q_{1,k_1})-y(r))H^{(0)}_{1;0;0}(r,q_{1,k_1})}\times$$
$$\Bigg[\sum_h \sum_{A\cup B=\{2,\dots,l\}} \sum_{\alpha=2}^{k_1}\sum_{I,J} H^{(h)}_{k_1-\alpha+1,\mathbf{k_B};m-|I|;n-|J|}(\{p_{1,\alpha},q_{1,\alpha},\dots,q_{1,k_1}\},\mathbf{S_B};\mathbf{p_{M/I}};\mathbf{q_{N/J}})$$
$$\times \frac{H^{(g-h)}_{\alpha-1,\mathbf{k_A};|I|;|J|}(\{r,q_{1,1},\dots,p_{1,\alpha-1},q_{1,\alpha-1}\},\mathbf{S_A};\mathbf{p_I};\mathbf{q_J})}{x(p_{1,\alpha})-x(r)}$$
$$+\sum_{\alpha=2}^{k_1}\frac{1}{x(p_{1,\alpha})-x(r)}\times$$
$$H^{(g-1)}_{\alpha-1,k_1-\alpha+1,\mathbf{k_{L/\{1\}}};m;n}(\{r,q_{1,1},\dots,p_{1,\alpha-1},q_{1,\alpha-1}\},\{p_{1,\alpha},q_{1,\alpha},\dots,q_{1,k_1}\},\mathbf{S_{L/\{1\}}};\mathbf{p_M};\mathbf{q_N})$$
$$+\sum_{i=2}^{l}\sum_{\alpha=1}^{k_i}\frac{1}{x(p_{i,\alpha})-x(r)}\times$$
$$H^{(g)}_{k_1+k_i,\mathbf{k_{L/\{1,i\}}};m;n}(\{S_1(r),p_{i,\alpha},q_{i,\alpha},p_{i,\alpha+1},\dots,q_{i,k_i},p_{i,1},\dots,q_{i,\alpha-1}\},\mathbf{S_{L/\{1,i\}}};\mathbf{p_M};\mathbf{q_N})+$$
$$\sum_h\sum_{A\cup B=\{2,\dots,l\}}\sum_{I,J} H^{(h)}_{k_1,\mathbf{k_A};|I|;|J|}(S_1(r),\mathbf{S_A};\mathbf{p_I};\mathbf{q_J})H^{(g-h)}_{\mathbf{k_B};m-|I|+1;n-|J|}(\mathbf{S_B};r,\mathbf{p_{M/\{I\}}};\mathbf{q_{N/\{J\}}})$$
$$+\sum_{h=1}^{g} H^{(h)}_{0;1;0}(r)H^{(g-h)}_{k_1,\dots,k_l;m;n}(S_1(r),S_2,\dots,S_l;p_1,\dots,p_m;q_1,\dots,q_n)$$
$$+H^{(g-1)}_{\mathbf{k_L};m+1;n}(\mathbf{S_K}(r);r,\mathbf{p_M};\mathbf{q_N})\Bigg] \tag{22.12}$$

It is a recurrence on $2g+L+n+m$. In the residue, the notation $q^{0,j}_{1,k_1}$, that has been introduced in the previous section, appears and j is non zero. This formula is valid to compute the Ising model generating functions (with a *rational* spectral curve). It is however possible to apply it with a *generic* spectral curve. In this case, the recurrence serves as a definition of the functions $H^{(g)}_{\mathbf{k_L};m;n}$, that are not necessarily generating functions of combinatorial objects such as maps. The order of the boundaries imports a priori. The spectral curve is present at several places in this formula:

- In order to know the location of $q^{0,j}_{1,k_1}$, one has to know the embedding of the spectral curve, namely the analytic functions $x(p)$, $y(q)$.
- In the right hand side, the function $H^{(0)}_{1;0;0}$ and potentially the 2-form $B(p,q)$ can appear. Both are directly linked to the spectral curve $\mathcal{S}$.

One can prove by induction on $2g+L+m+n$ the following:

Lemma 22.1. *$H^{(g)}_{\mathbf{k_L};m;n}$ has the following poles:*

$$\begin{cases} \text{in } p_{i,j} = q_{i',j'} \\ \text{in } p_i = q_{i',j'} \\ \text{in } p_{i,j} = q_{i'} \end{cases} \tag{22.13}$$

Differences with topological recursion: let us stress the differences between formula 22.12, and the formula of topological recursion 16.2 for $\omega_{g,n}$. First, a slight difference is that the invariants $H^{(g)}_{\mathbf{k_L};m;n}$ are functions and not differential forms. In order to get proper invariants one has to take into account the differential forms $dx(p)dy(q)$, that is to say, the invariants $h^{(g)}_{\mathbf{k_L};m;n}(\mathbf{S_L}; p_1, \dots, p_m; q_1, \dots, q_n)$ have rather this form:

$$\begin{aligned} h^{(g)}_{\mathbf{k_L};m;n}(\mathbf{S_L}; p_1, \dots, p_m; q_1, \dots, q_n) = \quad & H^{(g)}_{\mathbf{k_L};m;n}(\mathbf{S_L}; p_1, \dots, p_m; q_1, \dots, q_n) \times \\ & dx(p_{1,1}) \dots dx(p_{l,k_l}) dy(q_{1,1}) \dots dy(q_{l,k_l}) \\ & dx(p_1) \dots dx(p_m) dy(q_1) \dots dy(q_n). \end{aligned} \tag{22.14}$$

Second, although formula 22.12 is recursive on the topology $2-2g-L-n-m$ of the correlation functions, two features of topological recursion are missing:

- the residues are carried out on the variables p_i, and $q_{k_1}^{0,j}$, instead of the branch-points of the spectral curve. Also, the residues $q_{k_1}^{0,j}$ are very non local terms, as they are located in the non physical sheets of the spectral curve.

- The kernel of recursion is the following one:

$$\mathcal{K}(r,p,q) = \frac{H^{(0)}_{1;0;0}(p,q)}{H^{(0)}_{1;0;0}(r,q)(x(r)-x(p))(y(r)-y(q))} \tag{22.15}$$

  It is obviously different from the one of topological recursion defined in equation 16.1, as it involves the invariant $H^{(0)}_{1;0;0}$, and not the one-form ydx nor the two-form $B(p_1,p_2)$.

Remark 22.1. *The recursion for the generating functions $H^{(g)}_{\mathbf{k_L};m;n}$ solves the* loop equations *of those generating functions. Those loop equations are recursive relations "à la Tutte", and in the present case, they are determined from the 2-matrix model through Schwinger-Dyson equations. Schwinger-Dyson equations translate the fact that the expectation values of observables, that are formal integral over Hermitian matrices M_1 and M_2, are invariant under change of variable of M_1 and M_2.*

22.3 Symmetries of the generating functions

Looking at the combinatorial problem of counting weighted colored maps on a surface, some obvious symmetries arise. To be more precise, let us look at three types of transformations one can do.

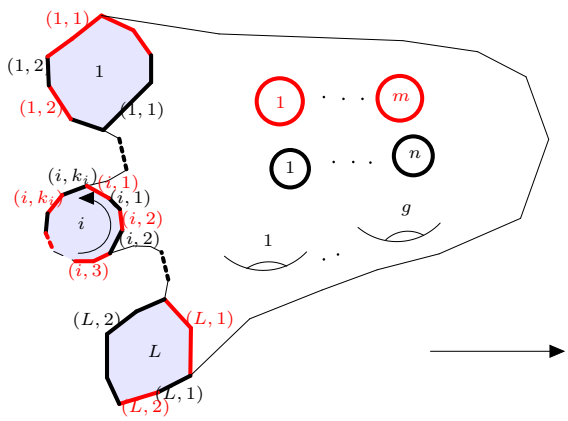

Figure 68: Boundary conditions before rotation

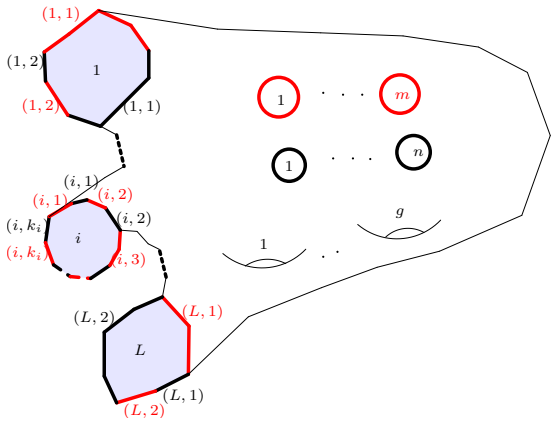

Figure 69: Boundary conditions after rotation

22.3.1 Rotation transformation

This transformation is illustrated in figures 68 and 69. It consists in rotating all the edges of a given boundary i, and leaving all the other boundaries unchanged. For a boundary i, let us note $\mathcal{R}_i$ the following rotation of the edges:

$$\begin{aligned} \mathcal{R}_i S_i &= \mathcal{R}_i(p_{i,1}, q_{i,1}, p_{i,2}, q_{i,2}, \ldots, p_{i,k_i}, q_{i,k_i}) && (22.16) \\ &= (p_{i,2}, q_{i,2}, p_{i,3}, q_{i,3}, \ldots, p_{i,k_i}, q_{i,k_i}, p_{i,1}, q_{i,1}) && (22.17) \end{aligned}$$

Any rotation of the edges of the i^{th} boundary is then a power of the operator $\mathcal{R}_i$. We extend the definition of this operator to the generating functions:

$$\mathcal{R}_i H^{(g)}_{\mathbf{k_L};m;n}(S_1, \ldots, S_L; m; n) = H^{(g)}_{\mathbf{k_L};m;n}(S_1, \ldots, \mathcal{R}_i S_i, \ldots, S_L; m; n). \tag{22.18}$$

22.3.2 Inversion transformation

The so-called inversion transformation represents, in this paper, the operation of changing the labelling of *all* the mixed boundaries from a clockwise ordering to a counter-clockwise ordering (see figures 70 and 71). Let us note $\mathcal{I}$ the operator corresponding to this transformation. Then, one has:

$$\forall i \in \{1, \ldots, L\} : \ \mathcal{I} S_i = (p_{i,1}, q_{i,k_i}, p_{i,k_i}, q_{i,k_{i-1}}, \ldots, p_{i,2}, q_{i,1}). \tag{22.19}$$

We define the action of $\mathcal{I}$ on the generating functions by:

$$\mathcal{I} H^{(g)}_{\mathbf{k_L};m;n}(S_1, \ldots, S_L; m; n) = H^{(g)}_{\mathbf{k_L};m;n}(\mathcal{I}S_1, \ldots, \mathcal{I}S_i, \ldots, \mathcal{I}S_L; m; n). \tag{22.20}$$

This is equivalent to consider the surface from the inside rather than from the outside.

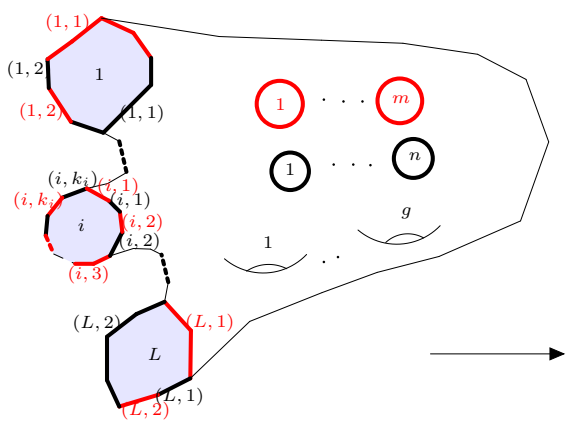

Figure 70: Boundary conditions before inversion

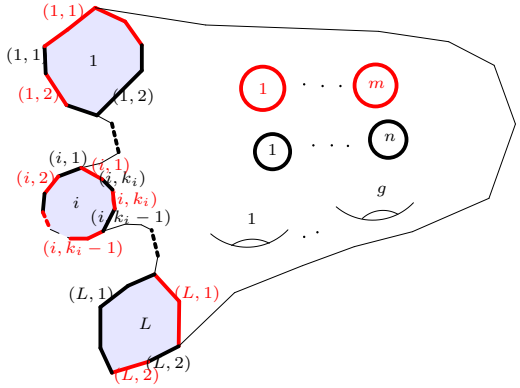

Figure 71: Boundary conditions after inversion: all the mixed boundaries have changed.

22.3.3 Symmetry under the exchange of boundaries

The symmetry exposed in the introductory section on symmetries of the formula of topological recursion concerns the permutation boundaries. In the same way for the invariants $H^{(g)}_{\mathbf{k_L};m;n}(S_1,\dots,S_L;m;n)$, one can ask if it is unchanged under $(S_1,\dots,S_L)\to(S_{\sigma(1)},\dots,S_{\sigma(L)})$ for any permutation $\sigma\in\mathfrak{S}_L$. Indeed, we mentioned that the order of the mixed boundaries $S_1,\dots,S_L$ imports a priori in the definition of the invariants through the recursion formula 22.12. However, from the point of view of the enumeration of colored maps, the symmetry is obvious, as it amounts to deform the underlying surface on which the random map is drawn, in order to exchange the boundaries. This operation does not change the structure of the graphs, so the counting is unchanged too. Hence, this symmetry shall be studied for generic spectral curves.

The group of permutations $\mathfrak{S}_L$ is generated by the transpositions $(1,i)$, $i=2,\dots,L$, so it is enough to study the transformations:

$$\mathcal{T}_i(S_1,S_2\dots,S_{i-1},S_i,S_{i+1},\dots,S_L)=(S_i,S_2,\dots,S_{i-1},S_1,S_{i+1},\dots,S_L), \tag{22.21}$$

whose action on the generating functions are:

$$\mathcal{T}_i H^{(g)}_{\mathbf{k_L};m;n}(S_1,\dots,S_L;m;n)=H^{(g)}_{\mathbf{k_L};m;n}(\mathcal{T}_i(S_1,\dots,S_L);m;n). \tag{22.22}$$

This transformation is pictured in figures 72 and 73.

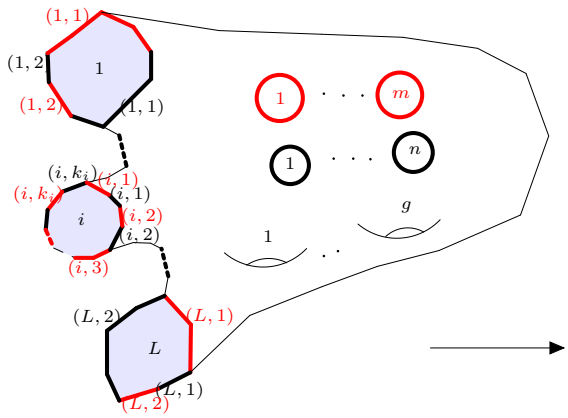

Figure 72: Boundary conditions before the exchange of boundaries

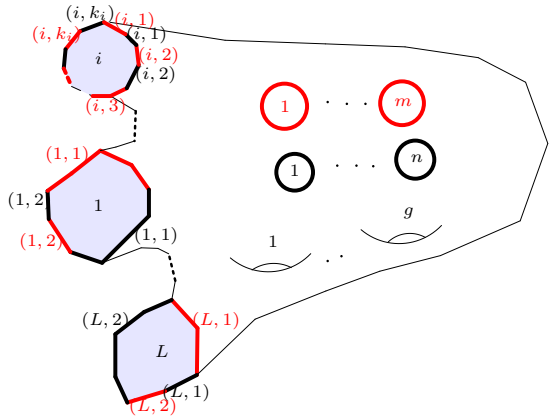

Figure 73: Boundary conditions after the exchange of mixed boundaries 1 and i.

23 Problematics and results

23.1 Generic spectral curve: problematics

The goal is to prove the invariance of the generating functions defined by the recurrence relation 22.12 under the rotation and the inversion transformations:

$$\mathcal{R}_i H^{(g)}_{\mathbf{k_L};m;n} = H^{(g)}_{\mathbf{k_L};m;n} \quad \forall i \in \{1,\dots,L\} \tag{23.1}$$

$$\mathcal{I} H^{(g)}_{\mathbf{k_L};m;n} = H^{(g)}_{\mathbf{k_L};m;n}. \tag{23.2}$$

Remark 23.1. *These invariances are trivially satisfied for the combinatorial problem of counting colored maps with given boundary conditions exposed in the previous section. In the generic case (i.e. for a generic spectral curve), the generating functions are only defined through the recurrence relation 22.12. The symmetries are then not obvious, as, for example, the parameter $p_{1,1}$ plays a special role regarding to the other p variables in the recursion.*

23.2 Notations

We shall use short hand notations for $H^{(0)}_{1;0;0}$:

$$H_{i,j} = H^{(0)}_{1;0;0}(p_{1,i}, q_{1,j}). \tag{23.3}$$

Also:

$$\begin{aligned} x_{ij} &= x(p_{1,i}) - x(p_{1,j}) \\ y_{ij} &= y(q_{1,i}) - y(q_{1,j}) \\ x_{rj} &= x(r) - x(p_{1,j}) \\ y_{rj} &= y(r) - y(q_{1,j}) \end{aligned}$$

$$H^{(0)}_{k;0;0}(p_{1,1}, q_{1,1}, \dots, p_{1,k}, q_{1,k}) = H^0_k(p_1, q_1, \dots, p_k, q_k)$$

Computing the generating function H^0_k by the recurrence formula 22.12, one sees that it contains terms proportional to H_{1j}:

$$H^0_k(p_1, q_1, \dots, p_k, q_k) = H_{1,j} a(\{p_i, q_i\}) + \text{terms not proportional to } H_{1,j},$$

so, in order to extract the content in $H_{1,j}$ from H^0_k, and with the previous equation notation, we define:

$$H^0_{k[j]}(\{p_i, q_i\}) = a(\{p_i, q_i\}).$$

Example 23.1. *In [Eynard and Orantin, 2008], the following generating function was explicitly computed:*

$$H^0_2(p_1, q_1, p_2, q_2) = \frac{H_{1,2}H_{2,1} - H_{1,1}H_{2,2}}{x_{1,2}y_{1,2}}. \tag{23.4}$$

We then have:

$$\begin{cases} H^0_{2[1]}(p_1, q_1, p_2, q_2) = -\frac{H_{2,2}}{x_{1,2}y_{1,2}} \\ H^0_{2[2]}(p_1, q_1, p_2, q_2) = \frac{H_{2,1}}{x_{1,2}y_{1,2}} \end{cases} \tag{23.5}$$

Another short hand notation is:

$$h(q) := \operatorname*{Res}_{p \to q} H(p, q)\, dx(p). \tag{23.6}$$

23.3 Known result for Ising model

In [Eynard and Orantin, 2005], the authors proved that the generating functions of planar random maps coupled to the Ising model with one mixed boundary could be written as a sum over planar link patterns. We will prove this decomposition in theorem 23.2 for generic spectral curves, so it is useful to recall the results obtained by Eynard and Orantin, in order to introduce the notations. The presentation of this section is adapted from section 4 of [Eynard and Orantin, 2005].

Let us consider one mixed boundary with k changes of colors. The fugacities are $x_1, y_1, \dots, x_k, y_k$, clockwisely. One can draw them as points located on a circle (see figure 74).

A first ingredient we need is the notion of planar permutations $\overline{\mathfrak{S}}_k$ of length k, which is a subset of the permutations $\mathfrak{S}_k$. The cycle $(1, 2, \dots, k)$ is denoted S.

A permutation $\sigma \in \mathfrak{S}_k$ is called planar if when one draws a straight line (that we call a link) between each pair $(x_j, y_{\sigma(j)})$, the lines don't intersect. The pattern formed by the lines associated with a planar permutation σ is called the link pattern of σ. The flipbook in bottom right hand side corner of this chapter shows a planar permutation

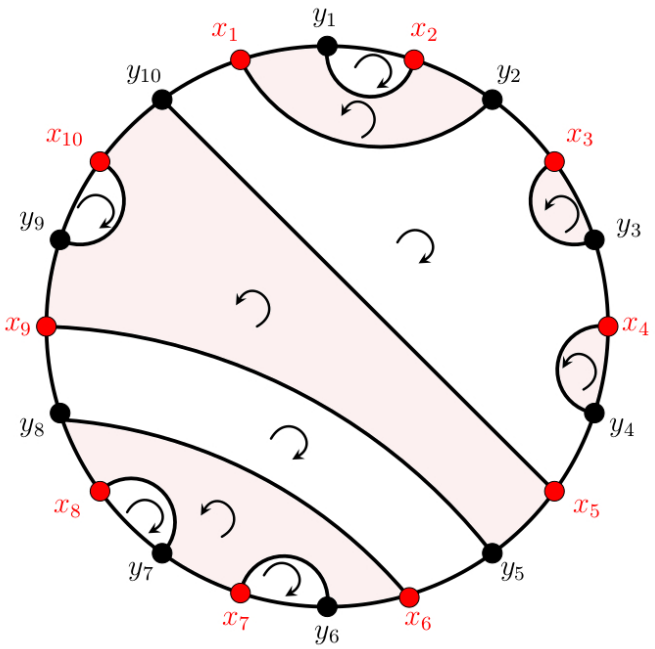

Figure 74: Link pattern on a boundary with 10 changes of colors. The arrows symbolize the orientations of the faces in which they sit.

of $\overline{\mathfrak{S}}_3$ (the lines are not straight for visibility). The $k+1$ faces of the link pattern are the cycles of σ and $S\sigma$.
Equivalently, $\sigma \in \mathfrak{S}_k$ is planar if

$$n_{cycles}(\sigma) + n_{cycles}(S\sigma) = k + 1,$$

where $n_{cycles}(\sigma)$ is the number of irreducible cycles composing the permutation σ.
We note $\overline{\mathfrak{S}}_k$ the set of planar permutation of rank k. The notation $\overline{\mathfrak{S}}_k(i_1, \ldots, i_k)$ is used when the permutation is on the set $\{i_1, \ldots, i_k\}$ instead of $\{1, \ldots, k\}$.
Last, the faces of the link pattern are given an orientation:

- if the face corresponds to a cycle of σ, the orientation is counterclockwise ;
- if the face is a cycle of $S\sigma$, the orientation is clockwise.

The order of a face is the number of links that belong to the face, which is also the length of the cycle.

Example 23.2. In figure 74, the planar permutation is $\sigma = (1,2)(5,10,9)(6,8,7)$, the cycle decomposition of σ and $S\sigma$ is

$$\begin{cases} \sigma = (1,2)(3)(4)(5,10,9)(6,8,7) \\ S\sigma = (1,3,4,5)(2)(10)(8)(7)(6,9). \end{cases} \tag{23.7}$$

The faces corresponding to cycles of σ are slightly colored (in red), and the faces of $S\sigma$ are simply white. The orientations are given by the arrows in the faces.

To each link pattern corresponding to a planar permutation σ, we associate a rational function $C_\sigma^{(k)}(x_1, y_1, \ldots, x_k, y_)$. This function is a product of rational functions $F^{(j)}$ over the faces of the link pattern. Therefore, the planar permutations σ are the underlying diagrams on which we sum, and the functions $F^{(j)}$, $C_\sigma^{(k)}$ depend on the structure of σ.
Let us consider a face of the link pattern. Let ℓ be its order, and suppose that, following its orientation, the fugacities are $x_{i_1}, y_{j_1}, \ldots, x_{i_\ell}, y_{j_\ell}$. Then to this face is associated the function $F^{(\ell)}(x_{i_1}, y_{j_1}, \ldots, x_{i_\ell}, y_{j_\ell})$, which is a rational function of the fugacities. The functions $F^{(\ell)}$ are defined recursively on ℓ:

Definition 23.1.

$$\begin{cases} F^{(1)}(x_1, y_1) = 1 \\ F^{(\ell)}(x_1, y_1, \ldots, x_\ell, y_\ell) = \sum_{j=1}^{\ell-1} \frac{F^{(j)}(x_1,\ldots,y_j)F^{(\ell-j)}(x_{j+1},\ldots,y_\ell)}{(x_\ell - x_1)(y_\ell - y_j)} \text{ for } \ell \geq 2. \end{cases} \tag{23.8}$$

For instance:

$$\begin{aligned} F^{(2)}(x_1, y_1, x_2, y_2) &= \frac{1}{(x_1 - x_2)(y_1 - y_2)} \\ F^{(3)}(x_1, y_1, x_2, y_2, x_3, y_3) &= \frac{1}{(x_3 - x_1)(y_3 - y_1)(x_2 - x_3)(y_2 - y_3)} - \\ &\quad \frac{1}{(x_3 - x_1)(y_2 - y_3)(x_1 - x_2)(y_1 - y_2)}. \end{aligned} \tag{23.9}$$

Now, for a link pattern, the product of all the faces functions gives the rational function $C_\sigma^{(k)}(x_1, y_1, \ldots, x_k, y_k)$. In more detail, the decomposition in cycle of σ and $S\sigma$ is:

$$\begin{cases} \sigma = \sigma_1 \sigma_2 \ldots \sigma_m \\ S\sigma = \tilde{\sigma}_1 \tilde{\sigma}_2 \ldots \tilde{\sigma}_n, \end{cases} \tag{23.10}$$

ℓ_j, $\tilde{\ell}_j$ are respectively the lengths of σ_j, $\tilde{\sigma}_j$. The cycles are:

$$\begin{aligned} \sigma_j &= (j_1, j_2, \ldots, j_{\ell_j}) \\ \tilde{\sigma}_j &= (\tilde{j}_1, \tilde{j}_2, \ldots, \tilde{j}_{\tilde{\ell}_j}). \end{aligned} \tag{23.11}$$

Therefore, following their orientations, the faces have these forms:

$$\begin{aligned} &(x_{j_1}, y_{j_2}, x_{j_2}, \ldots, x_{j_{\ell_j}}, y_{j_1}) \quad \text{for cycle } \sigma_j \\ &(x_{\tilde{j}_1}, y_{\tilde{j}_2 - 1}, x_{\tilde{j}_2}, \ldots, x_{\tilde{j}_{\tilde{\ell}_j}}, y_{\tilde{j}_1 - 1}) \quad \text{for cycle } \tilde{\sigma}_j. \end{aligned} \tag{23.12}$$

In the end, the function $C_\sigma^{(k)}$ is given by:

Definition 23.2.

$$C_\sigma^{(k)}(x_1, y_1, \dots, x_k, y_k) = \prod_{j=1}^{m} F^{(\ell_j)}(x_{j_1}, y_{j_2}, x_{j_2}, \dots, x_{j_{\ell_j}}, y_{j_1}) \times \prod_{j=1}^{n} F^{(\tilde{\ell}_j)}(x_{\tilde{j}_1}, y_{\tilde{j}_2 - 1}, x_{\tilde{j}_2}, \dots, x_{\tilde{j}_{\tilde{\ell}_j}}, y_{\tilde{j}_1 - 1}). \tag{23.13}$$

Once we have those functions, the theorem showed by Eynard and Orantin [Eynard and Orantin, 2005] is:

Theorem 23.1. *The generating functions of planar maps coupled to the Ising model with one mixed boundary having k changes of colors are given by the formula:*

$$H_{k;0;0}^{(0)}(x_1, y_1, \dots, x_k, y_k) = \sum_{\sigma \in \overline{\mathfrak{S}}_k} C_\sigma^{(k)}(x_1, y_1, \dots, x_k, y_k) \prod_{i=1}^{k} H_{i,\sigma(i)} \tag{23.14}$$

The proof of this result relies on the combinatorics of random maps, and independent of the recurrence relation 22.12, so it is not valid for generic spectral curves. Hereafter we give an example of application of this formula for planar maps with one mixed boundary of size 3.

Example 23.3. The set $\mathfrak{S}_3$ of planar permutations of size 3 has 5 elements. The generating function $H_{3;0;0}^{(0)}$ is therefore a sum of 5 terms, which we detail in the following table. The orientations of the faces having one link do not matter because their contribution is always 1, so they are not depicted for visibility.

Link pattern σ	$C_\sigma^{(3)}$	Contribution to $H_{3;0;0}^{(0)}$
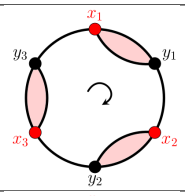	$F^{(3)}(x_1,y_1,x_2,y_2,x_3,y_3)$ $F^{(1)}(x_1,y_1)F^{(1)}(x_2,y_2)$ $F^{(1)}(x_3,y_3)$	$\frac{H_{1,1}H_{2,2}H_{3,3}}{x_{31}y_{23}}\left(\frac{1}{x_{23}y_{31}}-\frac{1}{x_{12}y_{12}}\right)$
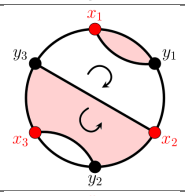	$F^{(2)}(x_1,y_1,x_2,y_3)$ $F^{(2)}(x_2,y_3,x_3,y_2)$ $F^{(1)}(x_1,y_1)F^{(1)}(x_2,y_3)$	$\frac{H_{1,1}H_{2,3}H_{3,2}}{x_{12}x_{23}y_{23}y_{31}}$
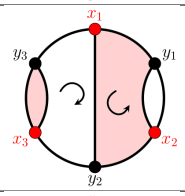	$F^{(2)}(x_1,y_2,x_2,y_1)$ $F^{(2)}(x_1,y_2,x_3,y_3)$ $F^{(1)}(x_2,y_1)F^{(1)}(x_3,y_3)$	$\frac{H_{1,2}H_{2,1}H_{3,3}}{x_{12}x_{31}y_{12}y_{23}}$
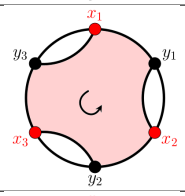	$F^{(3)}(x_1,y_3,x_3,y_2,x_2,y_1)$ $F^{(1)}(x_1,y_3)F^{(1)}(x_3,y_2)$ $F^{(1)}(x_2,y_1)$	$\frac{H_{1,3}H_{2,1}H_{3,2}}{x_{12}y_{12}}\left(\frac{1}{x_{23}y_{31}}-\frac{1}{x_{31}y_{23}}\right)$
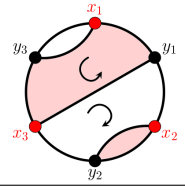	$F^{(2)}(x_1,y_3,x_3,y_1)$ $F^{(2)}(x_2,y_2,x_3,y_1)$ $F^{(1)}(x_1,y_3)F^{(1)}(x_2,y_2)$	$\frac{H_{1,3}H_{2,2}H_{3,1}}{x_{23}x_{31}y_{12}y_{31}}$

In the end, the generating function $H_{3;0;0}^{(0)}$ is the sum of the terms of the last column.

Besides this result, they showed the cyclic invariance of this formula:

Lemma 23.1. *The functions F, C and H are cyclically invariant. $\forall k \geq 0$, $\sigma \in \overline{\mathfrak{S}}_k$:*

$$\begin{aligned} F^{(k)}(x_1,y_1,\ldots,x_k,y_k) &= F^{(k)}(x_2,y_2,\ldots,x_k,y_k,x_1,y_1) \\ C_\sigma^{(k)}(x_1,y_1,\ldots,x_k,y_k) &= C_\sigma^{(k)}(x_2,y_2,\ldots,x_k,y_k,x_1,y_1) \\ H_{k,0,0}^{(0)}(x_1,y_1,\ldots,x_k,y_k) &= H_{k,0,0}^{(0)}(x_2,y_2,\ldots,x_k,y_k,x_1,y_1). \end{aligned} \tag{23.15}$$

23.4 Results

23.4.1 Preliminary result: rational functions of the faces

In [Eynard and Orantin, 2005], the rational functions $F^{(k)}$ were defined (see section 23.3).

Let us define, in the same manner, two other families of rational functions $F_a^{(k)}$ and $F_b^{(k)}$:

Definition 23.3. *The $F_a^{(k)}$'s:*

$$\begin{cases} F_a^{(1)}(x_1, y_1) = 1 \\ F_a^{(k)}(x_1, y_1, \ldots, x_k, y_k) = \sum_{j=1}^{k-1} \frac{F_a^{(j)}(x_1,\ldots,y_j) F_a^{(k-j)}(x_{j+1},\ldots,y_k)}{(x_{j+1}-x_1)(y_{j+1}-y_1)} \text{ for } k \geq 2 \end{cases} \tag{23.16}$$

The $F_b^{(k)}$'s:

$$\begin{cases} F_b^{(1)}(x_1, y_1) = 1 \\ F_b^{(k)}(x_1, y_1, \ldots, x_k, y_k) = \sum_{j=1}^{k-1} \frac{F_b^{(j)}(x_1,\ldots,y_j) F_b^{(k-j)}(x_{j+1},\ldots,y_k)}{(x_{j+1}-x_1)(y_k-y_1)} \text{ for } k \geq 2 \end{cases} \tag{23.17}$$

Then we have the following lemma:

Lemma 23.2. *For all $k \geq 1$, the functions $F^{(k)}$, $F_a^{(k)}$ and $F_b^{(k)}$ are equal. Moreover, their poles in x_1 are simple, located at x_j, $j = 2, \ldots, k$, and the residues are:*

$$\operatorname*{Res}_{x_1 \to x_j} F^{(k)}(x_1, \ldots, y_k) dx_1 = \frac{F^{(j-1)}(x_j, y_1 \ldots, x_{j-1}, y_{j-1}) F^{(k-j+1)}(x_j, \ldots, y_k)}{y_1 - y_j}. \tag{23.18}$$

This lemma entails the following one, that we use in section 25.2.4:

Lemma 23.3. *For $k \geq 2$ and $\sigma \in \overline{\mathfrak{S}}_k$, with the notations of [Eynard and Orantin, 2005], we have:*

$$C_\sigma^{(k)}(x_1, y_1, \ldots, x_k, y_k) = \sum_{i=j}^{k-1} \sum_{\rho \in \overline{\mathfrak{S}}_{k-i}} \sum_{\tau \in \overline{\mathfrak{S}}_i} \delta_{\sigma,\rho\tau} \frac{C_\rho^{(k-i)}(x_{i+1}, \ldots, y_k) C_\tau^{(i)}(x_1, \ldots, y_i)}{x_{1,i+1} y_{k,j}} \tag{23.19}$$

and

$$C_\sigma^{(k)}(x_1, \ldots, y_k) = -\sum_{i=j}^{k-1} \sum_{\rho \in \overline{\mathfrak{S}}_{k-i}} \sum_{\tau \in \overline{\mathfrak{S}}_i} \delta_{\sigma\circ(1,i+1),\rho\tau} \frac{C_\rho^{(k-i)}(x_{i+1}, \ldots, y_k) C_\tau^{(i)}(x_{i+1}, y_1, \ldots, y_i)}{x_{1,i+1} y_{k,j}} \tag{23.20}$$

23.4.2 Main theorem

We first focus on the case where there is only one mixed boundary (with $k \geq 2$ changes of colors on the boundary). Therefore, we want to compute $H_{k;0;0}^{(0)}(p_1, q_1, \ldots, p_k, q_k)$. The recurrence relation 22.12 yields only one sum –the first one– as the other ones individually vanish. Indeed:

- The second term vanishes because it requires $g \geq 1$.
- The third term vanishes because $l = 1$ (one boundary), so the sum has no term.
- The fourth term vanishes because $H_{0;1;0}^{(0)} = 0$.

- The fifth term vanishes because it requires $g \geq 1$.
- The last term vanishes because it requires $g \geq 1$.

So the recurrence 22.12 simplifies and we get:

$$H_k^0(p_1, q_1, \ldots, p_k, q_k) = \operatorname*{Res}_{r \to p_i, q_k^{0,j}} \frac{H_{1,k} dx(r)}{x_{r1} x_{ri} y_{kr} H_{r,k}} \sum_{\alpha=2}^{k} H_{k-\alpha+1}^0(p_\alpha, q_\alpha, \ldots, p_k, q_k) \times H_{\alpha-1}^0(r, q_1, \ldots, p_{\alpha-1}, q_{\alpha-1}). \tag{23.21}$$

The following theorem contains 4 parts. The first one allows to simplify the recurrence relation 23.21. The second and third one allows to compute explicitly H_k^0, and the last one to prove its symmetry.

Theorem 23.2. *For all $k \geq 1$, the following holds:*

- *The generating function H_k^0 belongs to the ring of polynomials $\mathbb{C}\left[\frac{1}{x_{i,j}}, \frac{1}{x_{i,j}}, H_{i,j}\right]\left[\frac{1}{y(p_l)-y(q_k)}, \frac{1}{H_{l,k}}\right]$, where $i, j = 1, \ldots, k$ and $l = 2, \ldots, k$. Moreover, it has degree at most 1 in $\frac{1}{y(p_l)-y(q_k)}$ and $\frac{1}{H_{l,k}}$, that is to say, there exist $[H_k^0]_{\text{Irr}}$, $a^{k,l}$, $b^{k,l}$, $c^{k,l,l'} \in \mathbb{C}\left[\frac{1}{x_{i,j}}, \frac{1}{x_{i,j}}, H_{i,j}\right]$ such that:*

$$H_k^0 = \left[H_k^0\right]_{\text{Irr}} + \sum_{j=2}^{k} \frac{a^{k,j}}{y(p_j) - y(q_k)} + \sum_{j=2}^{k} \frac{b^{k,j}}{H_{j,k}} + \sum_{j,j'=2}^{k} \frac{c^{k,j,j'}}{(y(p_j) - y(q_k)) H_{j',k}} \tag{23.22}$$

  We call $[H_k^0]_{\text{Irr}}$ the irreducible part of H_k^0.

- *With the notations of [Eynard and Orantin, 2005], the irreducible part of H_k^0 has the same form as in the Ising Model:*

$$\left[H_k^0\right]_{\text{Irr}}(p_i, q_i) = \sum_{\sigma \in \widetilde{\mathfrak{S}}_k} C_\sigma^{(k)}(x_1, y_1, \ldots, x_k, y_k) \prod_{j=1}^{k} H_{j,\sigma(j)} \tag{23.23}$$

- *For all $2 \leq j \leq k$, the functions $a^{k,j} + \sum_{j'=2}^{k} \frac{c^{k,j,j'}}{H_{j',k}}$ and $b^{k,j}$ vanish:*

$$a^{k,j} + \sum_{j'=2}^{k} \frac{c^{k,j,j'}}{H_{j',k}} = b^{k,j} = 0,$$

  so H_k^0 is equal to its so-called irreducible part.

- *The generating function H_k^0 is invariant under a rotation of its variables:*

$$H_k^0(p_1, q_1, \ldots, p_k, q_k) = H_k^0(p_2, q_2, \ldots, p_k, q_k, p_1, q_1). \tag{23.24}$$

The proof is given in section 25.2 below.

23.4.3 Removing one change of color and adding other boundaries

Removing one change of color This result defines an additional operator, effective at least for the case of one mixed boundary. Its effect is similar to the forgetful map of section 21.2: in one mixed boundary $S_1 = (p_1, q_1, \dots, p_{k_1}, q_{k_1})$, it erases one change of color, that is to say one pair of variable (p_i, q_i). This operator exists if there exists $q^* \in \Sigma$ such that it is a pole of y and x. For the spectral curves arising from the Ising model, two values of q match this condition: $q^* = 0$ and $q^* = \infty$.

Lemma 23.4. *The operator $\mathcal{O}_i$ defined as:*

$$\mathcal{O}_i(f) = \operatorname*{Res}_{q_i \to q^*} \frac{x(q_i)}{h(q_i)} dy(q_i) \operatorname*{Res}_{p_i \to q_i} f dx(p_i). \tag{23.25}$$

erases the i^{th} pair (p_i, q_i) from the generating function $H^{(0)}_{k_1;0;0}(S_1)$:

$$\forall 1 \leq i \leq k_1, \qquad \mathcal{O}_i H^{(0)}_{k_1;0;0}(S_1) = H^{(0)}_{k_1-1;0;0}(p_1, q_1, \dots, p_{i-1}, q_{i-1}, p_{i+1}, q_{i+1}, \dots, p_{k_1}, q_{k_1}). \tag{23.26}$$

The operator $\mathcal{O}_i$ matches the requirements of section 21.2: it depends only on the spectral curve – through q^*, x, y and h –, and on the variables p_i, q_i to delete, not on the other variables p_j, q_j, $j \neq i$.

Insertion of uniform boundaries The first extension concerns planar maps with one mixed boundary and several uniform boundaries, *i.e.* generating functions of this type:

$$H^{(0)}_{k;m;n}(\{p_1, q_1, \dots, p_k, q_k\}; p'_1, \dots, p'_m; q'_1, \dots, q'_n).$$

As we shall show in the following, it can be obtained by *insertion* of m red boundaries and n black boundaries through the action of insertion operators. We begin with defining these operators.

Definition 23.4. *Let δ^r_z (δ^b_z) be the insertions operator of a uniform red (resp. black) boundary at position z, defined by:*

$$\begin{cases} \delta^r_z Y(x(z_1)) = H^{(0)}_{0;2;0}(z_1, z) \\ \delta^r_z H^{(0)}_{0;2;0}(z_1, z_2) = H^{(0)}_{0;3;0}(z_1, z_2, z) \end{cases} \tag{23.27}$$

(respectively:

$$\begin{cases} \delta^b_z X(y(z_1)) = H^{(0)}_{0;0;2}(z_1, z) \\ \delta^b_z H^{(0)}_{0;0;2}(z_1, z_2) = H^{(0)}_{0;0;3}(z_1, z_2, z)) \end{cases} \tag{23.28}$$

Moreover, we impose the following rule:

$$\delta^r_z \operatorname*{Res}_{r \to p} = \operatorname*{Res}_{r \to z^p} \delta^r_z,$$

respectively

$$\delta_z^b \operatorname*{Res}_{r\to p} = \operatorname*{Res}_{r\to z^p} \delta_z^b$$

This definition suffices to define recursively the action of the insertion operators on any generating function $H^{(g)}_{\mathbf{k_L};m;n}$ via the topological recursion. First, as δ_z^r is a derivation at fixed $x(z)$, one can deduce its action on $x(y(q))$:

$$\delta_z^r x(y(q)) = -H^{(0)}_{0;2;0}(q,z)\frac{dx}{dy}(q).$$

For more general generating functions, we show that:

Lemma 23.5.

$$\delta_z^r H^{(g)}_{\mathbf{k_L};m;n}(S_1,\dots,S_L;\{p_i\};\{q_j\}) = H^{(g)}_{\mathbf{k_L};m+1;n}(S_1,\dots,S_L;p_1,\dots,p_m,z;q_1,\dots,q_n) \tag{23.29}$$

This lemma allows to state the result of this section, which extends the result of the theorem 23.2:

Theorem 23.3. *The invariants $H^{(0)}_{k;m;n}$ of genus 0, with one mixed boundary, m uniform red boundaries and n uniform black boundaries, are symmetric under $\mathcal{R}_1$ and $\mathcal{I}$*

24 Consequences

We know that in the Ising model, the generating functions $H^{(g)}_{\mathbf{k_L};m;n}$ enumerate random maps of fixed genus with specified boundary conditions. We may distinguish two parts here: the boundaries, whose configurations are specified by the structure of the fugacities $S_1,\dots,S_L;x_1,\dots,x_m;y_1,\dots,y_n$; and the bulk part, which is the enumeration of the maps relying on the boundaries. The weight of a map depends on the configuration of the boundaries (through the fugacities of the boundary edges), and on the configuration of the bulk. However, it is tempting to treat the generating functions $H^{(g)}_{\mathbf{k_L};m;n}$ as observables depending only on the boundaries, and not on the bulk, as if they arose from an effective theory on the boundaries. They can be seen as amplitudes of a configurations of spin chains located on the boundaries (section 24.1 hereafter). Those spin chains have complex interactions, as they are coupled to the bulk. But knowing that their amplitudes satisfy a recurrence relation of the type of equation 22.12, and without computing them explicitly, are there constraints to impose to those amplitudes, which constraint and simplify their expression ? We shall see that there are indeed such constraints, which can determine some generating functions without

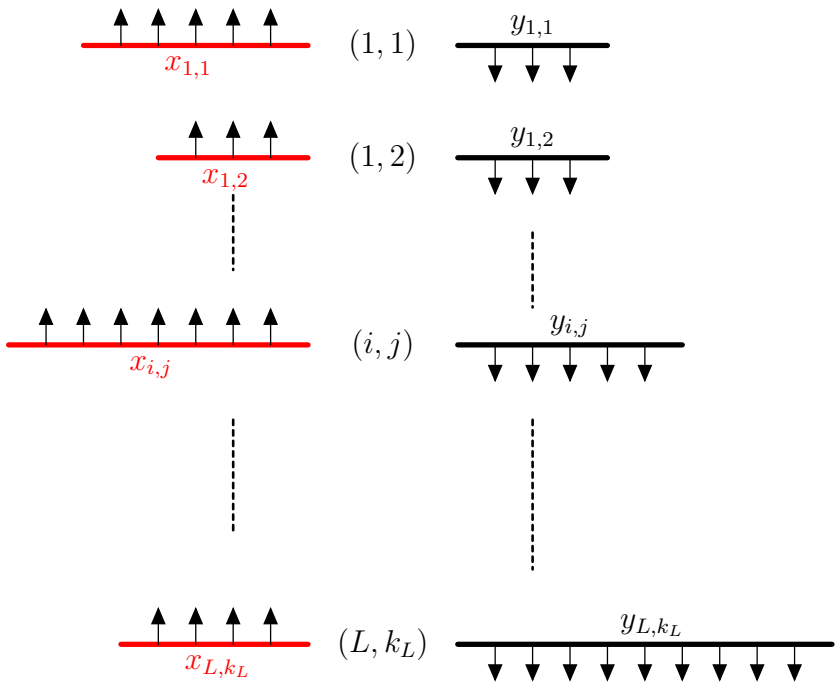

Figure 75: Variables assigned to chains of up spins (resp. of down spins). The red (resp. black) edges considered up to now are replaced by chains of up (resp. down) spins

resorting to the recursion 22.12.

This question, that we ask for generating functions stemming from the enumeration of random maps, can be extended to any generating function computed through formula 22.12 from a generic spectral curve. The same constraints still hold, but the proof relies on the symmetries of the generating functions. Therefore, theorem 23.2 allows to constraint the generating functions $H^{(0)}_{k;m;n}$.

24.1 Amplitudes of spin chains

Let us take k chains of consecutive up spins (resp. down spins), that we name $1, \dots, k$. To the chain i of up spins (resp. down spins) is associated the variable x_i (resp. y_i), see figure 75.

To a pair (π, π') of permutations of $\{1, \dots, k\}$ (there are $k!$ possible permutations on this set), one associates a set of circular spin chains:

- The right end of the i^{th} up spin chain is glued with the left end of the $\pi(i)^{\text{th}}$ down spin chain.
- The right end of the i'^{th} down spin chain is glued with the left end of the $\pi'^{-1}(i')^{\text{th}}$ up spin chain.

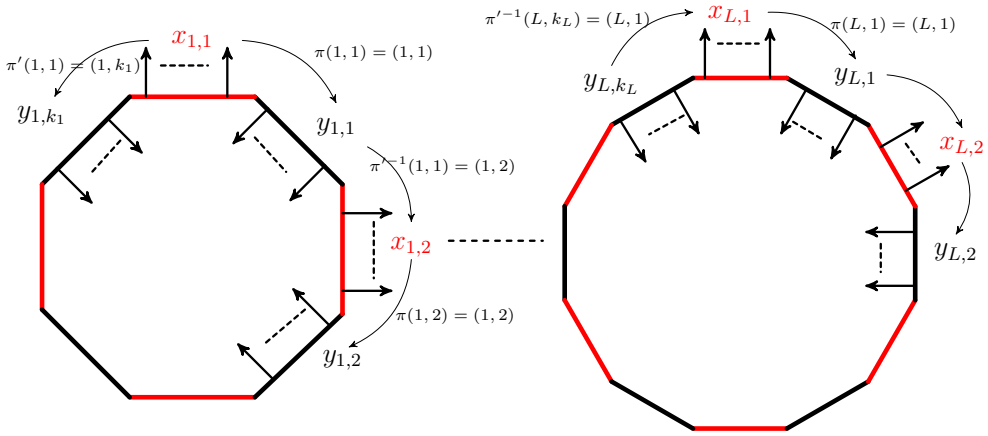

Figure 76: Set of circular spin chains made from the up spin chains $(1,1),\dots,(L,k_L)$, the down spin chains $(1,1),\dots,(L,k_L)$, and from the permutations (π,π') defined in equation 24.1.

The circular spin chains associated to (π,π') are the cycles of $\pi'^{-1}\circ\pi$.
In figure 76 is represented the set of circular spin chains corresponding to the permutations $\pi = \mathrm{Id}$ and π' on the set $\{(1,1),\dots,(1,k_1),(2,1),\dots,(2,k_2),\dots,(L,1),\dots,(L,k_L)\}$ defined by:

$$\begin{aligned} \pi &= \mathrm{Id} \\ \pi'((i,j)) &= \begin{cases} (i,k_i) \text{ if } j=1 \\ (i,j-1) \text{ else} \end{cases} \end{aligned} \tag{24.1}$$

If the permutation $\pi'^{-1}\circ\pi$ has L cycles of lengths $\{k_1,\dots,k_L\}$, with $i_1,\dots,i_L$ belonging to different cycles, one defines the following formal series in N:

$$\hat{H}_{\pi,\pi'} = \sum_{g=0}^{\infty} N^{2-2g-L} H^{(g)}_{\mathbf{k_L};0;0}\left(\{x_{i_1}, y_{\pi(i_1)},\dots,x_{(\pi'^{-1}\circ\pi)^{k_1-1}(i_1)}, y_{\pi((\pi'^{-1}\circ\pi)^{k_1-1})(i_1)}\},\dots, \{x_{i_L,\dots,y_{\pi((\pi'^{-1}\circ\pi)^{k_L-1})(i_L)}}\}\right).$$

The power of N is the Euler characteristic χ of a surface of genus g with L boundaries: $\chi = 2-2g-L$.
The coefficient of N^χ is the invariant defined previously for the Ising model on random maps. It counts *connected* maps of genus g. The following formal series allows to count, for a given coefficient, the connected and the *non-connected* invariants:

$$H_{\pi,\pi'}(x_1,\dots,x_k;y_1,\dots,y_k) = \exp\left(\hat{H}_{\pi,\pi'}(x_1,\dots,x_k;y_1,\dots,y_k)\right) \tag{24.2}$$

If $\pi'^{-1}\circ\pi$ has L cycles, the coefficient of N^χ is called the *amplitude* of genus $g = 1-\frac{\chi+L}{2}$ of the permutations (π,π'). It is a function of $(x_1,\dots,x_k)$, $(y_1,\dots,y_k)$, and is denoted

by $H^{(g)}_{\pi,\pi'}(x_1,\dots,x_k;y_1,\dots,y_k)$.
Last, we define the *matrix of amplitudes*:

$$H(x_1,\dots,x_k;y_1,\dots,y_k) = \{H_{\pi,\pi'}(x_1,\dots,x_k;y_1,\dots,y_k)\}_{\pi,\pi'\in\mathfrak{S}_k}. \tag{24.3}$$

We note it also $H_{\pi,\pi'}(\vec{x},\vec{y})$.

24.2 Constraints on the amplitudes

The constraints associated to the matrix of amplitudes are commutation relations with the matrix $\mathcal{M}$, defined as:

$$\begin{aligned}\mathcal{M}_{\pi,\pi'}(x_1,\dots,x_k;y_1,\dots,y_k;\xi,\eta) &= \prod_{i=1}^{k}\left(\delta_{\pi(i),\pi'(i)} - \frac{1}{Nc}\frac{1}{(x_i-\xi)(y_{\pi(i)}-\eta)}\right)\\ &= \mathcal{M}_{\pi,\pi'}(\vec{x};\vec{y};\xi,\eta).\end{aligned} \tag{24.4}$$

The parameters ξ and η are called the spectral parameters, for a reason given in next subsection on the matrix model. The parameter N is the size of the matrices when one considers the generating functions as expectation values of a matrix model. This parameter is the the same as the one used for the matrix of amplitudes, all the object defined here are viewed as formal series in N, including $\mathcal{M}$ which is a finite sum in powers of N.

Remark 24.1. *In equation 24.4, $\delta_{\pi(i),\pi'(i)} = 1$ if the circular chain containing the chain i has only two pieces: the chain i of up spins, and the chain $\pi(i)$ of down spins. One sees in this definition that the invariants H_{ij} play a special role, and that they can be considered as fundamental block for the construction of invariants.*

Then, under certain assumptions – developed in this section –, the following holds:

$$\forall\xi,\,\eta\ ,\ \ [H(x_1,\dots,x_k;y_1,\dots,y_k),\mathcal{M}(x_1,\dots,x_k;y_1,\dots,y_k;\xi,\eta)] = 0. \tag{24.5}$$

This commutation relation has to be understood as valid for every coefficient in the power series in N, for $[H,\mathcal{M}] \in \mathbb{C}[[N^{-1}]]$ is a formal series.
The equation 24.5 involves that the matrices H and $\mathcal{M}$ have the same eigenvectors. In order to determine entirely the matrix H, *i.e.* the amplitudes, one has to compute the eigenvectors of $\mathcal{M}$, and the eigenvalues of H (that can be expressed in terms of H_{ij}). The eigenvectors of the matrix $\mathcal{M}$ are amplitudes of a circular spin chains. Therefore, the knowledge of the invariants $H^{(g)}_{\mathbf{k_L};0;0}$ (that are sum over all maps having certain boundary conditions) is (indirectly) determined by a statistical physics model located on the boundaries. It is thus a sort of *AdS/CFT* correspondence for this class of

problems: the amplitudes of quantities depending on the bulk and on the boundaries of a surface are computable, by a duality principle, from a physical model on the boundaries.

Equation 24.5 imposes constraints on the amplitudes $H^{(g)}_{\pi,\pi'}$. For instance, we will show that it allows to determine recursively (on the size of the boundary) the amplitude $H^0_{k;0;0}$. Hereafter, we describe when relation 24.5 holds, for the case of matrix models and for the case of generating functions $H^{(g)}_{\mathbf{k_L};0;0}$ derived from the recursion relation 22.12.

24.2.1 Commutation in the matrix model

In the case where the matrix of amplitudes stems from the matrix model described above, the commutation of the matrix of amplitudes H and the matrix $\mathcal{M}$ is true for any power of N. The derivation of this result comes from a lemma of Eynard and Prats Ferrer [Eynard and Prats Ferrer, 2006]. Let us describe how one gets to the commutation of the matrices.

First, by the method introduced in section 5, we transform the partition function of the formal matrix model into a formal integral over the radial parts and the angular parts of M_1 and M_2. Namely, there exists $U \in U(N)$ (corresponding to the angular part), and $X = \mathrm{diag}(\xi_1, \ldots, \xi_N)$, $Y = \mathrm{diag}(\eta_1, \ldots, \eta_N)$ (the radial parts) such that:

$$\mathrm{Tr}\,(M_1^k M_2^\ell) = \mathrm{Tr}\,(X^k U Y^\ell U^\dagger). \tag{24.6}$$

It entails for the mixed boundaries:

$$\mathrm{Tr}\left(\prod_{i=1}^{k} \frac{1}{x_i - M_1}\frac{1}{y_i - M_2}\right) = \mathrm{Tr}\left(\prod_{i=1}^{k} \frac{1}{x_i - X} U \frac{1}{y_i - Y} U^\dagger\right). \tag{24.7}$$

This angular/radial decomposition allows to rewrite the expectation values of functions $\mathcal{O}$ implying traces of matrices M_1, M_2:

$$\begin{aligned}\langle \mathcal{O}(M_1, M_2)\rangle &\overset{\text{formal}}{=} \frac{1}{\mathcal{Z}} \int_{H_N \times H_N} dM_1 dM_2 \mathcal{O}(M_1, M_2) e^{-N\,\mathrm{Tr}\,(V_1(M_1)+V_2(M_2)-cM_1M_2)} \\ &\overset{\text{formal}}{=} \frac{1}{\mathcal{Z}} \int_{\mathbb{R}^N \times \mathbb{R}^N} dX\, dY \Delta(X)\Delta(Y) e^{-N\,\mathrm{Tr}\,(V_1(X)+V_2(Y))} \\ &\int_{U(N)} \mathcal{D}U e^{cNXUYU^\dagger} \mathcal{O}(X, UYU^\dagger).\end{aligned} \tag{24.8}$$

The measure over $U(N)$ is the Haar measure, and $\Delta(X) = \prod_{i<j}(\xi_i - \xi_j)$, $\Delta(Y) = \prod_{i<j}(\eta_i - \eta_j)$. In the case of random maps with fugacities $(x_1, \ldots, x_k); (y_1, \ldots, y_k) = \vec{x}; \vec{y}$, we associate an expectation value to a pair of permutations $\pi, \pi' \in \mathfrak{S}_k$. This expectation value is a formal series in N, and enumerates bi-colored random maps having

the Boltzmann weight described in the beginning of the chapter, whose boundaries are the cycles of $\pi'^{-1} \circ \pi$. For $m = 1, \ldots, n_{cycles}(\pi'^{-1} \circ \pi)$, let us note ℓ_m the length of the m^{th} cycle (which is the number of changes of colors of the m^{th} boundary). The function associated to the fugacities $\vec{x}, \vec{y}$ and the permutations π, π' is then:

$$\mathcal{O}_{\pi,\pi'}(M_1, M_2; \vec{x}, \vec{y}) = \prod_{m=1}^{n_{cycles}(\pi'^{-1}\circ\pi)} \left(\delta_{1,\ell_m} + \text{Tr} \prod_{i=1}^{\ell_m} \frac{1}{x_{m_i} - M_1} \frac{1}{y_{\pi(m_i)} - M_2} \right). \quad (24.9)$$

The expectation value associated is precisely the amplitude:

$$H_{\pi,\pi'}(\vec{x}; \vec{y}) = \langle \mathcal{O}_{\pi,\pi'}(M_1, M_2; \vec{x}, \vec{y}) \rangle \quad (24.10)$$

Therefore, using the previous angular/radial decomposition, we can write:

$$\begin{aligned} H_{\pi,\pi'}(\vec{x}; \vec{y}) &= \int_{\mathbb{R}^N \times \mathbb{R}^N} dX dY \Delta(X)\Delta(Y) e^{-N \,\text{Tr}\,(V_1(X)+V_2(Y))} \\ &\int_{U(N)} dU e^{cNXUYU^\dagger} \mathcal{O}_{\pi,\pi'}(X, UYU^\dagger; \vec{x}, \vec{y}). \end{aligned} \quad (24.11)$$

The angular integral can be carried out using a result of Eynard and Prats Ferrer [Eynard and Prats Ferrer, 2006]:

$$\int_{U(N)} dU e^{cNXUYU^\dagger} \mathcal{O}_{\pi,\pi'}(X, UYU^\dagger; \vec{x}, \vec{y}) = \sum_{\sigma \in \mathfrak{S}_N} (-1)^{\epsilon(\sigma)} \left(\prod_{i=1}^{N} \mathcal{M}(\vec{x}; \vec{y}; \xi_i, \eta_{\sigma(i)}) \right)_{\pi,\pi'}, \quad (24.12)$$

$\epsilon(\sigma)$ being the signature of the permutation. One has to be careful in the previous formula, as the permutations π, π' belong to $\mathfrak{S}_k$, k being the length of the vectors $\vec{x}, \vec{y}$, whereas σ belongs to $\mathfrak{S}_N$, where N is the size of the matrices X and Y. Now, a property in [Eynard and Prats Ferrer, 2006] states that the matrices $\mathcal{M}$ with different spectral parameters commute:

$$\forall \xi, \eta, \zeta, \chi \,, \qquad [\mathcal{M}(\vec{x}; \vec{y}; \xi, \eta), \mathcal{M}(\vec{x}; \vec{y}; \zeta, \chi)] = 0, \quad (24.13)$$

and that they are symmetric: $\mathcal{M} = \mathcal{M}^t$. It is therefore possible to diagonalize simultaneously those matrices in the angular integration 24.12, that is to say there exists a matrix V of size $k! \times k!$ independent of the spectral parameters, such that:

$$\mathcal{M}_{\pi,\pi'}(\vec{x}; \vec{y}; \xi, \eta) = \sum_{\rho \in \mathfrak{S}_k} V_{\pi,\rho}(\vec{x}, \vec{y}) \Lambda_\rho(\vec{x}, \vec{y}; \xi, \eta) V_{\pi',\rho}(\vec{x}, \vec{y}) \quad (24.14)$$

where Λ is a vector of size $k!$. The angular integration 24.12 simplifies into:

$$\sum_{\rho \in \mathfrak{S}_k} V_{\pi,\rho}(\vec{x}, \vec{y}) \det_{1 \le i,j \le N} (\Lambda_\rho(\vec{x}, \vec{y}; \xi_i, \eta_j)) V_{\pi',\rho}(\vec{x}, \vec{y}). \quad (24.15)$$

In the end, the amplitude is simply given by the radial integration:

$$H_{\pi,\pi'}(\vec{x};\vec{y}) = \begin{array}{c} \sum_{\rho\in\mathfrak{S}_k} V_{\pi,\rho}(\vec{x},\vec{y})V_{\pi',\rho}(\vec{x},\vec{y}) \\ \int_{\mathbb{R}^N\times\mathbb{R}^N} dXdY\Delta(X)\Delta(Y)e^{-N\,\mathrm{Tr}\,(V_1(x)+V_2(Y))}\det_{1\leq i,j\leq N}(\Lambda_\rho(\vec{x},\vec{y};\xi_i,\eta_j)) \end{array} \tag{24.16}$$

Two elements are important in the last formula. First, the matrix element $V_{\pi,\rho}$ are independent of the radial integration, as they do not depend on the spectral parameters. Second, the radial integration depends only on the permutation ρ. We can conclude that the matrix of amplitudes H is diagonalizable in the same basis as the matrices $\mathcal{M}$, so they commute. This shows that:

$$\forall\xi,\eta,\ \forall\vec{x},\vec{y},\qquad [H(\vec{x};\vec{y}),\mathcal{M}(\vec{x},\vec{y},\xi,\eta)]=0. \tag{24.17}$$

This demonstration, given by Eynard and Prats Ferres, uses extensively matrix integrals methods, but does not explicitly require the symmetries of the generating functions.

24.2.2 Commutation for generic spectral curves

If the invariants $H^{(g)}_{\mathbf{k_L};0;0}$, that satisfy by construction the recursive relation 22.12, are symmetric under the rotations $\mathcal{R}_i$ and the inversion $\mathcal{I}$, then the matrix of amplitudes commute with the matrix $\mathcal{M}$ (see [Eynard, 2016]):

$$\forall\xi,\ \eta\ ,\ \ [H(x_1,\dots,x_k;y_1,\dots,y_k),\mathcal{M}(x_1,\dots,x_k;y_1,\dots,y_k;\xi,\eta)]=0, \tag{24.18}$$

In this chapter, we have proven that the invariants $H^{(0)}_{k;0;0}$ (for which the Euler characteristic is $\chi = 1$) satisfy the symmetries. It allows to obtain the following commutation relation:

$$\forall\xi,\ \eta\ ,\ \ [H(x_1,\dots,x_k;y_1,\dots,y_k),\mathcal{M}(x_1,\dots,x_k;y_1,\dots,y_k;\xi,\eta)]^{(0)}=0, \tag{24.19}$$

where by $[]^{(0)}$, we mean the coefficient of N^0 in the formal series $[H(x_1,\dots,x_k;y_1,\dots,y_k),\mathcal{M}(x_1,\dots,x_k;y_1,\dots,y_k;\xi,\eta)]$ in N.

Example 24.1. *Let us look at the case $k=2$. There are 2 permutations:* Id *and* $(1,2)$. *The leading order coefficients in N of the matrix $H(x_1,x_2;y_1,y_2)$ are:*

π \ π'	Id	$(1,2)$
Id	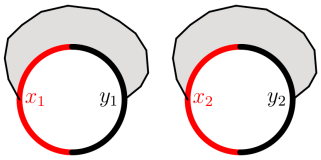 (N^2)	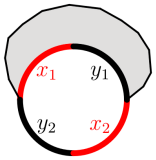 (N)
$(1,2)$	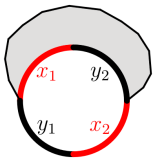 (N)	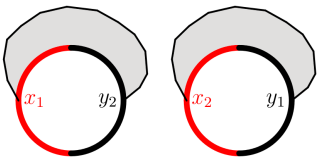 (N^2)

where, in the parenthesis is given the power of N corresponding to such amplitudes. The matrix $\mathcal{M}$ is given by:

π \ π'	Id	$(1,2)$
Id	$\left(1-\frac{1}{Nc}\frac{1}{(x_1-\xi)(y_1-\eta)}\right)\times\left(1-\frac{1}{Nc}\frac{1}{(x_2-\xi)(y_2-\eta)}\right)$	$\frac{1}{N^2c^2}\frac{1}{(x_1-\xi)(y_1-\eta)(x_2-\xi)(y_2-\eta)}$
$(1,2)$	$\frac{1}{N^2c^2}\frac{1}{(x_1-\xi)(y_1-\eta)(x_2-\xi)(y_2-\eta)}$	$\left(1-\frac{1}{Nc}\frac{1}{(x_1-\xi)(y_2-\eta)}\right)\times\left(1-\frac{1}{Nc}\frac{1}{(x_2-\xi)(y_1-\eta)}\right)$

In $[H(x_1,x_2;y_1,y_2),\mathcal{M}]=0$, the coefficient of N^0 yields the equation:

$$H^{(0)}_{2;0;0}(x_1,y_1,x_2,y_2)=\frac{H^{(0)}_{1;0;0}(x_1,y_2)H^{(0)}_{1;0;0}(x_2,y_1)-H^{(0)}_{1;0;0}(x_1,y_1)H^{(0)}_{1;0;0}(x_2,y_2)}{(x_1-x_2)(y_1-y_2)}. \quad (24.20)$$

Therefore the commutation relation 24.5 is constraining enough to determine entirely the generating function $H^{(0)}_{2;0;0}$

Actually, the commutation of the matrix of amplitudes and the matrix $\mathcal{M}$ allows to determine recursively the generating functions of planar one mixed boundaries amplitudes $H^{(0)}_{k;0;0}$. Indeed, we have the result:

Lemma 24.1. *Let $k\geq 2$, and assume $H^{(0)}_{k';0;0}$ is known $\forall k'<k$. Then $H^{(0)}_{k;0;0}$ is determined by the equation:*

$$[N^0][\mathcal{M}(\vec{x};\vec{y};0,0),H(\vec{x},\vec{y})]_{\mathrm{Id},S_k}=0, \quad (24.21)$$

where S_k is the cycle $(1,k,k-1,\dots,2)$ and $[N^0]$ means that we take the coefficient of N^0 of the formal series $[\mathcal{M},H]\in\mathbb{C}[[N^{-1}]]$.

Proof. We show that equation 24.21 allows to compute $H^{(0)}_{k;0;0}(x_1,y_1,\dots,x_k,y_k)=[N]H_{\mathrm{Id},S_k}$. This means that we have to show that, at the order N^0:

- Only the genus 0 parts of the $H_{\pi,\pi'}$ is present.

- The leading order in N of the commutator is N^0, and it involves $H^{(0)}_{\mathrm{Id},S_k}$.
- besides H_{Id,S_k}, there is no other $H_{\pi,\pi'}$ with $\pi'^{-1}\circ\pi$ being a cycle of length k. This means that the only amplitude with one boundary of length k is H_{Id,S_k}.

Point 1: writing the coefficient Id, S_k of the commutation relation gives:

$$\sum_{\pi\in\mathfrak{S}_k} \mathcal{M}_{\mathrm{Id},\pi} H_{\pi,S_k} - H_{\mathrm{Id},\pi}\mathcal{M}_{\pi,S_k}. \tag{24.22}$$

$\mathcal{M}_{\pi,\pi'}$ is a polynomial in N^{-1}. The leading order when $N\to\infty$ is at most N^0. The term $H_{\pi,\pi'}$ represents a sum over the genus of amplitudes with at least one boundary. The characteristic of amplitudes with genus $g\geq 1$ is therefore less or equal to $1-2g\leq -1$. This means that amplitudes with genus $g\geq 1$ contribute in the commutator at most in the coefficient of N^{-1}. Hence, in equation 24.21, only planar amplitudes are involved.
Point 2: The contribution to order N^1 of the commutator is worth:

$$H^{(0)}_{\mathrm{Id},S_k}\left([N^0]\mathcal{M}_{\mathrm{Id},\mathrm{Id}} - [N^0]\mathcal{M}_{S_k,S_k}\right) = H^{(0)}_{\mathrm{Id},S_k}(1-1) = 0, \tag{24.23}$$

so the commutator has leading order N^0. At this order, H_{Id,S_k} contributes in this way:

$$\begin{aligned} H^{(0)}_{\mathrm{Id},S_k}[N^{-1}]\left(\mathcal{M}_{\mathrm{Id},\mathrm{Id}}(\vec{x};\vec{y};0,0) - \mathcal{M}_{S_k,S_k}(\vec{x};\vec{y};0,0)\right) &= H^{(0)}_{\mathrm{Id},S_k}\sum_{i=1}^{k}\left(\frac{1}{x_i y_{S_k(i)}} - \frac{1}{x_i y_i}\right) \\ &\neq 0. \end{aligned} \tag{24.24}$$

The contribution of $H^{(0)}_{\mathrm{Id},S_k}$ is not null at the order N^0.
Point 3: take $\pi\neq\mathrm{Id}$ such that $S_k^{-1}\circ\pi$ is a cycle of length k. As $\pi\neq\mathrm{Id}$, there exists at least two integers i,j such that $\pi(i)\neq i$, $\pi(j)\neq j$. Therefore the leading order in N of $\mathcal{M}_{\mathrm{Id},\pi}$ is less or equal to N^{-2}. Therefore, $H_{\pi,S_k}\mathcal{M}_{\mathrm{Id},\pi}$ contributes to the coefficients N^m with $m\leq -1$. With the same argument, the terms $H_{\mathrm{Id},\pi}\mathcal{M}_{\pi,S_k}$ with $\pi\neq S_k$ such that π is a cycle, contribute to the coefficients N^m with $m\leq -1$. In the end, the only amplitude with one boundary of length k appearing at the order N^0 is H_{Id,S_k}.

□

Example 24.2. As an example, we show how to compute $H^{(0)}_{3;0;0}(x_1,y_1,x_2,y_2,x_3,y_3)$. It corresponds to the genus 0 part of the amplitude $H_{Id,(132)}(x_1,x_2,x_3;y_1,y_2,y_3)$. In the matrix H, we keep only the leading order terms in N, which consist in products of planar amplitudes with one boundary. Then, we apply the commutation relation $[N^0][H(\vec{x};\vec{y}),\mathcal{M}(\vec{x};\vec{y};\xi,\eta)]_{\mathrm{Id},S_3}=0$. We specialize the spectral parameters $\xi=\eta=0$. The matrix H is shown in the 6×6 following table.

π \ π'	Id	$(1,2)$	$(1,3)$	$(2,3)$	$(1,2,3)$	$(1,3,2)$
Id	$H_{1,1}H_{2,2}$ $H_{3,3}$ N^3	$H_2^0(x_1,y_1,x_2,y_2)$ $H_{3,3}$ N^2	$H_2^0(x_1,y_1,x_3,y_3)H_{2,2}$ N^2	$H_2^0(x_2,y_2,x_3,y_3)H_{1,1}$ N^2	$H_3^0(x_1,y_1,x_3,y_3,x_2,y_2)$ N^1	$H_3^0(x_1,y_1,x_2,y_2,x_3,y_3)$ N^1
(12)	$*$	$H_{1,2}H_{2,1}H_{3,3}$ N^3	$H_3^0(x_1,y_2,x_2,y_1,x_3,y_3)$ N^1	$H_3^0(x_1,y_2,x_3,y_3,x_2,y_1)$ N^1	$H_2^0(x_2,y_1,x_3,y_3)H_{1,2}$ N^2	$H_2^0(x_1,y_2,x_3,y_3)H_{2,1}$ N^2
(13)	$*$	$*$	$H_{1,3}H_{2,2}H_{3,1}$ N^3	$H_3^0(x_1,y_3,x_2,y_2,x_3,y_1)$ N^1	$H_2^0(x_1,y_3,x_2,y_2)H_{3,1}$ N^2	$H_2^0(x_2,y_2,x_3,y_1)H_{1,3}$ N^2
(23)	$*$	$*$	$*$	$H_{1,1}H_{2,3}H_{3,2}$ N^3	$H_2^0(x_1,y_1,x_3,y_2)H_{2,3}$ N^2	$H_2^0(x_1,y_1,x_2,y_3)H_{3,2}$ N^2
(123)	$*$	$*$	$*$	$*$	$H_{1,2}H_{2,3}H_{3,1}$ N^3	$H_3^0(x_1,y_2,x_3,y_1,x_2,y_3)$ N^1
(132)	$*$	$*$	$*$	$*$	$*$	$H_{1,3}H_{2,1}H_{3,2}$ N^3

The stars $*$ mean that the corresponding coefficient is the same as the one of the symmetric (with respect to the diagonal) coefficient.

The matrix element $[N^0][H(\vec{x};\vec{y}),\mathcal{M}(\vec{x};\vec{y};0,0)]_{\mathrm{Id},(1,3,2)}$ yields the equation:

$$\begin{aligned}
&\frac{H_{1,3}H_{2,1}H_{3,2}}{x_1x_2x_3y_1y_2y_3} - \frac{(H_{1,3}H_{2,1}-H_{1,1}H_{2,3})H_{3,2}}{x_2x_3y_2y_3(x_1-x_2)(y_1-y_3)} + \frac{H_{1,3}(H_{2,2}H_{3,1}-H_{2,1}H_{3,2})}{x_1x_3y_1y_3(x_3-x_2)(y_1-y_2)}\\
-&\frac{H_{1,1}H_{2,2}H_{3,3}}{x_1x_2x_3y_1y_2y_3} + \frac{(H_{1,2}H_{2,1}-H_{1,1}H_{2,2})H_{3,3}}{x_1x_3y_2y_3(x_1-x_2)(y_1-y_2)} + \frac{H_{2,2}(H_{1,3}H_{3,1}-H_{1,1}H_{3,3})}{x_2x_3y_1y_2(x_1-x_3)(y_1-y_3)}\\
&\qquad -\frac{H_{2,1}(H_{1,3}H_{3,2}-H_{1,2}H_{3,3})}{x_1x_2y_1y_2(x_1-x_3)(y_2-y_3)} + \frac{H_{1,1}(H_{2,3}H_{3,2}-H_{2,2}H_{3,3})}{x_1x_3y_1y_2(x_2-x_3)(y_2-y_3)}\\
+&H^{(0)}_{3;0;0}(x_1,y_1,x_2,y_2,x_3,y_3)\left[\frac{1}{x_1y_1}-\frac{1}{x_2y_1}+\frac{1}{x_2y_2}-\frac{1}{x_3y_2}-\frac{1}{x_1y_3}+\frac{1}{x_3y_3}\right] = 0.
\end{aligned} \tag{24.25}$$

This gives $H^{(0)}_{3;0;0}$ as a sum over link patterns (see the table of example 23.3 for the expression of the sum), which is consistent with the result of theorem 23.2.

It remains to extend the theorem to result to the more general cases $H^{(g)}_{\mathbf{k_L};m;n}$. Several ways of generalizing the result are under consideration. Yet, the most probable plan to tackle the problem is to show the rotational invariance in the following order:

1. Add uniform boundaries with insertion operators, and prove the rotation symmetry of $H^{(0)}_{k;m;n}$ (the invariants are still planar and have one mixed boundary).
2. Prove by induction on L that:
   - $H^{(0)}_{\mathbf{k_L};m;n}$ is invariant when one permutes the two boundaries S_1, S_2.
   - $H^{(0)}_{\mathbf{k_L};m;n}$ is symmetric under the rotations $\mathcal{R}_i$
3. Prove the theorem for genus $g \geq 1$.

If those generalizations are true, then formula 24.5 is true.

25 Proof of the results

25.1 Preliminary result

Proof. We prove this result by induction on k. It is clearly true for $k=1$, so let $k \geq 2$ and suppose the equality holds for all $1 \leq j \leq k-1$.
From the definitions 23.1-23.3, it is also clear that the three functions have simple poles in x_1 around the x_j's for $j \geq 2$. Let $2 \leq l_0+1 \leq k$. We compute the residues of the three functions around x_{l_0+1}.

$$\operatorname*{Res}_{x_1 \to x_{l_0+1}} F^{(k)}_a(x_1,\ldots,y_k)dx_1 \quad = \quad \frac{F^{(l_0)}_a(x_{l_0+1},y_1\ldots,x_{l_0},y_{l_0})F^{(k-l_0)}_a(x_{l_0+1},\ldots,y_k)}{y_1-y_{l_0+1}}$$

$$= \frac{F^{(l_0)}(x_{l_0+1}, y_1 \ldots, x_{l_0}, y_{l_0}) F^{(k-l_0)}(x_{l_0+1}, \ldots, y_k)}{y_1 - y_{l_0+1}}$$

(25.1)

So the residue for $F_a^{(k)}$ is of the right form.

$$\begin{aligned}
\operatorname*{Res}_{x_1 \to x_{l_0+1}} F^{(k)} dx_1 &= \sum_{j=l_0+1}^{k-1} \frac{F^{(k-j)}(x_{j+1}, \ldots, y_k)}{(x_k - x_{l_0+1})(y_k - y_j)} \operatorname*{Res}_{x_1 \to x_{l_0+1}} F^{(j)}(x_1, \ldots, y_j) \\
&= \sum_{j=l_0+1}^{k-1} \frac{F^{(k-j)}(x_{j+1}, \ldots, y_k)}{(x_k - x_{l_0+1})(y_k - y_j)} \frac{F^{(l_0)}(x_{l_0+1}, y_1 \ldots, x_{l_0}, y_{l_0})}{y_1 - y_{l_0+1}} \times \\
&\quad F^{(j-l_0)}(x_{l_0+1}, \ldots, y_j) \\
&= \frac{F^{(l_0)}(x_{l_0+1}, y_1 \ldots, x_{l_0}, y_{l_0})}{y_1 - y_{l_0+1}} \sum_{j=l_0+1}^{k-1} \frac{F^{(k-j)}(x_{j+1}, \ldots, y_k)}{(x_k - x_{l_0+1})(y_k - y_j)} \times \\
&\quad F^{(j-l_0)}(x_{l_0+1}, \ldots, y_j) \\
&= \frac{F^{(l_0)}(x_{l_0+1}, y_1 \ldots, x_{l_0}, y_{l_0}) F^{(k-l_0)}(x_{l_0+1}, \ldots, y_k)}{y_1 - y_{l_0+1}}
\end{aligned} \tag{25.2}$$

So we get the same residues for $F_a^{(k)}$ and $F^{(k)}$.

Last, for $F_b^{(k)}$:

$$\begin{aligned}
\operatorname*{Res}_{x_1 \to x_{l_0+1}} F_b^{(k)} dx_1 &= \sum_{j=l_0+1}^{k-1} \frac{F_b^{(k-j)}(x_{j+1}, \ldots, y_k)}{(x_{j+1} - x_{l_0+1})(y_k - y_1)} \operatorname*{Res}_{x_1 \to x_{l_0+1}} F_b^{(j)}(x_1, \ldots, y_j) \\
&\quad - \frac{F_b^{(l_0)}(x_{l_0+1}, y_1 \ldots, x_{l_0}, y_{l_0}) F_b^{(k-l_0)}(x_{l_0+1}, \ldots, y_k)}{y_k - y_1} \\
&= \sum_{j=l_0+1}^{k-1} \frac{F^{(k-j)}(x_{j+1}, \ldots, y_k)}{(x_{j+1} - x_{l_0+1})(y_k - y_1)} \frac{F^{(l_0)}(x_{l_0+1}, y_1 \ldots, x_{l_0}, y_{l_0})}{y_1 - y_{l_0+1}} \times \\
&\quad F^{(j-l_0)}(x_{l_0+1}, \ldots, y_j) - \frac{F^{(l_0)}(x_{l_0+1}, y_1 \ldots, y_{l_0}) F^{(k-l_0)}(x_{l_0+1}, \ldots, y_k)}{y_k - y_1} \\
&= \frac{F^{(l_0)}(x_{l_0+1}, y_1 \ldots, x_{l_0}, y_{l_0}) F^{(k-l_0)}(x_{l_0+1}, \ldots, y_k)}{y_k - y_1} \times \\
&\quad \left(-1 + \frac{y_k - y_{l_0+1}}{y_1 - y_{l_0+1}} \right) \\
&= \frac{F^{(l_0)}(x_{l_0+1}, y_1 \ldots, x_{l_0}, y_{l_0}) F^{(k-l_0)}(x_{l_0+1}, \ldots, y_k)}{y_1 - y_{l_0+1}}
\end{aligned} \tag{25.3}$$

Therefore, the functions $F^{(k)}$, $F_a^{(k)}$ and $F_b^{(k)}$ have the same poles in x_1, so they must be equal for all x_1. This ends the proof of the lemma. □

Proof. The proof follows exactly the same steps as the proof of theorem 4.1 in [Eynard and Orantin, 2005], but instead of using the recursive definition 23.1, we use the 2 others ones of definition 23.3. □

25.2 Proof of the theorem

The theorem is proved by induction on k. It is clearly true for $k = 1$, so for the rest of this section, let $k \geq 2$ and assume the theorem holds for H_j^0, $1 \leq j \leq k-1$. The scheme of the proof follows the points of the theorem.

- First, in section 25.2.1, we transform formula 23.21 into another one (equation 25.13). This allows us to show that H_k^0 belongs to the ring $\mathbb{C}\left[\frac{1}{x_{i,j}}, \frac{1}{x_{i,j}}, H_{i,j}\right]\left[\frac{1}{y(p_l)-y(q_k)}, \frac{1}{H_{l,k}}\right]$, and to give the degrees in $\frac{1}{y(p_l)-y(q_k)}$ and $\frac{1}{H_{l,k}}$.
- Second, in section 25.2.2, we give explicit expressions (from equation 25.13) for $a^{k,j} + \sum_{j'=2}^{k} \frac{c^{k,j,j'}}{H_{j',k}}$, $b^{k,j}$ and $[H_k^0]_{\text{Irr}}$. From the previous expressions, it is convenient to define $A^{k,j}$ and $B^{k,j}$ that are functions independent of p_1. This proves the first item of the theorem.
- Third, in section 25.2.3, we show that $[H_k^0]_{\text{Irr}}$ satisfies the formula 23.23 in the second item of the theorem. It requires to use the recurrence formulas of definition 23.3.
- We show that $A^{k,j} = 0$, then $B^{k,j} = 0$ in section 25.2.4, proving the third part, and allowing to compute H_k^0 explicitly (that is, not recursively).
- To conclude, in section 25.2.5, the symmetry of the generating functions follows from the previous results.

25.2.1 Transformation of the recurrence formula

We use the formula 23.21 and make some manipulations first:

$$H_k^0(p_i, q_i) = H_{1,k} \sum_{i=1}^{k-1} H_{k-i}^0(p_{i+1}, \ldots, q_k) \operatorname*{Res}_{r \to p_1, p_{i+1}, q_k^{0,j}} \frac{H_i^0(r, q_1, \ldots, p_i, q_i) dx(r)}{x_{r,i+1} x_{r,1}} \tag{25.4}$$

For a given j, we want to decompose the function H_i^0 on the basis of $\mathbb{C}[H_{1,j}]$. Let us introduce the subsets $\overline{\mathfrak{S}}_i^j \subset \overline{\mathfrak{S}}_i$ for $j \leq i$, of the planar permutations $\overline{\mathfrak{S}}_i$:

$$\overline{\mathfrak{S}}_i^j = \{\sigma \in \overline{\mathfrak{S}}_i \text{ s.t. } \sigma(1) = j\} \tag{25.5}$$

The $\overline{\mathfrak{S}}_i^j$'s form a partition of $\overline{\mathfrak{S}}_i$.
As the theorem is true for $i \leq k-1$, H_i^0 is a polynomial of degree 1 in $H_{1,j}$. Moreover, calling $H_{i[j]}^0$ the coefficient of $H_{1,j}$, we have:

$$H_i^0(r, q_1, \ldots, p_i, q_i) \quad = \quad \sum_{\sigma \in \overline{\mathfrak{S}}_i} C_\sigma^{(i)}(r, y_1, \ldots, x_i, y_i) H_{r,\sigma(1)} \prod_{l=2}^{i} H_{l,\sigma(l)}$$

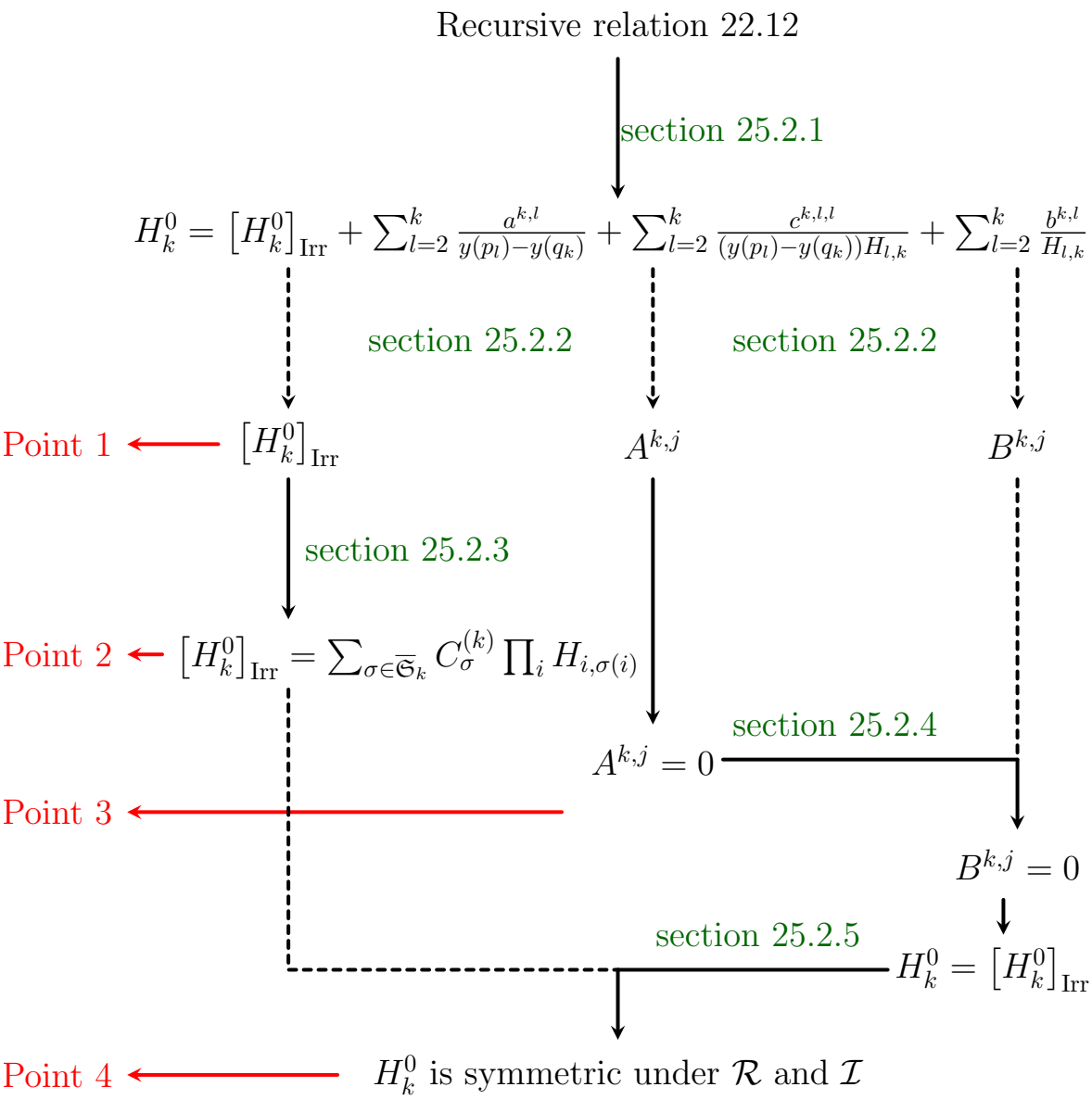

Figure 77: Scheme of the proof. Red arrows show when the successive points are proven.

$$
\begin{aligned}
&= \sum_{j=1}^{i} H_{r,j} \sum_{\sigma \in \overline{\mathfrak{S}}_i^j} C_\sigma^{(i)}(r, y_1, \ldots, x_i, y_i) \prod_{l=2}^{i} H_{l,\sigma(l)} \\
&= \sum_{j=1}^{i} H_{r,j} H_{i[j]}^0(r, q_1, \ldots, p_i, q_i)
\end{aligned}
\tag{25.6}
$$

The functions $H_{i[j]}^0$ belong to $\mathbb{C}\left[\frac{1}{x_{m,n}}, \frac{1}{y_{m,n}}, H_{r,s}\right]$ with $m, n = 1, \ldots, i$; $r = 2, \ldots, i$ and $s = 1, \ldots, i,\ s \neq j$.
Applying this decomposition of H_i^0:

$$
\begin{aligned}
H_k^0(p_s, q_s) &= H_{1,k} \sum_{i=1}^{k-1} H_{k-i}^0(p_{i+1}, \ldots, q_k) \operatorname*{Res}_{\substack{r \to p_{i+1} \\ q_k^{0,m}}}^{p_1} \sum_{j=1}^{i} \frac{H_{r,j} H_{i[j]}^0(r, q_1, \ldots, p_i, q_i) dx(r)}{x_{r,i+1} x_{r,1} y_{k,r} H_{r,k}} \\
&= H_{1,k} \sum_{i=1}^{k-1} H_{k-i}^0(p_{i+1}, \ldots, q_k) \sum_{j=1}^{i} \operatorname*{Res}_{\substack{r \to p_{i+1} \\ q_k^{0,m}}}^{p_1} \frac{H_{r,j} H_{i[j]}^0(r, q_1, \ldots, p_i, q_i) dx(r)}{x_{r,i+1} x_{r,1} y_{k,r} H_{r,k}}
\end{aligned}
\tag{25.7}
$$

For a given pair $1 \leq j \leq i \leq k-1$, we transform the factor inside the residue, using the identity:

$$
\frac{1}{y(q_k) - y(r)} = \frac{y(r) - y(q_j)}{(y(q_k) - y(r))(y(q_k) - y(q_j))} + \frac{1}{y(q_k) - y(q_j)}. \tag{25.8}
$$

Restating it with our notations, this gives:

$$
\frac{1}{y_{k,r}} = \frac{y_{r,j}}{y_{k,r} y_{k,j}} + \frac{1}{y_{k,j}} \tag{25.9}
$$

Remark 25.1. *This identity was used by Eynard and Orantin in [Eynard and Orantin, 2008] in order to compute H_2^0.*

We use it in the residue, so that we get:

$$
\begin{aligned}
H_k^0(p_i, q_i) &= H_{1,k} \sum_{i=1}^{k-1} H_{k-i}^0(p_{i+1}, \ldots, q_k) \sum_{j=1}^{i} \operatorname*{Res}_{\substack{r \to p_1 \\ p_{i+1} \\ q_k^{0,m}}} \left(\frac{y_{r,j}}{y_{k,r} y_{k,j}} \frac{H_{r,j} H_{i[j]}^0(r, q_1, \ldots, q_i) dx(r)}{x_{r,i+1} x_{r,1} H_{r,k}} \right. \\
&\quad \left. + \frac{1}{y_{k,j}} \frac{H_{r,j} H_{i[j]}^0(r, q_1, \ldots, p_i, q_i) dx(r)}{x_{r,i+1} x_{r,1} H_{r,k}} \cdot \right)
\end{aligned}
\tag{25.10}
$$

Now, it is possible to compute explicitly the residues. Indeed, we have to distinguish between the first term of the sum (on the first line), and the second one (on the second line).

First term Let us characterize the poles of $\frac{y_{r,j}}{y_{k,r}y_{k,j}}\frac{H_{r,j}H^0_{i[j]}(r,q_1,\ldots,p_i,q_i)dx(r)}{x_{r,i+1}x_{r,1}H_{r,k}}$ with respect to r.

- The equation 25.6 tells us that $H^0_{i[j]}$ is a rational function of $x(r)$, having poles in $x(r) \to x(p_l)$, $l = 2, \ldots, i$.
- $y_{r,j}H_{r,j} = \frac{E(x(r),y(q_j))}{x(r)-x(q_j)}$ is a rational function of $x(r)$, having no pole in $r \to q_j$.
- $y_{k,r}H_{r,k} = -\frac{E(x(r),y(q_k))}{x(r)-x(q_k)}$ is a rational function of $x(r)$, which does not vanish when $r \to q_k$, but vanishes when $r \to q_k^{0,m}$, $m \geq 1$.
- $\frac{y_{r,j}H_{r,j}}{y_{k,r}H_{r,k}}$ is a rational function of $x(r)$, regular when $x(r) \to \infty$.

Hence $\frac{y_{r,j}}{y_{k,r}y_{k,j}}\frac{H_{r,j}H^0_{i[j]}(r,q_1,\ldots,p_i,q_i)dx(r)}{x_{r,i+1}x_{r,1}H_{r,k}}$ is a rational function of $x(r)$, having poles in $x(r) \to x(p_l)$, $l = 1, \ldots, i+1$. Therefore, moving the contour $\mathcal{C}_1$ of integration for the residues $\operatorname*{Res}_{r\to p_1,p_{i+1},q_k^{0,m}}$ to the contour $\mathcal{C}_2$ (see figures 78 and 79):

$$\begin{aligned}
&\operatorname*{Res}_{r\to p_1,p_{i+1},q_k^{0,m}} \frac{y_{r,j}}{y_{k,r}y_{k,j}}\frac{H_{r,j}H^0_{i[j]}(r,q_1,\ldots,p_i,q_i)dx(r)}{x_{r,i+1}x_{r,1}H_{r,k}} \\
= \quad & -\sum_{l=2}^{i}\operatorname*{Res}_{r\to p_l}\frac{y_{r,j}}{y_{k,r}y_{k,j}}\frac{H_{r,j}H^0_{i[j]}(r,q_1,\ldots,p_i,q_i)dx(r)}{x_{r,i+1}x_{r,1}H_{r,k}} \\
= \quad & \sum_{l=2}^{i}\left(\frac{y(p_l)-y(q_j)}{(y(p_l)-y(q_k))y_{k,j}}\right)\frac{H_{l,j}}{H_{l,k}}\operatorname*{Res}_{r\to p_l}\frac{H^0_{i[j]}(r,q_1,\ldots,p_i,q_i)dx(r)}{x_{r,i+1}x_{r,1}} \\
= \quad & \sum_{l=2}^{i}\left(\frac{1}{y_{k,j}}+\frac{1}{y(p_l)-y(q_k)}\right)\frac{H_{l,j}}{H_{l,k}}\operatorname*{Res}_{r\to p_l}\frac{H^0_{i[j]}(r,q_1,\ldots,p_i,q_i)dx(r)}{x_{r,i+1}x_{r,1}}
\end{aligned} \tag{25.11}$$

Second term As there is no longer $y_{k,r}$ in the denominator of the second term, there is no pole around $r \to q_k^{0,m}$, then we can carry out the residues around $r \to p_1$ and $r \to p_{i+1}$ without difficulty, and we get:

$$\frac{1}{y_{k,j}}\frac{H_{1,j}}{H_{1,k}}\operatorname*{Res}_{r\to p_1}\frac{H^0_{i[j]}(r,q_1,\ldots,p_i,q_i)dx(r)}{x_{r,i+1}x_{r,1}} + \frac{1}{y_{k,j}}\frac{H_{i+1,j}}{H_{i+1,k}}\operatorname*{Res}_{r\to p_{i+1}}\frac{H^0_{i[j]}(r,q_1,\ldots,p_i,q_i)dx(r)}{x_{r,i+1}x_{r,1}} \tag{25.12}$$

Bringing the first and second terms together Equations 25.11 and 25.12 yield:

$$H^0_k(p_i,q_i) = \sum_{i=1}^{k-1}H^0_{k-i}(p_{i+1},\ldots,p_k,q_k)\sum_{j=1}^{i}\sum_{l=1}^{i+1}\frac{H_{1,k}H_{l,j}}{H_{l,k}y_{kj}}\operatorname*{Res}_{r\to p_l}\frac{H^0_{i[j]}(r,q_1,\ldots,p_i,q_i)dx(r)}{x_{r,1}x_{r,i+1}}$$

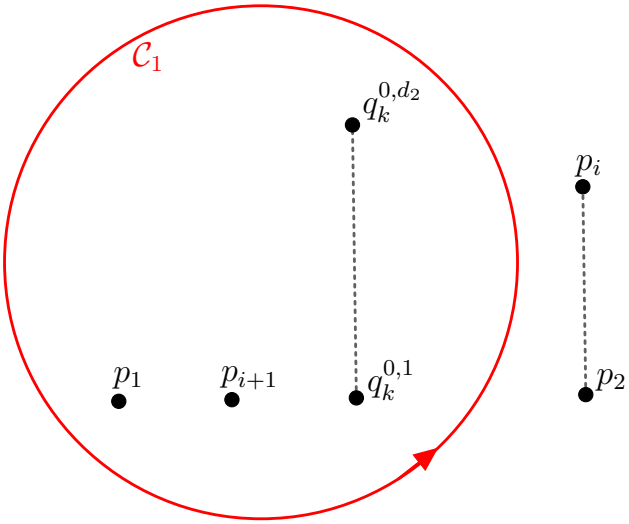

Figure 78: Contour of integration for the residue, and location of the poles.

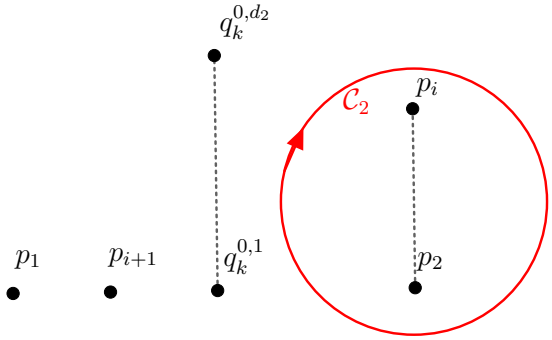

Figure 79: Deformed contour.

$$+\sum_{i=1}^{k-1} H^0_{k-i}(p_{i+1},\dots,q_k)\sum_{j=1}^{i}\sum_{l=2}^{i}\frac{H_{1,k}H_{l,j}}{H_{l,k}(y(p_l)-y(q_k))x_{l,1}x_{l,i+1}}\times \operatorname*{Res}_{r\to p_l} H^0_{i[j]}(r,q_1,\dots,p_i,q_i)dx(r) \tag{25.13}$$

This recursive formula is equivalent to equation 23.21. In the r.h.s.,

$$i \leq k-1 \qquad \text{and} \qquad k-i \leq k-1,$$

so the theorem applies to $H^0_i(r,q_1,\dots,p_i,q_i)$ and $H^0_{k-i}(p_{i+1},q_{i+1},\dots,p_k,q_k)$: they actually belong to $\mathbb{C}\left[H_{m,n},\frac{1}{x_{m,n}},\frac{1}{y_{m,n}}\right]$ (with, respectively, $m,n = 1,2,\dots,i$ and $m,n = i+1,\dots,k$). Therefore, we immediately see that H^0_k belongs to $\mathbb{C}\left[\frac{1}{x_{m,n}},\frac{1}{H_{m,n}},H_{m,n}\right]\left[\frac{1}{H_{m,k}},\frac{1}{y(p_m)-y(q_k)}\right]$.

Moreover, the degrees with respect to $\frac{1}{H_{m,k}}$ and $\frac{1}{y(p_m)-y(q_k)}$ are at most 1, and the monomials that are allowed when decomposing H^0_k in the ring $\mathbb{C}\left[\frac{1}{y(p_m)-y(q_k)},\frac{1}{H_{m,k}}\right]$ are

$$\frac{1}{y(p_m)-y(q_k)},\ \frac{1}{H_{m,k}} \qquad \text{and} \qquad \frac{1}{(y(p_m)-y(q_k))H_{m,k}}$$

(There can't be any term like

$$\frac{1}{(y(p_m)-y(q_k))(y(p_{m'})-y(q_k))},\ \frac{1}{H_{m,k}H_{m',k}} \text{ or } \frac{1}{(y(p_m)-y(q_k))H_{m',k}},\ m\neq m').$$

Therefore, the first point of the theorem is proven. We restate it in the following way: there exist $[H^0_k]_{\text{Irr}}$, $a^{k,l}$, $b^{k,l}$, $c^{k,l,l'} \in \mathbb{C}\left[\frac{1}{x_{i,j}},\frac{1}{x_{i,j}},H_{i,j}\right]$ such that:

$$H^0_k = \left[H^0_k\right]_{\text{Irr}} + \sum_{l=2}^{k}\frac{a^{k,l}}{y(p_l)-y(q_k)} + \sum_{l=2}^{k}\frac{b^{k,l}}{H_{l,k}} + \sum_{l=2}^{k}\frac{c^{k,l,l}}{(y(p_l)-y(q_k))H_{l,k}} \tag{25.14}$$

(it is similar to equation 23.22, but we don't allow (better, we proved that they vanished) $c^{k,l,l'}$ with $l \neq l'$). The polynomials $[H^0_k]_{\text{Irr}}$, $a^{k,l}$, $b^{k,l}$, $c^{k,l,l'}$ can be computed recursively by the recurrence equation 25.13 we just derived, and this is the aim of the following section.

25.2.2 Explicit expressions

Actually, instead of computing separately $a^{k,l}$, and $c^{k,l,l'}$, we need to compute a combination of $a^{k,l}$ and $c^{k,l,l}$ that is encoded in the quantity $A^{k,l}$.

Computation of the A's From the decomposition of H_k^0 in equation 25.14, we can transform it into:

$$H_k^0 = \left[H_k^0\right]_{\text{Irr}} + \sum_{l=2}^{k} \frac{b^{k,l}}{H_{l,k}} + \sum_{l=2}^{k} \frac{1}{y(p_l) - y(q_k)} \left(a^{k,l} + \frac{c^{k,l,l}}{H_{l,k}}\right). \tag{25.15}$$

We need to compute $a^{k,l} + \frac{c^{k,l,l}}{H_{l,k}}$ (it is the coefficient of $\frac{1}{y(p_l)-y(q_k)}$ when we decompose H_k^0 over the ring $\mathbb{C}\left[\frac{1}{y(p_l)-y(q_k)}\right]$). It is possible to do so if we look at the recurrence relation 25.13. We extract easily this coefficient:

$$a^{k,l} + \frac{c^{k,l,l}}{H_{l,k}} = \frac{H_{1,k}}{x_{l,1}} \sum_{i=l}^{k-1} \sum_{j=1}^{i} H_{k-i}^0(p_{i+1}, \ldots, q_k) \frac{H_{l,j}}{H_{l,k} x_{l,i+1}} \operatorname*{Res}_{r \to p_l} H_{i[j]}^0(r, q_1, \ldots, p_i, q_i) dx(r). \tag{25.16}$$

We define $A^{k,l}$ for $l \geq 2$ as:

$$\begin{aligned} A^{k,l}(q_1, p_2, q_2, \ldots, p_k, q_k) &= \sum_{i=l}^{k-1} \sum_{j=1}^{i} H_{k-i}^0(p_{i+1}, q_{i+1}, \ldots, p_k, q_k) \frac{H_{l,j}}{H_{l,k} x_{l,i+1}} \times \\ &\quad \operatorname*{Res}_{r \to p_l} H_{i[j]}^0(r, q_1, \ldots, p_i, q_i) dx(r). \end{aligned} \tag{25.17}$$

so that we rewrite the coefficient $a^{k,l} + \frac{c^{k,l,l}}{H_{l,k}}$ as:

$$a^{k,l} + \frac{c^{k,l,l}}{H_{l,k}} = \frac{H_{1,k}}{x_{l,1}} A^{k,l} \tag{25.18}$$

The $A^{k,l}$'s do not depend on p_1 from equation 25.17.
Then, equation 25.13 reads:

$$\begin{aligned} H_k^0(p_i, q_i) &= \sum_{i=1}^{k-1} H_{k-i}^0(p_{i+1}, \ldots, q_k) \sum_{j=1}^{i} \sum_{l=1}^{i+1} \frac{H_{1,k} H_{l,j}}{H_{l,k} y_{kj}} \operatorname*{Res}_{r \to p_l} \frac{H_{i[j]}^0(r, q_1, \ldots, p_i, q_i) dx(r)}{x_{r,1} x_{r,i+1}} \\ &\quad + \sum_{l=2}^{k} \frac{H_{1,k} A^{k,l}(q_1, p_2, q_2, \ldots, p_k, q_k)}{x_{l,1}(y(p_l) - y(q_k))} \\ &= \left[H_k^0\right]_{\text{Irr}} + \sum_{l=2}^{k} \frac{b^{k,l}}{H_{l,k}} + \sum_{l=2}^{k} \frac{H_{1,k}}{x_{l,1}} \frac{A^{k,l}}{y(p_l) - y(q_k)}. \end{aligned} \tag{25.19}$$

Computation of the b's Now, from equation 25.19, we have to decompose the first sum on $\mathbb{C}\left[\frac{1}{H_{l,k}}\right]$ to find the coefficients $b^{k,l}$ (and $[H_k^0]_{\text{Irr}}$ in the next section).
Let us take $l_0 \in \{1, \ldots, k\}$. From formula 25.19, the $\frac{1}{H_{1,k}}$ compensate with $H_{1,k}$ at the numerator, so we suppose $l_0 \geq 2$. The coefficient of $\frac{1}{H_{l_0,k}}$ in the first sum of equation 25.19 is:

$$\frac{H_{1,k}}{x_{l_0,1} H_{l_0,k}} \sum_{i=l_0}^{k-1} \frac{H_{k-i}^0(p_{i+1}, \ldots, q_k)}{x_{l_0,i+1}} \sum_{j=1}^{i} \frac{H_{l_0,j}}{y_{k,j}} \operatorname*{Res}_{r \to p_{l_0}} H_{i[j]}^0(r, q_1, \ldots, p_i, q_i) dx(r)$$

$$+\frac{H_{1,k}}{x_{l_0,1}H_{l_0,k}}{H^0_{k-l_0+1}}'(p_{l_0},\dots,q_k)\sum_{j=1}^{l_0-1}\frac{H_{l_0,j}}{y_{k,j}}H^0_{l_0-1[j]}(p_{l_0},q_1,\dots,p_{l_0-1},q_{l_0-1}) \quad (25.20)$$

where, by ${H^0_{k-l_0+1}}'$, we mean:

$${H^0_{k-l_0+1}}' = H^0_{k-l_0+1} - H^0_{k-l_0+1[k]} \quad (25.21)$$

As $k-l_0+1 \leq k-1$, the theorem stands for $H^0_{k-l_0+1}$, so we use it to compute ${H^0_{k-l_0+1}}'$:

$${H^0_{k-l_0+1}}'(p_{l_0},\dots,q_k) = \sum_{i=l_0}^{k-1}\frac{H^0_{k-i}(p_{i+1},\dots,q_k)}{x_{l_0,i+1}}\sum_{j'=l_0}^{i}\frac{H_{l_0,j'}}{y_{k,j'}}H^0_{i-l_0+1[j']}(p_{l_0},q_{l_0}\dots,q_i) \quad (25.22)$$

So, in the end, the coefficient b^{k,l_0} of $\frac{1}{H_{l_0,k}}$ is:

$$\begin{aligned} b^{k,l_0} &= \frac{H_{1,k}}{x_{l_0,1}}\sum_{i=l_0}^{k-1}\frac{H^0_{k-i}(p_{i+1},\dots,q_k)}{x_{l_0,i+1}}\left[\sum_{j=1}^{i}\frac{H_{l_0,j}}{y_{k,j}}\operatorname*{Res}_{r\to p_{l_0}}H^0_{i[j]}(r,q_1,\dots,p_i,q_i)dx(r)+\right.\\ &\left.\sum_{j=1}^{l_0-1}\frac{H_{l_0,j}}{y_{k,j}}H^0_{l_0-1[j]}(p_{l_0},q_1,\dots,p_{l_0-1},q_{l_0-1})\sum_{j'=l_0}^{i}\frac{H_{l_0,j'}}{y_{k,j'}}H^0_{i-l_0+1[j']}(p_{l_0},q_{l_0}\dots,q_i)\right]. \end{aligned} \quad (25.23)$$

We define $B^{k,l}$ as:

$$\begin{aligned} B^{k,l_0} &= \sum_{i=l_0}^{k-1}\frac{H^0_{k-i}(p_{i+1},\dots,q_k)}{x_{l_0,i+1}}\left[\sum_{j=1}^{i}\frac{H_{l_0,j}}{y_{k,j}}\operatorname*{Res}_{r\to p_{l_0}}H^0_{i[j]}(r,q_1,\dots,p_i,q_i)dx(r)+\right.\\ &\left.\sum_{j=1}^{l_0-1}\frac{H_{l_0,j}}{y_{k,j}}H^0_{l_0-1[j]}(p_{l_0},q_1,\dots,p_{l_0-1},q_{l_0-1})\sum_{j'=l_0}^{i}\frac{H_{l_0,j'}}{y_{k,j'}}H^0_{i-l_0+1[j']}(p_{l_0},q_{l_0}\dots,q_i)\right], \end{aligned} \quad (25.24)$$

so that the $B^{k,l}$'s are independent of p_1, and:

$$b^{k,l} = \frac{H_{1,k}}{x_{l,1}}B^{k,l}. \quad (25.25)$$

To sum up, when we decompose H^0_k over the ring $\mathbb{C}\left[\frac{1}{H_{l,k}},\frac{1}{y(p_l)-y(q_k)}\right]$, we have computed all the coefficients except the constant term $[H^0_k]_{\text{Irr}}$, which we do now.

Computation of the irreducible part We have given the expression of the $A^{k,l}$s (equation 25.17) and the $B^{k,l}$s (equation 25.24). We can use these expressions and equation 25.13 to compute $[H^0_k]_{\text{Irr}}$:

$$\left[H^0_k\right]_{\text{Irr}} = H^0_k - \sum_{l=2}^{k}\frac{H_{1,k}}{x_{l,1}}\frac{A^{k,l}}{y(p_l)-y(q_k)} - \sum_{l=2}^{k}\frac{H_{1,k}}{x_{l,1}}\frac{B^{k,l}}{H_{l,k}}. \quad (25.26)$$

More specifically, using equation 25.19:

$$\begin{aligned}\left[H_k^0\right]_{\text{Irr}} &= \sum_{i=1}^{k-1} H_{k-i}^0(p_{i+1},q_{i+1},\ldots,p_k,q_k)\sum_{j=1}^{i}\sum_{l=1}^{i+1}\frac{H_{1,k}H_{l,j}}{H_{l,k}y_{kj}}\operatorname*{Res}_{r\to p_l}\frac{H_{i[j]}^0(r,q_1,\ldots,q_i)dx(r)}{x_{r,1}x_{r,i+1}}\\ &\quad -\sum_{l=2}^{k}\frac{H_{1,k}}{x_{l,1}}\frac{B^{k,l}}{H_{l,k}}.\end{aligned} \tag{25.27}$$

As $\sum_{l=2}^{k}\frac{H_{1,k}}{x_{l,1}}\frac{B^{k,l}}{H_{l,k}}$ is the sum of the terms of the first line where the $\frac{1}{H_{l,k}}$s *are not* compensated by a $H_{l,k}$ on the numerator, the irreducible part corresponds to the sum of the terms in

$$\sum_{i=1}^{k-1} H_{k-i}^0(p_{i+1},q_{i+1},\ldots,p_k,q_k)\sum_{j=1}^{i}\sum_{l=1}^{i+1}\frac{H_{1,k}H_{l,j}}{H_{l,k}y_{kj}}\operatorname*{Res}_{r\to p_l}\frac{H_{i[j]}^0(r,q_1,\ldots,p_i,q_i)dx(r)}{x_{r,1}x_{r,i+1}} \tag{25.28}$$

where the $\frac{1}{H_{l,k}}$s *are* compensated, i.e. they cancel with some $H_{l,k}$ in the numerator. There are 2 cases:

- either $l=1$ and $\frac{1}{H_{l,k}}$ cancels out with $H_{1,k}$, so we get:

$$\sum_{i=1}^{k-1}\frac{H_{k-i}^0(p_{i+1},q_{i+1},\ldots,p_k,q_k)}{x_{1,i+1}}\sum_{j=1}^{i}\frac{H_{1,j}}{y_{kj}}H_{i[j]}^0(p_1,q_1,\ldots,p_i,q_i) \tag{25.29}$$

- either $l\geq 2$ and $\frac{1}{H_{l,k}}$ can only cancel with a $H_{l,k}$ coming from $H_{k-i}^0(p_{i+1},\ldots,q_k)$. So we need $l\geq i+1$. From the summation bounds, we also have $l\leq i+1$, so $l=i+1$ and we have all these terms:

$$\sum_{i=1}^{k-1}\frac{H_{k-i[k]}^0(p_{i+1},q_{i+1},\ldots,p_k,q_k)}{x_{i+1,1}}\sum_{j=1}^{i}\frac{H_{1,k}H_{i+1,j}}{y_{kj}}H_{i[j]}^0(p_{i+1},q_1,\ldots,p_i,q_i). \tag{25.30}$$

In the end, the irreducible part of H_k^0 is:

$$\begin{aligned}\left[H_k^0\right]_{\text{Irr}}(p_s,q_s) &= \sum_{i=1}^{k-1}\sum_{j=1}^{i}\frac{1}{x_{1,i+1}y_{k,j}}\left[H_{k-i}^0(p_{i+1},q_{i+1},\ldots,p_k,q_k)H_{1,j}H_{i[j]}^0(p_1,q_1,\ldots,q_i)\right.\\ &\quad \left.-H_{k-i[k]}^0(p_{i+1},q_{i+1},\ldots,p_k,q_k)H_{1,k}H_{i+1,j}H_{i[j]}^0(p_{i+1},q_1,\ldots,p_i,q_i)\right]\end{aligned} \tag{25.31}$$

We have thus decomposed the recursion relation in this way:

$$\begin{aligned}H_k^0(p_1,q_1,\ldots,p_k,q_k) &= \left[H_k^0\right]_{\text{Irr}}(p_1,q_1,\ldots,p_k,q_k)\\ &\quad +\sum_{j=2}^{k}\frac{H_{1,k}}{x_{j,1}}\frac{A^{k,j}(q_1,p_2,q_2,\ldots,p_k,q_k)}{y(p_j)-y(q_k)}\\ &\quad +\sum_{j=2}^{k}\frac{H_{1,k}}{x_{j,1}}\frac{B^{k,j}(q_1,p_2,q_2,\ldots,p_k,q_k)}{H_{j,k}}\end{aligned} \tag{25.32}$$

and given the expressions for $[H_k^0]_{\text{Irr}}$, $A^{k,l}$ and $B^{k,l}$.

25.2.3 Proof of the second point

From the expression of the irreducible part in equation 25.31, we first prove that $[H_k^0]_{\mathrm{Irr}}$ can be written this way:

$$\left[H_k^0\right]_{\mathrm{Irr}}(p_s,q_s)=\sum_{\sigma\in\overline{\mathfrak{S}}_k} D_\sigma^{(k)}(x_1,y_1,\ldots,x_k,y_k)\prod_{i=1}^{k}H_{i,\sigma(i)} \tag{25.33}$$

where $D_\sigma^{(k)}$ is a rational function of $x_i,\ y_j,\ i,j=1,\ldots,k$. Indeed, we have, from equation 25.31, and applying the hypothesis of recurrence to the H_i^0s and H_{k-i}^0 (it is legitimate because $i\leq k-1$ and $k-i\leq k-1$):

$$\begin{aligned}\left[H_k^0\right]_{\mathrm{Irr}}(p_s,q_s) \;=\; & \sum_{i=1}^{k-1}\sum_{j=1}^{i}\sum_{\rho\in\overline{\mathfrak{S}}_{k-i}}\sum_{\substack{\tau\in\overline{\mathfrak{S}}_i\\ \tau(1)=j}}\frac{C_\rho^{(k-i)}(x_{i+1},\ldots,y_k)C_\tau^{(i)}(x_1,\ldots,y_i)}{x_{1,i+1}y_{k,j}}\times\\ & \prod_{l=1}^{i}H_{l,\tau(l)}\prod_{m=i+1}^{k}H_{m,\rho(m)}\\ & -\sum_{i=1}^{k-1}\sum_{j=1}^{i}\sum_{\substack{\rho\in\overline{\mathfrak{S}}_{k-i}\\ \rho(i+1)=k}}\sum_{\substack{\tau\in\overline{\mathfrak{S}}_i\\ \tau(1)=j}}\frac{C_\rho^{(k-i)}(x_{i+1},\ldots,y_k)C_\tau^{(i)}(x_{i+1},y_1,\ldots,x_i,y_i)}{x_{1,i+1}y_{k,j}}\\ & H_{1,k}H_{i+1,j}\prod_{l=2}^{i}H_{l,\tau(l)}\prod_{m=i+2}^{k}H_{m,\rho(m)}\end{aligned} \tag{25.34}$$

We need to check that the following stands: if $\rho\in\overline{\mathfrak{S}}_{k-i}(i+1,\ldots,k)$, $\tau\in\overline{\mathfrak{S}}_i(1,\ldots,i)$, then

$$\begin{cases}\rho\tau\in\overline{\mathfrak{S}}_k\\ \text{if } \tau(1)=j,\ \rho(i+1)=k\Rightarrow\rho\tau\circ(1,i+1)\in\overline{\mathfrak{S}}_k\end{cases} \tag{25.35}$$

Proof. We show this graphically.

First case: If one takes $\rho\in\overline{\mathfrak{S}}_{k-i}(i+1,\ldots,k)$, it is equivalent to draw a system of non-intersecting arches on the disk $(i+1,\ldots,k)$. For $\tau\in\overline{\mathfrak{S}}_i(1,\ldots,i)$, it is equivalent to a system of non-intersecting arches on $(1,\ldots,i)$. If we open the disks and glue them according to figure 80, we see that $\rho\tau$ gives a system of non-intersecting arches on the disk $(1,\ldots,k)$, so $\rho\tau\in\overline{\mathfrak{S}}_k(1,\ldots,k)$.

Second case: From figures 81 and 82, one sees that, if $\rho\in\overline{\mathfrak{S}}_{k-i}(i+1,\ldots,k)$, $\rho(i+1)=k$ and $\tau\in\overline{\mathfrak{S}}_i(1,\ldots,i)$, $\tau(1)=j$, one can draw a system of (non-intersecting) arches on the disk $(1,\ldots,k)$ corresponding to the planar permutation $\rho\tau$ (it is represented in figure 81). Now, drawing the system of arches of $\rho\tau\circ(1,i+1)$ gives figure 82. Obviously, it is a system of non-intersecting arches of the disk $(1,\ldots,k)$, so $\rho\tau\circ(1,i+1)$ is a planar permutation: $\rho\tau\circ(1,i+1)\in\overline{\mathfrak{S}}_k(1,\ldots,k)$.

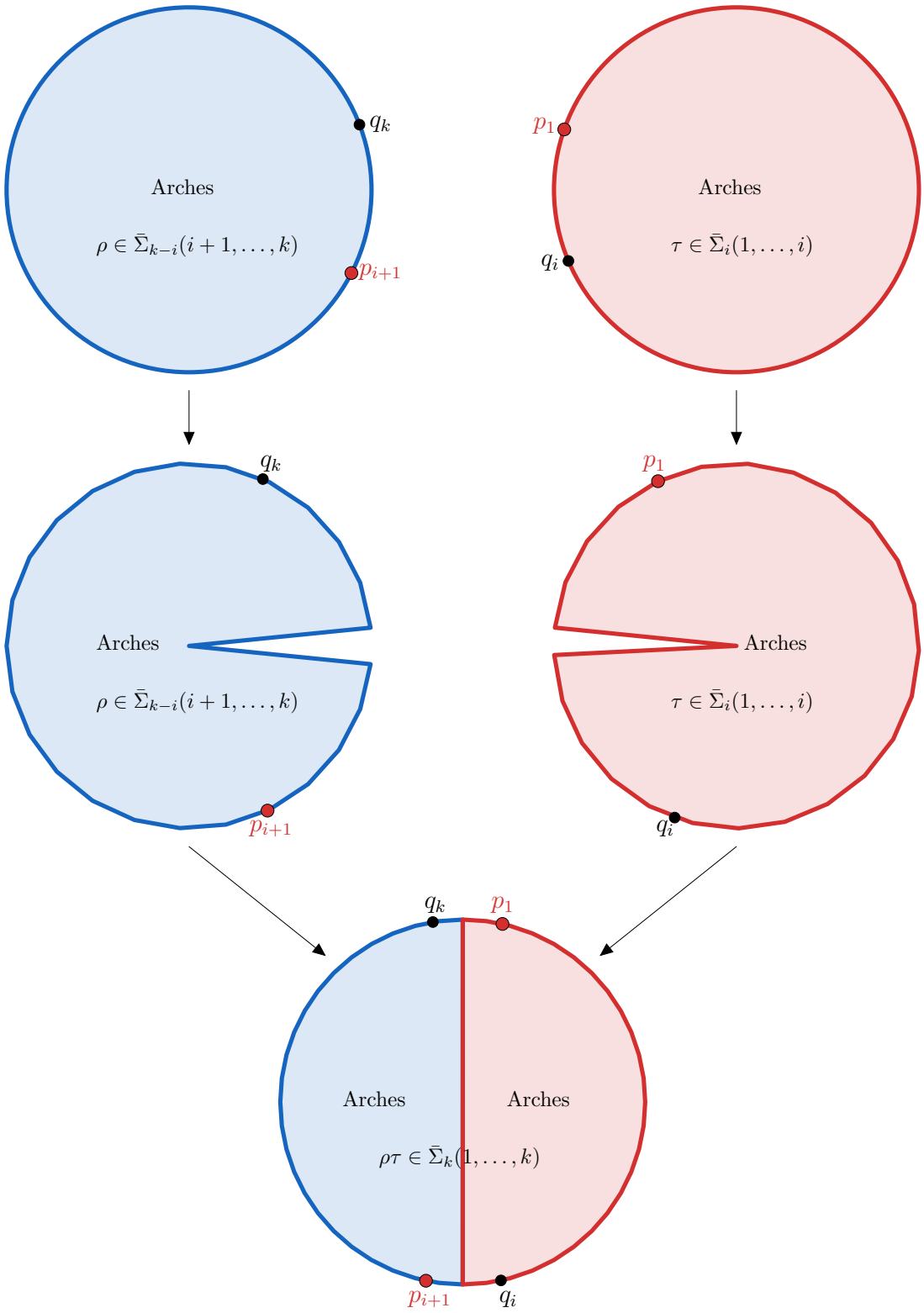

Figure 80: Gluing 2 systems of arches gives a system of non intersecting arches.

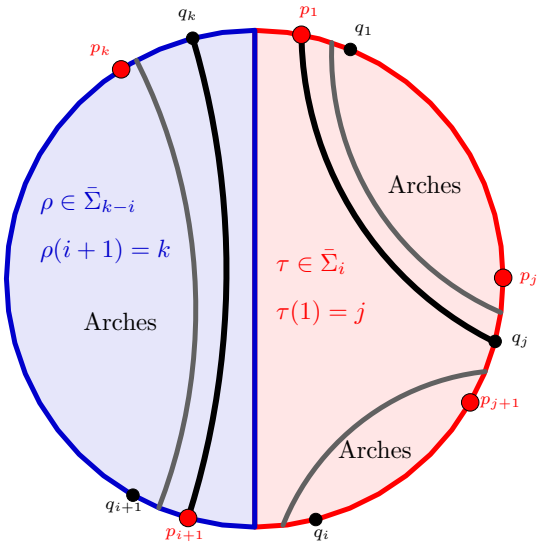

Figure 81: System of arches of $\rho\tau$

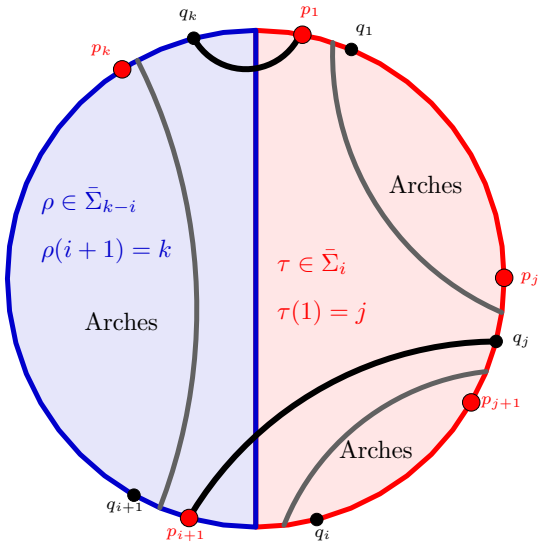

Figure 82: System of arches of $\rho\tau \circ (1, i{+}1)$

□

Therefore, the irreducible part admits a decomposition on planar permutations:

$$\left[H_k^0\right]_{\text{Irr}}(p_s, q_s) = \sum_{\sigma \in \overline{\mathfrak{S}}_k} D_\sigma^{(k)}(x_1, y_1, \ldots, x_k, y_k) \prod_{i=1}^{k} H_{i,\sigma(i)} \tag{25.36}$$

We need to show that for all $\sigma \in \overline{\mathfrak{S}}_k$, $D_\sigma^{(k)} = C_\sigma^{(k)}$. Let us take $\sigma \in \overline{\mathfrak{S}}_k$.
The proof splits in two parts:

$\sigma(1) = j$ **with** $j \leq k-1$ In this case, the permutation σ can only come from terms of the *first* 2 lines in equation 25.34. We then have:

$$D_\sigma^{(k)}(x_1, y_1, \ldots, x_k, y_k) = \sum_{i=j}^{k-1} \sum_{\rho \in \overline{\mathfrak{S}}_{k-i}} \sum_{\tau \in \overline{\mathfrak{S}}_i} \delta_{\sigma,\rho\tau} \frac{C_\rho^{(k-i)}(x_{i+1}, \ldots, y_k) C_\tau^{(i)}(x_1, \ldots, y_i)}{x_{1,i+1} y_{k,j}} \tag{25.37}$$

From section 23.4.1, the r.h.s is equal to $C_\sigma^{(k)}(x_1, y_1, \ldots, x_k, y_k)$.

$\sigma(1) = k$ Here, the permutation σ can only come from the *last* 2 lines of equation 25.34. Considering this, we get:

$$D_\sigma^{(k)}(x_1, y_1, \ldots, x_k, y_k) = -\sum_{i=j}^{k-1} \sum_{\rho \in \overline{\mathfrak{S}}_{k-i}} \sum_{\tau \in \overline{\mathfrak{S}}_i} \delta_{\sigma\circ(1,i+1),\rho\tau} \frac{C_\rho^{(k-i)}(x_{i+1}, \ldots, y_k) C_\tau^{(i)}(x_{i+1}, y_1, \ldots, y_i)}{x_{1,i+1} y_{k,j}} \tag{25.38}$$

And again, from section 23.4.1, the r.h.s is equal to $C_\sigma^{(k)}(x_1, y_1, \ldots, x_k, y_k)$.
Therefore, the second point is proven:

$$\left[H_k^0\right]_{\text{Irr}}(p_i, q_i) = \sum_{\sigma \in \overline{\mathfrak{S}}_k} C_\sigma^{(k)}(x_1, y_1, \ldots, x_k, y_k) \prod_{j=1}^{k} H_{j,\sigma(j)} \tag{25.39}$$

which is equation 23.23.

25.2.4 Proof of the third point

We show successively that $A^{k,l} = 0$ and $B^{k,l} = 0$. The main tool for this step is that we already know (see [Eynard and Orantin, 2008]) that H_k^0 has no pole in $p_i \to p_j$. Then, for all $l_0 \geq 2$, $\underset{p_1 \to p_{l_0}}{\text{Res}} H_k^0(p_s, q_s)dx(p_1) = 0$. So we have, $\forall l_0 \geq 2$:

$$\begin{aligned} &\underset{p_1 \to p_{l_0}}{\text{Res}} \left[H_k^0\right]_{\text{Irr}}(p_i, q_i)dx(p_1) \\ &+\frac{A^{(k,l_0)}(q_1, p_2, q_2, \ldots, p_k, q_k)}{y(p_{l_0}) - y(q_k)} \\ &+B^{(k,l_0)}(q_1, p_2, q_2, \ldots, p_k, q_k) \quad = \quad 0. \end{aligned} \tag{25.40}$$

From the expression of $B^{(k,l)}$ in equation 25.24 and the expression of $[H_k^0]_{\text{Irr}}$ in equation 25.31, one easily finds that:

$$\underset{p_1 \to p_{l_0}}{\text{Res}} \left[H_k^0\right]_{\text{Irr}}(p_i, q_i)dx(p_1) + B^{(k,l_0)}(q_1, p_2, q_2, \ldots, p_k, q_k) = 0 \tag{25.41}$$

So $A^{k,l} = 0$.
From the result of the third point, we know that the irreducible part of H_k^0 is the generating function of the Ising Model. We also know that the generating functions of the Ising Model have no pole at coinciding x_i (for both statements, see [Eynard and Orantin, 2005]). We then get:

$$\underset{p_1 \to p_{l_0}}{\text{Res}} \left[H_k^0\right]_{\text{Irr}}(p_i, q_i)dx(p_1) = 0 \tag{25.42}$$

so $B^{k,l} = 0$, and the third part of the theorem is true. The generating functions H_k^0 computed from the recursive relation 22.12 can be computed from the Ising model generating functions:

$$H_k^0(p_1, q_1, \ldots, p_k, q_k) = \sum_{\sigma \in \overline{\mathfrak{S}}_k} C_\sigma^{(k)}(x_1, y_1, \ldots, x_k, y_k) \prod_{j=1}^{k} H_{j,\sigma(j)}. \tag{25.43}$$

25.2.5 Conclusion

It is enough to use the proof of the symmetry of the generating functions in[Eynard and Orantin, 2005] to conclude about rotational the symmetry of H_k^0. This closes the proof of the theorem.

25.3 Removing one change of color from the boundary

Let us prove the lemma 23.4 for the operator $\mathcal{O}_1$ applied to the generating function $H_{k+1}^{(0)}(p_1, q_1, \ldots, p_{k+1}, q_{k+1})$. From the rotation symmetry proven in theorem 23.2, it is enough to prove the lemma: $\mathcal{O}_i = \mathcal{O}_1 \mathcal{R}_1^i$.
Let us suppose also that the spectral curve is such that there exists a common pole $q^* \in \Sigma$ of x and y.
From theorem 23.2, the generating function can be written as:

$$H_{k+1}^{(0)}(p_1, q_1, \ldots, p_{k+1}, q_{k+1}) = \sum_{\sigma \in \overline{\mathfrak{S}}_{k+1}} C_\sigma^{(k+1)}(x_1, y_1, \ldots, x_{k+1}, y_{k+1}) \prod_{i=1}^{k+1} H_{i,\sigma(i)}. \quad (25.44)$$

As we have:

$$\frac{1}{h(q_1)} \operatorname*{Res}_{p_1 \to q_1} dx(p_1) H(p_1, q_j) = \delta_{1,j}, \quad (25.45)$$

let us then carry out the following residue:

$$\frac{1}{h(q_1)} \operatorname*{Res}_{p_1 \to q_1} dx(p_1) H_{k+1}^{(0)}(S_{k+1}) = \sum_{\substack{\sigma \in \overline{\mathfrak{S}}_{k+1} \\ \sigma(1)=1}} C_\sigma^{(k+1)}(x(q_1), y_1, \ldots, x_{k+1}, y_{k+1}) \prod_{i=2}^{k+1} H_{i,\sigma(i)}.$$

It selects the link patterns with a link between p_1 and q_1. Then, using the point q^*, the following residue gives:

$$\begin{aligned} \operatorname*{Res}_{q_1 \to q^*} \frac{x(q_1)}{h(q_1)} dy(q_1) \operatorname*{Res}_{p_1 \to q_1} dx(p_1) H_{k+1}^{(0)}(S_{k+1}) &= \sum_{\tilde{\sigma} \in \overline{\mathfrak{S}}_k} C_{\tilde{\sigma}}^{(k)}(x_2, y_2, \ldots, x_{k+1}, y_{k+1}) \prod_{i=2}^{k+1} H_{i,\tilde{\sigma}(i)} \\ &= H_k^{(0)}(p_2, q_2, \ldots, p_{k+1}, q_{k+1}) \end{aligned}$$

Therefore the "forget map of the first pair of colors" is:

$$\mathcal{O}_1 = \operatorname*{Res}_{q_1 \to q^*} \frac{x(q_1)}{h(q_1)} dy(q_1) \operatorname*{Res}_{p_1 \to q_1} dx(p_1), \quad (25.46)$$

which proves lemma 23.4.

25.4 Insertion of uniform boundaries

Proof. This result is proven by induction, using the recursion 22.12 formula.

Initialization: Let us first apply the insertion operator to the generating function $H^{(0)}_{1;0;0}$. Using the Leibniz rule for the derivations:

$$\begin{aligned}
\delta_z^r H^{(0)}_{1;0;0}(p,q) &= \delta_z^r \frac{\prod_{i\neq 0}(y(q)-Y_i(x(p)))}{x(p)-X(y(q))} \\
&= \frac{\prod_{i\neq 0}(Y_i(x(p))-y(q))}{x(p)-X(y(q))}\left(\sum_{i\neq 0}\frac{H^{(0)}_{0;2;0}(p,z)}{y(q)-Y_i(x(p))}+\frac{H^{(0)}_{0;2;0}(q,z)}{x(p)-X(y(q))}\frac{dx}{dy}(q)\right) \\
&= -H^{(0)}_{1;0;0}(p,q)\left(\sum_{i\neq 0}\frac{H^{(0)}_{0;2;0}(p,z)}{y(q)-Y_i(x(p))}+\frac{H^{(0)}_{0;2;0}(q,z)}{x(p)-X(y(q))}\frac{dx}{dy}(q)\right)
\end{aligned}$$

It is possible to compute $H^{(0)}_{1;1;0}$ from the recursion formula, which gives:

$$\begin{aligned}
H^{(0)}_{1;1;0}(p,q;z) &= H^{(0)}_{1;0;0}(p,q)\operatorname*{Res}_{\substack{r\to \overset{p}{q^{0,j}}\\ z}}\frac{H^{(0)}_{0;2;0}(r,z)dx(r)}{(x(r)-x(p))(y(q)-y(r))} \\
&= H^{(0)}_{1;0;0}(p,q)\operatorname*{Res}_{\substack{r\to p^{i,0}\\ q}}\frac{H^{(0)}_{0;2;0}(r,z)dx(r)}{(x(r)-x(p))(y(r)-y(q))} \\
&= H^{(0)}_{1;0;0}(p,q)\left(\sum_{i\neq 0}\operatorname*{Res}_{r\to p^{i,0}}\frac{H^{(0)}_{0;2;0}(r,z)dx(r)}{(x(r)-x(p^{i,0}))(y(r)-y(q))}\right. \\
&\quad \left.+\operatorname*{Res}_{r\to q}\frac{dx}{dy}(r)\frac{H^{(0)}_{0;2;0}(r,z)dy(r)}{(x(r)-x(p))(y(r)-y(q))}\right) \\
&= -H^{(0)}_{1;0;0}(p,q)\left(\sum_{i\neq 0}\frac{H^{(0)}_{0;2;0}(p,z)}{y(q)-Y_i(x(p))}+\frac{H^{(0)}_{0;2;0}(q,z)}{x(p)-X(y(q))}\frac{dx}{dy}(q)\right)
\end{aligned}$$

Therefore:

$$\delta_z^r H^{(0)}_{1;0;0}(p,q) = H^{(0)}_{1;1;0}(p,q;z),$$

and a similar computation yields $\delta_z^b H^{(0)}_{1;0;0}(p,q) = H^{(0)}_{1;0;1}(p,q;z)$, which initializes the induction.

Induction: First, let us rewrite the recursion relation 22.12 in a more compact way, using the kernel $\mathcal{K}$ and the recursive terms $\mathrm{Rec}^{(g)}_{\mathbf{k_L};m;n}$:

$$H^{(g)}_{\mathbf{k_L};m;n} = \operatorname*{Res}_{\substack{p_{1,1}\\ r\to \tilde{q}^j_{1,k_1}\\ p_{i,\alpha}}}\mathcal{K}(r,p_{1,1},q_{1,k_1})\mathrm{Rec}^{(g)}_{\mathbf{k_L};m;n}(r)dx(r), \tag{25.47}$$

where:

$$\mathcal{K}(r,p,q) = \frac{H^{(0)}_{1;0;0}(p,q)}{H^{(0)}_{1;0;0}(r,q)(x(r)-x(p))(y(r)-y(q))}, \tag{25.48}$$

and

$$\begin{aligned}
&\mathrm{Rec}^{(g)}_{\mathbf{k_L};m;n}(r) = \\
&\sum_h \sum_{A\cup B=\{2,\ldots,l\}} \sum_{\alpha=2}^{k_1} \sum_{I,J} H^{(h)}_{k_1-\alpha+1,\mathbf{k_B};m-|I|;n-|J|}(\{p_{1,\alpha},q_{1,\alpha},\ldots,p_{1,k_1},q_{1,k_1}\},\mathbf{S_B};\mathbf{p_{M/I}};\mathbf{q_{N/J}}) \\
&\qquad \times \frac{H^{(g-h)}_{\alpha-1,\mathbf{k_A};|I|;|J|}(\{r,q_{1,1},\ldots,p_{1,\alpha-1},q_{1,\alpha-1}\},\mathbf{S_A};\mathbf{p_I};\mathbf{q_J})}{x(p_{1,\alpha})-x(r)} \\
&\qquad + \sum_{\alpha=2}^{k_1} \frac{1}{x(p_{1,\alpha})-x(r)} \times \\
&H^{(g-1)}_{\alpha-1,k_1-\alpha+1,\mathbf{k_{L/\{1\}}};m;n}(\{r,q_{1,1},\ldots,p_{1,\alpha-1},q_{1,\alpha-1}\},\{p_{1,\alpha},q_{1,\alpha},\ldots,p_{1,k_1},q_{1,k_1}\},\mathbf{S_{L/\{1\}}};\mathbf{p_M};\mathbf{q_N}) \\
&\qquad + \sum_{i=2}^{l} \sum_{\alpha=1}^{k_i} \frac{1}{x(p_{i,\alpha})-x(r)} \times \\
&H^{(g)}_{k_1+k_i,\mathbf{k_{L/\{1,i\}}};m;n}(\{S_1(r),p_{i,\alpha},q_{i,\alpha},p_{i,\alpha+1},\ldots,q_{i,k_i},p_{i,1},\ldots,p_{i,\alpha-1},q_{i,\alpha-1}\},\mathbf{S_{L/\{1,i\}}};\mathbf{p_M};\mathbf{q_N}) \\
&+ \sum_h \sum_{A\cup B=\{2,\ldots,l\}} \sum_{I,J} H^{(h)}_{k_1,\mathbf{k_A};|I|;|J|}(S_1(r),\mathbf{S_A};\mathbf{p_I};\mathbf{q_J}) H^{(g-h)}_{\mathbf{k_B};m-|I|+1;n-|J|}(\mathbf{S_B};r,\mathbf{p_{M/\{I\}}};\mathbf{q_{N/\{J\}}}) \\
&\qquad + \sum_{h=1}^{g} H^{(h)}_{0;1;0}(r) H^{(g-h)}_{k_1,\ldots,k_l;m;n}(S_1(r),S_2,\ldots,S_l;p_1,\ldots,p_m;q_1,\ldots,q_n) \\
&\qquad\qquad + H^{(g-1)}_{\mathbf{k_L};m+1;n}(\mathbf{S_K}(r);r,\mathbf{p_M};\mathbf{q_N}) \qquad (25.49)
\end{aligned}$$

According to the definition of the insertion operators, one gets:

$$\begin{aligned}
\delta^r_z H^{(g)}_{\mathbf{k_L};m;n}(\mathbf{S_L};p_M;q_N) &= \operatorname*{Res}_{\substack{p_{1,1}\\ r\to q^{0,j}_{1,k_1}\\ p_{i,\alpha}\\ z}} \delta^r_z \left[\mathcal{K}(r,p_{1,1},q_{1,k_1})\mathrm{Rec}^{(g)}_{\mathbf{k_L};m;n}(r)\right] dx(r) \\
&= \operatorname*{Res}_{\substack{p_{1,1}\\ r\to q^{0,j}_{1,k_1}\\ p_{i,\alpha}\\ z}} \Big(\delta^r_z\left[\mathcal{K}(r,p_{1,1},q_{1,k_1})\right]\mathrm{Rec}^{(g)}_{\mathbf{k_L};m;n}(r) \\
&\qquad + \mathcal{K}(r,p_{1,1},q_{1,k_1})\delta^r_z \mathrm{Rec}^{(g)}_{\mathbf{k_L};m;n}(r)\Big) dx(r)
\end{aligned}$$

In the last term, we have:

$$\delta^r_z \mathrm{Rec}^{(g)}_{\mathbf{k_L};m;n}(r) = \mathrm{Rec}^{(g)}_{\mathbf{k_L};m+1;n}(r) - H^{(g)}_{\mathrm{k_L};m;n}(r) H^{(0)}_{0;2;0}(r,z) \qquad (25.50)$$

(the term $H^{(g)}_{\mathrm{k_L};m;n}(r)H^{(0)}_{0;2;0}(r,z)$ comes from the red part of equation 25.49). Therefore:

$$\begin{aligned}
\delta^r_z H^{(g)}_{\mathbf{k_L};m;n}(\mathbf{S_L};p_M;q_N) &= \operatorname*{Res}_{\substack{p_{1,1}\\ r\to q^{0,j}_{1,k_1}\\ p_{i,\alpha}\\ z}} \Big(\mathcal{K}(r,p_{1,1},q_{1,k_1})\mathrm{Rec}^{(g)}_{\mathbf{k_L};m+1;n}(r) \\
&\qquad + \delta^r_z\left[\mathcal{K}(r,p_{1,1},q_{1,k_1})\right]\mathrm{Rec}^{(g)}_{\mathbf{k_L};m;n}(r) \\
&\qquad - \mathcal{K}(r,p_{1,1},q_{1,k_1}) H^{(g)}_{\mathrm{k_L};m;n}(r) H^{(0)}_{0;2;0}(r,z)\Big) dx(r) \\
&= H^{(g)}_{\mathbf{k_L};m+1;n}(\mathbf{S_L};p_M,z;q_N)
\end{aligned}$$

$$+ \operatorname*{Res}_{\substack{p_{1,1}\\ r\to q_{1,k_1}^{0,j}\\ p_{i,\alpha}\\ z}} \Big(\delta_z^r \left[\mathcal{K}(r,p_{1,1},q_{1,k_1})\right] \mathrm{Rec}^{(g)}_{\mathbf{k_L};m;n}(r) - \mathcal{K}(r,p_{1,1},q_{1,k_1}) H^{(g)}_{\mathrm{k_L};m;n}(r) H^{(0)}_{0;2;0}(r,z) \Big)\, dx(r)$$

It remains to show that the following holds:

$$\operatorname*{Res}_{\substack{p_{1,1}\\ r\to q_{1,k_1}^{0,j}\\ p_{i,\alpha}\\ z}} \delta_z^r \left[\mathcal{K}(r,p_{1,1},q_{1,k_1})\right] \mathrm{Rec}^{(g)}_{\mathbf{k_L};m;n}(r)dx(r) = \operatorname*{Res}_{\substack{p_{1,1}\\ r'\to q_{1,k_1}^{0,j}\\ z}} \mathcal{K}(r',p_{1,1},q_{1,k_1}) H^{(g)}_{\mathrm{k_L};m;n}(r') \times H^{(0)}_{0;2;0}(r',z)dx(r') \tag{25.51}$$

In order to make the term $\mathrm{Rec}^{(g)}_{\mathbf{k_L};m;n}(r)$ appear in the right hand side, we express $H^{(g)}_{\mathbf{k_L};m;n}(r')$ with the recursion relation, so that the right hand side is:

$$\operatorname*{Res}_{\substack{p_{1,1}\\ r'\to q_{1,k_1}^{0,j}\\ z}} \operatorname*{Res}_{\substack{r'\\ r\to q_{1,k_1}^{0,j}\\ p_{i,\alpha}}} \mathcal{K}(r',p_{1,1},q_{1,k_1}) \mathcal{K}(r,r',q_{1,k_1}) H^{(0)}_{0;2;0}(r',z) \mathrm{Rec}^{(g)}_{\mathrm{k_L};m;n}(r)dx(r)dx(r') \tag{25.52}$$

In order to get an expression similar to the left hand side, one has to exchange the residues in r and r'. Using the following rule:

$$\operatorname*{Res}_{r'\to p} \operatorname*{Res}_{r\to r'} = \operatorname*{Res}_{r\to p} \operatorname*{Res}_{r'\to p} - \operatorname*{Res}_{r'\to p} \operatorname*{Res}_{r\to p},$$

we end up, for the right hand side, with the following expression:

$$\operatorname*{Res}_{\substack{p_{1,1}\\ r\to q_{1,k_1}^{0,j}\\ p_{i,\alpha}\\ z}} \operatorname*{Res}_{\substack{p_{1,1}\\ r'\to q_{1,k_1}^{0,j}\\ z}} \mathcal{K}(r',p_{1,1},q_{1,k_1}) \mathcal{K}(r,r',q_{1,k_1}) H^{(0)}_{0;2;0}(r',z) \mathrm{Rec}^{(g)}_{\mathrm{k_L};m;n}(r)dx(r')dx(r). \tag{25.53}$$

Regarding the left hand side, we compute explicitly the action of the insertion operator on the kernel:

$$\delta_z^r \mathcal{K}(r,p,q) = \left(\frac{H^{(0)}_{1;1;0}(p,q;z)}{H_{p,q}} - \frac{H^{(0)}_{1;1;0}(r,q;z)}{H_{r,q}} - \frac{H^{(0)}_{0;2;0}(r,z)}{y(r)-y(q)} \right) \mathcal{K}(r,p,q) \tag{25.54}$$

The three terms can be expressed in this manner:

- First term

$$\frac{H^{(0)}_{1;1;0}(p,q;z)}{H_{p,q}} \mathcal{K}(r,p,q) = \operatorname*{Res}_{\substack{p\\ r'\to q^{0,j}\\ z}} \mathcal{K}(r',p,q) \mathcal{K}(r,r',q) H^{(0)}_{0;2;0}(r',z) \frac{x(r)-x(r')}{x(r)-x(p)} dx(r') \tag{25.55}$$

- Second term

$$-\frac{H^{(0)}_{1;1;0}(r,q;z)}{H_{r,q}}\mathcal{K}(r,p,q) = \operatorname*{Res}_{\substack{r'\to q^{0,j}_{z}}} \mathcal{K}(r',p,q)\mathcal{K}(r,r',q)H^{(0)}_{0;2;0}(r',z)\frac{x(r')-x(p)}{x(r)-x(p)}dx(r') \tag{25.56}$$

- Third term

$$-\frac{H^{(0)}_{0;2;0}(r,z)}{H_{r,q}}\mathcal{K}(r,p,q) = -\operatorname*{Res}_{r'\to r}\mathcal{K}(r',p,q)\mathcal{K}(r,r',q)H^{(0)}_{0;2;0}(r',z)dx(r') \tag{25.57}$$

Summing up these terms gives:

$$\delta^r_z\mathcal{K}(r,p,q) = \operatorname*{Res}_{\substack{p\\ r'\to q^{0,j}_{z}}} \mathcal{K}(r',p,q)\mathcal{K}(r,r',q)H^{(0)}_{0;2;0}(r',z). \tag{25.58}$$

Hence, the left hand side is equal to:

$$\operatorname*{Res}_{\substack{p_{1,1}\\ r\to q^{0,j}_{1,k_1}\\ p_{i,\alpha}\\ z}} \operatorname*{Res}_{\substack{p_{1,1}\\ r'\to q^{0,j}_{1,k_1}\\ z}} \mathcal{K}(r',p_{1,1},q_{1,k_1})\mathcal{K}(r,r',q_{1,k_1})H^{(0)}_{0;2;0}(r',z)\mathrm{Rec}^{(g)}_{\mathrm{k_L};m;n}(r)dx(r')dx(r), \tag{25.59}$$

which is equal to the right hand side, and finally proves by induction that

$$\delta^r_z H^{(g)}_{\mathbf{k_L};m;n}(\mathbf{S_L};p_M;q_N) = H^{(g)}_{\mathbf{k_L};m+1;n}(\mathbf{S_L};p_M,z;q_N). \tag{25.60}$$

Similar computations would give the result for the insertion of a uniform black boundary:

$$\delta^b_z H^{(g)}_{\mathbf{k_L};m;n}(\mathbf{S_L};p_M;q_N) = H^{(g)}_{\mathbf{k_L};m;n+1}(\mathbf{S_L};p_M;q_N,z). \tag{25.61}$$

□

Proof. The theorem is a consequence of theorem 23.2 and lemma 23.29. □

26 Extensions of the results

26.1 Toward several mixed boundaries

All the results obtained so far in this chapter concerns generating functions with one mixed boundary, and genus 0. But what do we have for higher genera, and several mixed boundaries ? The symmetries are not proven for those cases, but if we assume one invariance of the genus 0 generating functions, then the proof is straightforward. Namely, suppose in the next two sections, that:

$$\forall L \geq 2,\ \forall\{k_1,\dots,k_L\}, \qquad \mathcal{T}_2 H^{(0)}_{\mathbf{k_L};0;0} = H^{(0)}_{\mathbf{k_L};0;0}. \tag{26.1}$$

Let us show that, assuming this symmetry, the rotation symmetry and the symmetry under a permutation of mixed boundaries are statisfied.

26.1.1 Exchange of boundaries

For all $2 \leq i \leq L$, for all $k_1, \dots, k_L, m, n$, we prove that $\mathcal{T}_i H^{(g)}_{\mathbf{k_L},m,n} = H^{(g)}_{\mathbf{k_L},m,n}$. We simply need to prove the result for $m = n = 0$: to get the result for non null m, n, one simply uses the insertion of uniform boundary operators, and the result comes straightforwardly. The proof is done by recursion on $(L, k_1, \dots, k_L)$ (using the lexicographic order).

In that case, the recursion has three terms:

$$H^{(0)}_{\mathbf{k_L};0;0}(\mathbf{S_L}) = \operatorname*{Res}_{\substack{p_{i,\ell} \\ r \to q^{0,j}_{1,k_1}}} \frac{H^0_1(p_{1,1},q_{1,k_1})dx(r)}{H^0_1(r,q_{1,k_1})(x(r)-x(p_{1,1}))(y(r)-y(q_{1,k_1}))} \times$$
$$\Bigg[\sum_{\alpha=2}^{k_1} \sum_{\substack{A \sqcup B = \\ \{2,\dots,L\}}} \frac{H^{(0)}_{\alpha-1,\mathbf{k_A};0;0}(\{r,q_{1,1},\dots,q_{1,\alpha-1}\},\mathbf{S_A}) H^{(0)}_{k_1-\alpha+1,\mathbf{k_B};0;0}(\{p_{1,\alpha},\dots,q_{1,k_1}\},\mathbf{S_B})}{x(p_{1,\alpha})-x(r)}$$
$$+ \sum_{i=2}^{L} \sum_{\alpha=1}^{k_i} \frac{H^{(0)}_{k_1+k_i,\mathbf{k_{L/\{1,i\}}};0;0}(\{S_1(r),p_{i,\alpha},q_{i,\alpha},\dots,p_{i,\alpha-1},q_{i,\alpha-1}\},\mathbf{S_{L/\{1,i\}}})}{x(p_{i,\alpha})-x(r)}$$
$$+ \sum_{\substack{A \sqcup B = \\ \{2,\dots,L\}}} H^{(0)}_{k_1,\mathbf{k_A};0;0}(S_1(r),\mathbf{S_A}) H^{(0)}_{\mathbf{k_B};1;0}(\mathbf{S_B};r) \Bigg]. \tag{26.2}$$

There are three sums (two double sums and one simple sum) in the recurrence. We may refer to them in the following, as the 1^{st}, 2^{nd} and 3^{rd} sum.

The initialization of the recurrence is done for $L = 2$, and any k_1, $k_2 \in \mathbb{N}$. By assumption, one has $\mathcal{T}_2 H^{(0)}_{k_1,k_2}(S_1, S_2) = H^{(0)}_{k_1,k_2}(S_1, S_2)$, which initializes the recurrence. In the following, let us suppose $L \geq 2$

The second simplification we use is that, as we have the following identity on the transpositions:

$$(1, i) = (1, 2)(2, i)(1, 2),$$

and as we assume the invariance under $\mathcal{T}_2$, we just need to prove recursively the invariance of the generating function under the transposition of the boundaries 2 and i. Let us note $\mathcal{T}_{i,2}$ this transformation:

$$\mathcal{T}_{i,2}(S_1, S_2, \dots, S_L) = (S_1, S_i, \dots, S_{i-1}, S_2, S_{i+1}, \dots, S_L).$$

The hypothesis of recurrence is the following:

$$\forall i = 3, \dots, L, \qquad \mathcal{T}_{i,2} H^{(0)}_{\mathbf{k_L};0;0}(\mathbf{S_L}) = H^{(0)}_{\mathbf{k_L};0;0}(\mathbf{S_L}). \tag{26.3}$$

If it is true up to $(L, k_1, \dots, k_L)$, let us prove that it is true for $(L + 1, 1, k_1, \dots, k_L)$, and $(L, k_1 + 1, k_2, \dots, k_L)$. In both cases, we use formula 26.2 to compute $H^{(0)}_{1,\mathbf{k_L};0;0}(\{p, q\}, \mathcal{T}_i(\mathbf{S_L}))$ and $H^{(0)}_{k_1+1,\mathbf{k_{L/\{1\}}};0;0}(\{p, q, S_1\}, \mathcal{T}_i(\mathbf{S_{L/\{1\}}}))$. In the first case, only the 2^{nd} and 3^{rd} sum are present, whereas in the second case, the 3 sums are there.

In the equation 26.2, the first two sums are symmetric under the exchange $S_2 \leftrightarrow S_i$:

the symmetry amounts to rearrange the sum over $A \sqcup B = \{2, \dots, L\}$, and to apply the invariance of $H^{(0)}_{\alpha-1,\mathbf{S_A};0;0}$, $H^{(0)}_{k_1-\alpha+2,\mathbf{k_B};0;0}$ and $H^{(0)}_{k_1+k_j,\mathbf{k_{L/\{1,j\}}};0;0}(\{S_1(r), \mathcal{R}_j^{\alpha-1} S_j\}, \mathbf{S_{L/\{1,j\}}})$ under $\mathcal{T}_{i,2}$, $\forall i \geq 3$ by hypothesis of recurrence. In the last sum, the symmetry is manifest if one reorders the sum over $A \sqcup B = \{2, \dots, L\}$, and uses the invariance of

$$H^{(0)}_{k_1,\mathbf{k_A};0;0}(S_1(r), \mathbf{S_A}) H^{(0)}_{\mathbf{k_B};1;0}(\mathbf{S_B}; r)$$

when exchanging S_2 and S_i: this is the invariance under $\mathcal{T}_{i,2}$ $\forall i \geq 3$ and $\mathcal{T}_2$ by hypothesis of recurrence.
Therefore, the formulas computing $H^{(0)}_{1,\mathbf{k_L};0;0}$ and $H^{(0)}_{k_1+1,\mathbf{k_{L/\{1\}}};0;0}$ are respectively the same as the one computing $\mathcal{T}_{i,2} H^{(0)}_{1,\mathbf{k_L};0;0}$ and $\mathcal{T}_{i,2} H^{(0)}_{k_1+1,\mathbf{k_{L/\{1\}}};0;0}$, which prove that they are equal. This proves by recurrence that the generating functions $H^{(0)}_{\mathbf{k_L};m;n}$ are symmetric under a permutation of the mixed boundaries.

26.1.2 Rotation symmetry for several mixed boundaries

Once the symmetry under permutations of the mixed boundaries is proven, the rotation symmetry under $\mathcal{R}_i$ of generating function with several mixed boudaries of genus 0 comes also easily. As for the exchange of boundaries, we simply need to prove the result in the case where there is no uniform boundary. Adding uniform boundaries by applying insertion operators does not change the rotation symmetries. The proof is carried out by recurrence over $(L, k_1, \dots, k_L)$ with the lexicographic order. The initialization is done for $L = 1$, and any $k_1 \geq 1$: this is the result proved in the theorem 23.2:

$$\mathcal{R}_1 H^{(0)}_{k_1;0;0}(S_1) = H^{(0)}_{k_1;0;0}(S_1). \tag{26.4}$$

Then, suppose that the symmetries under $\mathcal{R}_i$ $\forall i = 1, \dots, L$ are satisfied up to order $(L, k_1, \dots, k_L)$. A first remark is that for $L > 1$, it is enough to prove the invariance under $\mathcal{R}_2$. Indeed, we have the following:

$$\mathcal{R}_i = \mathcal{T}_{i,2} \mathcal{R}_2 \mathcal{T}_{i,2}. \tag{26.5}$$

$\mathcal{T}_{i,2}$ leaves the generating functions invariants from previous section. The proof of invariance of $H^{(0)}_{1,\mathbf{k_L};0;0}$ and $H^{(0)}_{k_1+1,\mathbf{k_{L/\{1\}}};0;0}$ under $\mathcal{R}_2$ is the same as in the previous section, for the invariance under $\mathcal{T}_{i,2}$. In the end, one get:

$$\forall L \geq 1, \forall k_1, \dots, k_L, \forall m, n \leq 0, \forall 1 \leq i \leq L, \ \mathcal{R}_i H^{(0)}_{\mathbf{k_L};m;n} = H^{(0)}_{\mathbf{k_L};m;n}. \tag{26.6}$$

26.1.3 The exchange of boundaries 1 and 2.

For the two previous results to be true, it remains to show that the generating functions are not changed if one exchange boundaries 1 and 2. One could be tempted to apply the

proof of lemma 21.1. However, this recursive proof relies on the fact that the residues of topological recursion are local. The crucial fact of topological recursion is that it depends only on the Taylor expansion of the one-form $\omega_{0,1}$ close to the branchpoints, and on the Taylor expansion of the two-form $\omega_{0,2}$ at coinciding points. We stressed that the recursion of formula 22.12 is not local in the sense that the residues are done on all the sheets of the spectral curve (if one considers $q_{1,k_1}^{0,j}$). Those residues prevent from proving the symmetries recursively, uniquely using the master equation 22.12. This is why we had to find another formulation of the recursion, more convenient for our purposes in the one mixed boundary case. We ended up with a sum over link patterns, and the recursion does not involve residues any more.

This is why it is necessary to find another equivalent formulation of the recursion 22.12 to have a hope of proving the symmetries. What follows is purely speculative. In a first approach, it is tempting to extend the sum over planar link patterns to the case of several mixed boundaries on a genus g surface. It would then be necessary to define new functions for the faces, as they would not be all cellular (see figure 83). This approach would give a formula similar to the recursion computing the braided generating functions found by Borot and Eynard [Borot and Eynard, 2011] in the $O(n)$ loop model. Namely, their recursion is a sum over planar link pattern drawn on a genus g surfaces with boundaries.

A second approach would be to extend topological recursion to the case of mixed boundaries. Indeed, the residues of topological recursion are located at the branchpoints only, so they are local. However, the formula of topological recursion allows to compute generating functions which have uniform boundaries. This means that to each boundary is associated a parameter belonging to the spectral curve. A generalization of topological recursion would involve to generalize the kernel of recursion and the residues. For instance, if one looks at the generating function $H^{(g)}_{1,\dots,1;0;0}((p_1,q_1);(p_2,q_2);\dots;(p_k,q_k))$, it corresponds to an invariant associated to a surface of genus g with k mixed boundaries. To each boundary is associated a pair (p_i,q_i) of spectral parameters. It is tempting to formally write the following recursive formula:

$$\begin{aligned} H^{(g)}_{1,\dots,1;0;0}((p_1,q_1);(p_2,q_2);\dots;(p_k,q_k)) \;=\; & \sum_{\substack{(a,b)\\ dx(a)=0\\ dy(b)=0}} \text{“ Res ”}_{(s,t)\to(a,b)} \text{“}K_{a,b}\text{”}((s,t),(p_1,q_1))\times \\ & \Big[H^{(g-1)}_{1,\dots,1;0;0}((p,q);(\sigma_{a,b}(p,q));\dots;(p_k,q_k)) \\ & + {\sum_{\substack{g_1+g_2=g\\ I\sqcup J=\{2,\dots,k\}}}}' H^{(g_1)}_{1,\dots,1;0;0}((p,q);\mathbf{S_I})\times \\ & H^{(g_2)}_{1,\dots,1;0;0}(\sigma_{a,b}((p,q));\mathbf{S_J})\Big] \end{aligned} \tag{26.7}$$

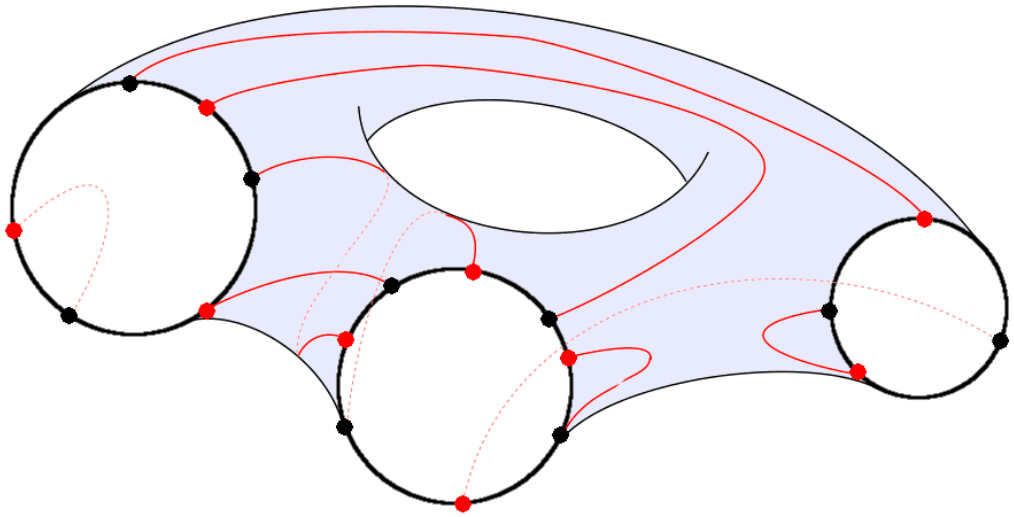

Figure 83: A non intersecting link pattern on a surface of genus 1 with 3 boundaries of lengths 2, 3 and 4. Some faces are no longer homeomorphic to a disk.

The quotation marks on the residues and the kernel are there to emphasize that this formula involves to find a generalization of the kernel and the residues so that it takes into account both parameters $(p, q) \in \Sigma^2$, and not only one. At the moment of writing this thesis, such generalization has not been found yet.

Part VII
Conclusion

Three aspects of random maps were investigated in this thesis. First, we studied a measure over the set of Delaunay triangulations, and showed that this very measure is the Weil-Petersson measure over the moduli space of punctured Riemann surfaces. Also, two local properties of the measure were proven, as preliminary steps toward the continuous limit of Delaunay triangulations. In the future, it is worth keeping on proving other properties of this measure in order to get a more substantial flavour of the continuous limit of the measure. Second, we computed explicitly the expectation values of observables defined on Strebel graphs. It allowed us to study different regimes for the marked perimeter of the one-point function when the size of the graphs grows to infinity. Then, once the interesting regime was identified, we implemented topological recursion in order to compute the expectation values in a more systematic way. Through the behaviour of the correlation functions, we could tag the continuous limit of Strebel graphs as a (3,2) minimal model dressed by gravity, corresponding to the pure quantum gravity. However, we got this result by considering the continuous limit of the observables accessible from the Chern class, which represent roughly half of the possible observables on Strebel graphs. It would be useful to study the other observables one can define on Strebel graphs, encoding for some of them the graph distance. Hence, we could have a glimpse of the continuous limit of Strebel graphs as metric spaces. Last, we studied the symmetry properties of the correlation functions of the Ising model on random maps. Those symmetries were not obvious from the recursive relation defining the correlation functions, and we showed the rotation and inversion symmetries for some cases. The generalization of this result is currently under study.

The continuous limit of generic random maps and its relation with Liouville quantum gravity is still a lively area of research: although we have many physical predictions for the large n limit, many of the statements are not proven yet. Also, the powerful procedure of topological recursion has not shown all its possibilities yet, and it is worth digging them.

In the forthcoming months, I intend to focus on the three following problems:

$\triangleright$ Find a combinatorial way to compute the correlation functions of the Ising model on random maps in order to find another recursive formula. The current

recursion comes from the resolution of loop equations coming from the matrix model. The combinatorial recursion would be found by exploring the interfaces between the red and black faces of the random maps. Then, it is probable that the recursive relation directly gives a sum over non intersecting link patterns. Such decomposition over link patterns simplifies considerably the symmetry properties of the correlation functions.

▷ Extend the topological recursion, first by applying it to other models. For instance, the r-spin model, for which the topological recursion allows to compute expectations of *ciliated* maps. Second, the extension would correspond also to a generalization of the topological recursion, in order to get a "topological recursion"-like formula for the correlations of the Ising model. Indeed, it has been stressed that the current recursion is different from topological recursion because of the non-locality of the residues.

▷ Third, investigate the algebraic properties of the correlation functions of the Ising model and of the $O(n)$ model, in order to relate them with integrable systems. This would involve to define operators (such as Dunkl operators) and algebras acting on the correlation functions. It is foreseen that the expectation values of the Ising model on random maps can be interpreted as amplitudes of a Calogero model. This relation must be strengthened.

A Special Functions

Here are some definitions and useful properties of special functions used in this thesis (dilogarithm and Bessel functions).
The dilogarithm Li_2 is defined by the series:

$$\mathrm{Li}_2(z) = \sum_{k=1}^{+\infty} \frac{z^k}{k^2}. \tag{A.1}$$

It is also the integral of the logarithm:

$$\mathrm{Li}_2(z) = -\int_0^z \frac{\ln(1-\zeta)}{\zeta} d\zeta. \tag{A.2}$$

Bessel functions of (complex) order ν is defined by the generating series

$$J_\nu(x) = \left(\frac{x}{2}\right)^\nu \sum_{k=0}^{\infty} \frac{(-1)^k}{\Gamma(k+1)\Gamma(k+\nu+1)} \left(\frac{x}{2}\right)^{2k}. \tag{A.3}$$

The modified Bessel functions of the first kind of order ν are given by:

$$I_\nu(x) = \left(\frac{x}{2}\right)^\nu \sum_{k=0}^{\infty} \frac{1}{\Gamma(k+1)\Gamma(k+\nu+1)} \left(\frac{x}{2}\right)^{2k}. \tag{A.4}$$

For $n \in \mathbb{Z}$, those Bessel functions are related by:

$$I_n(x) = \mathrm{i}^{-n} J_n(\mathrm{i}x) \tag{A.5}$$

For all $n \in \mathbb{Z}$, the modified Bessel functions of the first kind satisfy the recurrence relations:

$$\begin{aligned} I_{n-1}(x) - I_{n+1}(x) &= \frac{2n}{x} I_n(x) \\ I_{n-1}(x) + I_{n+1}(x) &= 2I'_n(x). \end{aligned} \tag{A.6}$$

B Explicit computation of the one point function

The one point function $f_n\left(L, \frac{L_1}{L}\right)$ can be computed in the same manner as the volumes V_n. For $n \geq 3$

$$\begin{aligned} f_n\left(L, \frac{L_1}{L}\right) &= Z_{n,1}(L; L_1) \\ &= 2\sum_{d_1=0}^{+\infty} \left\langle \left(\frac{1}{2}\sum_d \frac{L^{2d}}{2^d d!}\tau_d\right)^n \frac{L_1^{2d_1}}{2^{d_1} d_1!}\tau_{d_1} \right\rangle_0 \end{aligned}$$

$$= \frac{2}{2^n} \sum_{d_1,\ldots,d_{n+1}} \frac{L^{2(d_2+\cdots+d_{n+1})}}{2^{d_2+\cdots+d_{n+1}} d_2! \ldots d_{n+1}!} \frac{L_1^{2d_1}}{2^{d_1} d_1!} \langle \tau_{d_1} \ldots \tau_{d_{n+1}} \rangle_0 \tag{B.1}$$

Now:

$$\langle \tau_{d_1} \ldots \tau_{d_{n+1}} \rangle_0 = \frac{(n-2)!}{d_1! \ldots d_{n+1}!} \delta \left(n - 2 - \sum_{i=1}^{n+1} d_i \right). \tag{B.2}$$

So:

$$\begin{aligned} f_n\left(L, \frac{L_1}{L}\right) &= \frac{(n-2)! L^{2n-4}}{2} \sum_{d_1+\ldots d_{n+1}=n-2} \frac{1}{2^{2(d_2+\cdots+d_{n+1})}} \left(\frac{L_1}{2L}\right)^{2d_1} \frac{1}{(d_1! \ldots d_{n+1}!)^2} \\ &= \frac{(n-2)! L^{2n-4}}{2} [z^{2n-4}] I_0(z)^n I_0\left(z \frac{L_1}{L}\right) \\ &= \frac{(n-2)! L^{2n-4}}{2} \operatorname{Res}_{z\to 0} \frac{dz}{z^{2n-3}} I_0(z)^n I_0\left(z \frac{L_1}{L}\right) \\ &= \frac{(n-2)! L^{2n-4}}{2} \operatorname{Res}_{z\to 0} \frac{dz}{z} I_0(z)^2 e^{(n-2)(\ln I_0(z) - 2\ln z + \frac{1}{n-2} I_0(zL_1/L))}. \end{aligned} \tag{B.3}$$

C Change of the measure with a flip: proof of lemma 8.1

When the triangulation T undergoes a flip to give the triangulation T', only the two faces surrounding the edge change. So in the prepotentials $\mathcal{A}(T)$ and $\mathcal{A}(T')$, the only terms that differ are those implying the changed faces:

$$\mathcal{A}(T) - \mathcal{A}(T') = \mathrm{Vol}(124) + \mathrm{Vol}(234) - \mathrm{Vol}(123) - \mathrm{Vol}(134) \tag{C.1}$$

Therefore, the differences between $D(T)$ and $D(T')$ are located in the $D_{i,j}$ with $i, j \in \{1, 2, 3, 4\}$. As we are looking at the quantities $d_{(124)}$, the indices 1, 2 and 4 are not taken into account in the determinant. So the differences between $D(T)$ and $D(T')$ lay in $D_{3,3}$. By expanding the determinant with respect to the third line, we get:

$$d_{(124)}(T) - d_{(124)}(T') = [D_{3,3}(T) - D_{3,3}(T')] \det \left[D_{\{1,2,3,4\}}(T)\right] \tag{C.2}$$

Let us focus on the term $D_{3,3}(T) - D_{3,3}(T')$. Using the form $D = \frac{1}{4i}AEA^\dagger$, and noting $z_{ij} = z_i - z_j$ one gets:

$$D_{3,3}(T) - D_{3,3}(T') = \frac{1}{4i}\left[\sum_{e\to 3}\sum_{e' \text{ neighbour of } e} A_{3,e}E_{e,e'}\overline{A}_{3,e'}\right] \tag{C.3}$$

$$= \frac{1}{4i}\left[\frac{1}{z_{31}}\frac{-1}{\overline{z}_{32}} + \frac{1}{z_{32}}\frac{1}{\overline{z}_{31}} + \frac{1}{z_{31}}\frac{1}{\overline{z}_{34}} - \frac{1}{z_{34}}\frac{1}{\overline{z}_{31}} - \frac{1}{z_{32}}\frac{1}{\overline{z}_{34}} + \frac{1}{z_{34}}\frac{1}{\overline{z}_{32}}\right] \tag{C.4}$$

$$= \frac{1}{4i}\frac{z_{32}z_{34}\overline{z}_{31}\overline{z}_{42} + z_{31}z_{32}\overline{z}_{34}\overline{z}_{21} + z_{31}z_{34}\overline{z}_{32}\overline{z}_{14}}{|z_{31}|^2|z_{32}|^2|z_{34}|^2} \tag{C.5}$$

$$= \frac{1}{4i}\frac{N(z_3,\overline{z}_3)}{|z_{31}|^2|z_{32}|^2|z_{34}|^2} \tag{C.6}$$

The coefficient of the term $z_3^2\overline{z}_3$ in $N(z_3,\overline{z}_3)$ gives $\overline{z}_{42} + \overline{z}_{21} + \overline{z}_{14} = 0$. What is more, $\overline{N}(z) = -N(z)$, so N can be written as $N(z_3,\overline{z}_3) = az_3\overline{z}_3 + bz_3 - \overline{b}\overline{z}_3 + c$, with $a \in \mathrm{i}\mathbb{R}$, b and $c \in \mathrm{i}\mathbb{R}$ functions of z_i, $\overline{z}_i$, $i = 1, 2, 4$. Setting $\omega = -\frac{\overline{b}}{a}$ and $R^2 = -\frac{c}{a} + |a|^2$,

$$N(z_3,\overline{z}_3) = a[(z_3 - \omega)(\overline{z}_3 - \overline{\omega}) - R^2] \tag{C.7}$$

$N(z_3,\overline{z}_3) = 0$ is thus the equation of a circle for the point 3. As we have $N(z_i,\overline{z}_i) = 0$ for $i = 1, 2, 4$, the circle is the circumcircle of the face $f = (124)$, of center $\omega_f = \omega$ and radius $R_f = R$. The coefficient a is given by $a = z_{41}\overline{z}_{21} - z_{21}\overline{z}_{41}$, which is the (euclidean) area of the face (124). Eventually we have:

$$D_{3,3}(T) - D_{3,3}(T') = \mathrm{Area}(f)\frac{|z_3 - \omega_f|^2 - R_f^2}{|z_{31}|^2|z_{32}|^2|z_{34}|^2} \tag{C.8}$$

which proves the lemma 8.1.

D Refined lower bound for the volume: proof of theorem 8.3

The notations introduced here refer to the figure 41. Each edge of the triangle (abc) is surrounded by two faces. If we remove the point z_{n+1}, we obtain the Delaunay Triangulation for the points $\{z_1, \ldots, z_n\}$, and the triangle (abc) is one of its faces. Let us note $\theta_{(ab)}$, $\theta_{(bc)}$,and $\theta_{(ca)}$ the angles between the face $f = (abc)$ and the other face in contact with the edges (ab), (bc), and (ca) respectively.

Now, in formula 8.16, instead of computing the integral of the measure over the region $\mathcal{B}(f)$, we carry out the integral over the region $\mathcal{R}(f)$. The integrand is not changed: it is the measure of the Delaunay triangulation made of the 4 points a, b, c and z_{n+1}.

$$I_1 = \int_{\mathcal{R}(f)} d^2 z_{n+1} \det\left[D_{\{a,b,c\}}(T^D(\{a,b,c,z_{n+1}\}))\right]. \tag{D.1}$$

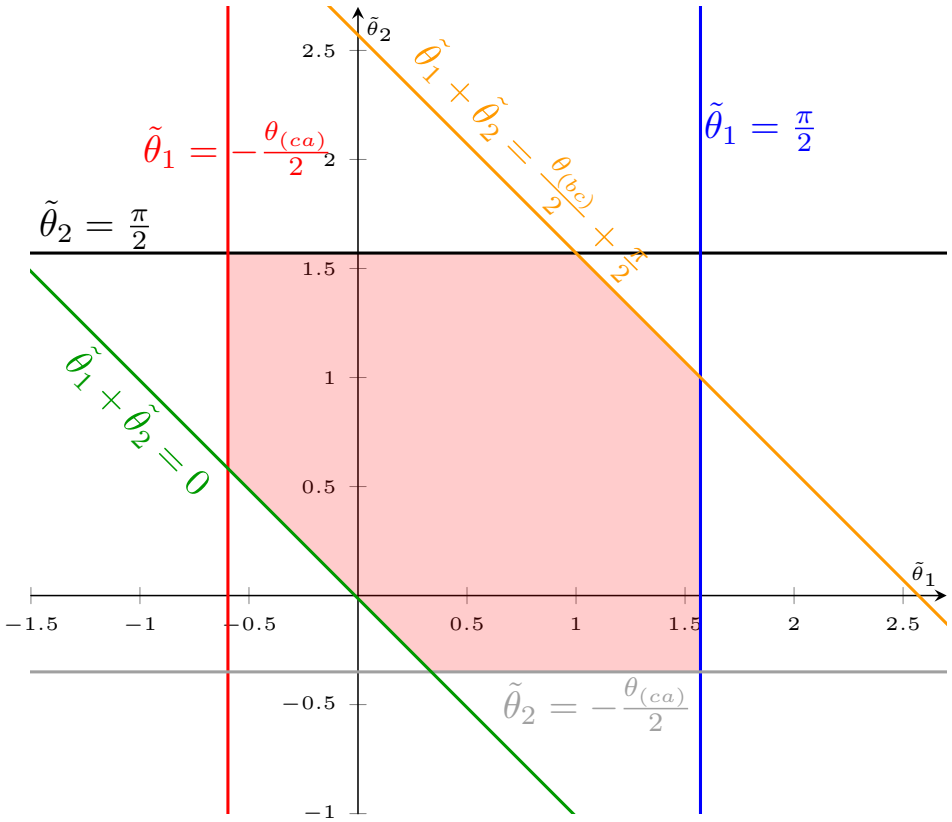

Figure 84: Domain on which $d\tilde{\theta_1} d\tilde{\theta_2}$ has to be integrated. We take here $\tilde{\theta}_i = \theta_i - \theta_i^{\min}$.

Then the computation of I_1 follows the same steps as for I, the only difference being the inequalities 8.19 satisfied by θ_1 and θ_2:

$$\theta_1^{\min} - \frac{\theta_{(ca)}}{2} \leq \theta_1 \leq \theta_1^{\min} + \frac{\pi}{2} \tag{D.2}$$

$$\theta_2^{\min} - \frac{\theta_{(ab)}}{2} \leq \theta_2 \leq \theta_2^{\min} + \frac{\pi}{2} \tag{D.3}$$

$$\theta_1^{\min} + \theta_2^{\min} \leq \theta_1 + \theta_2 \leq \theta_1^{\min} + \theta_2^{\min} + \frac{\theta_{(bc)}}{2} + \frac{\pi}{2} \tag{D.4}$$

The integral is then the area of the red region in figure 84. So we get:

$$I_1 = \frac{\pi^2}{16} + \frac{1}{16}[\theta_{(ab)}(2\pi - \theta_{(ab)}) + \theta_{(bc)}(2\pi - \theta_{(bc)}) + \theta_{(ca)}(2\pi - \theta_{(ca)})].$$

Then, following the same steps as for the previous lower bound, the result comes:

$$\int_{\mathbb{C}} d^2 z_{n+1} \det\left[D_{\{1,2,3\}}(T^D(\{z_1, \ldots, z_{n+1}\}))\right]$$
$$\geq \left[(n-2)\frac{\pi^2}{8} + \frac{1}{8} \sum_{e \in \mathcal{E}(T^D)} \theta(e)(2\pi - \theta(e))\right] \det\left[D_{\{1,2,3\}}(T^D(\{z_1, \ldots, z_n\}))\right]. \tag{D.5}$$

E Origamap

The equipped and courageous reader can do better than a 3d printer and build a bi-colored quadrangulation on a torus with 2 boundaries, by following this tutorial. Some pictures are here to help to the construction of the map.

- **Duration:** approximately 30 minutes.
- **Equipment:** liquid glue, scissors, printed version of this appendix.

Steps:

1. Cut the pattern along the plain thick lines, in order to get two pieces of paper. They constitute two parts of the torus.
2. For each piece, fold the pattern along the dashed thick lines, except the dashed lines neighbouring the areas labeled “1” and “7”. The strips “2” and “4” must be folded in the opposed way with respect to the other strips.
3. On each piece of paper, glue the areas “1” to the neighboring triangle. Then glue the area “2”.
4. Glue the two pieces of paper together along the areas “3”, in such a way that the strips “4” cannot touch each other.
5. Then, glue successively the areas “4”, “5”, “6” and “7”.
6. The origamap should look like a square donut, see figure 86.

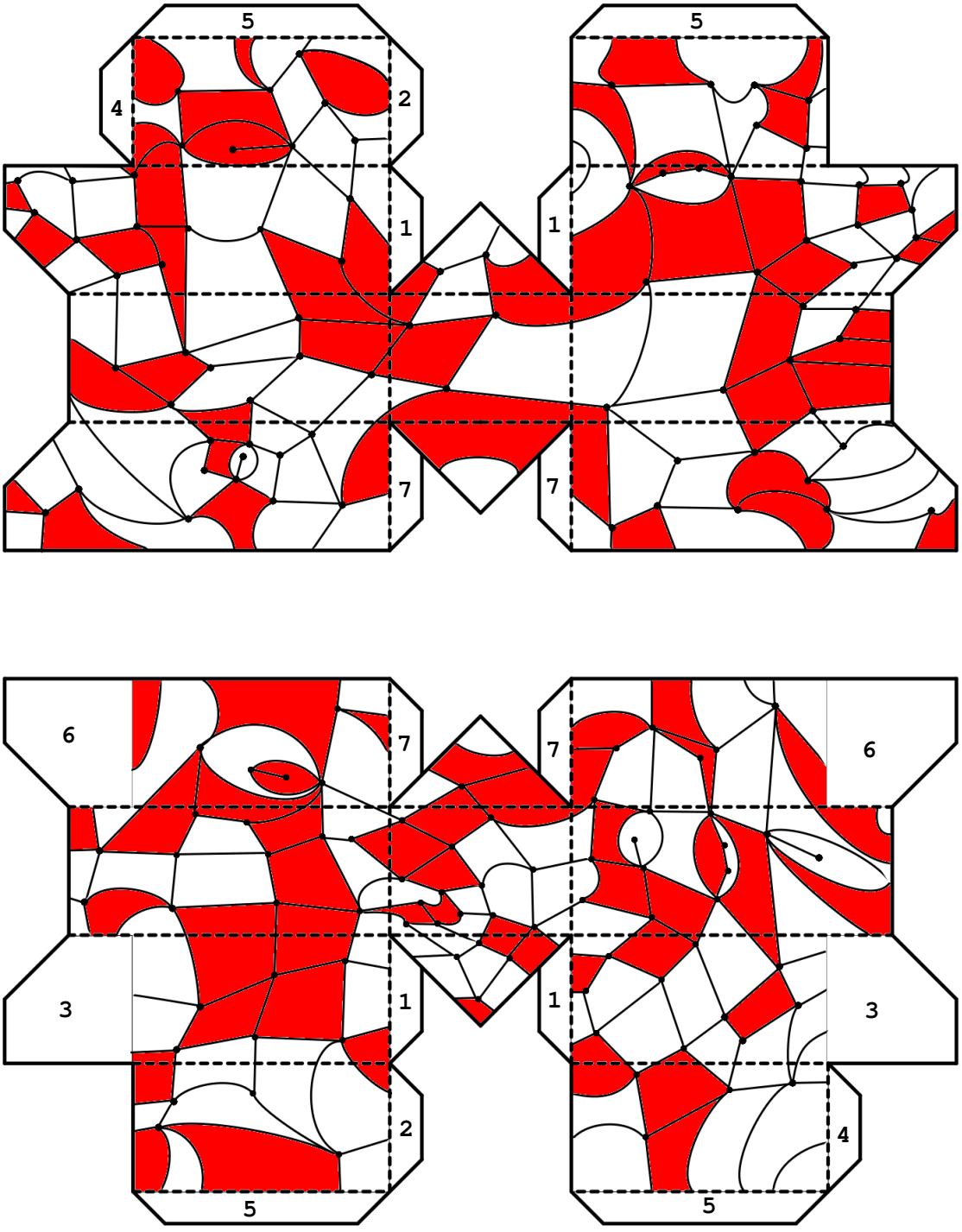

Figure 85: Pattern for the construction of a bi-colored quadrangulation on a torus with 2 boundaries.

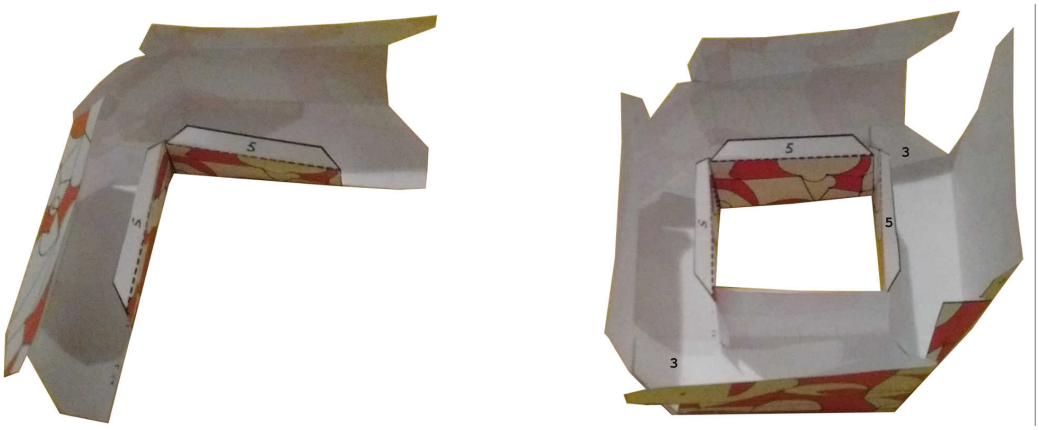

Figure 86: Pictures of the map in construction. On the left hand side, it is after step 3 ; on the right hand side, it is after step 4.

F Synthèse des résultats

On présente dans cette annexe une synthèse de certains résultats de la thèse, chapitre par chapitre.

F.1 Propriétés locales d'une mesure définie sur les triangulations de Delaunay et modèles de gravité topologique en 2D

Dans ce chapitre, on étudie diverses propriétés d'une mesure définie sur les triangulations de Delaunay.

Definition F.1. *Etant donnés n points du plan complexe $z_1, \dots, z_n \in \mathbb{C}$ distincts deux à deux, une triangulation de Delaunay de ces points est un graphe tel que:*

- *les nœuds du graphe sont $z_1, \dots, z_n$;*
- *toutes les faces, y compris la face externe, sont de degré 3 ;*
- *l'intérieur du cercle circonscrit de chaque face ne contient aucun nœud.*

On note T^D la structure (c'est-à-dire les relations d'adjacence entre les nœuds) d'une triangulation de Delaunay. On note $\mathcal{V}(T)$, $\mathcal{E}(T)$ et $\mathcal{F}(T)$ respectivement l'ensemble des nœuds, des arêtes et des faces d'une triangulation T.

Une propriété importante de telles triangulations est que pour chaque configuration de points $\{z_1, \ldots, z_n\}$, il existe une unique triangulation de Delaunay de cette configuration. À chaque arête de la triangulation est associé un angle, de la façon suivante :

Definition F.2. *Soit $e = (z_i, z_j)$ une arête de T^D, et $f_1 = (z_i, z_j, z_k)$, $f_2 = (z_i, z_\ell, z_j)$ les faces adjacentes à e. On note ω_1, ω_2 les centres respectifs des cercles circonscrits aux triangles f_1 et f_2. Alors l'angle θ_e associé à e est défini par :*

$$\theta_e = \widehat{(\omega_1 z_j \omega_2)}.$$

L'ensemble des angles d'une triangulation est noté θ. Pour toute arête d'une triangulation de Delaunay, on a $0 \leq \theta_e \leq \pi$.

La configuration d'angles associée à une triangulation de Delaunay satisfait deux contraintes.

1. La première contrainte est locale : soit v un nœud de T^D, alors

$$\sum_{e \mapsto v} \theta_e = 2\pi,$$

   où $e \mapsto v$ est une notation qui signifie que la somme porte sur les arêtes incidentes en v.

2. La seconde est globale : soit $\mathcal{C}$ un cycle du graphe dual T^D ; on note $\mathcal{C}^*$ l'ensemble des arêtes de T^D qui intersectent le contour $\mathcal{C}$, alors

$$\sum_{e \in \mathcal{C}^*} \theta_e \geq 2\pi.$$

Ce qu'on appelle une triangulation de Delaunay est la donnée (T^D, θ) de la structure et de la configuration d'angles. La taille d'une triangulation de Delaunay est le nombre de nœuds de la triangulation. Un autre intérêt des triangulations de Delaunay est qu'elles satisfont une propriété d'invariance conforme :

Proposition F.1. *Soit $\{z_1, \ldots, z_n\} \subset \mathbb{C}$ une configuration de points distincts deux à deux, et $\varphi \in \mathrm{SL}_2(\mathbb{C})$ une transformation de Möbius. Alors $\{z_1, \ldots, z_n\}$ et $\{\varphi(z_1), \ldots, \varphi(z_n)\}$ ont la même structure et la même configuration d'angles : ces configurations ont la même triangulation de Delaunay.*

Un espoir est que dans la limite continue (lorsque la taille n tend vers l'infini), le modéle limite conserve cette propriété d'invariance conforme. On note $\mathfrak{D}_n =$

$\mathbb{C}^n/\mathrm{SL}_2(\mathbb{C})$ l'ensemble des triangulations de Delaunay de taille n. On définit une mesure sur $\mathfrak{D}_n$:

$$d\nu_n(T,\theta) = \text{uniforme}(T) \prod_{e\in\mathcal{E}(T)} d\theta_e \prod_{v\in\mathcal{V}(T)} \delta\left(2\pi - \sum_{e\mapsto v}\theta_e\right) \prod_{mathcalC} \Theta\left(\sum_{e\in\mathcal{C}^*}\theta_e - 2\pi\right),$$

où Θ est la fonction de Heaviside. C'est la mesure de Lebesgue sur les angles, où les contraintes, locale d'une part et globale d'autre part, sont imposées. En terme des coordonnées des points, cette mesure a la forme suivante :

$$d\nu_n(T,\theta) = \mathcal{D}^T_{\{i,j,k\}}(z_1,\dots,z_n) \prod_{\substack{v=1\\ v\neq i,j,k}}^{n} d^2 z_v,$$

$\mathcal{D}^T_{\{i,j,k\}}$ étant le jacobien pour passer de la description en termes d'angles à la description en termes des coordonnées des points. Ce dernier est défini que T soit la triangulation de Delaunay ou pas. David et Eynard ont montré [David and Eynard, 2014] que la mesure utilisée est Kählerienne, et que ce jacobien peut s'écrire sous la forme d'un déterminant :

$$\mathcal{D}^T_{\{i,j,k\}}(z_1,\dots,z_n) = 2^{n-3}\det\left[D_{i,j,k}(z_1,\dots,z_n)\right],$$

ce qui permet de définir une 2-forme

$$\Omega_{\mathscr{D}} = \frac{1}{2\mathrm{i}}\sum_{u,v=1}^{n} D_{u,v}\, dz_u \wedge d\bar{z}_v.$$

Les résultats de ce chapitre sont de deux ordres. D'abord, on relie la mesure sur les triangulations de Delaunay à la mesure de Weil-Petersson sur l'espace des modules des surfaces de Riemann marquées de genre 0. Ensuite, on prouve 2 propriétés, de maximalité d'une part et de croissance d'autre part. Ces deux propriétés sont des étapes préliminaires à une possible étude de la limite continue des triangulations de Delaunay. Les résultats sont donc les suivants. On montre d'abord que la 2-forme $\Omega_{\mathscr{D}}$ est proportionnelle à la 2-forme de Weil-Petersson $\Omega_{\mathscr{W}\mathscr{P}}$:

Théorème F.1. *La 2-forme $\Omega_{\mathscr{D}}$ admet l'expression:*

$$\Omega_{\mathscr{D}} = \frac{1}{2}\sum_{f\in\mathcal{F}(T)} \frac{d|z_i-z_j|}{|z_i-z_j|}\wedge\frac{d|z_j-z_k|}{|z_j-z_k|} + \frac{d|z_j-z_k|}{|z_j-z_k|}\wedge\frac{d|z_k-z_i|}{|z_k-z_i|} + \frac{d|z_k-z_i|}{|z_k-z_i|}\wedge\frac{d|z_i-z_j|}{|z_i-z_j|},$$

et

$$\Omega_{\mathscr{D}} = \frac{1}{2}\Omega_{\mathscr{W}\mathscr{P}}.$$

Ceci a pour conséquence directe que les formes volumes $d\nu_n$ (sur $\mathfrak{D}_n$) et $d\nu_n^{\mathscr{W}\mathscr{P}}$ (sur $\overline{\mathcal{M}}_{0,n}$) sont égales. La propriété de maximalité de la mesure est formulée ainsi :

Théorème F.2. *Soit $\{z_1, \ldots, z_n\} \subset \mathbb{C}$ une configuration de points distincts. Soit T une triangulation générique construite sur ces points (T n'est pas nécessairement la structure de la triangulation de Delaunay de la configuration), et T^D la structure de la triangulation de Delaunay associée à cette configuration. Alors le jacobien associé à T^D est maximal :*

$$\mathcal{D}^T_{\{i,j,k\}}(z_1, \ldots, z_n) \leq \mathcal{D}^{T^D}_{\{i,j,k\}}(z_1, \ldots, z_n)$$

Enfin, la propriété de croissance est la suivante.

Théorème F.3. *Soient $z_1, \ldots, z_{n+1} \in \mathbb{C}$, et T_n, T_{n+1} les structures des triangulations de Delaunay de $\{z_1, \ldots, z_n\}$ et $\{z_1, \ldots, z_{n+1}\}$ respectivement. Alors :*

$$\int_{\mathbb{C}} d^2 z_{n+1} \det\left[D_{1,2,3}(T_{n+1})\right] \geq (n-2)\frac{\pi^2}{8} \det\left[D_{1,2,3}(T_n)\right].$$

F.2 Limite continue des fonctions de corrélation définies sur les graphes de Strebel

Les graphes de Strebel ont été introduits par Penner [Penner, 1988].

Definition F.3. *Un graphe de Strebel de genre g et de taille n est un graphe ruban cellulaire métrique et trivalent, qui a n faces, et qui peut être plongé dans une surface de genre g. On note $\mathscr{S}_{g,n}$ l'ensemble des graphes de Strebel de taille n et genre g. Le périmètre de la face i est noté P_i. On note $\mathscr{S}_{g,n}(L_1, \ldots, L_n)$ la strate constituée des graphes de Strebel de genre g et taille n, tels que le périmètre de la face i est L_i.*
Étant donné un graphe ruban trivalent Γ, on note $\mathcal{V}(\Gamma)$, $\mathcal{E}(\Gamma)$, $\mathcal{F}(\Gamma)$ respectivement l'ensemble des nœuds, arêtes, faces de Γ, et pour $e \in \mathcal{E}(\Gamma)$, la longueur associée à e est notée ℓ_e, et l'ensemble des longueurs est ℓ.
La mesure $d\nu_{g,n}^{L_1,\ldots,L_n}$ sur $\mathscr{S}_{g,n}(L_1, \ldots, L_n)$ est la mesure de Lebesgue sur les longueurs :

$$d\nu_{g,n}^{L_1,\ldots,L_n}(\Gamma, \ell) = \prod_{e \in \mathcal{E}(\Gamma)} d\ell_e \prod_{f \in \mathcal{F}(\Gamma)} \delta(P_f - L_f)$$

La strate de référence dans ce chapitre est $\mathscr{S}_{0,n}(L)$: on considère les graphes de Strebel planaires tels que tous les périmètres sont égaux à L. Les fonctions à k-points font intervenir les strates $\mathscr{S}_{0,n+k}(L; L_1, \ldots, L_k)$, où les n premières faces ont pour périmètre L, et les k dernières faces ont les périmètres $L_1, \ldots, L_k$. Les fonctions de corrélation sont :

- le volume $V_n(L)$ de la strate $\mathscr{S}_{0,n}(L)$: $V_n(L) = \int_{\mathscr{S}_{0,n}(L)} d\nu_{0,n}^L(\Gamma, \ell)$, on encode les volumes dans la fonction génératrice

$$\mathcal{V}(\mu, L) = \sum_{n=3}^{\infty} \frac{\mu^n}{n!} V_n(L)$$

- la fonction à k-points est le volume de la strate $\mathscr{S}_{0,n+k}(L; L_1, \ldots, L_k)$: $Z_{n,k}(L; L_1, \ldots, L_k) = \int_{\mathscr{S}_{0,n+k}(L;L_1,\ldots,L_k)} d\nu_{0,n}^{L;L_1,\ldots,L_k}(\Gamma, \ell)$, qu'on encode dans la fonction génératrice

$$\mathcal{Z}_k(\mu, L; L_1, \ldots, L_k) = \sum_{n=3}^{\infty} \frac{\mu^n}{n!} Z_{n,k}(L; L_1, \ldots, L_k).$$

En utilisant le théorème de Kontsevich [Kontsevich, 1992], on calcule explicitement les fonctions génératrices des fonctions à k points.

Théorème F.4. *Les fonctions génératrices $\mathcal{V}$ et $\mathcal{Z}_k$ ont les expressions suivantes :*

$$\frac{\partial^3}{\partial \mu^3} \mathcal{V}(\mu, L) = \frac{I_0(u)^4}{2I_0(u) - uI_1(u)}$$

$$\mathcal{Z}_k(\mu, L; L_1, \ldots, L_k) = \frac{\partial^{k-3}}{\partial \mu^{k-3}} \left(\mu^k L^{2k} \left[\frac{1}{u^{2k}} \frac{I_0(u)^4}{2I_0(u) - uI_1(u)} \prod_{i=1}^{k} I_0(uL_i/L) \right]_+ \right)$$

où I_0, I_1 sont des fonctions de Bessel modifiées du premier type ; $[\ ]_+$ signifie qu'on ne garde que les puissance positives dans la série génératrice en μ ; et u est une fonction des paramètres μ, L

$$\mu L^2 = \frac{u^2}{I_0(u)}.$$

On se sert de ces expressions pour étudier la limite n grand du volume V_n et de la fonction à un point $Z_{n,1}$. Pour le volume, le comportement dominant s'obtient en étudiant la singularité de la fonction génératrice $\mathcal{V}(\mu, L)$ lorsque μ atteint le rayon de convergence μ_c.

$$V_n(L) \underset{n\to\infty}{\sim} C\ n! A(L)^n n^{-\frac{7}{2}}$$

où $A(L) = \frac{L^2}{2\mu_c L^2}$. Pour la fonction à un point, on distingue trois régimes pour le périmètre L_1 de la face marquée. On note $\ell = \frac{1}{n}\frac{L_1}{L}$:

1. $\ell \underset{n\to\infty}{\to} 0$;
2. $\ell \underset{n\to\infty}{\sim} \ell_0$;
3. $\ell \underset{n\to\infty}{\to} \infty$.

On applique la méthode du point-selle pour les différents régimes, et on obtient le comportement suivant

$$\ln \frac{Z_{n,1}(L; L_1)}{n! L^{2n} n^{-2}} \underset{n\to\infty}{\sim} n\ \ln A_i(\ell) + n\ell x_0(\ell),$$

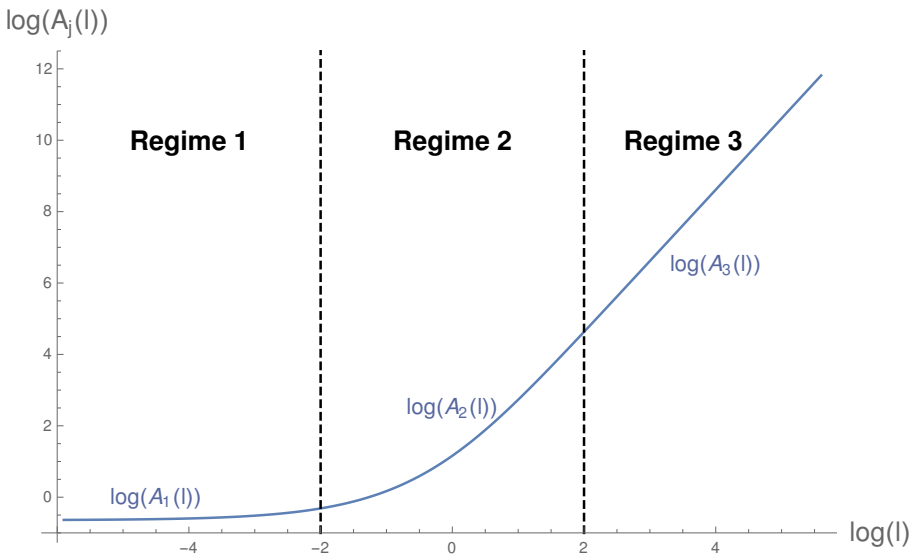

Figure 87: Comportement asymptotique de la fonction à un point pour les différents régimes : $\ln A_i(\ell)$ en fonction de $\ln \ell$.

où $A_i(\ell)$ est une fonction de ℓ valide dans le régime i, et $x_0(\ell)$ est une fonction de ℓ valide dans tous les régimes. Le comportement de la fonction à un point est résumé dans le graphique de la figure 87. On déduit de cette étude asymptotique que le régime où la fonction à un point ne présente pas un comportement simple est le régime 2 : $\ell = O(1)$.

F.3 Courbe spectrale associée aux graphes de Strebel

Afin d'avoir une vue englobante des fonctions de corrélation, celles-ci sont encodées dans la courbe spectrale du modèle. Pour calculer les fonctions de corrélation à partir de la courbe spectrale, il faut appliquer la récurrence topologique, procédure développée par Eynard et Orantin [Eynard and Orantin, 2007]. Dans le cas des graphes de Strebel, la courbe spectrale $\mathcal{S}(\mu, L)$, qui dépend des paramètres du modèle, est la donnée de 5 objets : une surface de Riemann Σ (dans notre cas $\Sigma = \overline{\mathbb{C}}$) ; une courbe Σ_0 ($\Sigma_0 = \mathbb{C}$) ; deux fonctions méromorphes $x(\mu, L)$, $y(\mu, L)$: $\Sigma \to \Sigma_0 = \mathbb{C}$; une forme bi-différentielle méromorphe $\omega_{0,2} \in \mathcal{M}^1(\Sigma) \otimes^{\text{sym}} \mathcal{M}^1(\Sigma)$ dont les seuls pôles sont doubles et se situent aux points coïncidents avec ce comportement $\omega_{0,2}(z_1, z_2) \underset{z_1 \to z_2}{\sim} \frac{dz_1 \otimes dz_2}{(z_1 - z_2)^2} +$ analytique. Pour résumer, la courbe spectrale est donnée par le quintuplet :

$$\mathcal{S}(\mu, L) = (\overline{\mathbb{C}}, \mathbb{C}, x(\mu, L), y(\mu, L), \omega_{0,2}).$$

Pour les graphes de Strebel forme bi-différentielle est $\omega_{0,2}(z_1, z_2) = \frac{dz_1 \otimes dz_2}{(z_1 - z_2)^2}$, et les fonctions x, y sont données par :

$$\begin{cases} x(\mu, L; z) = z^2 + \frac{u^2}{L^2} \\ y(\mu, L; z) = z - \frac{\mu L^2}{2u} \sum_{k=0}^{\infty} \frac{L^{2k} I_{k+1}(u)}{(2k+1)!! u^k} z^{2k+1} \end{cases}$$

où les fonctions de Bessel modifiées du premier type I_k, et le paramètre u apparaissent. L'objectif étant l'étude de la limite continue des graphes de Strebel, on étudie le comportement de la courbe spectrale lorsque les paramètres μ, L, et plus précisément le paramètre μL^2, tendent vers la valeur critique $\mu_c L^2$. Comme on le voit sur la figure 88, à cette valeur, la courbe spectrale est singulière. Pour obtenir une courbe spectrale critique non singulière, il faut redimensionner les fonctions x, y en fonction du paramètre ($\mu L^2 - \mu_c L^2$, et on obtient le résultat :

Théorème F.5. *Notons* $x_0 = \frac{u_c^2}{L^2}$, $A = \frac{u_c}{L^2} \sqrt{\frac{2I_0(u_c)}{u_c^2 - 4}}$ *et* $B = (u_c^2 - 4)^{\frac{1}{4}} \frac{(2I_0(u_c))^{\frac{3}{4}}}{6L\sqrt{u_c}}$ *trois constantes, et notons* ξ *la paramétrisation suivante :*

$$z = (\mu_c L^2 - \mu L^2)^{\frac{1}{4}} \left(\frac{2u_c^2 I_0(u_c)}{9(u_c^2 - 4)} \right)^{\frac{1}{4}} \xi.$$

Alors les fonctions $x(\mu, L)$, $y(\mu, L)$, *après un redimensionnement, ont les limites suivantes:*

$$\lim_{\mu \to \mu_c} \frac{x(\mu, L; z) - x_0}{A(\mu_c L^2 - \mu L^2)^{\frac{1}{2}}} = \xi^2 - 2 = \tilde{x}(\xi)$$

$$\lim_{\mu \to \mu_c} \frac{y(\mu, L; z)}{B(\mu_c L^2 - \mu L^2)^{\frac{3}{4}}} = \xi^3 - 3\xi = \tilde{y}(\xi).$$

Cela donne la courbe spectrale critique suivante :

$$\tilde{S} = \left(\overline{\mathbb{C}}, \mathbb{C}, \tilde{x}, \tilde{y}, \frac{d\xi_1 \otimes d\xi_2}{(\xi_1 - \xi_2)^2} \right)$$

$$\begin{cases} \tilde{x}(\xi) = \xi^2 - 2 \\ \tilde{y}(\xi) = \xi^3 - 3\xi \end{cases}$$

La courbe spectrale critique est celle du modèle minimal (3,2) [Douglas, 1990], qui est une réduction de la hiérarchie KdV. Di Francesco et Kutasov [Di Francesco and Kutasov, 1990] ont relié ce mod'ele minimal à une théorie des champs conforme ayant une charge centrale nulle $c_{\text{matiere}} = 0$, couplée à la théorie de Liouville. Cela est supposé correspondre à la gravité pure. Ainsi, la limite continue des fonctions de corrélations définies sur les graphes de Strebel correspond à une théorie conforme de charge centrale nulle, habillée par la gravité. La figure 89 synthétise le raisonnement des deux chapitres sur les graphes de Strebel, qui permet de déduire la limite continue des fonctions de corrélation.

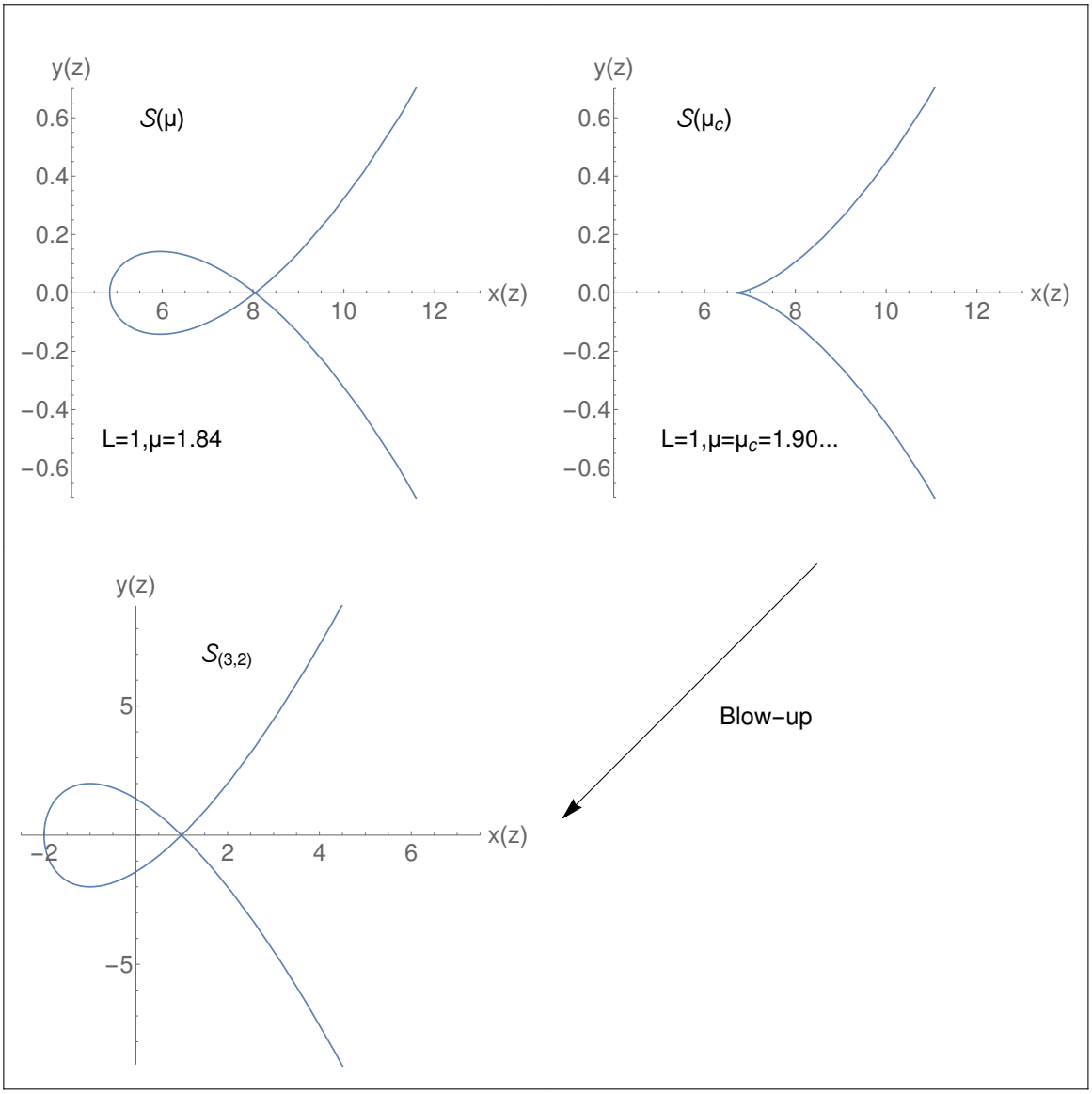

Figure 88: Intersection des fonctions $x(\mu, L)$, $y(\mu, L)$ avec le plan $x, y \in \mathbb{R}$ pour différentes valeurs du paramètre μL^2. Le premier graphe correspond à une valeur générique du paramètre ; le deuxième correspond à $\mu L^2 = \mu_c L^2$, et la courbe spectrale est singulière ; enfin le troisième graphe est la représentation de $\tilde{x}$, $\tilde{y}$, c'est-à-dire de la courbe spectrale critique, obtenue à partir de la courbe spectrale au paramètre critique après redimensionnement.

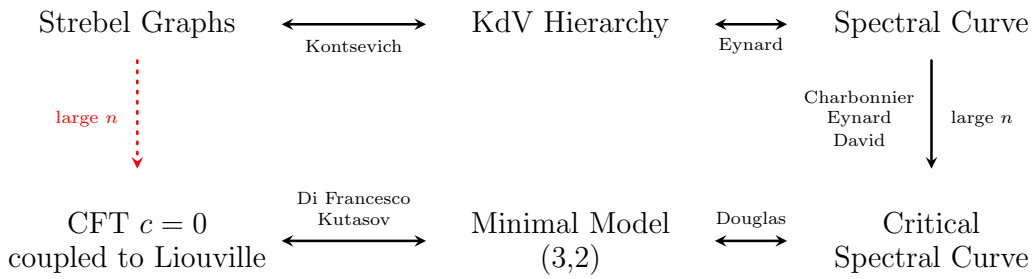

Figure 89: Schéma récapitulatif pour les graphes de Strebel

F.4 Invariances de fonctions de corrélation dans le modèle d'Ising

Dans ce chapitre, des propriétés de symétries de fonctions de corrélations inspirées du modèle d'Ising sur cartes aléatoires sont étudiées. On considère des fonctions de corrélation de genre g, avec L bords dits "mixtes", m bords dits "uniformes et rouges", et n bords dits "uniformes et noirs".

- Le bord mixte i est noté S_i, et sa longueur est notée k_i. On associe au i-ème bord mixte les $2k_i$ variables $(p_{i,1}, q_{i,1}, p_{i,2}, q_{i,2}, \dots, p_{i,k_i}, q_{i,k_i})$ (ces variables sont ordonnées).

- Au i-ème bord uniforme rouge (resp. noir) on associe la variable p_i (resp. q_i).

Alors la fonction de corrélation de genre g, à L bords mixtes $S_1, \dots, S_L$, m bords uniformes rouges et n bords uniformes noirs, est notée

$$H^{(g)}_{\mathbf{k_L};m;n}(S_1, \dots, S_L; p_1, \dots, p_m; q_1, \dots, q_n).$$

Ces fonctions de corrélations sont définies par récurrence sur $2g + \sum_{i=1}^{L} k_i + m + n$, la formule ayant été dérivée par Eynard et Orantin [Eynard and Orantin, 2008] :

$$
\begin{aligned}
&H^{(g)}_{\mathbf{k_L};m;n}(\mathbf{S_L}; p_1, \dots, p_m; q_1, \dots, q_n) = \\
&\operatorname*{Res}_{r \to p_{1,1}, p_{i,\alpha}, p_j, q^{0,j}_{1,k_1}} \frac{H^{(0)}_{1;0;0}(p_{1,1}, q_{1,k_1}) dx(r)}{(x(p_{1,1}) - x(r))(y(q_{1,k_1}) - y(r)) H^{(0)}_{1;0;0}(r, q_{1,k_1})} \times \\
&\Bigg[\sum_h \sum_{A \cup B = \{2,\dots,l\}} \sum_{\alpha=2}^{k_1} \sum_{I,J} H^{(h)}_{k_1-\alpha+1, \mathbf{k_B}; m-|I|; n-|J|}(\{p_{1,\alpha}, q_{1,\alpha}, \dots, q_{1,k_1}\}, \mathbf{S_B}; \mathbf{p_{M/I}}; \mathbf{q_{N/J}}) \\
&\times \frac{H^{(g-h)}_{\alpha-1, \mathbf{k_A}; |I|; |J|}(\{r, q_{1,1}, \dots, p_{1,\alpha-1}, q_{1,\alpha-1}\}, \mathbf{S_A}; \mathbf{p_I}; \mathbf{q_J})}{x(p_{1,\alpha}) - x(r)} \\
&+ \sum_{\alpha=2}^{k_1} \frac{1}{x(p_{1,\alpha}) - x(r)} \times \\
&H^{(g-1)}_{\alpha-1, k_1-\alpha+1, \mathbf{k_{L/\{1\}}}; m; n}(\{r, q_{1,1}, \dots, p_{1,\alpha-1}, q_{1,\alpha-1}\}, \{p_{1,\alpha}, q_{1,\alpha}, \dots, q_{1,k_1}\}, \mathbf{S_{L/\{1\}}}; \mathbf{p_M}; \mathbf{q_N}) \\
&+ \sum_{i=2}^{l} \sum_{\alpha=1}^{k_i} \frac{1}{x(p_{i,\alpha}) - x(r)} \times \\
&H^{(g)}_{k_1+k_i, \mathbf{k_{L/\{1,i\}}}; m; n}(\{S_1(r), p_{i,\alpha}, q_{i,\alpha}, p_{i,\alpha+1}, \dots, q_{i,k_i}, p_{i,1}, \dots, q_{i,\alpha-1}\}, \mathbf{S_{L/\{1,i\}}}; \mathbf{p_M}; \mathbf{q_N}) + \\
&\sum_h \sum_{A \cup B = \{2,\dots,l\}} \sum_{I,J} H^{(h)}_{k_1, \mathbf{k_A}; |I|; |J|}(S_1(r), \mathbf{S_A}; \mathbf{p_I}; \mathbf{q_J}) H^{(g-h)}_{\mathbf{k_B}; m-|I|+1; n-|J|}(\mathbf{S_B}; r, \mathbf{p_{M/\{I\}}}; \mathbf{q_{N/\{J\}}}) \\
&+ \sum_{h=1}^{g} H^{(h)}_{0;1;0}(r) H^{(g-h)}_{k_1,\dots,k_l; m; n}(S_1(r), S_2, \dots, S_l; p_1, \dots, p_m; q_1, \dots, q_n) \\
&+ H^{(g-1)}_{\mathbf{k_L}; m+1; n}(\mathbf{S_K}(r); r, \mathbf{p_M}; \mathbf{q_N}) \Bigg]
\end{aligned}
$$

Trois opérateurs agissent sur les variables de bords des fonctions de corrélation :

1. la rotation $\mathcal{R}_i$ du bord mixte i, qui agit de la manière suivante :

$$\mathcal{R}_i S_i = (p_{i,2}, q_{i,2}, p_{i,3}, q_{i,3}, \dots, p_{i,k_i}, q_{i,k_i}, p_{i,1}, q_{i,1}),$$

   et dont l'action sur les fonctions de corrélations est simplement

$$
\begin{aligned}
\mathcal{R}_i H^{(g)}_{\mathbf{k_L}; m; n}(S_1, \dots, S_L; p_1, \dots, p_m; q_1, \dots, q_n) = \\
H^{(g)}_{\mathbf{k_L}; m; n}(S_1, \dots \mathcal{R}_i S_i, \dots, S_L; p_1, \dots, p_m; q_1, \dots, q_n).
\end{aligned}
$$

2. L'inversion $\mathcal{I}$ de tous les bords mixtes est la transformation qui inverse l'ordre des variables de tous les bords mixtes :

$$\forall i \in \{1, \dots, L\} \qquad \mathcal{I} S_i = (p_{i,1}, q_{i,k_i}, p_{i,k_i}, q_{i,k_i-1}, \dots, p_{i,2}, q_{i,1}),$$

et dont l'action sur les fonctions de corrélations est :

$$\mathcal{I}H^{(g)}_{\mathbf{k_L};m;n}(S_1,\dots,S_L;p_1,\dots,p_m;q_1,\dots,q_n) = H^{(g)}_{\mathbf{k_L};m;n}(\mathcal{I}S_1,\dots,\mathcal{I}S_L;p_1,\dots,p_m;q_1,\dots,q_n).$$

3. L'échange $\mathcal{T}_i$ des bords mixtes S_1 et S_i :

$$\mathcal{T}_i H^{(g)}_{\mathbf{k_L};m;n}(S_1,\dots,S_L;p_1,\dots,p_m;q_1,\dots,q_n) = H^{(g)}_{\mathbf{k_L};m;n}(S_i,\dots,S_{i-1},S_1,S_{i+1},\dots,S_L;p_1,\dots,p_m;q_1,\dots,q_n)$$

L'objectif du chapitre est de prouver que les fonctions de corrélation définies par la formule de récurrence sont invariantes sous ces trois opérations. On prouve le théorème suivant :

Théorème F.6. *Les fonctions de corrélation planaires ($g = 0$), à un bord mixte ($L = 1$) de taille k et sans bord uniforme ($m = n = 0$) ont l'expression suivante :*

$$H^{(0)}_{k;0;0} = \sum_{\substack{\text{systemes de liens}\\ \text{planaires}}}$$

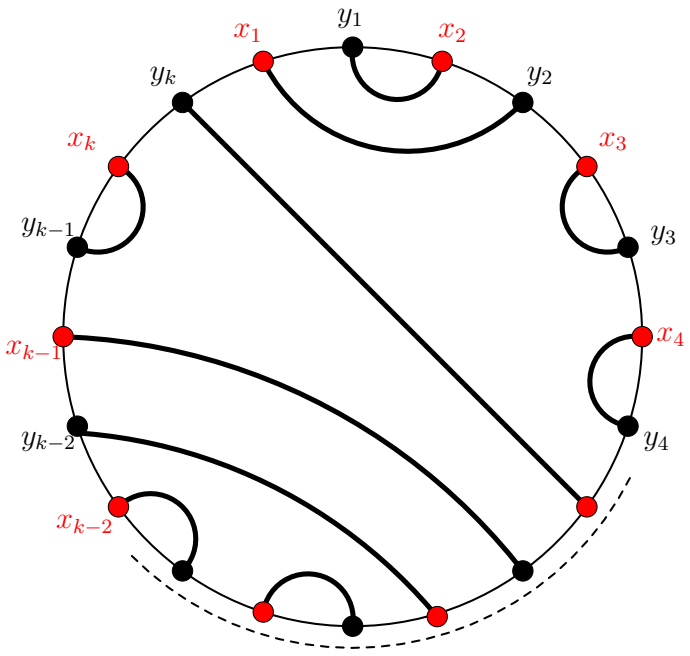

Dans cette formule, chaque diagramme est un système de liens planaire. Le cercle sur lequel sont dessinés les points rouges et noirs représente le bord mixte de taille k. Chaque point rouge (resp. noir) porte une étiquette x_i (resp. y_i), qui est une fonction de p_i (resp. q_i). Les variables sont orientées dans le sens horaire le long du cercle. Un système de liens est un couplage tel que chaque point rouge est relié à un unique point noir. Il est planaire si on peut dessiner le système de liens à l'intérieur du cercle sans que les liens ne se croisent.
Chaque diagramme ainsi dessiné a un poids, qui est le produit de poids locaux :

- chaque lien entre x_i et y_j a le poids $H^{(0)}_{1;0;0}(\{p_i, q_j\})$.
- Une face de taille ℓ a un poids $F^{(\ell)}(x_{j_1}, y_{j_1}, x_{j_2}, y_{j_2}, \dots, x_{j_\ell}, y_{j_\ell})$:

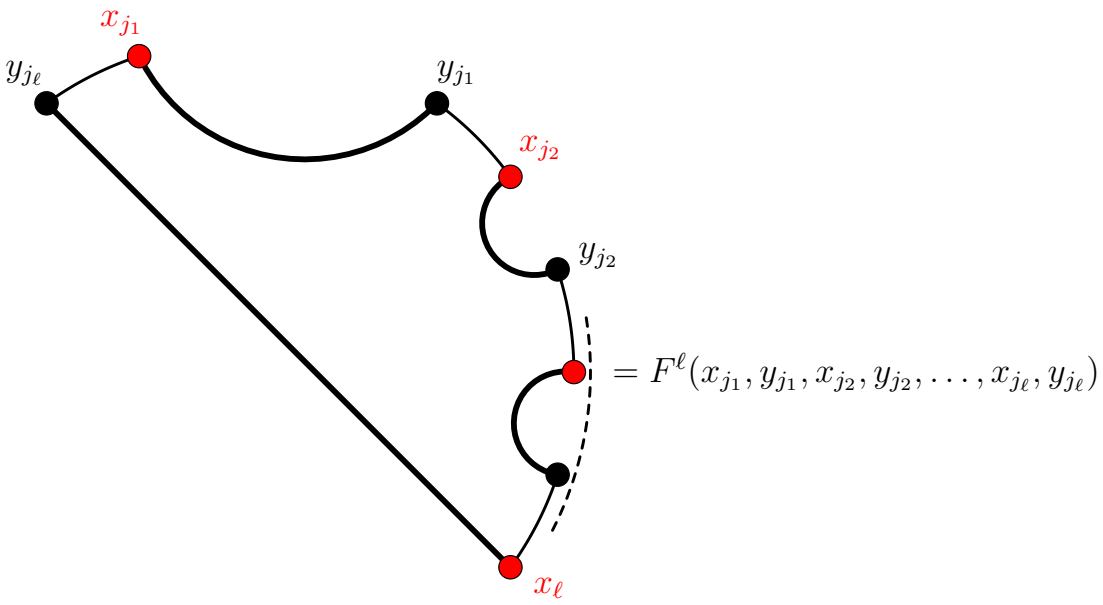

Les fonctions $F^{(\ell)}$ sont définies par la formule de récurrence suivante :

$$\begin{cases} F^{(1)}(x_1, y_1) = 1 \\ F^{(\ell)}(x_1, y_1, \dots, x_\ell, y_\ell) = \sum_{j=1}^{\ell-1} \frac{F^{(j)}(x_1,\dots,y_j)F^{(\ell-j)}(x_{j+1},\dots,y_\ell)}{(x_\ell - x_1)(y_\ell - y_j)}. \end{cases}$$

Une conséquence directe de ce théorème est que ces fonctions de corrélation sont invariantes par rotation et inversion du bord mixte.

Corollaire F.1. *Pour tout $k \in \mathbb{N}$,*

$$\mathcal{R}_1 H^{(0)}_{k;0;0}(\{p_1, q_1, \dots, p_k, q_k\}) = H^{(0)}_{k;0;0}(\{p_1, q_1, \dots, p_k, q_k\}),$$

$$\mathcal{I} H^{(0)}_{k;0;0}(\{p_1, q_1, \dots, p_k, q_k\}) = H^{(0)}_{k;0;0}(\{p_1, q_1, \dots, p_k, q_k\}).$$

En introduisant les opérateurs d'insertion de bords uniformes rouges (resp. noirs), on étend ce résultat à des fonctions de corrélation plus génerales :

Definition F.4. *On note δ^r_p (resp. δ^b_q) l'opérateur d'insertion d'un bord uniforme rouge (resp. noir), défini par :*

$$\begin{cases} \delta^r_p Y(x(p_1)) = H^{(0)}_{0;2;0}(p_1, p) \\ \delta^r_p H^{(0)}_{0;2;0}(p_1, p_2) = H^{(0)}_{0;3;0}(p_1, p_2, p) \\ \delta^r_p \operatorname*{Res}_{r\to z} = \operatorname*{Res}_{r\to \overset{z}{p}} \delta^r_p \end{cases}$$

(resp.

$$\begin{cases} \delta_q^b X(y(q_1)) = H^{(0)}_{0;0;2}(q_1, q) \\ \delta_q^b H^{(0)}_{0;0;2}(q_1, q_2) = H^{(0)}_{0;3;0}(q_1, q_2, q) \\ \delta_q^b \underset{r\to z}{\mathrm{Res}} = \underset{r\to \overset{z}{q}}{\mathrm{Res}} \delta_q^b) \end{cases}$$

Alors ces opérateurs permettent d'nseérer des bords uniformes dans les fonctions de corrélation :

Théorème F.7. *Pour l'insertion d'un bord uniforme rouge :*

$$\delta_p^r H^{(g)}_{\mathbf{k_L};m;n}(S_1, \dots, S_L; \{p_i\}; \{q_j\}) = H^{(g)}_{\mathbf{k_L};m+1;n}(S_1, \dots, S_L; \{p_i\} \cup \{p\}; \{q_j\})$$

et de même pour l'insertion d'un bord uniforme noir, on applique l'opérateur δ_q^b.

Grâce à ces opérateurs d'insertion, on montre le corollaire suivant :

Corollaire F.2. *Pour tous $k, m, n \in \mathbb{N}$,*

$$\mathcal{R}_1 H^{(0)}_{k;m;n}(\{p_{1,1}, q_{1,1}, \dots, p_{1,k}, q_{1,k}\}, p_1 \dots, p_m; q_1, \dots, q_n) = H^{(0)}_{k;m;n}(\{p_{1,1}, q_{1,1}, \dots, p_{1,k}, q_{1,k}\}, p_1 \dots, p_m; q_1, \dots, q_n),$$

$$\mathcal{I} H^{(0)}_{k;m;n}(\{p_{1,1}, q_{1,1}, \dots, p_{1,k}, q_{1,k}\}, p_1 \dots, p_m; q_1, \dots, q_n)$$
$$H^{(0)}_{k;m;n}(\{p_{1,1}, q_{1,1}, \dots, p_{1,k}, q_{1,k}\}, p_1 \dots, p_m; q_1, \dots, q_n).$$

References

[I] Charbonnier, S., Eynard, B. and David, F. (2018) Large Strebel Graphs and (3,2) Liouville CFT. *Ann. Henri Poincaré*, https://doi.org/10.1007/s00023-018-0662-x .

[II] Charbonnier, S., David, F. and Eynard, B. (2017) Local properties of the random Delaunay triangulation model and topological 2D gravity arXiv:1701.0258

[Ambjørn and Watabiki, 1995] Ambjørn, J. and Watabiki, Y. (1995) Scaling in quantum gravity. *Nucl. Phys. B*, 445(1):129–142 (1995)

[Andersen - Borot - Chekhov - Orantin, 2017] Andersen, J.E., Borot, G., Chekhov, L.O. and Orantin, N. (2017) The ABCD of topological recursion. *arXiv:*1703.03307

[Belavin et al., 1984] Belavin, A.A., Polyakov, A.M., Zamolodchikov, A.B. (1984) Infinite conformal symmetry in two-dimensional quantum field theory. *Nucl. Phys. B*, 241(2):333–380 (1984)

[Bobenko and Springborn, 2004] Bobenko, A. I. and Springborn, B. A. (2004) Variational principles for circle patterns and Koebe's theorem. *Trans. Amer. Math. Soc.*, 356:659–689 (2004)

[Borot and Eynard, 2011] Borot, G. and Eynard, B. (2011) Enumeration of maps with self-avoiding loops and the $O(n)$ model on random lattices of all topologies *J. Stat. Mech.* P01010 (2011)

[Bouttier - Di Francesco - Guitter, 2004] Bouttier, J., Di Francesco, P., Guitter, E. (2004) Planar maps as labeled mobiles. *Electron. J. Combin.* , 11(1) Research paper 69, 27 pp. (2004)

[Brévilliers, 2008] Brévilliers, M. (2008) Construction of the segment Delaunay triangulation by a flip algoritm. *tel-00372365*

[Brézin et al., 1978] Brézin, E., Itzykson, C., Parisi, G. and Zuber, J.B. (1978) Planar diagrams. *Commun. Math. Phys.*, 59(1):35–51 (1978)

Budd, T. , private communication, April 2014.

[David, 1985] David, F. (1985) Planar diagrams, two-dimensional lattice gravity and surface models. *Nucl. Phys. B 257*, 257 [FS14]:45–58 (1985)

[David, 1988a] David, F. (1988) Conformal field theories coupled to 2-d gravity in the conformal gauge. *Mod. Phys. Lett. A*, 03:1651–1656 (1988)

[David, 1988b] David, F. (1988) Sur l'entropie des surfaces aléatoires. *C. R. Acad. Sci. Paris*, 307 Série II:1051–1053 (1988)

[David and Eynard, 2014] David, F. and Eynard, B. (2014) Planar maps, circle patterns and 2D gravity. *Ann. Inst. Henri Poincaré Comb. Phys. Interact. 1* , 139-183 (2014)

[David et al., 2015] David, F., Kupiainen, A., Rhodes, R. and Vargas, V. (2015) Liouville Quantum Gravity on the Riemann Sphere. *Commun. Math. Phys.*, 10.1007/s00220-016-2572-4.

[Deligne and Mumford, 1969] Deligne, P. and Mumford, D. (1969) The irreducibility of the space of curves of given genus *Publ. Math. IHES* 36:75–109 (1969)

[Di Francesco et al., 1995] Di Francesco, P., Ginnsparg, P. and Zinn-Justin, J. (1995) 2D gravity and random matrices. *Phys. Rep.*, 254(1-2):1–333 (1995)

[Di Francesco and Kutasov, 1990] Di Francesco, P. and Kutasov, D. (1990). Unitary minimal models coupled to 2D quantum gravity. *Nucl. Phys. B*, 342:589–624 (1990)

[Distler and Kawai, 1989] Distler, J. and Kawai, H. (1989) Conformal field theory and 2-d quantum gravity. *Nucl. Phys. B*, 321(2):509–527 (1989)

[Dorn and Otto, 1994] Dorn, H. and Otto, H.-J. (1994) Two and three point functions in Liouville theoy. *Bucl. Phys. B*429, 375:388 (1994)

[Douglas, 1990] Douglas, M. R. (1990) Strings in less than one dimension and the generalized KdV hierarchies. *Phys. Lett. B*, 238(2-4):176–180 (1990)

[Duplantier et al., 2014] Duplantier, B., Miller, J. and Sheffield, S. (2014) Liouville quantum gravity as mating of trees. *arXiv:*1409.7055.

[Eynard, 2007] Eynard, B. (2007) Recursion between Mumford volumes of moduli spaces. *Unpublished,* arXiv:0706.4403

[Eynard, 2011] Eynard, B. (2011) Intersection numbers of spectral curves. *Unpublished,* arXiv:1104.0176

[Eynard, 2016] Eynard, B. (2016) Counting surfaces. *Springer* 2016, ISBN: 9783764387969

[Eynard and Orantin, 2005] Eynard, B. and Orantin, N. (2005) Mixed correlation functions in the 2-matrix model, and the Bethe Ansatz. *JHEP* 0508:028 (2005)

[Eynard and Orantin, 2007] Eynard, B. and Orantin, N. (2007) Invariants of algebraic curves and topological expansion. *Commun. Numb. Theor. Phys.*, 1(2):347–452 (2007)

[Eynard and Orantin, 2008] Eynard, B. and Orantin, N. (2008) Topological expansion and boundary conditions. *JHEP* 0806:037 (2008)

[Eynard and Prats Ferrer, 2006] Eynard, B. and Prats Ferrer, A. (2006) 2-matrix versus complex matrix model, integrals over the unitary group as triangular integrals Commun. Math. Phys. 264:115–144 (2006)

[Harer - Zagier, 1986] Harer, J. and Zagier, D. (1986) The Euler characteristic of the moduli space of curves. *Invent. Math.* , 85(3):457-485 (1986)

['t Hooft, 1974] 't Hooft, G. (1974) A planar diagram theory for strong interactions *Nucl. Phys. B.*, 72(3):461–473 (1974)

[Kaufmann et al., 1996] Kaufmann, R., Manin, Yu., and Zagier, D. (1996) Higher Weil-Petersson Volumes of Moduli Spaces of Stable n-Pointed Curves. *Commun. Math. Phys.* 181, 763:787 (1996)

[Kazakov, 1986] Kazakov, V.A. (1986) Ising model on a dynamical planar random lattice: exact solution. *Phys. Lett. A*, 119:140–144 (1986)

[Knizhnik - Polyakov - Zamolodchikov, 1988] Knizhnik, V., Polyakov, A., and Zamolodchikov, A. (1988) Fractal structure of 2d-gravity. *Mod. Phys. Lett. A*, 03:819–826 (1988)

[Koebe, 1936] Koebe, P. (1936) Kontaktprobleme der konformen Abbildung. *Ber. Sächs. Akad. Wiss. Leipzig, Math.-Phys. Kl.*, 88:141–164 (1936)

[Kontsevich, 1992] Kontsevich, M. (1992) Intersection theory on the moduli space of curves and the matrix Airy function. *Commun. MAth. Phys.*, 147:1–23 (1992)

[Kontsevich and Soibelman, 2017] Kontsevich, M. and Soibelman, Y. (2017) Airy structures and symplectic geometry of topological recursion *arXiv:*1701.09137

[Kupiainen et al., 2017] Kupiainen, A., Rhodes, R. and Vargas, V. (2017) Integrability of Liouville theory: proof of the DOZZ formula. *arXiv*:1707.08785

[Lawson, 1972] Lawson, C.L. (1972) Transforming Triangulations. *Discrete Mathematics*, 3:365-372 (1972)

[Le Gall, 2013] Le Gall, J.-F. (2013). Uniqueness and universality of the Brownian map. *Ann. Probab.*, 41:2880–2960 (2013)

[Manin and Zograf, 2000] Yu. Manin, P. Zograf (2000) Invertible cohomological field theories and Weil-Petersson volumes. *Ann. Inst. Fourier*, 50(2):519-535 (2000)

[Miermont, 2009] Miermont, G. (2009) Random maps and their scaling limits *Prog. Prob.* 61:197–224 (2009)

[Miermont, 2013] Miermont, G. (2013) The Brownian map is the scaling limit of uniform random plane quadrangulations. *Acta Math.*, 210:319–401 (2013)

[Mirzakhani, 2007] Mirzakhani, M. (2007) Weil-Petersson volumes and intersection theory on the moduli space of curves. *J. Amer. Math. Soc.*, 20:1–23 (2007)

[Mulase and Penkava, 1998] Mulase, M. and Penkava, M. (1998) Ribbon graphs, quadratic differentials on Riemann surfaces, and algebraic curves defined over $\overline{Q}$. *Asian J. Math.*, 2(4):875–920 (1998)

[Penner, 1987] Penner, R. C. (1987) The decorated Teichmüller space of punctured surfaces. *Comm. Math. Phys.*, 113:299–339 (1987)

[Penner, 1988] Penner, R. C. (1988) Perturbation series and the moduli space of Riemann surfaces. *Journal of Diff. Geom.*, 27:35–53 (1988)

[Polyakov, 1974] Polyakov, A.M. (1981) Non-Hamiltonian approach to conformal quantum field theory. *Zh. Eksp. Teor. Fiz.*, 66:23–42 (1974)

[Polyakov, 1981] Polyakov, A.M. (1981) Quantum geometry of bosonic strings. *Physics Letters B*, 103(3):207–210 (1981)

[Ribault, 2014] Ribault, S. (2014) Conformal field theory on the plane. *arXiv:*hep-th/1406.4290

[Rivin, 1994] Rivin, I. (1994) Euclidean structures on simplicial surfaces and hyperbolic volume. *Annals of Mathematics*, 139:553–580 (1994)

[Schaeffer, 1998] Schaeffer, G. (1998) Conjugaison d'arbres et cartes combinatoires aléatoires. *PhD Thesis*, Université Bordeaux I (1998)

[Strebel, 1984] Strebel, K. (1984) Quadratic Differentials. *Springer, New York* 1984, ISBN: 9783662024140

[Teschner, 1995] Teschner, J. (1995) On the Liouville three point function. *Phys. Lett. B*, 363:65–70 (1995)

[Tutte, 1962] Tutte, W.T. (1962) A census of planar triangulations. *Canad. J. Math.*, 14:21–38 (1962).

[Vargas, 2017] Vargas, V. (2017) Lecture notes on Liouville theory and the DOZZ formula. *arXiv:*1712.00829

[Zamolodchikov and Zamolodchikov, 1995] Zamolodchikov, A.B. and Zamolodchikov, A.B. (1995) Structure constants and conformal bootstrap in Liouville field theory. *arXiv:*hep-th/9506136

[Zamolodchikov and Zamolodchikov, 1996] Zamolodchikov, A.B. and Zamolodchikov, A.B. (1996). Conformal bootstrap in Liouville field theory. *Nucl. Phys. B*, 477(2):577–605 (1996)

[Zograf, 1993] Zograf, P. (1993) The Weil-Petersson volume of the moduli space of punctured spheres. *Contemp. Math.*, 150:367-372 (1993)

université PARIS-SACLAY
ÉCOLE DOCTORALE
Physique en île-de-France (EDPIF)

Titre: Théorie de Liouville et cartes aléatoires

Mots clés: Théorie de Liouville, cartes aléatoires, gravité quantique, triangulations de Delaunay, graphes de Strebel, modèle d'Ising

Résumé: Cette thèse explore divers aspects des cartes aléatoires par l'étude de trois modèles. Dans un premier temps, nous examinons les propriétés d'une mesure définie sur l'ensemble des triangulations de Delaunay planaires comportant n sommets, qui est un modèle de cartes où les arêtes sont décorées par des angles. Nous montrons ainsi que la mesure est égale à la mesure de Weil-Petersson sur l'espace des modules des surfaces de Riemann planaires marquées. Sont aussi montrées deux propriétés de la mesures, premiers pas d'une étude de la limite continue de ce modèle. Dans un deuxième temps, nous définissons des fonctions de corrélations sur les graphes de Strebel planaires isopérimétriques à n faces, qui sont des cartes métriques trivalentes. Les périmètres des faces sont fixés. Nous recourons au théorème de Kontsevich pour calculer les fonctions de corrélations en termes de nombres d'intersection de classes de Chern sur l'espace des modules des surfaces de Riemann. Pour la fonction à une face marquée, la limite des grandes cartes est examinée via l'approximation du point-selle, pour différents régimes du périmètre de la face marquée, et nous déduisons le régime où le comportement de la fonction de corrélation n'est pas trivial. Les fonctions de corrélations peuvent être calculées de manière systématique par la récurrence topologique. Partant, nous calculons la courbe spectrale de notre modèle, ce qui nous permet de montrer qu'il existe une courbe spectrale critique. Nous déduisons de cette courbe critique que la limite continue des graphes de Strebel isopérimétriques est un modèle minimal de type (3,2), habillé par la théorie de Liouville. Cela correspond bien à la gravité pure. Enfin, nous abordons la question des symétries dans le modèle d'Ising sur cartes aléatoires. Certaines fonctions de corrélations de ce modèle comptent le nombre de cartes bicolores avec des faces marquées, les bords, ayant des conditions aux bords mixtes, calculées par récurrence à partir de la courbe spectrale du modèle. Nous prouvons ici que, pour des courbes spectrales génériques, les fonctions de corrélations des cartes à un bord mixte sont symétriques par rotation et par inversion du bord mixte. Nous décrivons ensuite les conséquences de telles symétries, suggérant une possible reformulation du modèle en termes de chaînes de spins.

Title: Liouville theory and random maps

Keywords: Liouville theory, random maps, quantum gravity, Delaunay triangulations, Strebel graphs, Ising model

Abstract: This thesis explores several aspects of random maps through the study of three models. First, we examine the properties of a measure defined on the set of planar Delaunay triangulations with n vertices, a model in which the edges of the maps are decorated with angles. We show that the measure is the Weil-Petersson volume form on the moduli space of planar Riemann surfaces having n marked points. Two other properties, first steps toward the continuous limit study of the model, are also shown. Second, we define correlation functions on isoperimetric planar Strebel graphs with n faces, which are trivalent maps whose edges are decorated by positive lengths, and whose faces have a fixed perimeter. Kontsevich's theorem allows us to compute the correlation functions in terms of the intersection numbers of Chern classes of moduli space of Riemann surfaces. The continuous limit of the one-point function is computed in different regimes for the perimeter of the marked face via the saddle-point approximation. We identify the regime in which the behaviour of the one-point function is not trivial. The correlation functions can be computed in a systematic way by the Topological Recursion. To do so, we compute the spectral curve of the model, and show that there exists a critical spectral curve. We deduce from the latter that the continuous limit of isoperimetric Strebel graphs is a (3,2) minimal model dressed by Liouville theory: it corresponds to pure gravity. Last, we address the problem of symmetries in the Ising model on random maps. Some correlation functions of this model count the bi-colored maps with marked faces having mixed boundary conditions. They are computed via a recursive formula and the spectral curve of the model. We prove here that the correlation functions of maps with one mixed boundary, computed from the recursive relation with generic spectral curve, are invariant under rotation and inversion of the mixed boundary. We describe the consequences of such symmetries, suggesting a possible reformulation of the model in terms of spin chains.

Université Paris-Saclay
Espace Technologique / Immeuble Discovery
Route de l'Orme aux Merisiers RD 128 / 91190 Saint-Aubin, France